BYG·DTU

DANMARKS
TEKNISKE
UNIVERSITET

DTU

AALBORG WHITE®

Erik Pram Nielsen

The durability of white Portland cement to chemical attack

SUMMARY

In terms of volume, the severest conditions that reinforced concrete structures are subjected to usually involve some form of attack by chlorides. These include marine environments, roads and bridges exposed to de-icing salt, etc. The time it takes for the chlorides to reach the reinforcement is the main parameter used to predict the service life of the concrete structures.

Much effort has been spent in understanding the processes resulting in the ingress of chlorides in concrete structures exposed to aggressive environments, and in predicting its service life. However, to date it has not been possible to accurately predict the time for chloride ions to reach the reinforcement of concrete structures without carrying out extensive and time consuming laboratory experiments to calibrate the service life models.

It is generally agreed that when chlorides ingress into concrete, part of these become fixed to the cement paste hydrates through processes generally referred to as chloride binding. Furthermore, the rate at which these ions ingress into concrete is also known to be highly dependent on the available porosity. The aim of this study was to provide a more reliable model for predicting the ingress rate of chlorides in cement-based materials.

A thermodynamic model for the phase equilibria in hydrated Portland cement based on application of the phase rule, was developed and then verified experimentally during this investigation. The experiments were conducted on three types of Portland cement with varying composition (one grey and two white Portland cements). This approach was extended to include the reactions resulting in the binding of chlorides and alkalis. The model's accuracy to predict chloride binding in Portland cement pastes at any content of chloride, alkalis, sulfates and carbonate was verified experimentally, and found to be consistent with available data in the literature. Furthermore, the model was shown to be equally valid for the phase assemblage identified in 25 year old PC pastes exposed to NaCl.

Chloride binding in Portland cement pastes is highly dependent on the content of alkalis; the higher content of alkalis the lower amount of bound chloride at any total content of chloride. Contrary to conventional wisdom, the content of alumina was shown to only play a relative minor role in the overall extent of chloride binding, as the major part of chloride is bound by the C-S-H phase.

As alkalis are transported at a much slower rate into concrete than chlorides, low-alkali Portland cements should be used in aggressive environments containing chlorides. Furthermore, owing to the minor effect of alumina on chloride binding, low-alkali low-aluminate Portland cements could arguably be recommended for aggressive marine environments providing maximum protection to both chloride transport and sulfate attack.

The increased chloride binding capacity obtained by reducing the alkali content of the cement also reduces the ratio of chloride to hydroxyl ions in the pore solution (i.e. ratios at 0.50-0.60 are typically given as the chloride threshold value for reinforcement corrosion) as long as the content of alkalis is lower than $Na_2O_{eq} < 0.30$-0.35. This occurs even though the initial pH of the pore solution is of course also lower at these low alkali contents.

The model was introduced into an existing finite element model for the ingress of chlorides into concrete accounting for its multi-component nature, and the composite theory was used for predicting the diffusivity of each ion based on the phase assemblage in the hydrated Portland cement paste. Excellent agreement was found between the chloride ingress and phase assemblage profiles predicted by the model, and those determined experimentally on w/p 0.45 Portland cement pastes exposed to 650 mM NaCl for 70 days.

RESUMÉ (IN DANISH)

Klorider forbindes normalt med de værst tænkelige miljøer for placering af armerede betonkonstruktioner. Disse kan være havvandsmiljø, eller veje og brokonstruktioner udsat for tøsalte i vinterperioderne. Den tid der går indtil kloriderne når ind til armeringen, hvorefter armeringskorrosion kan påbegyndes, anvendes oftest som udtryk for betonkonstruktioners levetid.

Man har i de seneste årtier haft stor fokus på at opnå forståelse for de mekanismer der resulterer i indtrængning af klorider i beton. Det egentlige formål er at bringe sig i stand til at skønne en armeret betonkonstruktions levetid så nøjagtigt som muligt. Eksisterende levetidsmodeller er dog endnu ikke i stand til at kunne forudsige en given betons levetid uden empirisk kalibrering til resultater fra omfattende, tidskrævende forsøg. Anvendeligheden af opnåede resultater er desværre også begrænset til præcis den valgte betonsammensætning. Derfor kan levetidsmodeller heller ikke anvendes til at udvælge den optimale bindersammensætning til et givet eksponeringsmiljø.

Det er alment kendt, at en betydelig andel af de indtrængende klorider fastgøres til mineralerne i cementpastaen under indtrængningsforløbet. Denne proces er normalt benævnt kloridbinding. Derudover er der også generel accept for at hastigheden hvorved kloridioner trænger igennem beton er afhængig af cementpastaens porøsitet. Det overordnede mål i dette projekt er at udvikle en model til kvantificering af disse egenskaber på baggrund af den kemiske sammensætning af cementen.

En termodynamisk model til at forudsige faseselskabet i hærdnet Portland cement er udviklet, med udgangspunkt i fasereglen. Modellen er verificeret på baggrund af forsøg på tre typer Portland cement med forskellig sammensætning (en grå og to hvide cementer). Modellen blev videreudviklet således at reaktioner af klorider og alkalier med hydrater i cementpastaen blev inkluderet. Modellens nøjagtighed til at forudsige kloridbinding i hærdet cementpasta til ethvert indhold af klorid, alkali, karbonat og sulfat, er bevist i rapporten. Modellens forudsigelser er i god overensstemmelse med resultater fra uafhængige forsøg i litteraturen, samt med resultater fra 25 år gamle cementpastaprøver eksponeret til NaCl.

Kloridbinding i Portlandcementpastaer er meget afhængig af cementens indhold af alkalier; jo højere alkaliindhold desto lavere kloridbinding til ethvert totalt indhold af klorider. I modsætning til almen viden, har aluminium en beskeden indflydelse på kloridbinding fordi langt hovedparten af klorider bindes i C-S-H fasen.

Alkalier trænger meget langsomt ind i beton i forhold til klorider, og derfor bør lav-alkali Portland cementer anvendes i kloridholdigt aggressivt eksponeringsmiljø. Givet den lave effekt af aluminiumindholdet på kloridbinding, bør lav-alkali, lav-aluminat Portland cementer anvendes i aggressive miljøer hvor både klorid og sulfat er til stede. Derved sikres sulfatbestandighed.

Selv om den initiale pH-værdi i porevæsken reduceres ved at sænke alkali indholdet, så vil den øgede kloridbindingskapacitet i Portland cementer med $Na_2O_{æqv.}$ lavere end 0.30-0.35 vægt-% også reducere forholdet Cl/OH i porevæsken, der normalt forbindes med tærskelværdien for armeringskorrosion.

Modellen blev introduceret i en eksisterende finit element model for diffusion i multikomponent væske, sammen med en kompositteori model for estimering af effektive diffusionskoefficienter. Modellens skøn på kloridindtrængning viste god overensstemmelse med de målte på v/p 0.45 cementpastaer (tre forskellige cementtyper) efter 70 døgns eksponering i 650 mM Na

FOREWORD

This thesis, revised according to minor suggestions by the Assessment Committee, was written by Erik Pram Nielsen and is the result of a three year project commenced in July 2001, in collaboration between Aalborg Portland A/S, Denmark, and the Department of Civil Engineering at the Technical University of Denmark (DTU). The Ph.D. candidate was employed by the enterprise during the entire project.

Associate Professor Mette R. Geiker, Department of Civil Engineering (DTU), and Scientific Manager Duncan Herfort, Aalborg White Research and Development Centre, supervised the project. The thesis was defended on July 2nd 2004 and Professor Fred Glasser (University of Aberdeen), Chief Engineer Steen Rostam (COWI) and Associate Professor Henrik Stang (DTU) acted as Assessment Committee.

The following publications resulted from the findings during the course of the project, except the last publication which was prepared during the project but based on work undertaken as MSc project. Copies are attached at the end on the thesis.

- Nielsen, E.P., Herfort, D. and Geiker, M.R., The durability of white Portland cement to chloride and sea water attack. NCR – Workshop Proceedings No.3. Nordic Miniseminar – Durability of exposed concrete containing secondary cementitious materials. Hirtshals, November 21-23, 2001.

- Nielsen, E.P., Herfort, D., Geiker, M.R. and Hooton, R.D., Effect of solid solution of AFm phases on chloride binding. Proceedings of the 11th International Congress on the Chemistry of Cement, Durban, South Africa, 11-16 May 2003.

- Nielsen, E.P., Herfort, D. and Geiker, M.R., Phase equilibria in hydrated Portland cement. Submitted for publication in Cement and Concrete Research in June 2003.

- Nielsen, E.P., Herfort, D. and Geiker, M.R., Binding of chloride and alkalis in Portland cement systems. Submitted for publication in Cement and Concrete Research in June 2003.

- Nielsen, E.P., Thrysøe, J., Herfort, D. and Geiker, M.R., Performance of white Portland cement in aggressive environment. Proceedings of the 7th International Conference of Concrete in Hot and Aggressive Environments. Bahrain, 13-15 October 2003.

- Nielsen, E.P., Herfort, D. and Geiker, M.R., Chloride binding in the $CaO\text{-}SiO_2\text{-}Al_2O_3\text{-}SO_3\text{-}Na_2O\text{-}CO_2\text{-}H_2O$ system for Portland cement. Proceedings of the International Symposium on Advances in Concrete through Science and Engineering, March 21-24, Northwestern University, Evanston, Illinois, 2004.

- Nielsen, E.P. and Geiker, M.R., Chloride diffusion in partially saturated cementitious material. Cement and Concrete Research (33), pp. 133-138, 2003.

ACKNOWLEDGEMENTS

CONTENTS

1 Introduction

Durability is one of the most important properties to be considered in the design of reinforced concrete structures exposed to aggressive environments, e.g. sea water and de-icing salts. The service life of a reinforced concrete structure in marine environments can be described by two stages (**Tuutti [1982]**): the initiation and the propagation period. For exposure to sea water or de-icing salts, the initiation period is defined by the time taken from initial exposure to the aggressive environment until a concentration of chloride at the depth of the reinforcement able to initiate corrosion, has been reached. However, even though corrosion of the reinforcement is in progress the structure may still meet the service requirements for several years without high maintenance costs. The largest economic benefit though is probably obtained by prolonging the initiation period through, among others, proper concrete mix selection, smart structural design and proper on-site placement of the concrete. The focus of the present project is placed on the processes resulting in the ingress of chlorides in concrete exposed to aggressive environments, which eventually trigger corrosion of the reinforcement.

The transport of chlorides in concrete is an extremely complex process. Depending on the environment surrounding the concrete structure, the ingress of chloride ions results from a combination of several mechanisms: diffusion, capillary suction, permeation, evaporation, freeze/thaw processes, etc. Even in the same structure, e.g. a bridge pylon, mechanisms differ remarkably. Some parts of the structure are permanently submerged, some are exposed to water tides, and others are subjected to splash. It is therefore normally chosen to simplify prediction models by assuming diffusion to be the acting mechanism, corresponding to ingress of chlorides in submerged concrete. The predictions are thereafter transferred to other environments by empirical correlation.

Even in the simplified diffusion case, several factors affect the rate of ingress of chloride ions: the porosity of the concrete, degree of saturation, presence of cracks (both micro and macrocracks), chloride binding capacity of the concrete (acting as a buffer for the ingress of chlorides), temperature, connectivity of capillary pores, connectivity of ITZ (interfacial transition zones around aggregate particles), reaction of the concrete with other species (e.g. carbonation, sulfate attack), etc.

Many different models for predicting the service life of reinforced concrete structures exist. Most commonly, these are based on predictions from the extrapolation of chloride ingress profiles measured by accelerated testing of a specific concrete (e.g. in **HETEK83 [1997]**). The extrapolation of short term observations of chloride ingress from accelerated testing can be obtained by empirical, physically based or probabilistic approaches, according to **Truc [2000]**. "Empirical" models are mainly based on the error-function solution to Fick's 2. law of diffusion, which is restricted to diffusion in porous media where, among other limitations, no interaction between species in solution and hydrates in the cement paste or between ions in solution occur, and the environmental loading is constant. A so-called apparent diffusion coefficient measured at a certain time of exposure is therefore applied to predict the ingress after e.g. 100 years. Interaction of species with the hydrates of the cement paste, environmental properties, temperature, etc, is accounted for by empirical factorisation. The "physically based" models use finite element modelling techniques, where the transport of chlorides is regarded in multi-component solutions, as is the case for concrete pore solution, to account for interaction between the different species in solution (e.g. **Truc [2000]**) and the hydrates of the cement paste. Sometimes the chemical activity of the ions in solution is included (**Samson et al. [2001]**). Unfortunately, the interaction of species in solution with the hydrates, as well as the porosity available for the transport of ions, can only be included through fitting to experimentally determined ingress profiles on a specific concrete. The "probabilistic" models are extensions of the "empirical" models that account for the many sources of error arising from inhomogeneity

of the concrete, varying environmental load, production defects, etc, by means of statistical treatment of a large amount of data (see e.g. **Lindvall [2001]**).

Common to most, if not all service life prediction models is that they cannot accurately predict the performance of a concrete in e.g. a marine environment without previously carrying out extensive measurements (**Truc [2000]**) to calibrate e.g. chloride binding, chloride concentration at the surface of the concrete, capillary porosity of the concrete, etc. Some authors (e.g. **Palecki and Setzer [2001]**) have even stated that service life prediction of High Performance Concrete is an impossible task and recommend focusing on the development of guidelines and rules for material selection and casting, etc, instead. There is no doubt among concrete experts that the degradation of a reinforced concrete structure is an extremely complex process, where a large number of factors play a significant role. Nevertheless, research in understanding the basic mechanisms of chloride ingress should not be neglected. The more parameters quantifiable by theoretically sound models, the less parameters needing experimental calibration. Some processes may or may not have been oversimplified in the literature, a question which can only be resolved through understanding of the mechanisms involved.

In the State of the Art report **HETEK53 [1996]** on chloride penetration in concrete, several processes were highlighted as significant variables on the service life of reinforced concrete structures that were not thoroughly understood at that time. Several studies have described the physical transport of ions in the multi-component concrete pore solution (e.g. **Truc [2001]** and **Samson et al.[2001]**), as well as attempting to account for varying environmental loading on the structure (e.g. cyclic chloride and environmental loading in e.g. the Mejlbro-Poulsen model in **HETEK83 [1997]** and **Lindvall [2001]**). However, to the best of my knowledge far fewer studies (e.g. in **Bentz [1997]**), have focused on quantifying the microstructure of hydrated Portland cement pastes in order to predict porosity, and on quantifying the reactions between the pore solution and the hydrate phases in the cement paste. This is probably due to the common practise of describing relevant parameters by empirical testing, e.g. describing chloride binding by measurement of the so-called chloride binding isotherms, direct measurement of porosity, etc. But are we measuring realistic values? If chloride binding was dependent on e.g. alkalis, should we not account for transport of these when measuring chloride binding isotherms? Do we use the appropriate measurement techniques for capillary porosity? Many conflicting conclusions are found in the literature which suggests the need for a better understanding of the basic mechanisms. In many cases, hypotheses are derived from empirical observations focusing on the measured value itself, instead of from an understanding of the mechanisms leading to a measured property.

Much development has occurred in the field of durability of concrete with respect to development of accelerated testing procedures, as e.g. the development of chloride migration techniques (e.g. in **Tang [1996]**), which are useful, powerful and easily applicable techniques. However, the immediate question that arises is how reliable are they when we do not yet fully understand the mechanisms during non-steady state diffusion processes resulting e.g. from the chloride binding mechanism?

When designing a new concrete structure for a certain aggressive environment, one could ask the question; which of all the commercially available cement types and supplementary cementitious materials, and mixing proportions, will perform best? Even if the selection is restricted to a certain cement type, e.g. Portland cement, and additional requirements like ASTM Type V for sulfate attack, a large number of possible candidates will still exist. The only way to make a relatively fast selection of the three or four most realistic solutions is to rely on guidelines written by recognised institutions (e.g. *fib*, ACI, RILEM). However, many of these are based solely on interpretations of empirical observations which may not necessarily apply for all cement types, environmental loads, etc.

White Portland cement clinker differs from other Portland cement clinker by having a much lower iron content, which makes it harder to burn. White Portland cement is therefore a specialised product, but is today generally only used for applications where colour is the primary objective. An often overlooked advantage of the much lower iron content in white Portland cement is the improved durability that this can be expected to result in. Since iron forms the high density, low volume FH_3 phase, a lower content of iron should result in a higher relative volume of hydrate phases, and therefore a lower capillary porosity. This, in part, results in higher strengths and lower penetrability. The very low contents of alkalis significantly reduce the risk of alkali-silica reaction with the aggregate. Furthermore, the white Portland cement produced at Aalborg Portland A/S has a very low content of Al_2O_3 and therefore very high sulfate resistance, but its properties with respect to binding of chlorides may be questionable: if most chloride is taken up by aluminium-bearing phases, its binding capacity will be low, but if most is taken up by the C-S-H, it may have high chloride binding capacity. Hence the focus in the present investigation is to predict the phase assemblage in hydrated Portland cements, as well as understanding and quantifying the reactions of chlorides and sulfates with the hydrates in the hydrated Portland cement paste.

It appears that in order for service life prediction models to become more reliable, accurate models for predicting the microstructure of hydrated cement paste are needed. Once the microstructure is properly described, the reactions between the hydrates and different ions in solution should be resolved (e.g. chloride binding and sulfate attack). To develop such a model was the main objective for the present project. It is expected that the implementation of a model that predicts the phase equilibria in hydrated Portland cement pastes at any content of chlorides and sulfates in a Finite Element Model for diffusion in multi-component solutions, where the effective diffusion coefficients are predicted from the actual phase assemblage by use of composite theory, will result in a powerful tool for evaluating the performance of different binder types without prior experimental calibration.

Another very important feature is that once the composition of the pore solution can be predicted as a function of depth, the threshold values for chloride induced reinforcement corrosion can be computed in terms of ratio of chloride to hydroxyl ions in solution (as mentioned in e.g. **Saremi and Mahallati [2002]**), hence relating the chloride ingress model directly to the concept of service life. The proposed model will certainly not become the final solution to service life prediction problems, but will hopefully be a useful tool for understanding and quantifying other factors affecting service life in later studies.

This work is a continuation of work carried out in an earlier Ph.D. project (**Juel [2003]**). The concepts and ideas are further developed for quantification of the phase assemblage in hydrated Portland cement and to understanding and quantifying the reactions of hydrated Portland cement with aggressive ions.

1.1 Objectives of the study

The project is based on the idea that the transport rate of aggressive ions can be predicted from the chemical composition and microstructure of the material. The phase rule can be applied for predicting the stable or metastable phase equilibrium assemblage in hydrated Portland cement paste. The residual or capillary porosity available for transport of ions can be calculated from the relative contents of phases and knowledge of the phase densities. Assuming equilibrium it should therefore be possible to quantify the effect of reactions of aggressive ions such as chlorides, sulfates and alkalis, with the hydrated assemblage, and to predict the composition of the resulting pore solution. By application of existing composite theory (**Fuglsang-Nielsen [2004]**), the effective diffusion coefficients of all species in solution can be predicted from the phase assemblage. Ultimately, this can be introduced in a Finite Element Model for simulating the diffusion of chloride in multi-component solutions, and allow for an accurate prediction of the ingress of chlorides in a cementitious material as a function of time.

Once the composition of the pore solution can be predicted, the threshold values for chloride induced reinforcement corrosion, expressed in terms of the ratio of chloride to hydroxyl ions in solution, can be calculated, and then used for service life prediction.

The objectives of the project were the following:

- To develop a thermodynamically based model for predicting the equilibrium phase assemblage in hydrated Portland cement pastes.

- To describe and quantify the reactions resulting in the binding of chloride ions, as well as the reactions involved in sulfate attack, and to subsequently use this information to accurately predict the phase assemblage in a hydrated Portland cement paste at any content of chloride, alkalis, sulfate and carbonate.

- To develop a service life model constructed as a Finite Element Model, for predicting the diffusion of chlorides in the multi-component solution of cementitious material coupled with the priorly developed thermodynamic model and the composite theory.

It is expected that the model will allow optimization regarding the selection of cement type and, particularly with regard to white Portland cement, which supplementary cementitious materials are best suited to specific exposure environments. The model could be used for service-life prediction and re-evaluation of concrete structures exposed to chloride and sulfate rich environments.

1.2 Outline of the report

Chapter 2 deals with the phase equilibria in hydrated Portland cement. The phase rule is described and an example of its application, together with the application of phase diagrams, is given at the beginning of the chapter. Thereafter, phase equilibria in hydrated Portland cement is discussed starting from the simple system $CaO-SiO_2-H_2O$ to the system where all relevant components for Portland cement in chloride and sulfate containing environments are included. A model for predicting the phase equilibria in hydrated Portland cement at varying contents of sulfates, chloride, alkalis and carbonate is developed through this chapter (see attached CD), and verified against available data from the literature.

The properties of the materials used in this investigation are given in **appendix B**, the experimental procedures are described in **appendix C**, the relevant compositional properties of the phases included are given in **appendix D**, and the results from phase equilibria studies are given in **appendix E**. EDS-analyses are found on the attached CD.

Chapter 3 deals with the phase equilibria in hydrated Portland cement pastes with partial replacement by silica fume and slag. The application of the phase equilibria model in such pastes is discussed.

Chapter 4 deals with the effect of sulfates on chloride binding in Portland cement pastes. The results obtained from the corresponding experiments are found in **appendix F**.

Chapter 5 deals with the phase equilibria in 25 year old Portland cement pastes exposed to NaCl. The phase equilibria model is tested for how well it predicts long term equilibrium assemblages.

Chapter 6 deals with the development of a theoretical service life prediction model where the phase equilibria model is included in the finite element model for diffusion in multi-component solutions, and combined with the composite theory to predict the diffusivity of the cement paste. The codes for this program are found in **appendix G** and the attached CD.

Chapter 7 presents a discussion on the practical implications and applications of the findings in this investigation.

Chapter 8 summarizes the phase diagrams relevant for describing chloride binding in hydrated Portland cement pastes.

Chapter 9 concludes the report and chapter 10 suggests topics for further investigation.

Due to poor quality of mortars prepared for sulphate expansion test, no meaningful results on this subject were obtained and discussion has therefore been excluded from the written thesis.

The planned XRD-analyses were not performed due to technical problems with the equipment.

2   Phase equilibria in hydrated Portland cement

Portland cement clinker mainly consists of the clinker phases C_3S ($3CaO.SiO_2$) and C_2S ($2CaO.SiO_2$) and, to varying extents, C_3A ($3CaO.Al_2O_3$) and C_4AF ($4CaO.Al_2O_3.Fe_2O_3$). Upon grinding of the clinkers, $CaSO_4$ is added to regulate setting of the finished cement. The $CaSO_4$ may be present as a mixture of gypsum, hemihydrate and anhydrite. The chemical composition and the normative Bogue composition of the Portland cements examined in this study are found in **appendix B**, as well as the nomenclature applied for each of them in the text. **Appendix C** describes the experimental procedures and **appendix E** and **F** the results obtained from phase equilibria experiments.

Portland cement is unstable in the presence of water, resulting in a solid matrix of reaction products after hydration. In order to understand the phase equilibria in the hydrated Portland cement system it is appropriate to begin with the more simple system $CaO-SiO_2-H_2O$, and progressively add components until the complex system where all significant components are present, is reached. Equilibrium is a static condition in which no changes occur in the macroscopic properties of a system with time. This implies a balance of all potentials that may cause change. In engineering practice, the assumption of equilibrium is normally justified when it leads to results of satisfactory accuracy (**Putnis and McConnell [1980]**).

The number of independent variables that must be arbitrarily fixed to establish the intensive state of a system, i.e., the degrees of freedom F, is given by the 'phase rule' of J. Willard Gibbs. For non-reacting systems, the phase rule takes the form

$$P + F = C + 2$$

eq. 2.1

where P = number of phases, and C = number of chemical species or components (**Putnis and McConnell [1980]**).

The intensive state of a system at equilibrium is established when its temperature, pressure, and the compositions of all phases are fixed. These are therefore phase rule variables, but they are not all independent. The phase rule gives the number of variables from this set which must be arbitrarily specified to fix all remaining phase-rule variables. The formulation of the rule for systems at constant temperature and pressure is reduced to

$$P + F = C$$

eq. 2.2

and if the composition of all phases in the system are fixed and independent, the term becomes

$$P = C$$

eq. 2.3

A system obeying this relationship is said to be invariant.

As an example of the application of the phase rule, a system containing water and dissolved $CaSO_4$ can be regarded (see **Table 2.a**).

Table 2.a: *Example of the application of the phase rule in a two-component system. Note: applies at constant pressure and temperature*

Case 1: $[Ca^{2+}] \cdot [SO_4^{2-}]$ < solubility product for precipitation of gypsum (i.e. unsaturated solution). Source of Ca^{2+} and SO_4^{2-} is $CaSO_4$.	Case 2: $[Ca^{2+}] \cdot [SO_4^{2-}]$ = solubility product for precipitation of gypsum (i.e. saturated solution). Source of Ca^{2+} and SO_4^{2-} is $CaSO_4$.
$[Ca^{2+}]$ $[SO_4^{2-}]$	$[Ca^{2+}]$ $[SO_4^{2-}]$ $CaSO_4.2H_2O$
There is only 1 phase present (i.e. the solution with a certain chemical composition), and there must be 1 (and only 1) degree of freedom as the concentration of the pore solution can change upon addition/extraction of $CaSO_4$, until the solubility product for gypsum is achieved. Following applies	There are two phases present in the system (i.e. the pore solution and precipitated gypsum), and there are no degrees of freedom because once the solubility of gypsum is exceeded the concentration remains constant, and all additional $CaSO_4$ precipitates as gypsum. Hence
$P + F = C \rightarrow 1 + 1 = C \rightarrow \underline{C = 2}$	$P + F = C \rightarrow 2 + 0 = C \rightarrow \underline{C = 2}$
The components of the system are H_2O and $CaSO_4$. The composition of the solution can be expressed as x wt.% $CaSO_4$ and (1-x) wt.% H_2O.	The components of the system are H_2O and $CaSO_4$. The composition of the solution can be expressed as y wt.% $CaSO_4$ and (1-y) wt.% H_2O, and that of gypsum as 79.1 wt.% $CaSO_4$ and 20.9 wt.% H_2O.
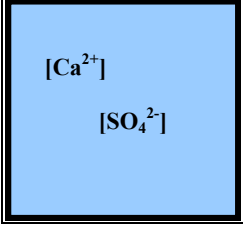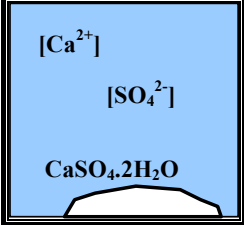
One may have imagined the system in **Table 2.a** composed by three components instead (e.g. H_2O, CaO and SO_3), or even four (e.g. Ca, S, O, H). However, the number of components in a system is defined as the <u>minimum</u> number of chemical species from which the chemical composition of all phases can be described.

Phase diagrams have been applied for many years within fields of study such as geology and high temperature cement chemistry for cement production. However the phase rule and phase diagrams are rarely applied to describe the phase equilibria in Portland cement pastes. In the following, a few examples are given on the application of phase diagrams within metamorphic geology. Figures and text are mainly based on **Mason [1978]**.

A mineral assemblage is a function of temperature, pressure and composition. At a given temperature and pressure conditions of formation, a rock with a certain chemical composition will be composed of a certain mineral assemblage. Minerals usually have constant proportions of oxides and can plot as points in the so-called phase diagrams. Rocks are composed of several components, but a diagram expressing the mineral assemblages within a three-component system represents the typical number of components that are represented in a 2-dimensional plot, i.e. as a triangle where the components are placed at each corner of the diagram. It is therefore common practice to plot the three component system of interest and to note which phases (minerals) are in excess outside the diagram. When a mineral is told to be in excess it simply implies that any phase assemblage observed in the diagram includes that phase.
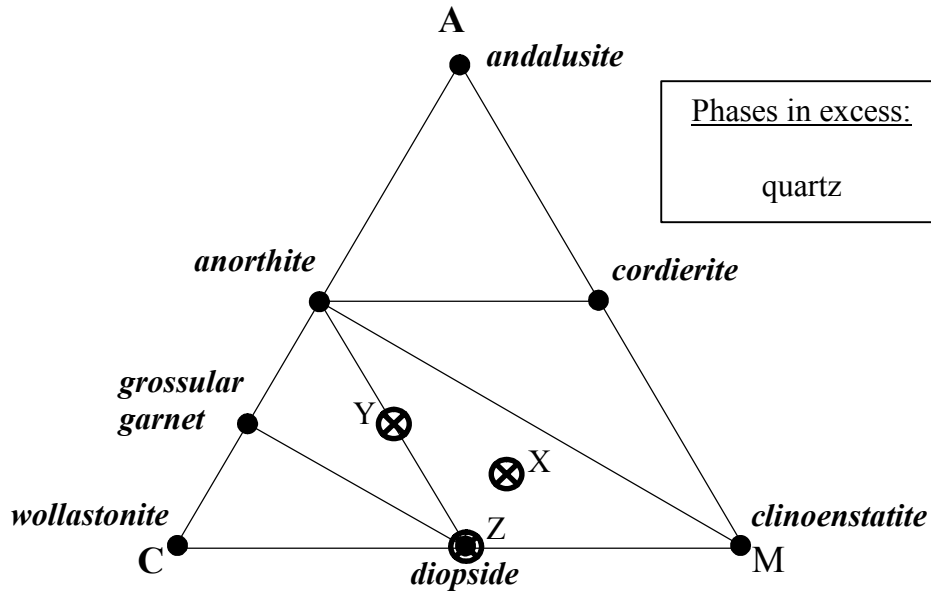
Fig. 2.1: *Example of an ACF (Al$_2$O$_3$-CaO-MgO) phase diagram (adapted from* **Mason [1978]***)*

The phase diagram of a subsystem Al$_2$O$_3$-CaO-MgO with quartz present as an excess phase (plotting outside the sub-ternary diagram) at low pressure and high temperature metamorphic conditions is shown in **Fig. 2.1**. The phase assemblage of a rock with chemical composition corresponding to "X" will be anorthite+diopside+clinoenstatite+quartz. The assemblage in "Y" will be anorthite+diopside+quartz, and in "Z" diopside+quartz. The system has four components (i.e. CaO, Al$_2$O$_3$, MgO and SiO$_2$) and an invariant assemblage at constant temperature and pressure (i.e. no degrees of freedom) consisting of 4 phases, as is the case for "X". "Y" is univariant as there is one degree of freedom (i.e. one phase missing) and "Z" is divariant as the assemblage has two degrees of freedom (i.e. two phases missing). This means that any decrease/increase in the content of one of the components will result in,

- for "X"; a change in the relative contents of the three phases.

- for "Y"; the formation of an extra phase.

- for "Z"; the formation of two extra phases (but only one phase if no Al$_2$O$_3$ is added).

The tie-lines in **Fig. 2.1** cannot be randomly selected, as phase diagrams have to represent phase assemblages that actually do occur for the specific system at a given temperature and pressure. The tie-lines are therefore either predicted from thermodynamic data on the free energies, or drawn by experimental observations.

Some minerals can undergo ionic exchanges of one major element for another in the crystal structure (i.e. solid solution). This is illustrated as a line in a phase diagram, or an area if ionic exchanges of more than one major element occur. **Fig. 2.2** shows an example of this in a subsystem Al$_2$O$_3$-Fe$_2$O$_3$-MgO in equilibrium with quartz and muscovite as excess phases. Chloritoid, garnet and chlorite have limited ranges of substitution of Fe^{2+} for Mg^{2+}. A rock with composition P will have an assemblage of chlorite+chloritoid+garnet +muscovite+quartz, where the composition of chlorite, chloritoid and garnet are those of ct$_p$, cd$_p$ and g$_p$, respectively. This assemblage is invariant. A rock with composition Q will have an assemblage of chlorite+chloritoid+muscovite+quartz, where the composition of chloritoid and chlorite are those of cd$_q$ and ct$_q$. This assemblage on the other hand is univariant as there is one degree of freedom that allows for the change in composition of chloritoid and chlorite upon changing the amount of one component.
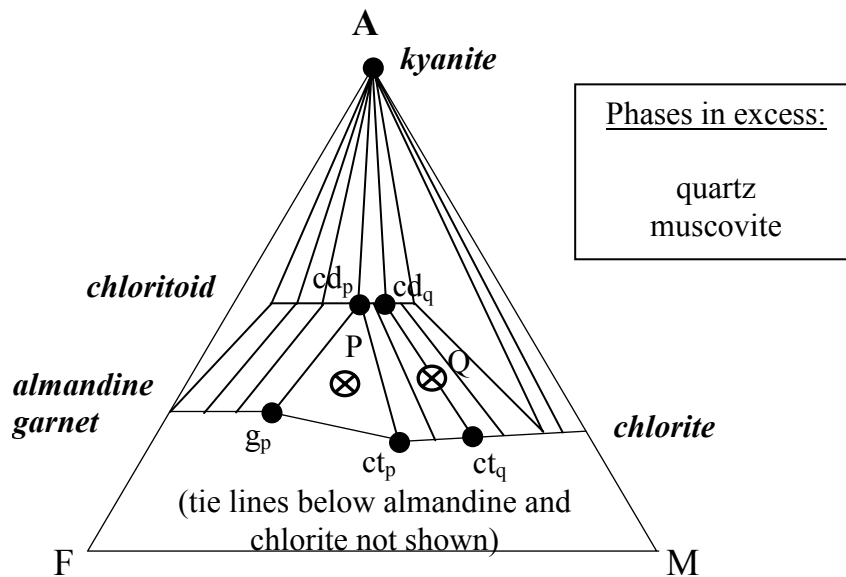
Fig. 2.2: *Example of a Thomson AFM (Al₂O₃-Fe₂O₃-MgO) phase diagram (adapted from* **Mason [1978]***)*

Phase diagrams such as the shown above can be used for quantification purposes as the location of the chemical composition in the diagram indicates the content of each phase relative to the others.

As mentioned earlier, a mineral assemblage is a function of pressure and temperature as well. **Fig. 2.3** shows the stability relationships of andalusite, kyanite, and sillimanite at varying temperature and pressure. All three minerals have the same chemical composition but have different crystal structures. Roughly speaking, kyanite is stable at relative high pressure, whilst sillimanite is stable at relative high temperature.
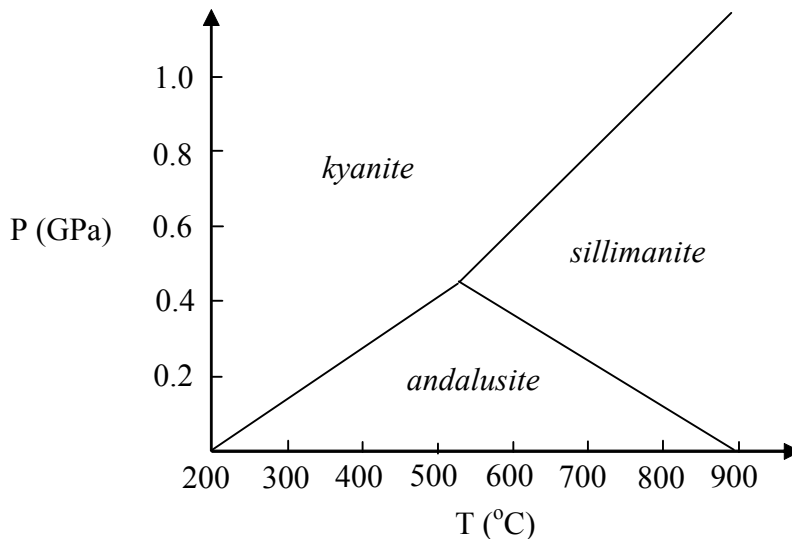
Fig. 2.3: *Stability relations of andalusite, kyanite and sillimanite in the Al₂SiO₅ (adapted from* **Mason [1978]***)*

Fig. 2.4 shows the univariant curves for the breakdown of muscovite. In assemblages saturated with SiO_2, muscovite will react to form K-feldspar (in this example sanidine) and andalusite upon heating corresponding to the left-hand curve in **Fig. 2.4**. If the assemblage is under-saturated with SiO_2, a higher temperature is needed to breakdown muscovite, and furthermore, it

will form K-feldspar and corundum instead. The breakdown occurs at temperatures corresponding to the right-hand curve in **Fig. 2.4**.
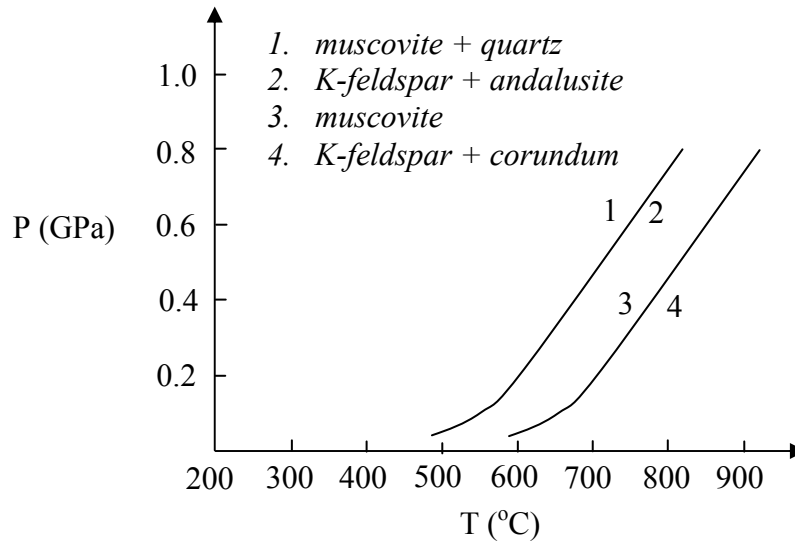
Fig. 2.4: *Univariant curves for the breakdown of muscovite (adapted from* **Mason [1978]***)*

Figs. 2.3 and **2.4** can be superimposed to construct a diagram linking the stability ranges of mineral assemblages with several members from which the mode of formation of rocks can be discussed. This is shown in **Fig. 2.5**.
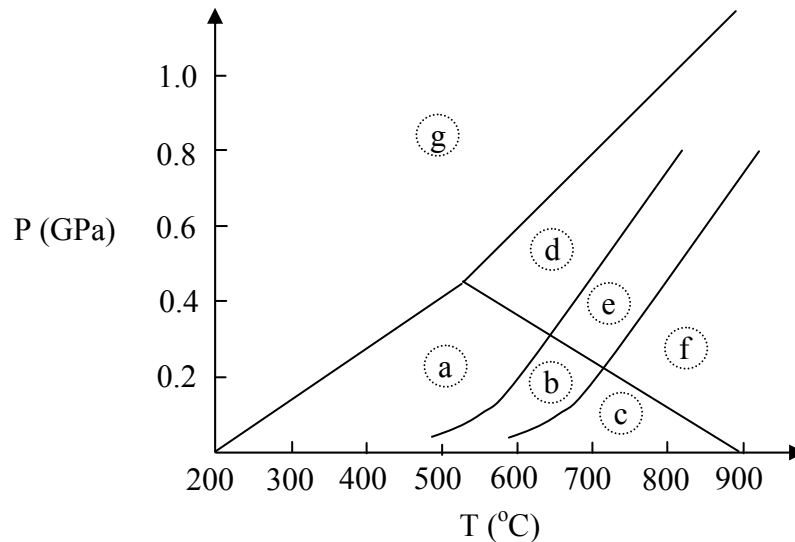
Fig. 2.5: *Superimposition of* **Figs. 2.3** *and* **2.4** *(adapted from* **Mason [1978]***)*

Fig. 2.6 shows the phase diagrams applicable for each of the numbered fields in **Fig. 2.5**.
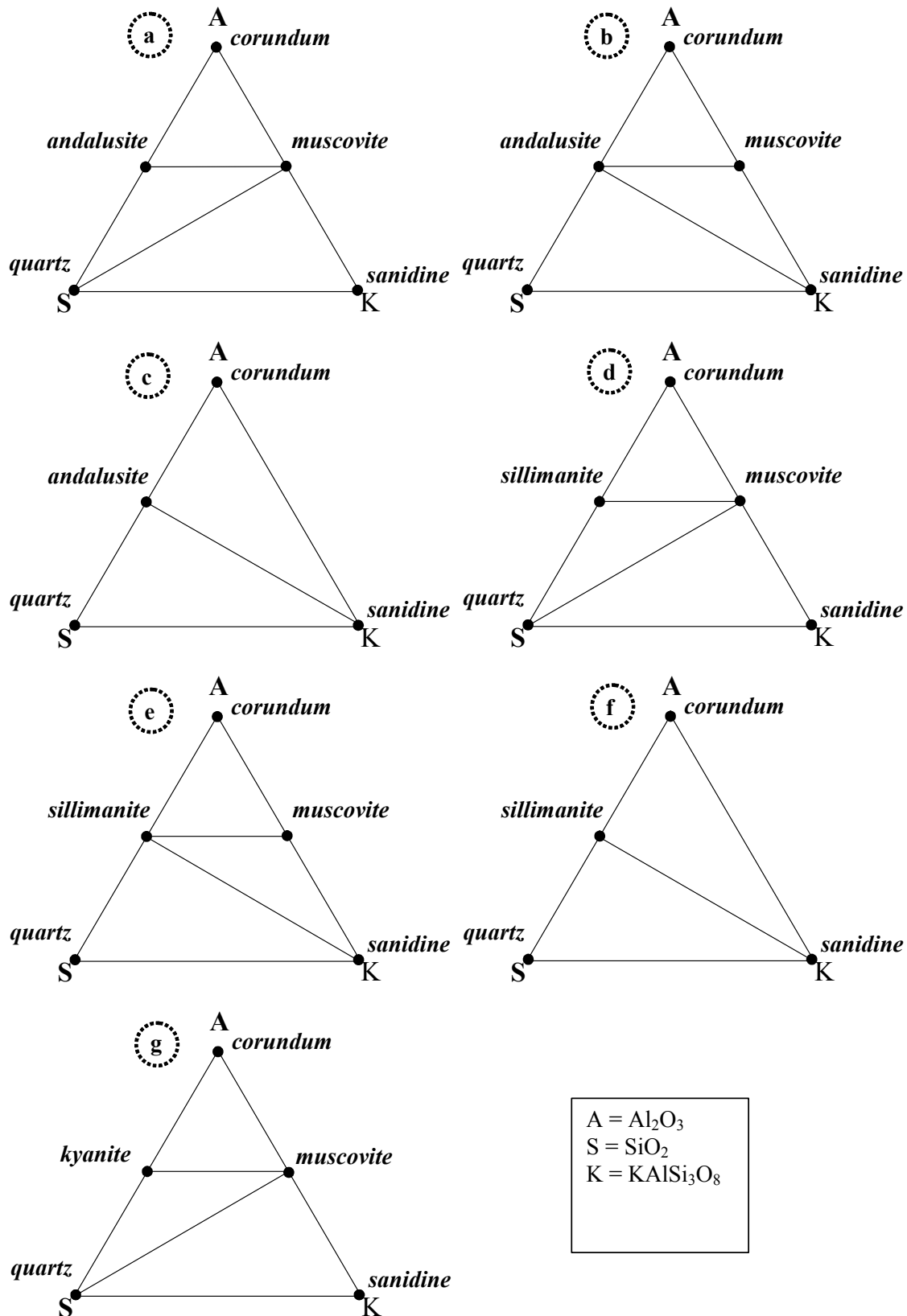
Fig. 2.6: *Phase diagrams showing mineral assemblages stable within the numbered temperature-pressure fields of* **Fig. 2.5** *(adapted from* **Mason [1978]***)*

Combining the phase diagrams shown in **Fig. 2.6** and the univariant curves for the stability ranges of the mineral assemblages in **Fig. 2.5**, the pressure and temperatures of formation of rocks can be predicted. It must be noted that high pressures and temperatures as the shown in the figures above are only observed at large depths from the earth's surface. However, the kinetics of

recrystallisation of metamorphic rocks is extremely slow and it may take several millions of years (**Mason [1978]**). Furthermore, the solid-solid reactions become so slow upon cooling to near surface temperatures that the assemblages can be regarded as metastable.

The above are just a few examples of how these types of condensed or "sub-"phase diagrams are used in metamorphic geology. The author hopes that the reader has been given the impression of how phase diagrams are used extensively in other fields and assuming equilibrium condition to prevail (albeit locally) should be equally applicable to chemically altered concrete.

In Portland cements, it is in most cases convenient to express the system in terms of the oxide components of interest, i.e. SiO_2 (S), CaO (C), Al_2O_3 (A), SO_3 ($\bar{S}$), Fe_2O_3 (F), CO_2 ($\bar{C}$), Na_2O and K_2O. The letters in parenthesis indicate the chosen abbreviation in the present study. In the presence of water, the component H_2O (H) is added to the list. <u>This thesis deals with the phase equilibria of hydrated Portland cements at around $20^{o}C$.</u>

2.1 CaO-SiO$_2$-H$_2$O

Fig. 2.7 illustrates the phase diagram for the three-component system CaO-SiO$_2$-H$_2$O (from **Taylor [1997]**). CaO and SiO_2 results from the dissolution of the clinker phases C_2S and C_3S (although only C_3S is included in the figure) and, depending on the overall concentration of each species in solution, precipitate according to the diagram.

A fully hydrated Portland cement paste is composed of a poorly crystalline calcium silicate hydrate phase ($C_{1.75}SH_4$, see **Paper III (appendix A)** for its properties such as density and evaporable water content), calcium hydroxide (CH) and the pore solution, corresponding to the lower lightly shaded region in **Fig. 2.7**. This particular region, consisting of three phases, is invariant according to the 'phase rule' (i.e. F=0). The composition of each of these phases must therefore be constant upon any addition or removal of CaO or SiO_2, as long as the overall composition lies within that particular field.

The Ca/Si ratio of the C-S-H at 1.75 is in good agreement with the observations in **Taylor [1997]**, **Richardson [2000]** and **Famy et al. [2002]**. The C-S-H is divided by some authors (e.g. **Richardson [2000]** and **Famy et al. [2003]**) in two types of reaction products, i.e. outer and inner. The difference observed in chemical composition between inner and outer product C-S-H in **Richardson [2000]** is chosen by the present author to be related to non-equilibrium conditions, as the cement pastes studied in that investigation contained 50% slag, which was enough to exhaust the $Ca(OH)_2$ (clearly observed by the EPMA analyses in that publication) implying most likely a decalcification of the C-S-H that undoubtly changes the Ca/Si ratio of the C-S-H. The observations in **Famy et al. [2003]** show a much closer chemical composition between the inner and outer reaction products of the C-S-H, supporting the assumption in this study that only one C-S-H phase exists with a certain chemical composition. Any deviations from that is the result of non-equilibrium conditions. Further properties of the C-S-H are discussed in **section 2.2**.

If the relative content of SiO_2 increases significantly, which would be the case of Portland cement pastes with large contents of silica fume, CH may become exhausted, resulting in the presence of only two phases in the subsystem (i.e. a C-S-H phase with Ca/Si molar ratio between 0.80 and 1.75, and the pore solution). Furthermore one degree of freedom will exist, which allows for the change in the Ca/Si ratio of the C-S-H as a function of the relative contents of SiO_2 and CaO. The lower limit for the Ca/Si molar ratio in the C-S-H appears to be approx. 0.80 (**Taylor [1997]**), which is why any further addition of SiO_2 beyond that point would result in the formation of a silicate hydrate phase (SH_x). The system would again be invariant as the number of components equals the number of phases (upper lightly shaded region in **Fig. 2.7**).
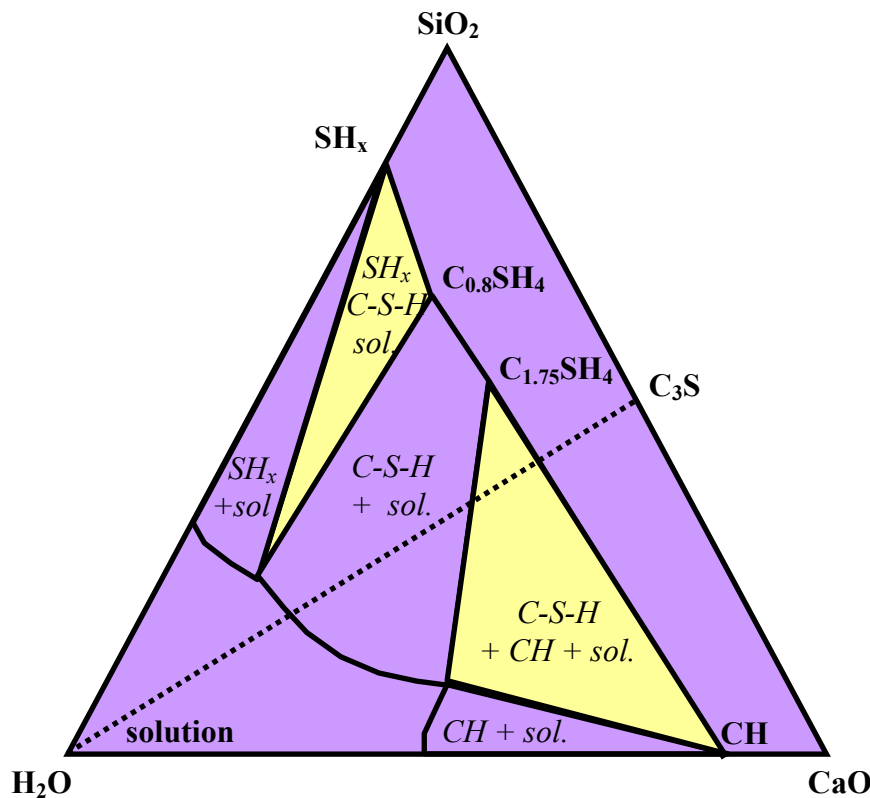
Fig. 2.7: *Phase diagram for the system CaO-SiO$_2$-H$_2$O from* **Taylor[1997]***, with own adjustments. The lightly shaded regions indicate invariant assemblages*

2.2   CaO-Al$_2$O$_3$-SO$_3$-SiO$_2$-H$_2$O

The contents of Al$_2$O$_3$ and SO$_3$ in Portland cements are low compared to CaO and SiO$_2$. Although substantial CaO combines with Al$_2$O$_3$ and SO$_3$ the phase relationships above remain essentially the same. In hydrated Portland cement pastes, this would only result in a change in the relative amount of CH to C-S-H.

It should be noted that a significant amount of the Al$_2$O$_3$ and SO$_3$ is incorporated in the C-S-H phase (see **Paper III (appendix A)**) in fully hydrated Portland cement systems. **Fig. 2.8** shows single spot EDS-analyses on 7 different WPC(12) samples plotted as S/Ca and Al/Ca vs. Si/Ca (molar ratios). The accuracy of the EDS measurements is discussed in **appendix C**. The phases of interest for the following are the shown in the figures (the location of each phase in the figures can be calculated from the composition of each mineral). The stable phase assemblage in these pastes is expected to consist mainly of C-S-H, CH and monocarbonate, and to a minor extent of ettringite and calcite (for more information on how this is predicted see **section 2.5**). The two trace lines in the upper figure of **Fig. 2.8** connect C-S-H with monocarbonate; and C-S-H with CH/calcite. The two trace lines in the lower figure connect C-S-H with ettringite; and C-S-H with CH/monocarbonate/calcite. All plots located away from the endmember composition of the minerals are a mixture of two or more phases.

In order to provide an estimate of the S/Ca, Al/Ca and Si/Ca ratio of the C-S-H, these parameters can be iteratively changed until the best fit of the trace lines to the actual measured plots is obtained, evaluated from R^2-values for the S/Ca, Al/Ca and Si/Ca ratios. For Si/Ca lower than the predicted for the C-S-H, the distance of each measured plot of Al/Ca or S/Ca ratio to the nearest trace line in vertical direction is evaluated. At Si/Ca higher than the predicted for the composition of the C-S-H, the measured Al/Ca and S/Ca ratios are evaluated against the predicted Al/Ca and S/Ca in the C-S-H. The R^2-value for Si/Ca is obtained through evaluation of the horizontal distance of each measured plot to the trace lines in the upper figure in **Fig. 2.8**.
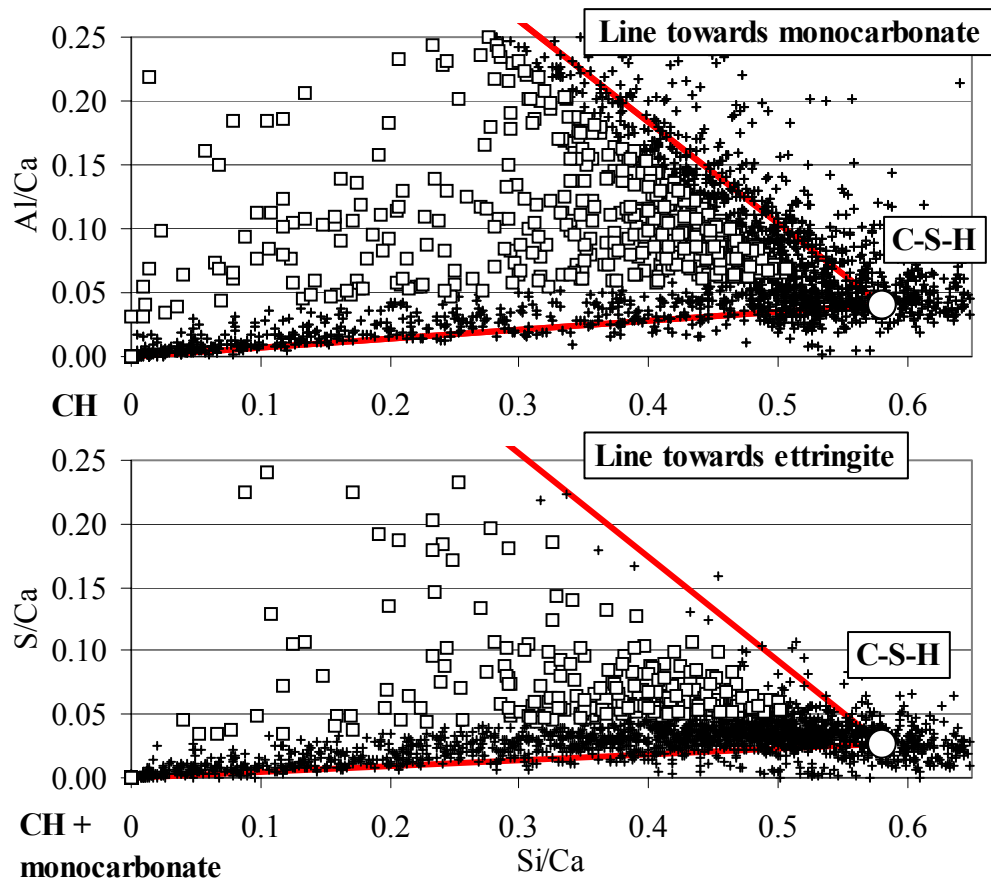
Fig. 2.8: *Selected single spot EDS-analyses on 7 different 6-months old WPC(12) pastes (approx. 300 points for each paste) at w/p 0.70 to predict the S/Ca, Al/Ca and Si/Ca in the C-S-H. 1.0 mass% of cement was replaced by CaCO₃*

All plots left from the Si/Ca corresponding to that of the C-S-H, and comprehended between the two trace lines, represent a mixture of three or more phases. To ease the fitting of the measured plots to the trace lines, all points located within the region obtained when displacing vertically the trace lines (-0.03 displacement for the upper trace lines, while +0.03 for the lower) are omitted. Excluded points are marked with squares.

The best fit was obtained for the C-S-H having a composition of S/Ca = 0.026 (R^2 = 0.68), Al/Ca = 0.040 (R^2 = 0.91) and Si/Ca = 0.58 (R^2 = 0.67). The corresponding best fit for the results on the WPC(4) pastes was obtained for C-S-H having a composition of S/Ca = 0.029 (R^2 = 0.50), Al/Ca = 0.039 (R^2 = 0.80) and Si/Ca = 0.56 (R^2 = 0.74). Best fit is to be understood as the composition resulting in maximum values for the three R^2-values. The calculations from which these results were obtained can be found on the spreadsheets in the attached CD (CSH_WPC(12) and CSH_WPC(4), respectively). The content of the C-S-H with respect to Al_2O_3 and SO_3 are chosen to S/Ca = 0.03 and Al/Ca = 0.04, which also are in accordance with the measured in **Famy et al. [2002]**. Furthermore, the earlier chosen Ca/Si molar ratio of the C-S-H becomes verified by these results, as a Ca/Si ratio at 1.75 corresponds to Si/Ca at ~ 0.57.

Many investigations are found in the literature where synthetic systems are studied for understanding hydration and reactions in Portland cements. However, it must be noted that results obtained from analyses on artificially generated C-S-H (as in e.g. **Hong and Glasser [1999]**), although they do provide very important information, cannot directly be applied to a Portland cement as e.g. Al_2O_3, SO_3 and Fe_2O_3 (shown later in the report) are included in the structure of C-S-H in Portland cement pastes. The observations of **Kuzel and Pöllmann [1991]** during hydration of C_3A in presence of $Ca(OH)_2$ and gypsum may also differ from that in Portland cement pastes.

As mentioned earlier, a mineral assemblage at constant temperature and pressure is a function of the total chemical composition of the system, and this should be remembered when carrying out investigations in more simple subsystems.

Fig. 2.9 illustrates the aqueous phase diagram for the system CaO-Al_2O_3-SO_3-SiO_2-H_2O. Coloured areas indicate possible stable assemblages in Portland cement pastes. The aqueous phase diagram is an adaption of the findings by **Damidot and Glasser [1993]**, and the invariant points in the diagram do not necessarily correspond to the scale given in the axes.

According to **Fig. 2.9**, the phase assemblage in a system with pore solution composition shown as "c" (i.e. a system with high contents of Al_2O_3 relative to SO_3) will consist of $C_{1.75}SH_4$, CH, monosulfate ($C_3A.C\overline{S}.H_{12}$) and a hydroxy-AFm phase. Any minor addition/removal of one of the components will only result in a change in the relative amount of the phases, but not in the composition of these (not even the pore solution). However, if a significant amount of SO_3 is added to the system, all the hydroxy-AFm phase is converted to monosulfate and, after exhaustion of the hydroxy-AFm phase, the composition of the pore solution will change to that of "b". Thereafter, ettringite ($C_3A.3C\overline{S}.H_{32}$) can begin to form at the expense of monosulfate upon further addition of SO_3. At high contents of SO_3 relative to Al_2O_3, all monosulfate is converted to ettringite, and then the composition of the pore solution can change to that of "a". Thereafter, gypsum is formed upon further addition of SO_3. Each of these assemblages is invariant and, therefore, the composition of the phases within each assemblage remains constant as well.
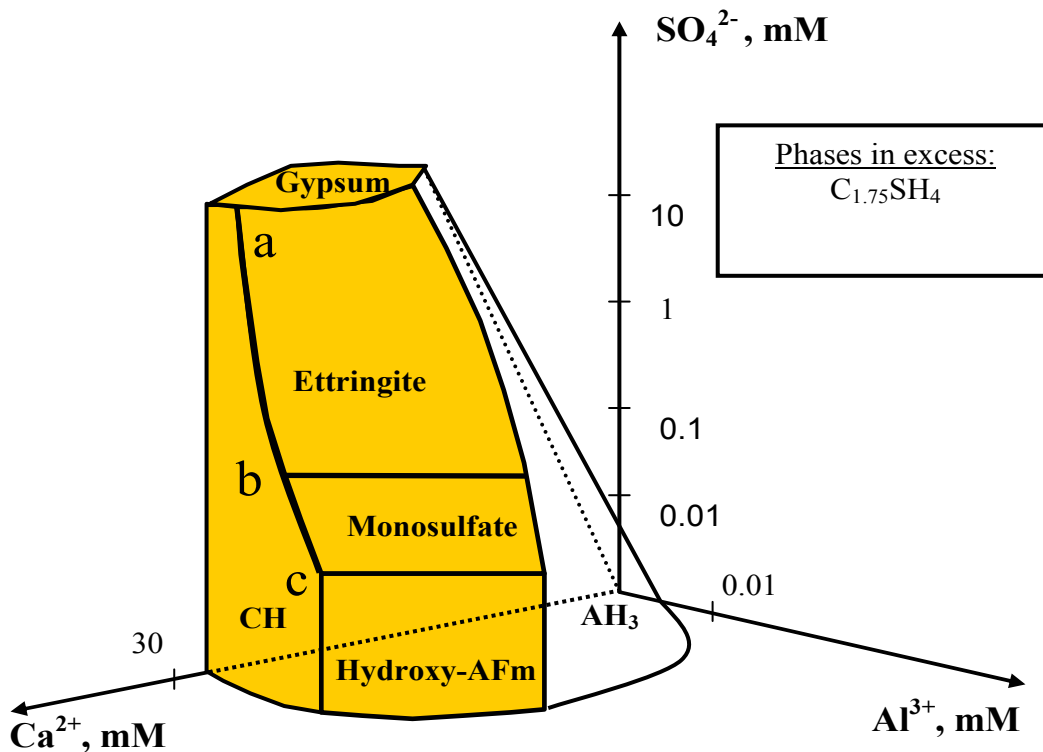
Fig. 2.9: *Aqueous phase diagram for the system CaO-Al_2O_3-SO_3-SiO_2-H_2O, for the case where $C_{1.75}SH_4$ is stable. <u>Adapted</u> from* **Damidot and Glasser [1993]***; Invariant points a, b and c do not necessarily correspond to the scale given in the axes*

At ages less than one year or so the composition of the hydroxy-AFm phase is most likely to be C_4AH_{13} (e.g. in **Taylor [1997]**) or C_4AH_{18} (e.g. in **Kuzel and Pöllmann [1991]**), but in older pastes the more stable phase hydrogarnet, C_3AH_6, is likely to occur instead (**Taylor [1997]** and **Damidot and Glasser [1995]**).

The main source of Al_2O_3 is the clinker mineral C_3A, and the source of SO_3 is mainly from the addition of $CaSO_4$ (as either gypsum, hemihydrate or anhydrite) during grinding of the clinkers. These minerals, as well as C_3S and C_2S, react relatively fast (**Taylor [1997]**), which is why after relatively short hydration times (after a few months of hydration) the phase assemblage of the hydrated part of the cement can be assumed to be metastable.

2.3 $CaO-Al_2O_3-SO_3-Fe_2O_3-SiO_2-H_2O$

Conventional Portland cements (i.e. grey cements) contain significant amounts of Fe_2O_3 in contrast to white Portland cements.

Fe_2O_3 is mainly present in the clinker mineral C_4AF. The main advantage of a relatively high content of Fe_2O_3 is its lowering of the melting temperature in the kiln, thereby reducing the cost of production (**Taylor [1997]**). However, C_4AF has a very slow rate of hydration, resulting in slower contribution to strength and, when it has reacted, to lower ultimate strengths due to the formation of high density hydration products.

As mentioned in **Taylor [1997]**, several investigators have noted that the Fe/Ca molar ratio in the product of iron containing phases tends to be higher than that of the starting material and have concluded that an iron (III) oxide or hydroxide is formed. **Teoreanu et al. [1979]** concluded that the hydration at ordinary temperature included FH_3 (goethite), which also is in accordance with the findings by **Fukuhara et al. [1981]**. According to **Taylor and Newbury [1984]** the tendency to form iron oxide or hydroxide may be connected with the fact that Al^{3+} can migrate easily through the paste, whilst Fe^{3+}, due to its lower solubility, cannot and is thus largely confined to the space originally occupied by the anhydrous material from which they came.

From my own findings in **Paper III** and **Paper IV (appendix A)**, Fe_2O_3 is likely to form FH_3 on hydration, but Fe_2O_3 appears to be incorporated to some extent in the C-S-H structure corresponding to a Fe/Ca molar ratio of approx. 0.02 and agrees with the findings in **section 2.5** and **2.6** where the presence of iron introduces an extra degree of freedom to the system. This could also explain the much higher contents of Al_2O_3 and SO_3 in the C-S-H of grey Portland cement pastes (by carrying out same procedure as done for the data in **Fig. 2.8** but on OPC pastes). The best fit to the EDS-plots was obtained for a composition of the C-S-H at S/Ca = 0.048 (R^2 = 0.78), Al/Ca = 0.057 (R^2 = 0.97) and Si/Ca = 0.58 (R^2 = 0.75). The incorporation of iron has no apparent effect on the Si/Ca of the C-S-H.

The calculations can be assessed in the spreadsheet CSH_OPC in the attached CD.

2.4 $CaO-Al_2O_3-SO_3-Fe_2O_3-CO_2-SiO_2-H_2O$

Kuzel and Pöllmann [1991] studied the system $CaO-Al_2O_3-CaSO_4-CaCO_3-H_2O$. In relatively young systems (hydrated for less than a month), the phases identified were hemicarbonate ($C_3A.\frac{1}{2}C\overline{C}.\frac{1}{2}CH.H_{11.5}$), monocarbonate ($C_3A.C\overline{C}.H_{12}$), monosulfate, ettringite, and calcium hydroxide. At increasing contents of $CaCO_3$ the amount of monocarbonate was found to increase compared to that of hemicarbonate, and the content of monosulfate was reduced. The system cannot be in equilibrium because the phase rule is not satisfied (i.e. there is one phase too many, as the solution itself is a phase of the assemblage). **Damidot and Glasser [1995]** concluded that hemicarbonate is only stable at low concentrations of carbonate and sulfate, and high concentrations of calcium, whilst monocarbonate is stable over a wider range of concentrations, and further suggested that monocarbonate forms preferentially in systems were alkalis are present. The reason for this was attributed to the common ion effect, which reduces the concentration of calcium, while increasing the concentration of sulfate, aluminate and carbonate.
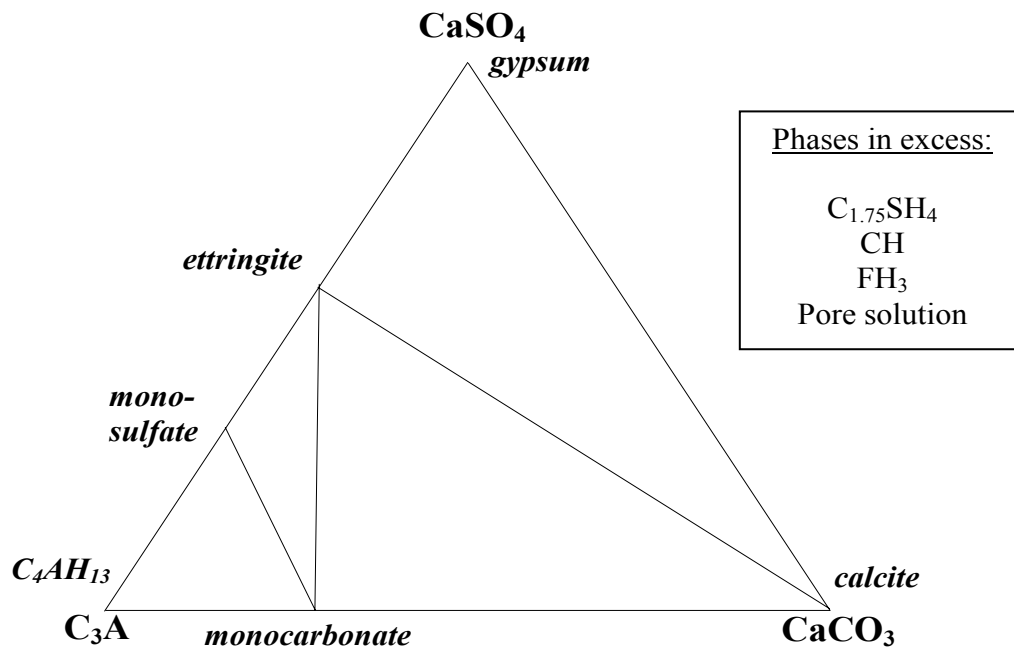
Fig. 2.10: Ternary subsystem C_3A-$CaSO_4$-$CaCO_3$, in Portland cement systems. *C_3A does not refer to the normative content C_3A in the clinker, but to the total Al_2O_3. (Note: this figure is revised in **chapter 4***)

The ternary subsystem C_3A-$CaSO_4$-$CaCO_3$ shown in **Fig. 2.10** is expected to be applicable for Portland cement pastes. For convenience, $CaCO_3$, $CaSO_4$, and C_3A are chosen as components rather than CO_2, SO_3 and Al_2O_3. This is valid as long as these components occur as stoichiometric units in all hydrate phases in the system. In order to avoid misinterpretation, it is noted that the component C_3A in **Fig. 2.10** does not refer to the normative content C_3A in the clinker, but to the total amount of Al_2O_3 in the system (i.e. including the Al_2O_3 present in the C_4AF and silicates).

The verification of the phase assemblage in hydrated Portland cement pastes with the components mentioned previously is presented in **Paper III (appendix A)** and **Juel [2003]**.

2.5   Model for the phase equilibria in hydrated Portland cement

In a fully hydrated Portland cement, which as a first approximation is invariant at constant temperature and pressure, the relative contents of phases of known composition present can be calculated by solving 'n' equations for 'n' unknowns, where 'n' is the number of components and phases. Since the system is invariant, the composition of each of the phases must remain constant. Relevant physical properties of the phases described earlier in this report can be found in the literature (e.g. **Taylor [1997]** and **Lea [1970]**). The properties selected for this investigation are the given in **appendix D**.

A fully hydrated Portland cement paste has typically seven major components (i.e. SiO_2, Al_2O_3, CaO, Fe_2O_3, SO_3, CO_2, H_2O). The systems described in **sections 2.1** to **2.4** are therefore relevant to the following. According to the phase rule, a maximum of seven phases (six hydrate phases and the pore solution) can be formed at constant temperature and pressure. From the aqueous phase diagram in **Fig. 2.9** it is deduced that, as $Ca(OH)_2$ is always present in hydrated Portland cements, four assemblages are possible (given in **Table 2.b**).

Table 2.b: *Possible assemblages in hydrated Portland cement.*

1.	C_4AH_{13}, monosulfate, monocarbonate, …	
2.	monosulfate, ettringite, monocarbonate, …	$C_{1.75}SH_4$, FH_3, CH, Pore solution
3.	Ettringite, monocarbonate, calcite, ...	
4.	Ettringite, calcite, gypsum, ...	

A Portland cement paste consisting of 99 g. WPC(4), 1 g. calcite and 70 g. H_2O (corresponding to w/p = 0.70), will have the chemical composition in **Table 2.c**.

Table 2.c: *Components in a w/p 0.70 paste of 99 g. WPC(4), 1 g. calcite and 70 g. H_2O*

SiO_2	Al_2O_3	Fe_2O_3	CaO	SO_3	CO_2	H_2O
24.62	1.86	0.33	68.70	2.18	0.56	70.00

For each of the possible four assemblages, the following system of equations can be solved (**Juel [2003]**),

$$\begin{bmatrix} W_{C1}^{P1} & W_{C1}^{P2} & W_{C1}^{P3} & W_{C1}^{P4} & W_{C1}^{P5} & W_{C1}^{P6} & W_{C1}^{P7} \\ W_{C2}^{P1} & W_{C2}^{P2} & W_{C2}^{P3} & W_{C2}^{P4} & W_{C2}^{P5} & W_{C2}^{P6} & W_{C2}^{P7} \\ W_{C3}^{P1} & W_{C3}^{P2} & W_{C3}^{P3} & W_{C3}^{P4} & W_{C3}^{P5} & W_{C3}^{P6} & W_{C3}^{P7} \\ W_{C4}^{P1} & W_{C4}^{P2} & W_{C4}^{P3} & W_{C4}^{P4} & W_{C4}^{P5} & W_{C4}^{P6} & W_{C4}^{P7} \\ W_{C5}^{P1} & W_{C5}^{P2} & W_{C5}^{P3} & W_{C5}^{P4} & W_{C5}^{P5} & W_{C5}^{P6} & W_{C5}^{P7} \\ W_{C6}^{P1} & W_{C6}^{P2} & W_{C6}^{P3} & W_{C6}^{P4} & W_{C6}^{P5} & W_{C6}^{P6} & W_{C6}^{P7} \\ W_{C7}^{P1} & W_{C7}^{P2} & W_{C7}^{P3} & W_{C7}^{P4} & W_{C7}^{P5} & W_{C7}^{P6} & W_{C7}^{P7} \end{bmatrix} \begin{bmatrix} P_{1,total} \\ P_{2,total} \\ P_{3,total} \\ P_{4,total} \\ P_{5,total} \\ P_{6,total} \\ P_{7,total} \end{bmatrix} = \begin{bmatrix} C_{1,total} \\ C_{2,total} \\ C_{3,total} \\ C_{4,total} \\ C_{5,total} \\ C_{6,total} \\ C_{7,total} \end{bmatrix}$$

eq. 2.4

where $P_{m,total}$ is the total content of phase "m" in the system, W_{Cj}^{Pm} is the weight percentage of the component "j" in phase "m", and $C_{j,total}$ is the total content of the component "j". For the components listed in **Table 2.c** the results from such calculations are the presented in **Table 2.d**.

Table 2.d: *Calculated four possible phase assemblages for a hydrated w/p 0.70 paste of 99 g. WPC(4), 1 g. calcite and 70 g. H_2O. Units in gram.*

Assemblage 1		Assemblage 2		Assemblage 3		Assemblage 4	
$C_{1.75}SH_4$	98.5	$C_{1.75}SH_4$	98.5	**$C_{1.75}SH_4$**	**98.5**	$C_{1.75}SH_4$	98.5
CH	36.9	CH	35.8	**CH**	**35.8**	CH	35.8
FH_3	0.4	FH_3	0.4	**FH_3**	**0.4**	FH_3	0.4
Pore solution	30.6	Pore solution	28.0	**Pore solution**	**29.7**	Pore solution	29.2
C_4AH_{13}	-8.2	Ettringite	9.2	**Ettringite**	**2.4**	Ettringite	4.9
Monosulfate	3.6	Monosulfate	-10.0	**Calcite**	**1.1**	Calcite	1.3
Monocarb.	7.2	Monocarb.	7.2	**Monocarb.**	**1.2**	Gypsum	-1.0

Assemblage 3 in **Table 2.d** is the only possible assemblage to form due to the negative values appearing in the other assemblages.

When neglecting the bulk shrinkage of the paste, the hydrated assemblage is expected to occupy the same volume as that of the anhydrous cement, calcite and water, i.e. 99/3.15 + 1/2.72 + 70/1 = 101.8 cm³. The assemblage calculated in **Table 2.d** (i.e. assemblage 3) only occupies 95.3 cm³ when applying the densities given in **appendix D**. This discrepancy is due to the chemical shrinkage of the paste, and according to the calculations, the amount of imbibed water during

hydration in an open system is $101.8 - 95.3 = 6.5$ cm^3. The volume fraction of each phase in the assemblage is given in **Table 2.e**.

Table 2.e: *Volume fraction of phases in a saturated (i.e. open system), hydrated w/p 0.70 paste of 99 g. WPC(4), 1 g. calcite and 70 g. H$_2$O*

C$_{1.75}$SH$_4$	45.6 %	Physical properties relevant for the calculations:
CH	15.5 %	
FH$_3$	0.1 %	
Pore solution	36.5 %	Capillary porosity, 36.0 vol.-% or
Ettringite	1.3 %	20.5 mass-% capillary water
Calcite	0.4 %	Evaporable water content, 31.1 mass-%
Monocarbonate	0.6 %	

See **Paper III (appendix A)** for further details of the calculation of evaporable water content (i.e. water release upon drying at 105°C), as well as loss of ignition when conditioning at 1000°C.

It should be remembered that the phase rule as described earlier, applies only for metastable or stable assemblages. That is, where reactions have gone to completion or where the rate of reaction is so slow that the assumption of metastability becomes justified. For hydrated Portland cement pastes in this study it is reasonable to assume that equilibrium conditions apply after two or three months of hydration, because reaction of the unhydrated clinker proceeds very slowly at this stage (e.g. **Taylor [1997]**). The validity of this assumption is, however, dependent on the composition, reactivity and fineness of the cement, including supplementary materials, the water-to-cement ratio, etc. If the degree of hydration of each of the clinker phases is known or can be reasonably predicted, the calculations described earlier can be performed based on the amount of components that have reacted so far. An example of that is given in **Paper III (appendix A)**.

By further development of this model, processes as sulfate attack, chloride binding, carbonation, etc. can be simulated, and their consequences become easier to understand.

2.6   CaO-Al$_2$O$_3$-SO$_3$-Fe$_2$O$_3$-CO$_2$-CaCl$_2$-SiO$_2$-H$_2$O

The system CaO-Al$_2$O$_3$-SO$_3$-Fe$_2$O$_3$-CO$_2$-CaCl$_2$-SiO$_2$-H$_2$O is described thoroughly in **Paper II (appendix A)** and the main findings are summarized in this section.

The presence of Cl is described by the component CaCl$_2$ as it is incorporated stoichiometrically in the chloride containing AFm phase in Portland cement systems, i.e. Friedel's salt, C$_3$A.CaCl$_2$.10H$_2$O (**Taylor [1997]**). The system has 8 components and can therefore only form a maximum of 8 phases at constant temperature and pressure. If invariant conditions apply, the ternary subsystem in **Fig. 2.11** is expected to apply. Once again the subsystem is expressed by the components C$_3$A, CaSO$_4$ and CaCl$_2$ as they are included stoichiometrically in all of the hydrates of the system.
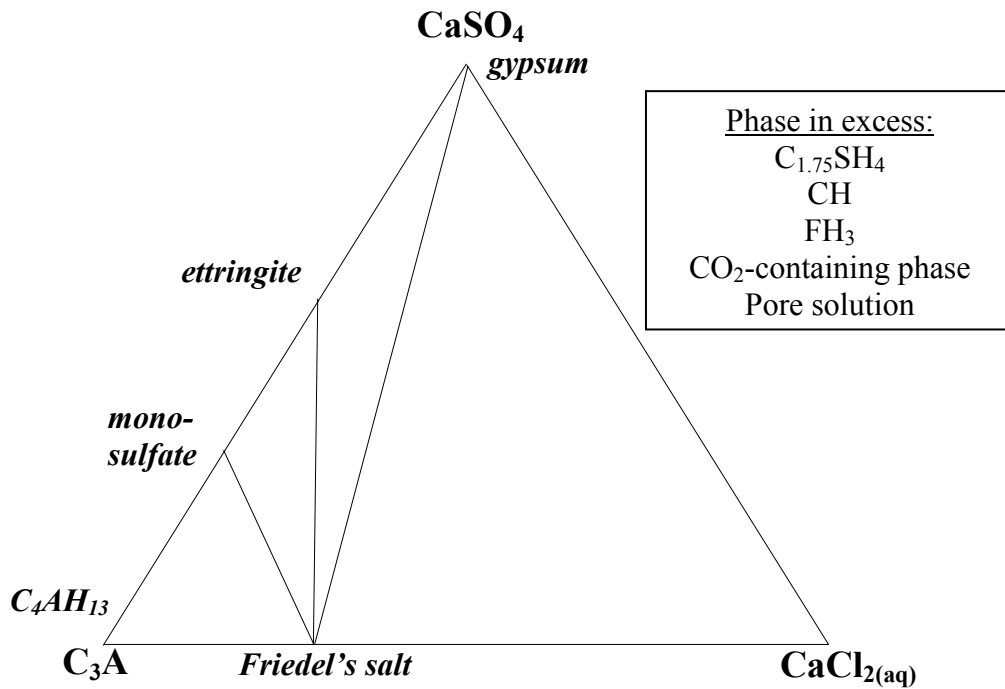
Fig. 2.11: *Ternary subsystem C_3A-$CaSO_4$-$CaCl_2$ in Portland cement systems. C_3A does not refer to the normative content C_3A in the clinker, but to the total Al_2O_3. (**Note:** this figure is revised in* **chapter 4***)*

In order to better visualize the connexion between the ternary subsystems in **Fig. 2.10** and **2.11**, the ternary subsystem C_3A-$CaCO_3$-$CaCl_2$ is illustrated in **Fig 2.12**. The phase diagrams in **Figs. 2.10**, **2.11** and **2.12** can be combined to select the relevant phase assemblages for describing chloride binding in hydrated Portland cement pastes.
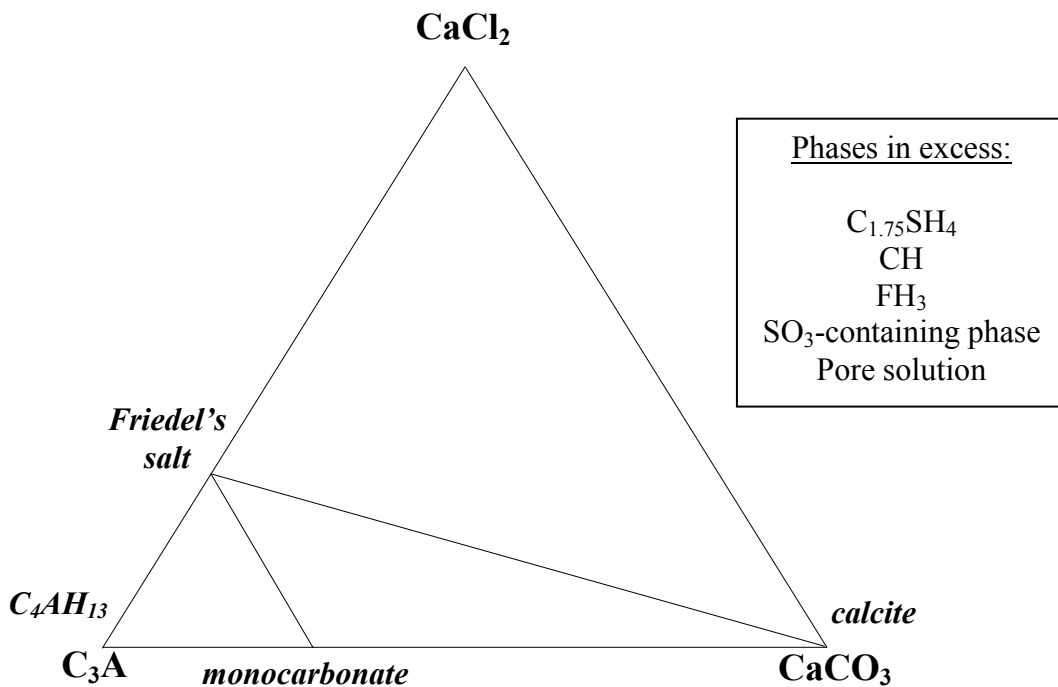
Fig. 2.12: *Ternary subsystem C_3A-$CaCO_3$-$CaCl_2$ in Portland cement systems. C_3A does not refer to the normative content C_3A in the clinker, but to the total Al_2O_3 (**Note:** this figure is revised in* **chapter 9***)*

From the above phase diagrams, the addition of $CaCl_2$ to a system starting out with a mixture of monosulfate, hydroxy-AFm and monocarbonate, should result in the sequence of five 8-phase assemblages shown in **Table 2.f**.

Table 2.f: *Predicted sequence of phase assemblages resulting from $CaCl_2$ addition to hydrated Portland cement with relative high $C_3A/CaSO_4$ ratio*

1.	Hydroxy-AFm, monosulfate, monocarbonate and Friedel's salt	
2.	monosulfate, ettringite, monocarbonate and Friedel's salt	Phases in excess: C-S-H, portlandite, goethite and pore solution
3.	ettringite, calcite, monocarbonate and Friedel's salt	
4.	ettringite, calcite, gypsum and Friedel's salt	
5.	calcite, gypsum, Friedel's salt, + (degree of freedom, i.e. [Cl⁻] can increase in pore solution)	

According to the phase rule, no degrees of freedom are possible in assemblages 1 to 4 since each assemblage consists of 8 components and the maximum number of phases (i.e. 8). An important constraint imposed by this invariance is that the composition of all phases must remain constant within each assemblage. However, once the total binding capacity is used up only seven phases exist giving one degree of freedom (assemblage no. 5). This degree of freedom would allow the $CaCl_2$ concentration to increase in the pore solution upon further addition, until it eventually becomes saturated with respect to $CaCl_2.2H_2O$.

A $CaCl_2$-binding isotherm for the sequence of reactions described above, at a constant level of alkalis, would be expected to develop as illustrated in **Fig. 2.13**. The small increases in concentration of free chloride ions are the result of probable differences in the composition of the pore solution between assemblages.
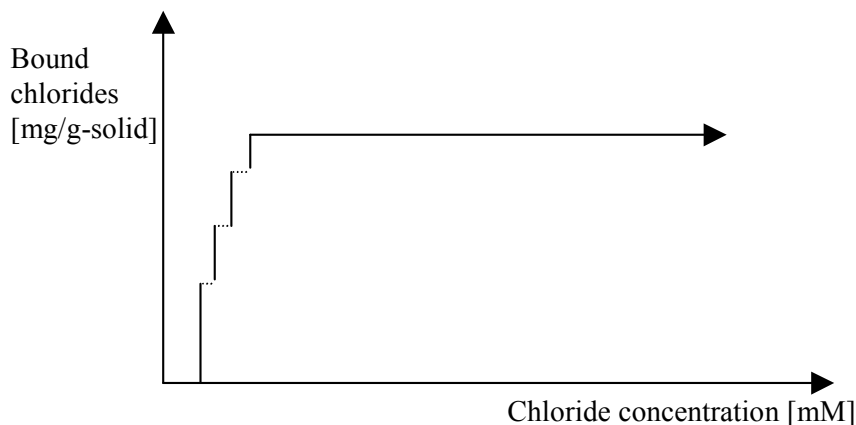
Fig. 2.13: *Schematic $CaCl_2$ binding isotherm in a series of invariant assemblages.*

This hypothetical isotherm for $CaCl_2$ has not been reported in the literature. Instead, the relationship between bound and free chlorides is invariably described as a continuous curve best described by the Langmuir or Freundlich models (as used in e.g. **Tang and Nilsson [1993]**). This implies either non-equilibrium conditions, which is unlikely, or solid solution between two or more phases. The latter would reduce the number of phases and, therefore, provide one or more degrees of freedom, which would allow the chloride concentration to increase in the pore solution as a function of the total chloride content in the system. In the absence of sulfate and carbonate, a likely candidate for this solid solution would be the hydroxy-AFm - Friedel's salt solid solution phase reported in **Birnin-Yauri and Glasser [1998]** albeit at very low concentrations of chloride. In the presence of carbonate, a solid solution between monocarbonate and Friedel's salt has also been reported (**Herfort and Juel [2001]** and **Juel and Herfort [2002b]**), and this would be the most likely phase to occur in realistic systems which must always contain some carbonate.

In systems without CO_2 monosulfate could be expected to form a solid solution with Friedel's salt instead, as observed for a few samples in **Juel [2003]**.

Based on the results from the experiments described in **appendix C,** and the corresponding results in **appendix E**, a solid solution was found between Friedel's salt and monocarbonate for all of the specimens examined, introducing a degree of freedom to the system. Hence, the phase diagram in **Fig. 2.12** must be revised, which is done in **chapter 9**. This permits the relative content of Friedel's salt to increase in the AFm$_{ss}$ (where "ss" denotes solid solution), along with a concomitant increase in the concentration of chloride ions in both the pore solution and in the C-S-H phase. The phase rule is satisfied as long as a single relationship exists for the distribution of Cl between all three phases regardless of C_3A and C-S-H contents, which was clearly observed in this investigation. The relationship between the concentration of Cl in the C-S-H phase and the AFm$_{ss}$ (**Fig. 2.14**) appears to be independent of the alkali content. However, a difference in the binding in the AFm$_{ss}$ and C-S-H phase between the white and grey cements was observed and is attributed to the presence of iron in the grey cement, which adds an extra degree of freedom probably due to a solid solution of iron in the C-S-H phase.
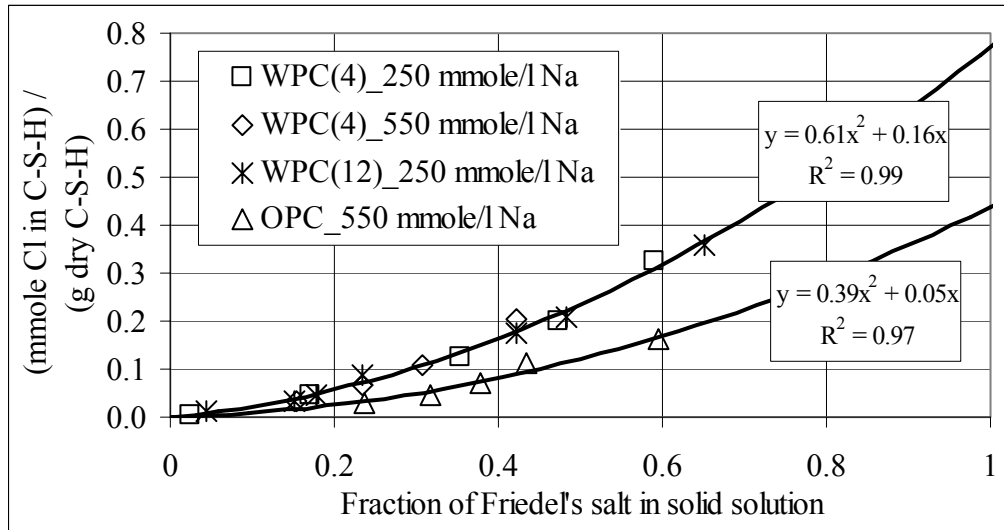
Fig. 2.14: *Cl/Ca molar ratio in the C-S-H versus fraction of Friedel's salt in the solid solution phase Friedel's salt-monocarbonate, for all cements and alkali contents.*

The relationship in **Fig. 2.14** can be understood more readily from the ternary subsystem shown in **Fig. 2.15** which is constructed from the data for the white Portland cements at approximately 250 mM Na concentration. This diagram should apply to any white Portland cement in which the concentration of Na in the pore solution is fixed at approximately 250 mM. The relationship can be used to calculate the overall binding capacity, i.e. the relationship between the free and bound chlorides, from the overall hydrate phase assemblage.
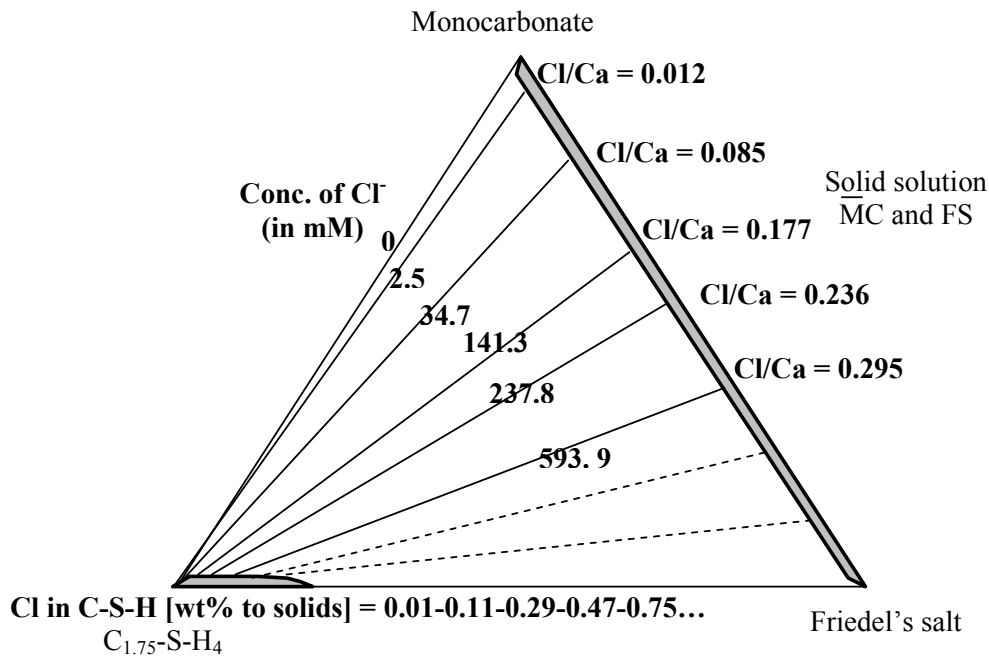
Fig. 2.15: *Pseudo ternary system for 'C-S-H'-Friedel's salt-Monocarbonate at an approximated Na concentration in solution of ~250 mM. Solid tie lines and corresponding chloride concentrations were determined in this study. The dashed lines are extrapolated from this. The relation is expected dependent on temperature*

2.7 $CaO-Al_2O_3-SO_3-Fe_2O_3-CO_2-CaCl_2-Na_2O/K_2O-SiO_2-H_2O$

In the following, sodium and potassium are considered to have the same properties and to show similar behaviour, which is supported by the observation in **Hong and Glasser [1999 and 2002]**.

The presence of sodium in a chloride containing cement paste system has to be defined by at least two additional components. In the solid phases it can be described by the element NaOH (which can be expressed by the relative contents of the components Na_2O and H_2O), whilst the components Na_2O, NaCl and H_2O must be defined in the pore solution in order to express the presence of NaCl and NaOH. At low concentrations of chloride, the composition of the pore solution can be expressed by relative contents of NaCl, Na_2O, and H_2O. Once all the sodium is balanced by chlorides, any further addition of chlorides can be expressed by the increase in $CaCl_2$ concentration, where Ca^{2+} is released from the solid phases.

Hong and Glasser [1999 and 2002] investigated the incorporation of alkalis (both sodium and potassium) up to equilibrium concentrations of 300 mM in artificially prepared C-S-H and introduced a distribution ratio, R_d, defined by the concentration of sodium or potassium in the C-S-H phase divided by the concentration in the pore solution, expressed as ml/g ([mmol alkali in C-S-H / g-dry C-S-H] / [mmol alkali in solution / ml solution]). The R_d value was found to be independent of the content of alkalis in the system, but strongly dependent on the Ca/Si ratio of the C-S-H. The distribution ratio for alkalis was found in this investigation to play a very significant role on the chloride binding in hydrated Portland cement pastes.

The overall global reaction taking place in hydrated Portland cement pastes, found in my own investigations, is given in **Table 2.g**, accounting for the total content of alkalis and the relative amount of solution to solid paste (see **paper IV (appendix A)** for details). This reaction is divided into two parts; one for the C-S-H which contains alkalis, the other for the alkali-free C-S-H. The reaction not only describes the distribution of chlorides between the C-S-H, AFm solid solution and pore solution, but also the change in Ca^{2+}, OH^- and alkali concentrations in the pore solution. The distribution function (see **Fig. 2.14**) for chlorides between the C-S-H and the solid

solution phase is independent of the alkali content, but is dependent on the iron content of the system.

Table 2.g: *Complete reaction describing the binding of chloride by the C-S-H and AFm phases, and the composition of the pore solution*

1.a) Chloride binding in PC pastes in which Na is still present in the C-S-H, and no AFm phases other than monocarbonate are present.

$$\mathbf{b} \cdot [C_3A.CaCO_3.11H_2O]_{(s)} + \mathbf{a} \cdot [1.75CaO.SiO_2.\mathbf{z}NaOH.4H_2O]_{(s)} +$$
$$+ (\mathbf{(k+1)} \cdot \mathbf{y} \cdot \mathbf{a} + \mathbf{b} \cdot \mathbf{x}) \, CaCl_{2 \,(aq)} + \mathbf{2 \cdot 0.83 \cdot k \cdot y \cdot a} \, NaOH_{(aq)}$$
$$\downarrow$$
$$\mathbf{2 \cdot k \cdot y \cdot a} \, NaCl_{(aq)} + \mathbf{a} \, [1.75CaO.SiO_2.\mathbf{(z-0.34 \cdot k \cdot y)}NaOH.\mathbf{y}CaCl_2.4H_2O]_{(s)}$$
$$+ \mathbf{k \cdot y \cdot a} \, Ca(OH)_{2 \,(s)} + \mathbf{b} \, [C_3A.CaCl_{2 \,(x)}.CaCO_{3 \,(1-x)}.11H_2O]_{(s)} + \mathbf{b \cdot x} \, CaCO_{3 \,(s)}$$
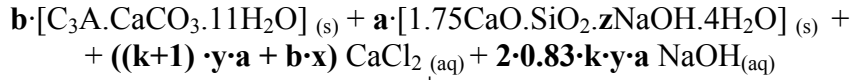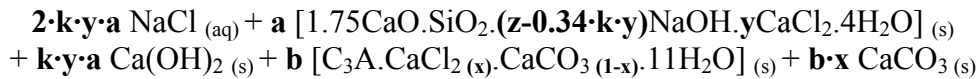
1.b) Chloride binding in PC pastes in which Na is still present in the C-S-H, and other AFm phases than monocarbonate are present
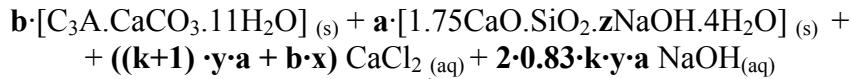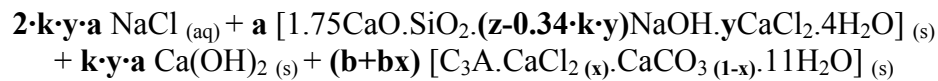
$$\mathbf{b} \cdot [C_3A.CaCO_3.11H_2O]_{(s)} + \mathbf{a} \cdot [1.75CaO.SiO_2.\mathbf{z}NaOH.4H_2O]_{(s)} +$$
$$+ (\mathbf{(k+1)} \cdot \mathbf{y} \cdot \mathbf{a} + \mathbf{b} \cdot \mathbf{x}) \, CaCl_{2 \,(aq)} + \mathbf{2 \cdot 0.83 \cdot k \cdot y \cdot a} \, NaOH_{(aq)}$$
$$\downarrow$$
$$\mathbf{2 \cdot k \cdot y \cdot a} \, NaCl_{(aq)} + \mathbf{a} \, [1.75CaO.SiO_2.\mathbf{(z-0.34 \cdot k \cdot y)}NaOH.\mathbf{y}CaCl_2.4H_2O]_{(s)}$$
$$+ \mathbf{k \cdot y \cdot a} \, Ca(OH)_{2 \,(s)} + \mathbf{(b+bx)} \, [C_3A.CaCl_{2 \,(x)}.CaCO_{3 \,(1-x)}.11H_2O]_{(s)}$$

2. Chloride binding in Portland cement pastes with alkali-free C-S-H

$$\mathbf{b} \cdot [C_3A.CaCl_{2 \,(m)}.CaCO_{3 \,(1-m)}.11H_2O]_{(s)} + (\mathbf{b \cdot x + y \cdot a}) \, CaCl_{2 \,(aq)} +$$
$$+ \mathbf{a} \, [1.75CaO.SiO_2.\mathbf{(z/0.34 \cdot k)}CaCl_2.4H_2O]_{(s)}$$
$$\downarrow$$
$$\mathbf{a} \cdot [\, \mathbf{(1.75-y)}CaO.SiO_2.\mathbf{(z/(0.34 \cdot k) + y)}CaCl_2.\mathbf{(4 - y)}H_2O]_{(s)} + \mathbf{y \cdot a} \, Ca(OH)_{2 \,(s)} +$$
$$+ \mathbf{b} \cdot [C_3A.CaCl_{2 \,(m + x)}.CaCO_{3 \,(1-m-x)}.11H_2O]_{(s)} + \mathbf{b \cdot x} \, CaCO_{3 \,(s)}$$
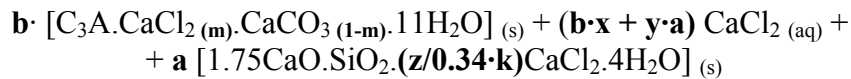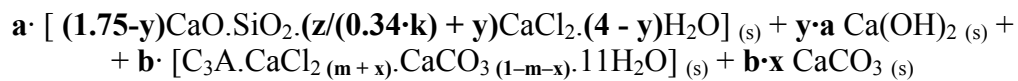
Note: in eq.2, for each mol of $CaCl_2$ bound by the C-S-H, **(PS/a)**/75 mol $CaCl_2$ remain in solution, where PS denotes the amount of solution in millilitre (i.e. pore solution + exposure solution, if applicable).

- '**x**' denotes the fraction of Friedel's salt in the AFm solid solution phase; '**y**' denotes the content of $CaCl_2$ in the C-S-H, in mol/mol, and is related to '**x**' as follows,

In the iron-free case (white Portland cement)

$$\mathbf{y} = 0.0601 \, \mathbf{x}^2 + 0.0164 \, \mathbf{x}$$

In the iron-containing case (grey Portland cement)

$$\mathbf{y} = 0.0376 \, \mathbf{x}^2 + 0.0046 \, \mathbf{x}$$

- '**a**' is the content of C-S-H, in mol; '**b**' is the initial content of monocarbonate, in mol.

- '**z**' is the molar ratio of NaOH, in the chloride-free C-S-H, to C-S-H, i.e. in mol/mol. This can be calculated from the initial Rd, i.e. 0.65 (see the text), which is a general value, independent of water to powder ratio.

- '**k**' is defined as

$$\mathbf{k} = \mathbf{z} \cdot \mathbf{(PS/a)} \cdot 25 / (0.83 \cdot 0.81 \cdot \mathbf{M_{w,C-S-H}} \cdot \mathbf{Rd_0}) = \mathbf{z} \cdot \mathbf{(PS/a)} \cdot 0.2354 \text{ , where } \mathbf{PS} \text{ is the}$$
amount of solution in milliliter (i.e. pore solution + exposure solution, if applicable).

- '**m**' denotes the fraction of Friedel's salt in the solid solution phase at the chloride content where all alkalis have been released to the pore solution from the C-S-H.

2.8 Model for phase equilibria in hydrated Portland cement, incl. chloride and alkali

An Excel spreadsheet is included in the enclosed CD which includes the model in **section 2.5** and the relationships in **section 2.7** for predicting the assemblage in hydrated Portland cement at any content of chloride, alkalis, sulfate and carbonate. *In this report, whenever reference to "model in **section 2.8**" or "model for phase equilibria in hydrated PC including chloride and alkali" is given, it refers to the combination of the phase equilibria model in **section 2.5** with the relations found in **Table 2.g**.*

As described in **sections 2.7**, three degrees of freedom are present in a hydrated Portland cement paste in aggressive marine or de-icing salts environments. This section deals with the modelling of chloride binding in the presence of alkalis in hydrated Portland cement pastes by application of the phase rule. As the number of phases does not equal the number of components, some adjustments are needed. The procedure adopted is described in the following starting with a Portland cement paste with a composition as that in **Table 2.c**. Chloride is then added to the system as two different sources: $CaCl_2$ and $NaCl$.

The calculations are carried out by initially neglecting the presence of alkalis and chloride. Therefore, the procedure is the same as described in **section 2.5**. The initial assemblage will be that of assemblage 3 in **Table 2.d**. In **Table 2.h**, the equations in **Table 2.g** have been used to predict the resulting assemblage of the cement paste upon addition of 15 mmol $CaCl_2$ (i.e. 30 mmol Cl), as well as upon addition of 30 mmol NaCl. Note that the lowest value of pH allowed in the calculations is 12.5 (approx. 30 mM OH^-), which is in agreement with the lowest pH measured in this investigation (see **appendix E**).

Table 2.h: *Predicted assemblage upon addition of 15 mmol $CaCl_2$ and 30 mmol NaCl to the water saturated assemblage 3 in* **Table 2.d** (1.06 wt.% chloride to anhydrous powder)

WPC(4) + 15 mmol $CaCl_2$		WPC(4) + 30 mmol NaCl	
$C_{1.75}SH_4$	98.5	$C_{1.75}SH_4$	98.5
CH	36.3	CH	35.8
FH_3	0.4	FH_3	0.4
Pore solution	35.8	Pore solution	36.0
Ettringite	2.4	Ettringite	2.4
Calcite	1.2	Calcite	1.1
Monocarb.	0.5	Monocarb.	0.7
Friedel's salt	0.6	Friedel's salt	0.4
Pore solution:		Pore solution:	
$[Na^+]$ = 108 mM		$[Na^+]$ = 491 mM	
$[Cl^-]$ = 140 mM		$[Cl^-]$ = 414 mM	
$[Ca^{2+}]$ = 31 mM		$[Ca^{2+}]$ = 15 mM	
$[OH^-]$ = 30 mM		$[OH^-]$ = 107 mM	

It is observed that the composition of the pore solution varies substantially depending on the additional components associated with the chloride attack, at any given total chloride content. This illustrates how complex the ingress of aggressive substances from, e.g. seawater, into concrete becomes. As will be treated in **chapter 6**, the ingress of ions in solution is dependent on many factors, such as their charge and mobility, but the ultimate driving force is the gradient in concentration throughout the concrete section. It is therefore important for the cement paste matrix to be able to reduce the concentration of chlorides (when dealing with the time to chloride induced reinforcement corrosion) in order to reduce the driving force towards the reinforcement. The calculations above reveal the strong negative influence of alkalis on binding

of chlorides, which is why the rate of ingress of other species such as alkalis also needs to be included if an accurate prediction on the ingress rate of chlorides is to be achieved. However, it should be noted that for seawater exposure, sulfate resisting capacity of the cement also becomes a decisive factor (see **chapters 4** and **7**).

The model described may serve as an appropriate tool to compare the chloride binding capacity of different Portland cements and allow for a better design of service life based on the optimum choice of the Portland cement for use in a given environment.

As an indication of the accuracy of the model, the experimentally determined concentrations of chloride and sodium in the exposure solution for the different cement types tested for the development of the model are plotted against the concentrations predicted by the model, in **Fig. 2.16**. An excellent agreement is found (R^2 value of 0.99 for both figures).
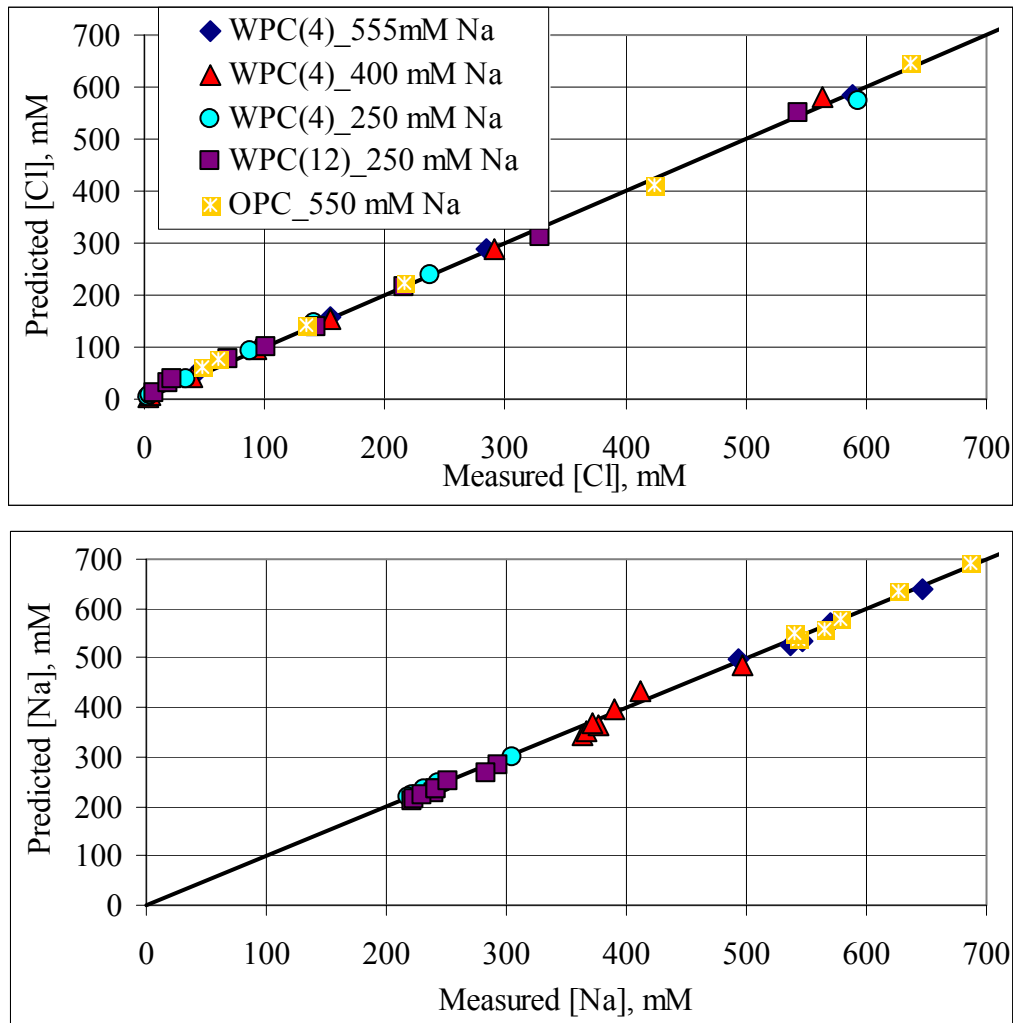
Fig. 2.16: *Experimentally determined concentrations of chloride and sodium in solution against the predicted by the model in this section. Predicted values are 1% higher than the measured (R^2 = 0.99), for both figures*

2.9   Comparison with data from the literature

Considerable experimental data on chloride binding in Portland cement pastes is found in the literature. However, the data is rarely given in sufficient detail to be tested using the model described in this thesis. Not only are the chemical composition of the cement and mixing proportions needed, but the exact composition and amount of exposure solution before and after exposure are usually absent. The author chooses not to select results from pore solution expression techniques because one of the main requirements for applying the phase rule as mentioned previously would be unsatisfied, i.e. the pressure of the system is changed dramatically during the procedure.

The results found in **Korzen [1998]** (some of them published in **Jensen et al.[2000]**) satisfy the required level of documentation in order to test their data against the model described here. Korzen studied the chloride binding isotherms of different Portland cement pastes at different w/p ratios and temperatures. The chloride source was NaCl and the amount of exposure solution prior to and after exposure was noted, as well as its initial composition, and the amount of exposed cement paste.

The model described in **section 2.8** was applied to the chemical composition of the white Portland cement paste (cement is the same product from the same manufacturer) in **Korzen [1998]** mixed at w/p 0.50 and the added amounts of chloride and sodium, to predict the equilibrium assemblage. **Fig. 2.17** compares the chloride concentrations in the pore solution predicted by the model and those measured in **Korzen [1998]**.
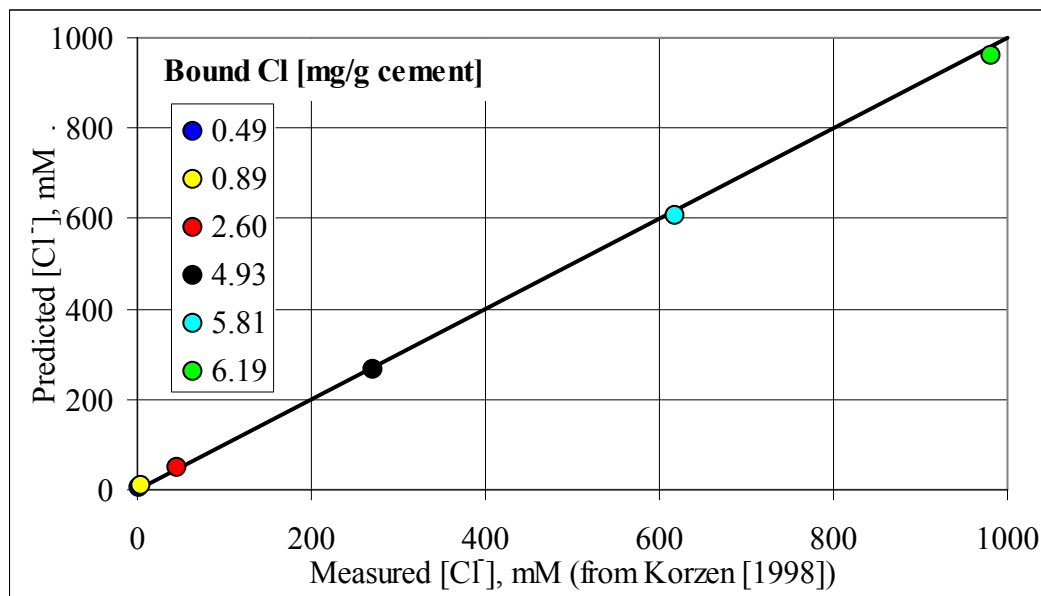
Fig. 2.17: *Comparison between predicted concentration of chlorides in the pore solution by the model in* **section 2.8***, and determined experimentally in* **Korzen [1998]***, from absorption of chlorides of a white Portland cement (same type as WPC(4)) paste at w/p = 0.50. Predicted values are 1% lower than the measured ($R^2 = 1.00$)*

Unfortunately, Korzen did not measure the concentration of alkalis in the pore solution at equilibrium, which is why those values cannot be compared. The concentration of alkalis was only reported prior to exposure.

After equilibrium was achieved for chloride absorption, Korzen removed 2.2 ml of the surrounding exposure solution for analysing purposes, and added 8 ml lime-saturated water to study the desorption of chlorides. **Fig. 2.18** compares the chloride concentrations predicted by the model when making corrections for this, and the results obtained by Korzen.
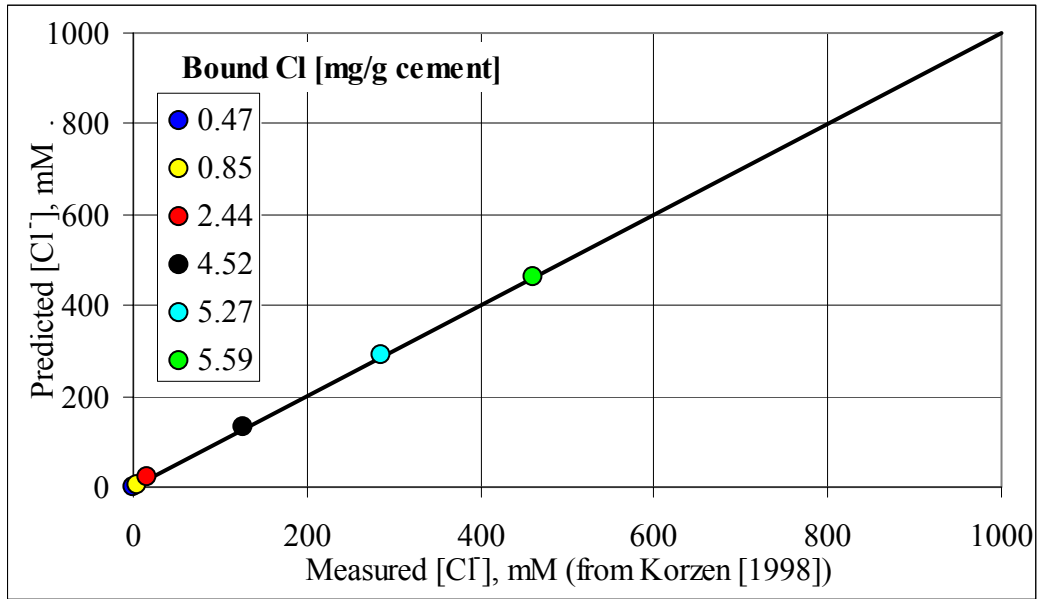
Fig 2.18: *Comparison between chloride concentrations measured in* **Korzen [1998]** *and those predicted by the model described in* **section 2.8**, *at equilibrium of the samples in* **Fig. 2.17** *upon removal of approx. 2.2 ml exposure solution and addition of 8 ml lime-saturated water. Predicted values are 1% higher than the measured ($R^2 = 0.99$)*

Furthermore, Korzen studied the absorption and desorption of chlorides on a grey Portland cement (composition similar to that of the OPC in this study) paste at w/p = 0.50, and **Fig. 2.19** and **2.20** shows the comparison between the values predicted by the model and the results obtained experimentally by Korzen, from absorption and desorption, respectively.
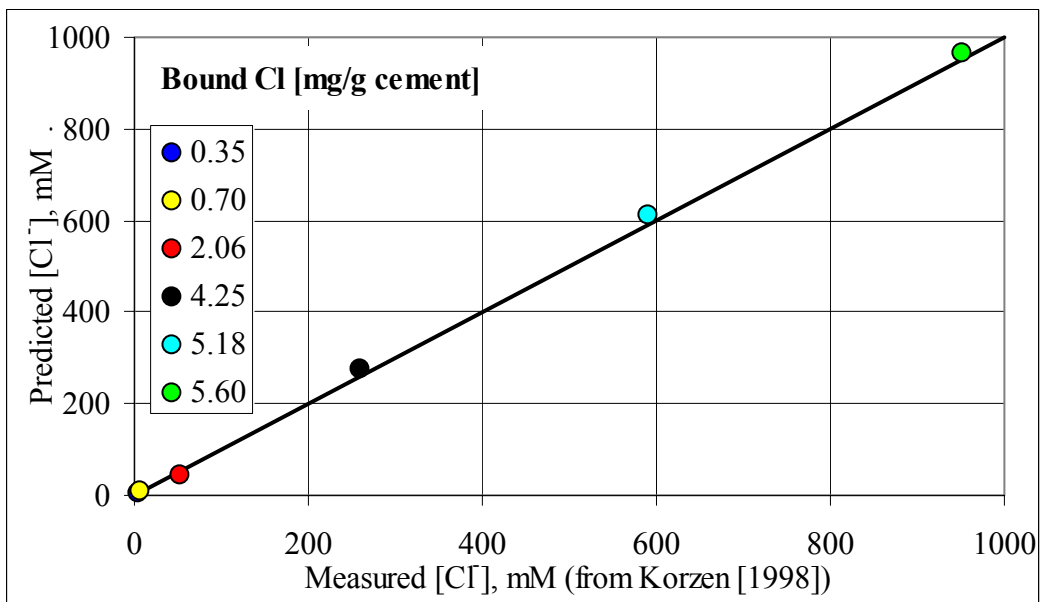
**Fig. 2.19:** *Comparison between predicted concentration of chlorides by the model in* **section 2.8**, *and determined experimentally in* **Korzen [1998]**, *from absorption of chlorides of a grey Portland cement (composition similar to that of OPC) paste at w/p = 0.50. Predicted values are 1% higher than the measured ($R^2 = 0.99$)*
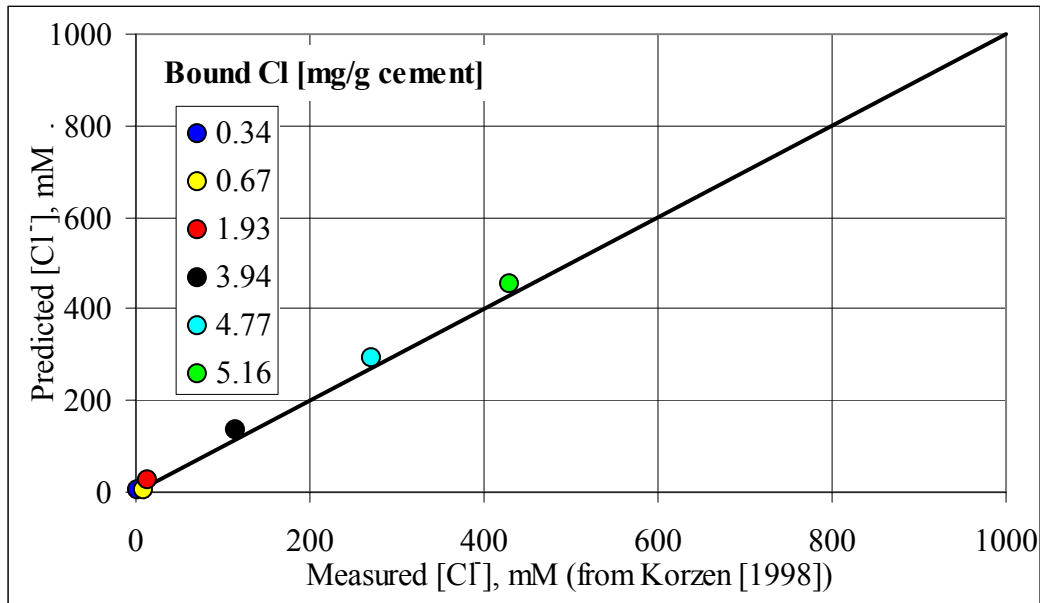
Fig. 2.20: *Comparison between chloride concentrations measured in* **Korzen [1998]** *and the predicted by the model described in* **section 2.8**, *at equilibrium of the samples in* **Fig. 2.19** *upon removal of approx. 2.2 ml exposure solution and addition of 8 ml lime-saturated water. Predicted values are 4% higher than the measured ($R^2 = 0.99$)*

Excellent agreement is also found for the grey cement (i.e. R^2 value at 0.99). It should be noted that the high volume ratio of exposure solution to sample results in only small variations in the predictions of chloride concentration upon a change in the composition of the cement. This is because a significant amount of chlorides has to be released or absorbed by the cement paste to significantly change the composition of the pore solution. However, for a similar exposure environment, the amount of bound chloride in the grey cement (see **Fig. 2.19**) measured by Korzen is approx. 25% to 6% (corresponding to lowest and highest concentration of chlorides, respectively) lower than that of the white cement (see **Fig. 2.17**).
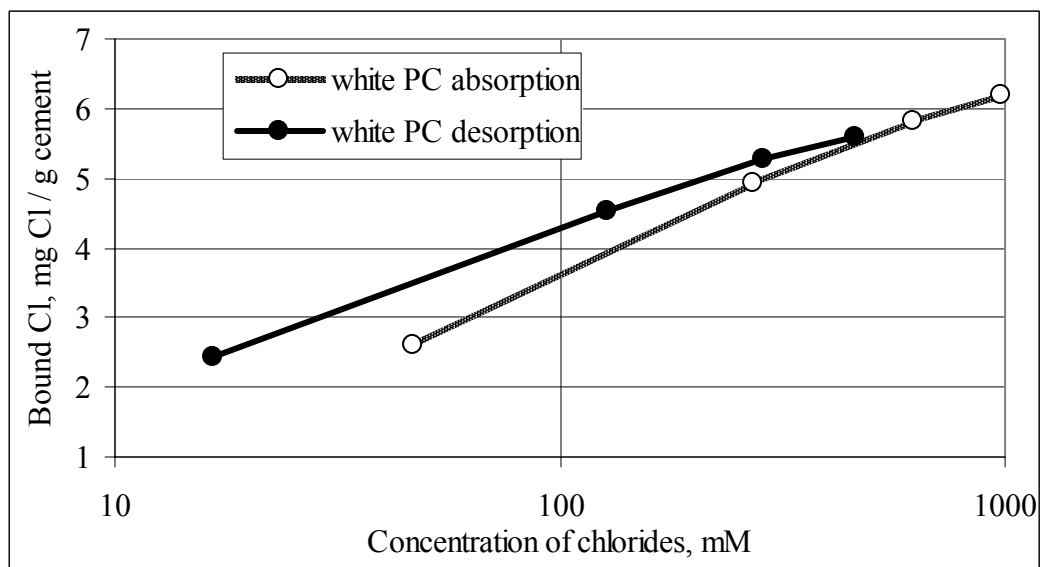
Fig. 2.21: *Chloride binding isotherms for the white PC during absorption and desorption based on the data measured in* **Korzen [1998]**

The chloride isotherms for the white Portland cement, both for absorption and desorption, are plotted in **Fig. 2.21**. It is a common observation elsewhere that the relative content of bound

chloride is higher after desorption than absorption. Some authors have suggested (e.g. **Jensen et al [2000]**) that a significant portion of the chloride is bound to the high specific surface area of the C-S-H phase by a process of physical adsorption, and that these forces are strong enough to fix the chloride ions to the surface of the C-S-H during leaching of chlorides. After applying the model described earlier it is clear that this explanation is unnecessary, and the desorption isotherm is purely a result of re-equilibration in response to a reduction in the alkali content of the system.

Korzen [1998] did not monitor the time for equilibrium during absorption and desorption and therefore, no comments on any differences in kinetics between these processes can be given. Equilibrium was already achieved at the first measurement on the chloride concentration in the exposure solution, which were carried out after 3 and 6 weeks of exposure for chloride absorption and desorption, respectively.

2.10 Effect of cement composition on chloride binding and threshold values

In this section, the model in **section 2.8** is used to identify the effect of relevant changes to the composition of the cement on chloride binding and chloride threshold values. **Fig. 2.22** illustrates the predicted concentration of chlorides in the pore solution of a WPC(4) and OPC paste, respectively, at a constant content of chlorides of 3.5 mg Cl/g-cement, upon varying the total content of Na_2O_{eq} and Al_2O_3.
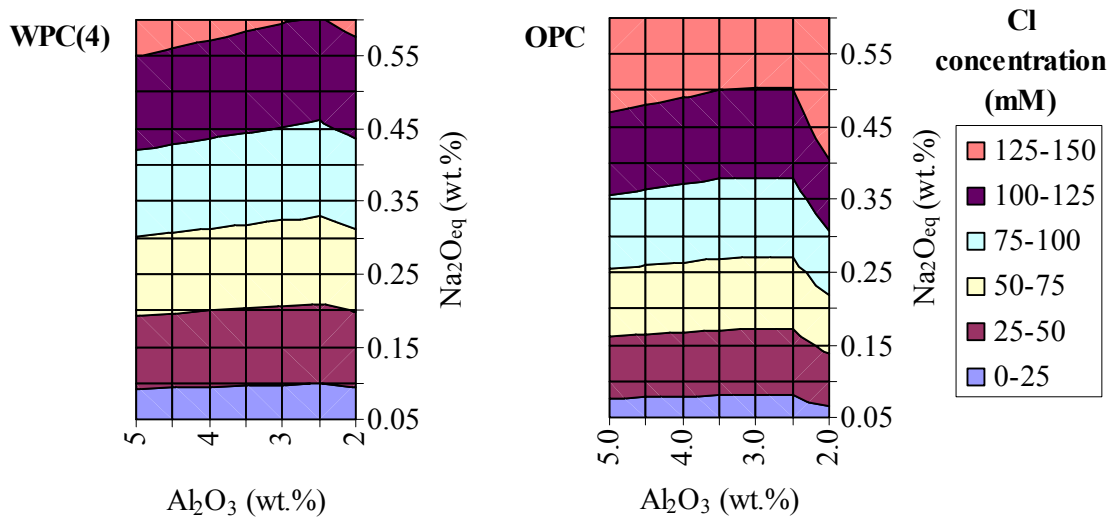
Fig. 2.22: *Predicted concentration of chloride in the pore solution upon varying the content of alkalis and aluminate, at a constant total chloride content of 3.5 mg Cl / g cement. Left graph starting with initial composition of WPC(4) and right graph of OPC*

The content of Al_2O_3 is seen to have a relative minor effect on the chloride binding compared to the alkalis. Similarly, the content of Fe_2O_3 (i.e. WPC(4) vs. OPC) also has a relative minor effect even though it was shown in **section 2.6** that the absorption of chlorides by the C-S-H is much higher in iron free Portland cements (i.e. white PC). The chloride distribution between the C-S-H and AFm solid solution is different for the two cements, but adds up to a similar amount of total bound chlorides, thereby explaining the minor difference observed in **Fig. 2.22**.

Alkalis (expressed as Na_2O_{eq}) have a significant effect on chloride binding in Portland cement pastes. The higher the alkali content, the higher the fraction of chlorides in the pore solution. Of all chemical parameters studied, alkalis showed the largest effect. From this, it could be concluded that any Portland cement exposed to chlorides should have a very low content of alkalis in order to maximize the binding capacity of the paste.

A low alkali content of the powder will result in a lowering of the pH in the pore solution of the paste, increasing the risk of pitting and subsequent corrosion of the reinforcement. Chloride induced reinforcement corrosion is normally regarded as the main degradation mechanism in concrete structures exposed to marine environments. Corrosion of reinforcement is expected to occur when the Cl/OH-ratio in the pore solution at the depth of the reinforcement is higher than 0.5-0.6 (e.g. **Saremi and Mahallati [2002]**).

As the initial content of alkalis of the powder relates to the amount of OH$^-$ in the resulting pore solution, the increased binding capacity by a reduction in alkali content has to be high enough to result in similar or better performance in terms of chloride threshold value. **Fig. 2.23** illustrates the calculated Cl/OH-ratio in the pore solution of a WPC(4) and OPC paste at w/p 0.50 for varying contents of Al_2O_3 and Na_2O_{eq}, but at constant total content of chlorides, corresponding to 3.5 mg Cl/g cement.
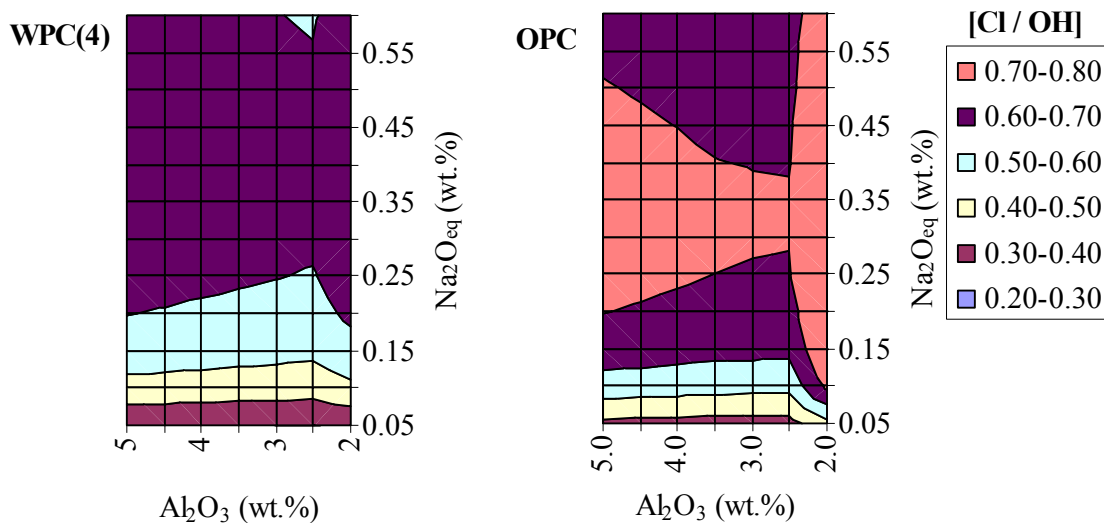
Fig. 2.23: *Predicted [Cl/OH]-ratios in the pore solution upon varying the content of alkalis and aluminate, at a constant total chloride content of 3.5 mg Cl / g cement. Left graph starting with initial composition of WPC(4) and right graph of OPC*

A reduction in alkali content (to Na_2O_{eq} levels lower than approx. 0.35) results in decreased Cl/OH in the pore solution, resulting in improved protection against reinforcement corrosion. However, a reduction in Na_2O_{eq} content from e.g. 0.60 to 0.40 will result in increased Cl/OH, therefore decreasing the protection against reinforcement corrosion.

Again, the content of Al_2O_3 is observed to have a smaller influence than the alkali content, except at Al_2O_3 contents below 2.5 % where chlorides are mostly taken up by the C-S-H phase. In this region, the higher uptake of chloride in white Portland cements becomes very pronounced. For increasing contents of Al_2O_3 above 2.5% the Cl/OH is increased. At any content of Na_2O_{eq} and Al_2O_3 (for Na_2O_{eq} lower than approx. 0.35), the Cl/OH ratio in the pore solution is lower in the iron-free paste (i.e. white PC).

The effect of the content of Al_2O_3 only becomes significant in systems with high (roughly > 1 % CO_2) contents of CO_2. This is illustrated for the WPC(4) w/p = 0.50 paste in **Fig. 2.24**, where 2 mass% of the cement has been replaced by $CaCO_3$.
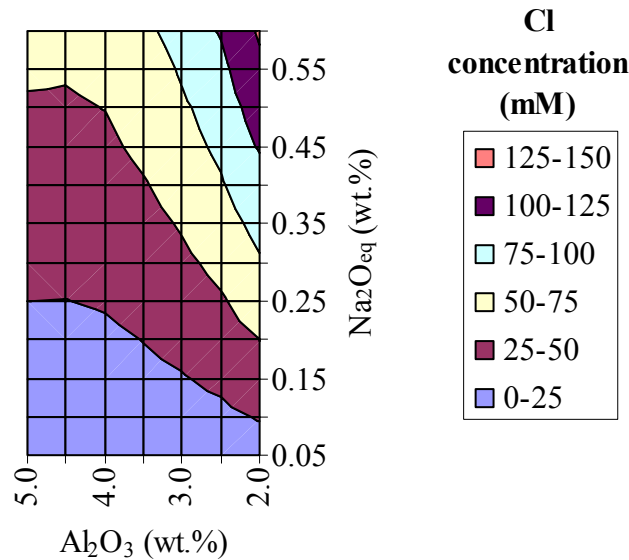
Fig. 2.24: *Chloride concentration in the pore solution of a w/p 0.50 paste, at constant content of chlorides (3.5 mg Cl/g cement), where 2 mass% of the cement has been replaced by CaCO₃. Starting with the initial composition of WPC(4)*

The increased binding capacity of the paste at high contents of Al_2O_3 result from the larger amount of monocarbonate formed initially in the cement paste upon hydration, which goes into solid solution with Friedel's salt, being able to incorporate significantly higher amounts of chloride.

However, it should be remembered that a typical requirement to Portland cements in aggressive environments is sulfate resistance, which limits the maximum content of Al_2O_3. For the white Portland cement in **Fig. 2.24**, this corresponds to a Al_2O_3 content of approx. 2 wt.% (i.e. C_3A content of 5 %). Furthermore, in **chapter 4** it will be shown that the decrease in chloride binding capacity upon sulfate addition becomes more severe the higher the content of Al_2O_3.

2.11 Some limitations of the model

- The model is restricted to Portland cement pastes with or without supplementary cementing materials (see **chapter 3**) at temperatures around 20°C. All of the presented phase diagrams are dependent on temperature.

- The w/p of the cement paste matrix has to be high enough to ensure a residual capillary porosity at complete hydration, i.e. w/p > approx. 0.40. Where the content of cementitious powder is too high compared to that of water, the internal pressure of the capillary water in the cement paste will become lower than 1 atm, resulting in an extra degree of freedom of the system.

- The model is only valid for hydrated Portland cement pastes where the degree of hydration is high enough (i.e. reactions proceed at a slow rate) to justify the assumption of metastable or stable equilibrium.

- The Ca/Si of the paste has to be high enough to ensure the presence of both $C_{1.75}$-S-H_4 and CH in the stable assemblage. However, if the addition of SiO_2 is high enough to use up the CH phase, the assemblage can still be calculated as being composed of a $C_{1.75}$-S-H_4 and a $C_{0.8}$S-H_4 (in order to ensure as many equations as unknowns), where the actual C-S-H solid solution phase is of course in reality a mixture of the two end-member phases. This would require a study of the absorption properties of this C-S-H with respect to alkalis and chloride, to be able to calculate the composition of the pore solution.

- MgO is assumed to only form $Mg(OH)_2$ upon hydration. This is justified for Portland cements because of the very low contents. However, in cements with higher MgO contents, or replacement by cementitious materials with high MgO content, hydrotalcite or magnesium silicate hydrates may form and some discrepancies may result, although it is unclear whether the presence of the latter phases represents true equilibrium conditions or is a result of chemical inhomegeneity.

3 Chloride binding in pastes with silica fume and granulated blast furnace slag

Pure Portland cement concretes are rarely found in modern European concrete exposed to aggressive environments. Generally, supplementary cementitious materials as silica fume, slag or fly ash, or a combination of these are used, which is why binding of chloride in such systems needs to be studied. In this investigation, only binding in silica fume and slag containing pastes was examined, and the findings are described in the following. The composition of the supplementary materials is given in **appendix B** and all obtained results are given in **appendix E**.

3.1 Silica fume

The addition of silica fume (approximately 95% SiO_2) to a Portland cement results in enhanced formation of C-S-H at the expense of $Ca(OH)_2$ (see **Fig. 2.7**). If the addition is high enough, $Ca(OH)_2$ may be completely used up and the C-S-H is then progressively decalcified (i.e. lowering of Ca/Si molar ratio in the C-S-H, as illustrated in **Fig. 2.7**). However, the addition of silica fume is normally not larger than 5-10 mass % to anhydrous cement, which is normally insufficient to remove all of the $Ca(OH)_2$.

If $Ca(OH)_2$ is present as a stable phase in hydrated paste, the relationships described in the previous sections are expected applicable because the same solid phases are present.

In this investigation, only one cement with replacement of silica fume was tested, i.e. WPC(4) with 10 mass % silica fume (denoted WPC(4)_10%SF). The content of Al_2O_3 and SO_3 are very low for this particular Portland cement and are further lowered by the dilution with silica fume. This results in a total content of these components lower than what is needed to obtain Al/Ca and S/Ca molar ratios in the C-S-H of 0.04 and 0.03 (see **section 2.2**), as would be expected in normal hydrated Portland cement paste. Therefore, the C-S-H becomes under-saturated with respect to Al^{3+} and S^{6+}, and the paste has two extra degrees of freedom. Given that no extra components were introduced to the system, two phases must disappear in order for the phase rule to be satisfied. By carrying out calculations as those performed in **Table 2.d**, it is found that the exhausted phases are the otherwise expected sulfur containing phase (which in this case would have been ettringite), and monocarbonate.

Fig 3.1 shows the result of 1300 randomly distributed EDS-spot analyses on a polished section of a hydrated WPC(4)_10%SF paste, plotted in terms of S/Ca vs. Si/Ca molar ratios. Even though the number of analyses is high, there is clearly no trend towards monosulfate or ettringite (no trend-lines between the C-S-H, at approx. [Si/Ca,S/Ca] = [0.57,0.025], and the plots for the composition of monosulfate and ettringite), which is consistent with the above. Furthermore, it is observed that $Ca(OH)_2$ is present in the system, i.e. the number of plots tending towards the point [0,0] is much larger than can be explained by the minor presence of calcite.
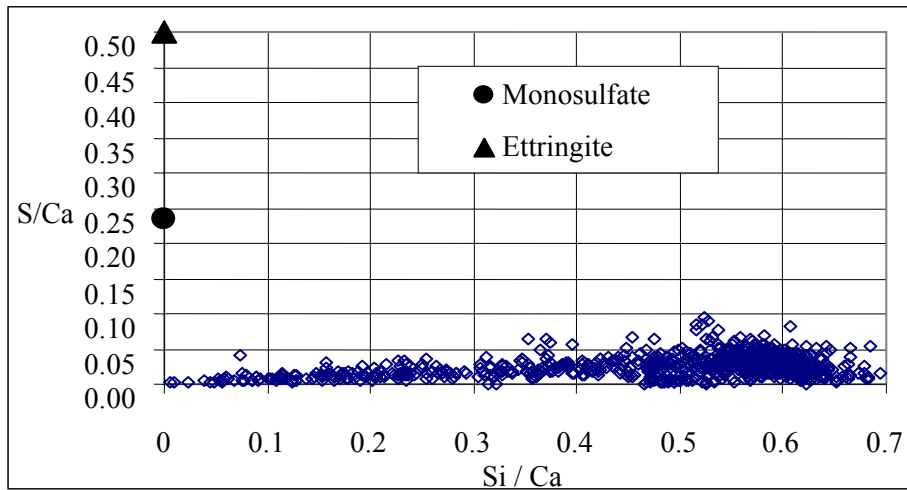
Fig. 3.1: *S/Ca vs. Si/Ca of 1300 randomly distributed EDS-analyses of a hydrated WPC(4)_10%SF*

The content of Al^{3+} and S^{6+} in the C-S-H can normally be predicted from the EDS plots as those in **Fig. 3.2**. However the scattering of the points makes this difficult, which is why the Al/Ca and S/Ca molar ratios are set at 0.033 and 0.029 respectively, as these values correspond to all Al^{3+} and S^{6+} being present in the C-S-H, when carrying calculations similar to those in **Table 2.d**. This is in agreement with the plots in **Fig. 3.2**.
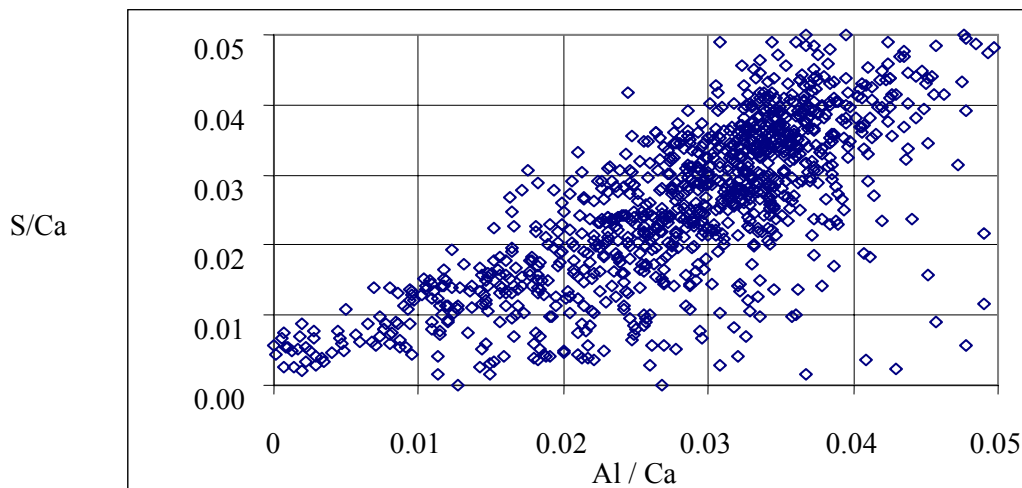
Fig. 3.2: *S/Ca vs. Al/Ca of 1300 randomly distributed EDS-analyses of a hydrated WPC(4)_10%SF*

Given the absence of AFm and AFt phases, and the overall under-saturation of the C-S-H phase with respect to Al_2O_3, Friedel's salt cannot form from additions of chloride, i.e. all bound chloride is likely to be found in the C-S-H. Confirming this, no trend-lines towards monocarbonate, Friedel's salt or a solid solution of Friedel's salt and monocarbonate were observed from the EDS-analyses (see the attached CD).

The reactions that were presented in **Table 2.g** are still expected to apply (when removing the reactions involving monocarbonate), as the exchange ratio of $CaCl_2$ for NaOH in the C-S-H is expected to be unchanged, relating thereby the composition of the C-S-H and the pore solution. However, the distribution ratio for alkalis, Rd_0, is likely to be affected by the changes in composition of the C-S-H (i.e. change in Al/Ca and S/Ca), similar to the change in Rd_0 brought about by a change in Ca/Si ratio in the C-S-H, as observed in **Hong and Glasser [1999]** (where Rd_0 increased for decreasing Ca/Si in C-S-H).

For the investigated paste (WPC(4)_10%SF) the Rd_0 is set to 1.0, predicted as the intersection point with the y-axis of Rd vs. chloride content in **Fig. 3.3**. Note that a change in Rd of ± 0.1 affects the predicted chloride and sodium concentrations by less than 4 %.
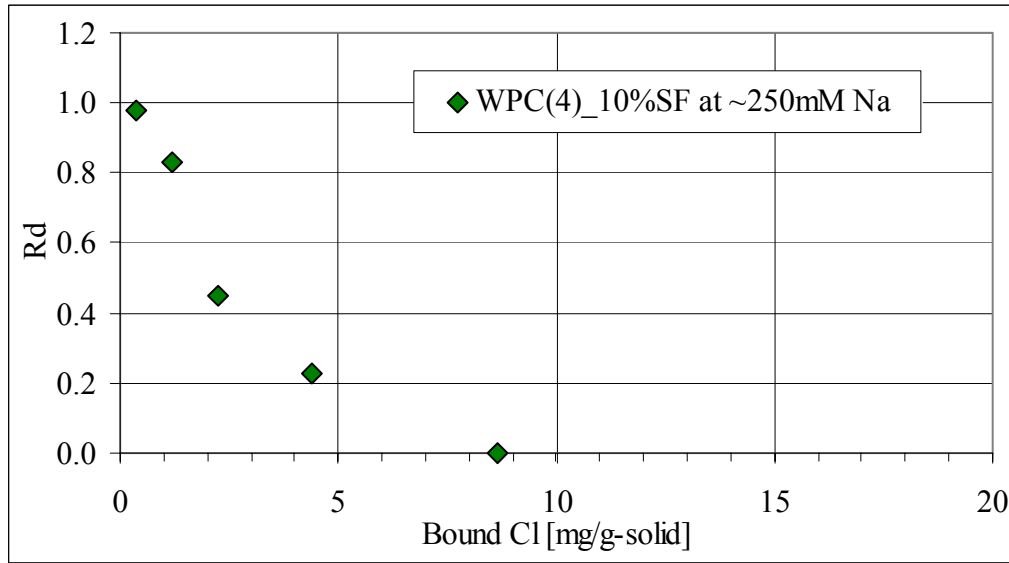
Fig. 3.3: *Rd vs. chloride content in the paste WPC(4)_10%SF, at nearly constant alkali concentration*

Fig. 3.4 and **Fig 3.5** show the comparison between the values predicted by the model in **section 2.8**, (Rd_0 at 1.0), and those measured (found in **appendix E**). **Fig. 3.4** compares the chloride concentration, while the concentration of alkalis is compared in **Fig. 3.5**.
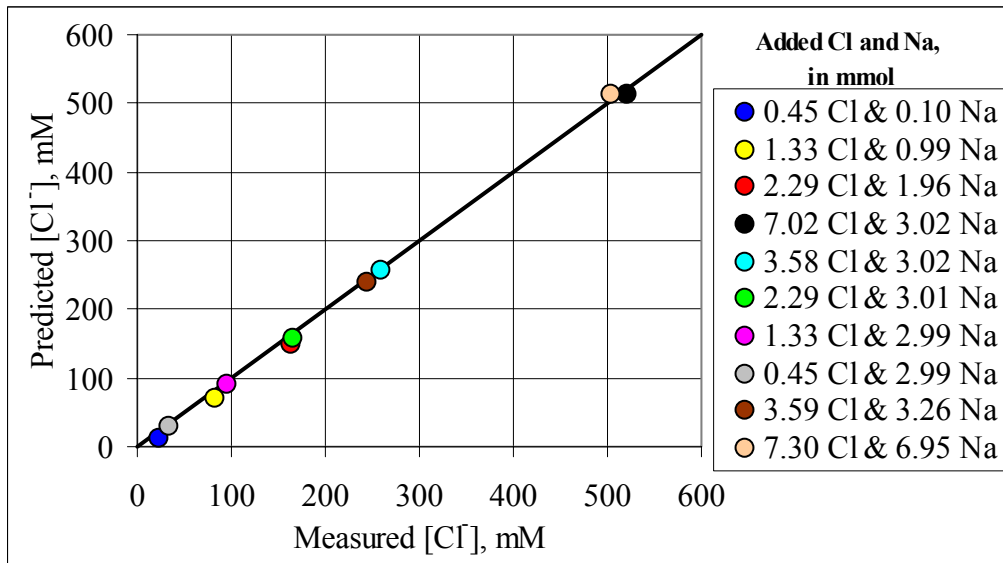
Fig. 3.4: *Comparison between predicted and measured concentration of chlorides in the pore solution of hydrated WPC(4)_10%SF. Adjustments: Al/Ca and S/Ca in C-S-H set to 0.033 and 0.029, respectively, and Rd_0 = 1.0. The line of equality is shown in the figure. Predicted values are 2% higher than the measured (R^2 = 0.99)*
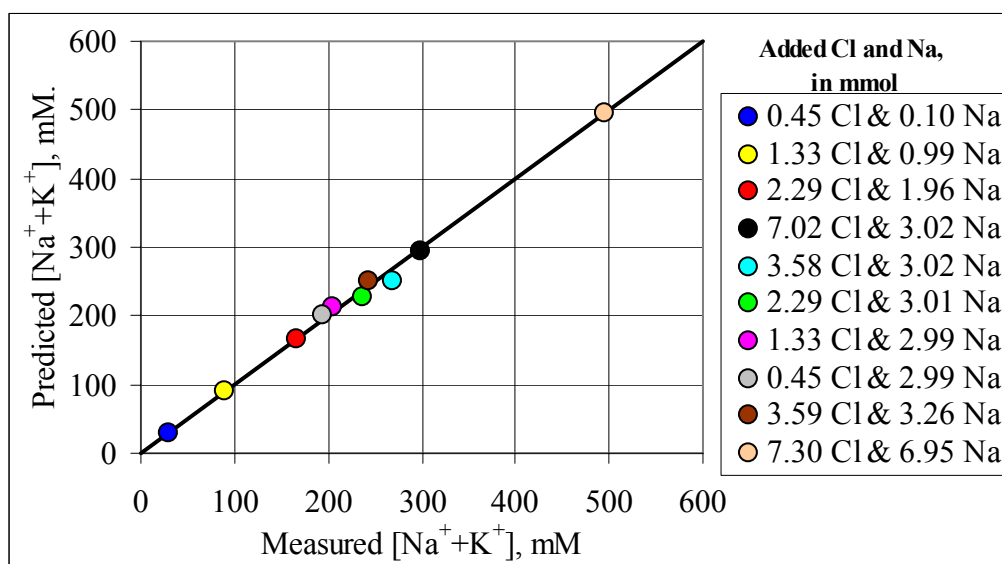
Fig. 3.5: *Comparison between predicted concentration of sodium following the described approach, and the measured on samples of hydrated WPC(4)_10%SF. Adjustments: Al/Ca and S/Ca in C-S-H set to 0.033 and 0.029, respectively, and $Rd_0 = 1.0$. The line of equality is shown in the figure. Predicted values are 1% lower than the measured ($R^2 = 0.99$)*

Excellent agreement between the predicted values and those determined experimentally was found. Thus, the model appears to be applicable to Portland cement pastes with a certain level of replacement by silica fume but it should be noted that major errors can be expected if the addition of silica fume is high enough to use up $Ca(OH)_2$.

3.2   Granulated Blast Furnace Slag

The replacement of Portland cement by 30 mass % very fine (Blaine = 1300 m^2/kg) granulated blast furnace slag (slag) was studied for two different cement types, i.e. WPC(4) and OPC, and these pastes are denoted WPC(4)_30%slag and OPC_30%slag. The experimental procedure is described in **appendix C** and the results from the experiments are presented in **appendix E**.

Fig. 3.6 shows 300 EDS-spot analyses of WPC(4)_30%slag. The Si/Ca and S/Ca ratio appears to be quite well defined at 0.62 and 0.03, respectively. This indicates that the C-S-H in this particular paste is decalcified, which is inconsistent with the presence of $Ca(OH)_2$ in the assemblage and suggests non-equilibrium conditions. The C-S-H appears to be relatively inhomogeneous with respect to the content of alumina (see right-hand figure in **Fig. 3.6**), when comparing the scattering in Al/Ca and S/Ca plots. Furthermore, the Al/Ca is much higher than observed in Portland cement pastes, i.e. at approximately 0.07 or higher. This was not expected as no phase has disappeared allowing an extra degree of freedom. Nevertheless, this must result from non-equilibrium conditions probably due to different hydration rates of slag and cement with very different chemical composition resulting in local zones with different chemical composition. This is dealt with later in this section.
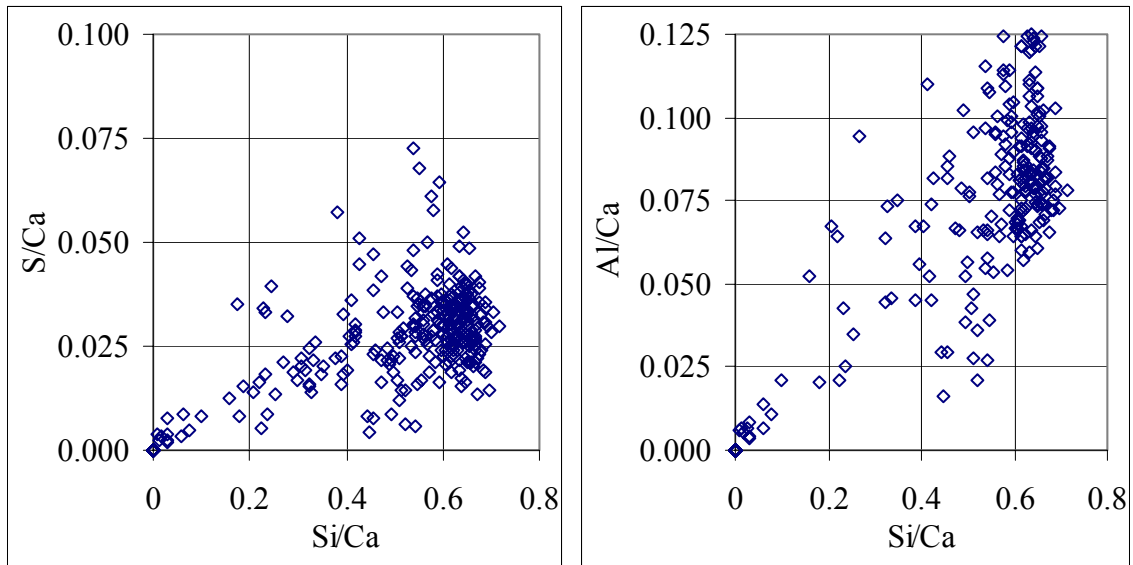
Fig 3.6: *300 EDS-spot analyses on a WPC(4)_30%slag paste. Left-hand figure illustrates S/Ca vs. Si/Ca, whilst right-hand figure illustrates Al/Ca vs. Si/Ca*

The initial distribution ratio for alkalis is affected by the change in composition of the C-S-H. A value of 0.9 for Rd_0 seems to be appropriate when predicting the intersection point of the plots of Rd against chloride content (see **Fig. 3.7**). Again, a change in Rd of ± 0.1 affects the predicted chloride and sodium concentrations by less than 3 %.
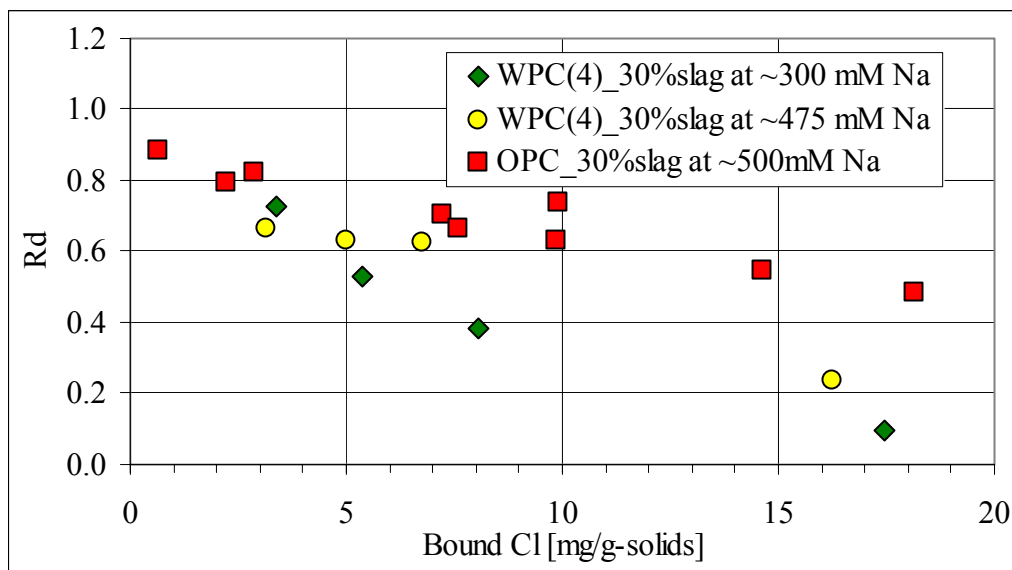
Fig. 3.7: *Rd vs. chloride content in the pastes WPC(4)_30%slag and OPC_30%slag, in different series with nearly constant alkali concentration*

Applying the model described in **section 2.8** to the experimental data for the WPC(4)_30%slag pastes, with the small adjustments mentioned above (see note below the figures), resulted in the correlation curves for chloride and sodium concentrations presented in **Fig. 3.8** and **3.9**, respectively.
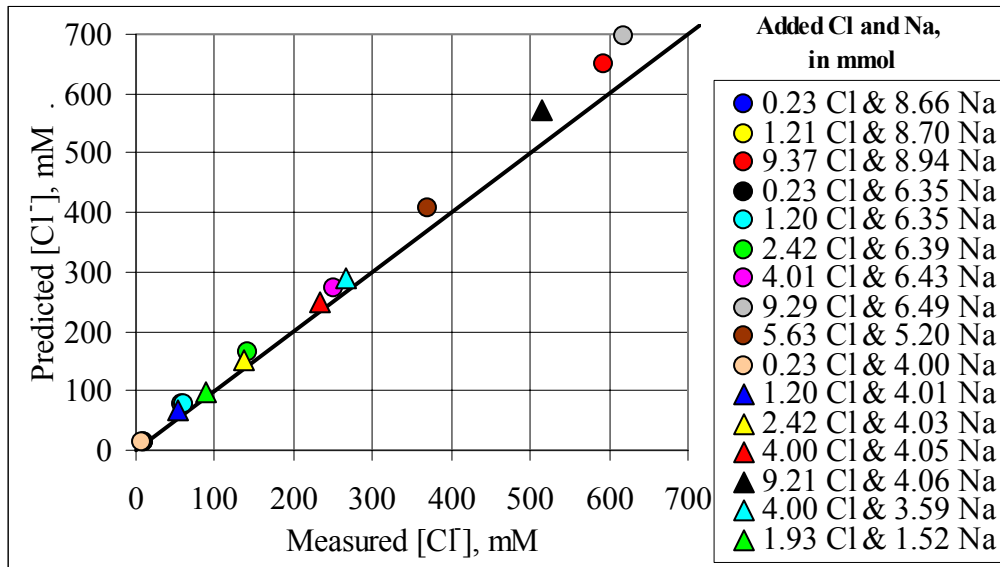
Fig. 3.8: *Comparison between predicted concentration of chlorides following the described approach, and the measured on samples of hydrated WPC(4)_30%slag. Adjustments: Al/Ca in C-S-H set to 0.07, and Rd_0 = 0.9. The line of equality is shown in the figure. Predicted values are 9% higher than the measured (R^2 = 0.99)*
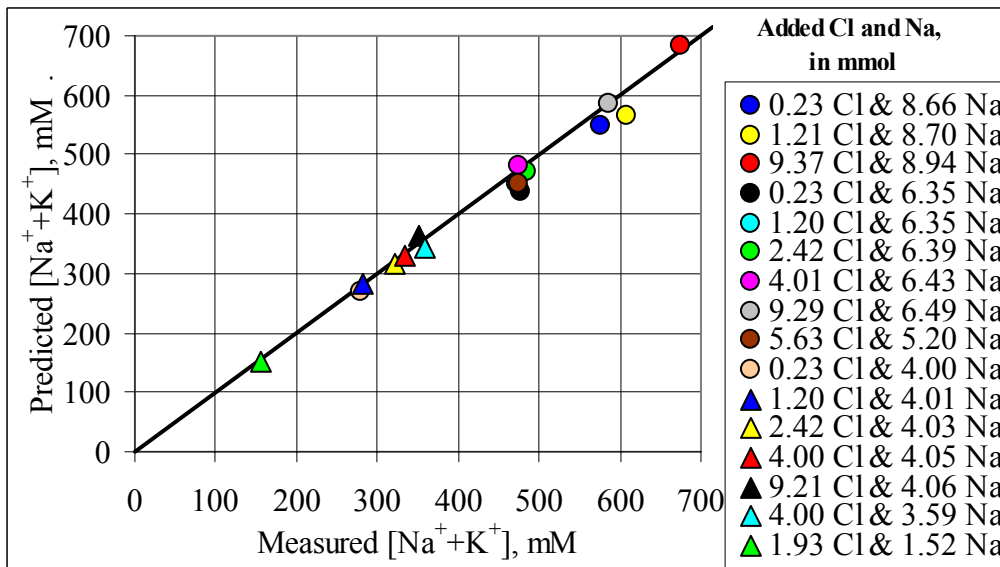
Fig. 3.9: *Comparison between predicted concentration of sodium following the described approach, and the measured on samples of hydrated WPC(4)_30%slag. Adjustments: Al/Ca in C-S-H set to 0.07, and Rd_0 = 0.9. The line of equality is shown in the figure. Predicted values are 2% lower than the measured (R^2 = 0.97)*

Again, good agreement is found between the predicted values and those measured experimentally, even though a significant part of the Portland cement has been replaced by slag. **Fig. 3.10** and **3.11** present similar plots for the OPC_30%slag pastes obtained when applying the same adjustments as for the WPC(4)_30%slag.

The agreement between predicted and measured concentrations is similar to the observed for WPC(4)_30%slag.
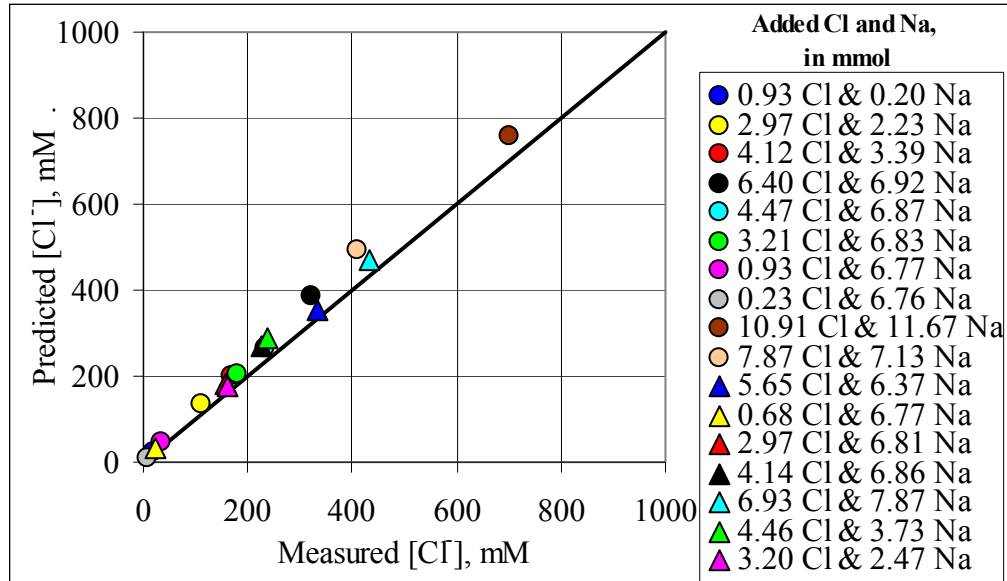
Fig. 3.10: *Comparison between predicted concentration of chlorides following the described approach, and the measured on samples of hydrated OPC_30%slag. Adjustments: Al/Ca in C-S-H set to 0.07, and $Rd_0 = 0.9$. The line of equality is shown in the figure. Predicted values are 10% higher than the measured ($R^2 = 0.96$)*
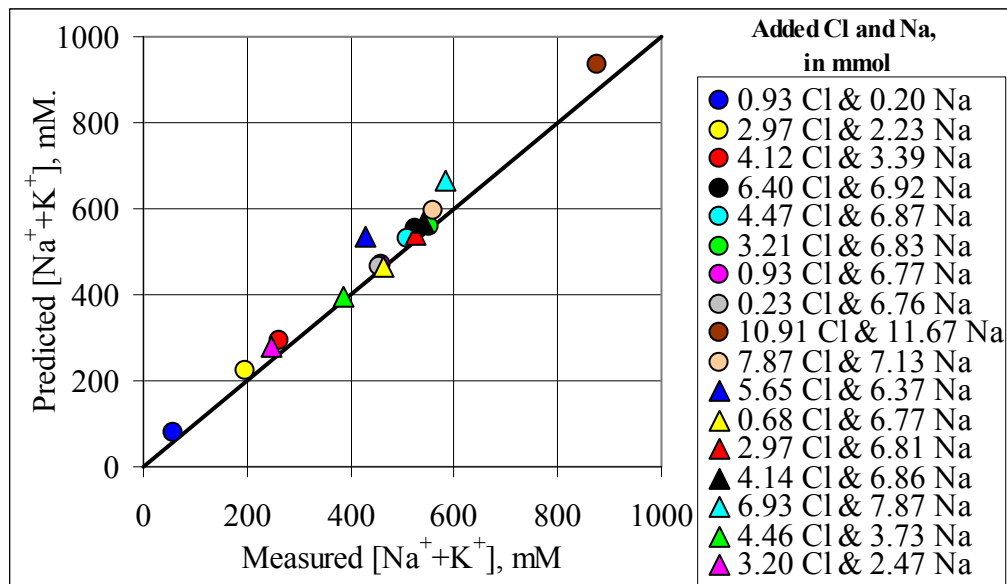

Fig. 3.11: *Comparison between predicted concentration of sodium following the described approach, and the measured on samples of hydrated OPC_30%slag. Adjustments: Al/Ca in C-S-H set to 0.07, and $Rd_0 = 0.9$. The line of equality is shown in the figure. Predicted values are 6% higher than the measured ($R^2 = 0.97$)*

It should be noted that for the previous calculations complete hydration was assumed for the slag and cement in the paste. This is probably not true although the degree of hydration must be fairly high, but was chosen in order to ease the calculations. Good agreement was still found between the predicted and measured values.

The composition of the slag (high content of Al_2O_3 and MgO) may result in some changes in the phase equilibria of the hydrated paste. Mg-silicate gels or hydrotalcite phases may form during the hydration process at very high contents of Mg^{2+} (**Gollop and Taylor [1996]**), but at low or

intermediate contents of Mg^{2+}, unreacted MgO or $Mg(OH)_2$ is likely to be stable (**Taylor and Newbury [1984]**). **Fig. 3.12** shows 300 EDS-spot analyses on a WPC(4)_30%slag plotted in terms of Mg/Ca vs. Al/Ca. A hydrotalcite phase, which basically is composed of alternating layers of $Mg(OH)_2$ and $Al(OH)_3$ (natural mineral has composition $[Mg_{0.75}Al_{0.25}(OH)_2](CO_3)_{0.125}(H_2O)_{0.5}$) would be recognised in such a figure by plots placed along a line with a slope close to 3. This procedure was used in **Gollop and Taylor [1996]** to identify hydrotalcite in slag blended cements.
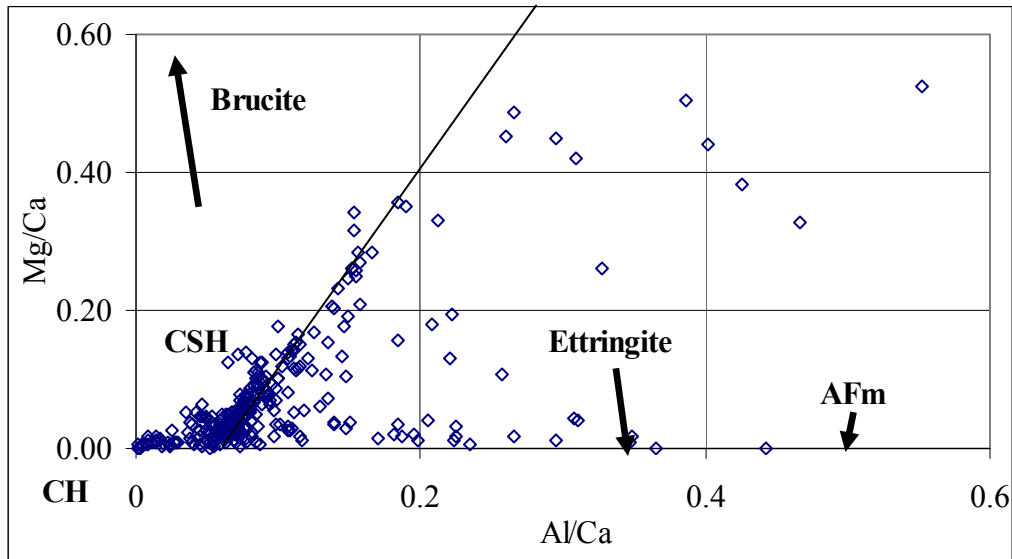
Fig. 3.12: *300 EDS-spot analyses on a WPC(4)_30%slag paste, plotted in terms of Mg/Ca vs. Al/Ca. Plots along the trend line through the composition of the C-S-H with a slope of 3.0 suggest the presence of a hydrotalcite phase*

The plots in **Fig. 3.12** suggest the presence of a hydrotalcite phase with a Mg/Al close to 3 judging from the plots lying along the trend line that crosses the composition of the C-S-H. No plots are located above the trend line, suggesting that no brucite is present in the hydrated assemblage. It is likely that the addition of slag to the cements studied resulted in the formation of a hydrotalcite phase instead of brucite. As the number of phases has not been increased, the number of degrees of freedom in the system is unchanged and can explain why the relations in **Table 2.g** for predicting the binding of chlorides still apply satisfactorily. No trends were found when plotting Mg/Ca vs. Si/Ca, which otherwise would have suggested the presence of a Mg-silicate hydrate phase. By further examination of the sample in the Electron microscope, it was found that the only places where relative high amounts of Mg was detected by EDS-analyses was in small inclusions where it was combined with Al, Si and Ca. This appeared to be unreacted slag grains. Furthermore, a large degree of chemical inhomegeneity was observed over the cross-section of the sample. Unfortunately, no XRD measurements were possible and further comments on this matter are omitted.

Figs. 3.13 present similar plots as those in **Fig. 3.12** but for a WPC(12) paste. This sample has been exposed to a solution initially of 960 mM $MgSO_4$ for 6 months. The concentration of magnesium at the time of examination was approx. 0.5 mM. The total content of MgO in the paste is approximately 3 times higher than that in the WPC(4)_30%slag in **Fig. 3.12**. In contrast to the observation in the paste with 30% slag, the plots do not suggest the presence of a hydrotalcite phase, but brucite instead (i.e. plots above the trend line with slope 3.0). The average Mg/Si ratio at approx. 1.0 for all the EDS-spot analyses corresponded approx. to the expected ratio from the chemical composition and the increased Mg content from the exposure solution, i.e. Mg/Si ratio of 0.9. This suggests that the high w/p ratio allowed the diffusion of Mg^{2+} to the core of the sample, instead of a layering of brucite at the surface of the specimen as observed in e.g. **Glasser [2001]**. Upon further examination of the sample in the Electron

microscope, large crystals of brucite (up to 20 μm) were identified when combined with EDS-analysis. These were distributed over the hole cross-section of the samples, together with gypsum and small amounts of $Ca(OH)_2$.

Based on the compared assemblages, non-equilibrium applies either for the pastes with 30% slag or the presented in **Figs. 3.13**. When noting that the composition of the C-S-H in the pastes with slag replacement differ from all other studied in this investigation, it is most likely that these pastes have not yet reached equilibrium.
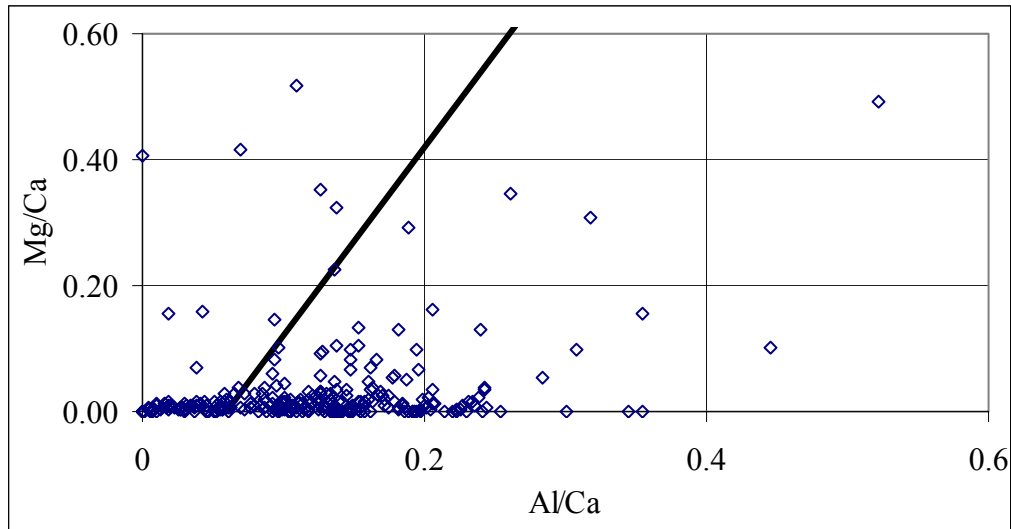
Fig. 3.13: *300 EDS-spot analyses of the WPC(12) paste with approximately 6 mass % MgO from exposure for 6 months to MgSO$_4$*

4 Effect of sulfates on chloride binding

The reaction of sulfates with hydrated Portland cement can easily be included in the model in **section 2.5** by increasing the relative amount of SO_3 in the system. This initially results in a change in the relative contents of AFm and AFt phases, as was illustrated in **Fig. 2.10**. If the source of sulfates is $CaSO_4$ or $(Na/K)_2SO_4$, the cations can be expressed as relative contents of CaO, Na_2O and/or K_2O, and the reactions involving these components was already described in **sections 2.1** to **2.7**. No extra degree of freedom is initially introduced by exposure of a hydrated Portland cement paste to sulfates. In the case where sulfates are introduced as $MgSO_4$, the corresponding amount of added MgO is introduced as an extra component resulting in the formation of brucite (i.e. $Mg(OH)_2$, see final discussion in the previous chapter).

It is therefore possible from the relationships found in **Table 2.g** to predict the phase assemblage in a hydrated Portland cement at any content of chloride and alkali, as well as sulfates, regardless of whether the source is $MgSO_4$, $CaSO_4$ or $(Na/K)_2SO_4$.

A series of one month old WPC(4) and WPC(12) w/p 0.70 pastes (with 1 mass % replacement by calcite) were allowed to react with varying contents $MgSO_4$ at a constant initial content of NaCl, in order to study the effect of sulfates on chloride binding in PC pastes after 5 months of exposure. The experimental procedure is described in **appendix C** and the results obtained are presented in **appendix F**. It should be noted that a single paste specimen of WPC(4) and one of WPC(12) were exposed to much higher contents of $MgSO_4$, corresponding to approx. 12.0 mmol per 8.25 gram paste, but at different combinations of sodium and chloride (see **appendix F**).

The model in **section 2.8** was used to calculate the composition of the pore solution at equilibrium. The concentrations of chloride predicted by the model against those determined experimentally are shown in **Fig. 4.1**, and the predicted alkali concentrations against the experimentally obtained concentrations are shown in **Fig. 4.2**. For each of the series of pastes, additions of $MgSO_4$ up to 1.25 mmol did not lead to the formation of gypsum, but only to the formation of more ettringite at the expense of AFm phases. The composition of the C-S-H and other minerals in the assemblage remained constant. Gypsum was only observed to form at additions of 12.0 mmol $MgSO_4$. In this particular case, the S/Ca molar ratio in the C-S-H increased from approx. 0.03 to 0.10. This suggests that at the point where the last AFm phase disappears, the resulting degree of freedom allows for the incorporation of more SO_3 in the C-S-H until approx. S/Ca 0.10 (this corresponds to the univariant conditions applying where the pore solution changes composition from "b" to "a" in the more simple system in **Fig. 2.9**, right after monosulfate is used up). Thereafter, gypsum is formed at the expense of portlandite, and the degree of freedom disappears (until of course all the $Ca(OH)_2$ is used up). **Table 4.a** shows the possible phase assemblages in the SiO_2-Al_2O_3-SO_3-Fe_2O_3-CaO-MgO-Na_2O-CO_2-$CaCl_2$-NaCl-H_2O system (note that NaCl is added to the components as it was described in **section 2.7** that the presence of chlorides and alkalis required the definition of a new component, besides $CaCl_2$ and Na_2O, to describe the phase assemblage) expected from the findings so far in this investigation, upon progressive addition of SO_3 to an assemblage initially consisting of C_4AH_{13}, monosulfate and a solid solution of Friedel's salt and monocarbonate. **Fig. 4.3** illustrates this process on the ternary subsystems C_3A-$CaSO_4$-$CaCO_3$ and C_3A-$CaSO_4$-$CaCl_2$. The S/Ca in the C-S-H is allowed to increase from assemblage 3 to 4.
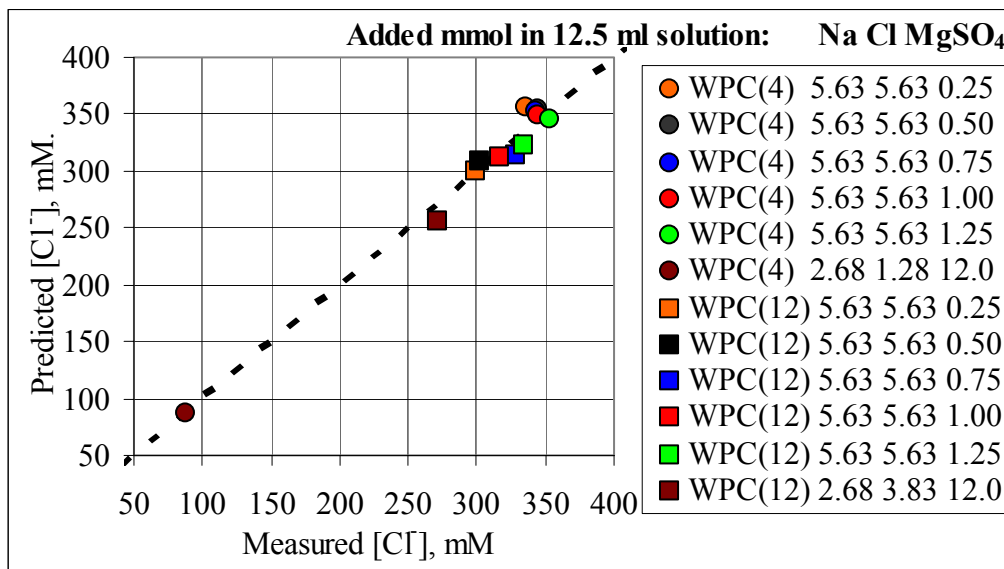
Fig. 4.1: *Comparison between predicted chloride concentrations by applying the model in* **section 2.8** *and those measured experimentally, at varying additions of MgSO₄. Legends indicate amount of Na, Cl and MgSO₄ (in mmol) dissolved in 12.5 ml exposure solution. Adjustment: for the two samples exposed to 12 mmol MgSO₄, S/Ca in C-S-H set to 0.10, and model corrected for formation of thaumasite (see* **Table 4.e and Fig. 4.4***).* R^2 *value at 0.98*
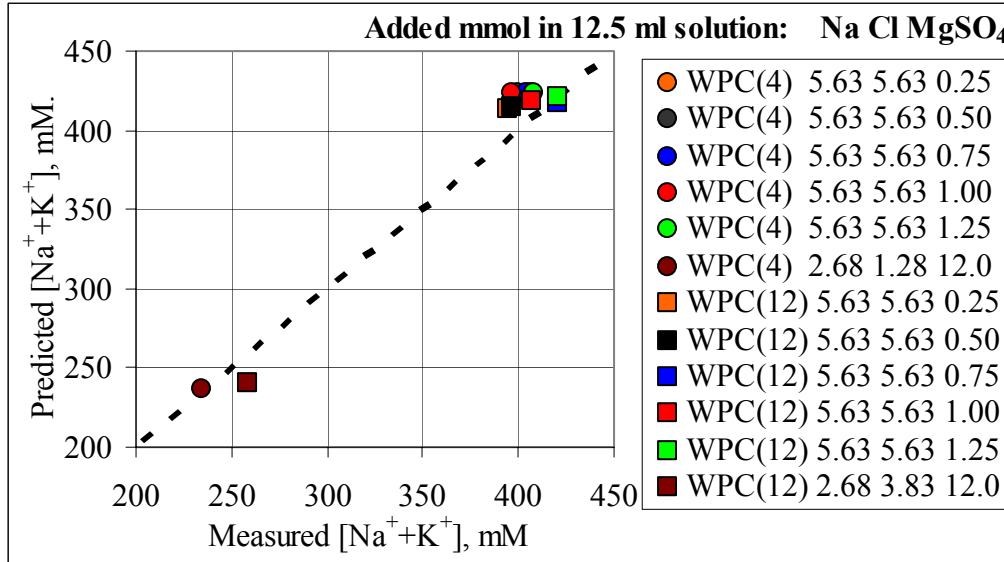
Fig. 4.2: *Comparison between predicted alkali concentrations by applying the model in* **section 2.8** *and those measured experimentally, at varying additions of MgSO₄. Legends indicate amount of Na, Cl and MgSO₄ (in mmol) dissolved in 12.5 ml exposure solution. Adjustment: for the two samples exposed to 12 mmol MgSO₄, S/Ca in C-S-H set to 0.10, and model corrected for formation of thaumasite (see* **Table 4.e and Fig. 4.4***) .* R^2 *value at 0.97*

Table 4.a: *Expected phase assemblages in hydrated Portland cement pastes containing CO_2 exposed to chlorides and sulfates. System SiO_2-Al_2O_3-SO_3-Fe_2O_3-CaO-MgO-Na_2O-CO_2-$CaCl_2$-NaCl-H_2O, based on* **Figs. 2.10** *and* **2.11** *and findings in* **section 2.6** *and* **2.7**

No.	Phases in the subsystem C_3A-$CaSO_4$-$CaCO_3$-$CaCl_2$	Phases in excess	Degrees of freedom
1.	C_4AH_{13} + monosulfate, + Friedel's salt – monocarbonate solid solution		3
2.	monosulfate + ettringite + Friedel's salt – monocarbonate solid solution	C-S-H CH FH$_3$ MH Pore solution	3
3.	ettringite + calcite + Friedel's salt – monocarbonate solid solution		3
4.	Friedel's salt + ettringite + calcite + gypsum		2
5.	Friedel's salt + calcite + gypsum		3
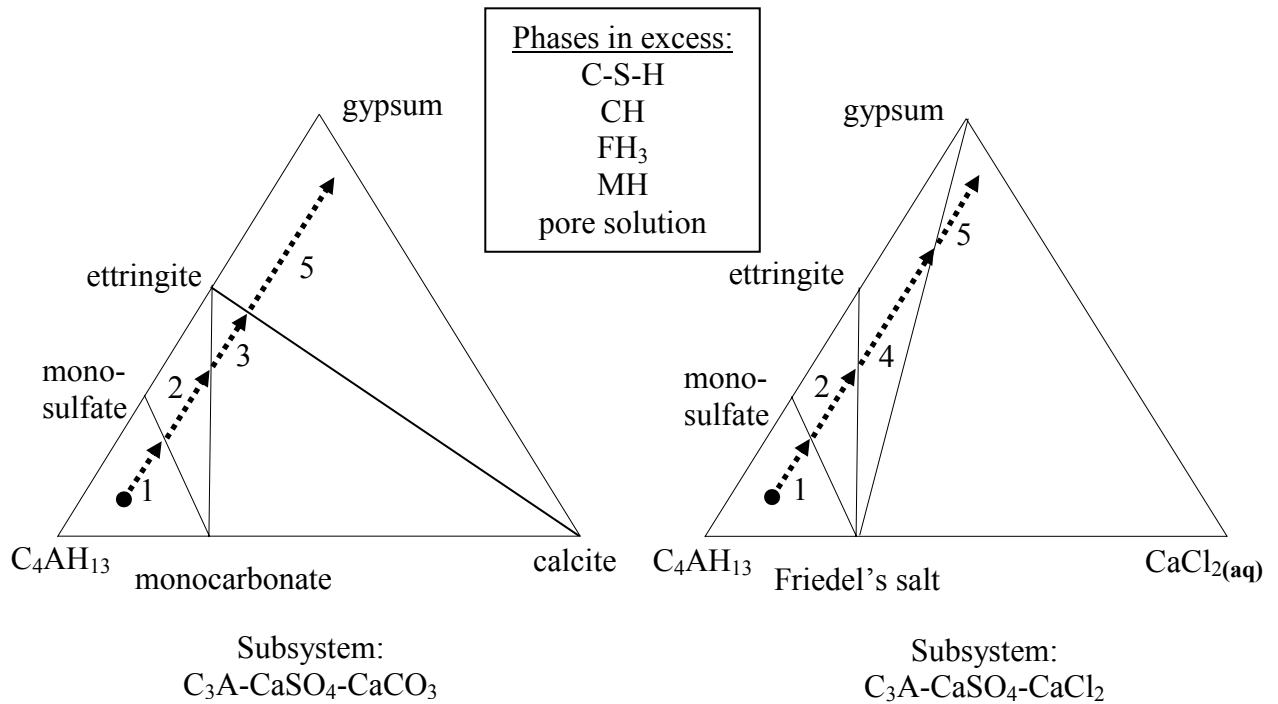
Fig. 4.3: *Illustration of the expected development of the phase assemblage upon addition of SO_3 to an assemblage initially consisting of C_4AH_{13}, monosulfate and a solid solution between Friedel's salt in the ternary subsystems C_3A-$CaSO_4$-$CaCO_3$ (left-hand) and C_3A-$CaSO_4$-$CaCl_2$ (right-hand). Numbers in the figures indicate the corresponding assemblage in* **Table 4.a**. *(Note: this figures are revised later in this section)*

For the lower additions of $MgSO_4$, the predicted assemblage was compared to the measured Cl/Ca ratio in the monocarbonate-Friedel's salt solid solution phase. **Table 4.b** shows the predicted assemblage of sample "WPC(12) 5.63 5.63 0.75" (corresponding to a WPC(12) paste exposed to 12.5 ml solution containing 5.63 mmol Na, 5.63 mmol Cl and 0.75 mmol $MgSO_4$) and the EDS-measurements plotted in terms of Cl/Ca vs. Al/Ca, for comparison between

predicted and measured Cl/Ca molar ratio in the solid solution phase. The good correlation found shows that the model in **section 2.8** can be used directly to predict the stable assemblage in Portland cement pastes exposed to sulfates.

Table 4.b: *Predicted Cl/Ca in solid solution phase of assemblage "WPC(12) 5.63 5.63 0.75" (5.63 mmol Na, 5.63 mmol Cl and 0.75 mmol $MgSO_4$ dissolved in 12.5 ml solution) against measured by EDS-analyses*

	mass %
C-S-H	**52.6**
CH	**14.8**
goethite	**0.1**
brucite	**1.3**
pore solution	**17.7**
calcite	**0.7**
ettringite	**5.7**
monocarbonate	**4.5**
Friedel's salt	**2.6**

Figure: Plot of Cl/Ca versus Al/Ca. Legend: ● Monosulfate/monocarbonate, ▲ Ettringite, ■ FS. Data points (open diamonds) trend upward to an "Estimated Cl/Ca" point (red dot) near Al/Ca = 0.5, Cl/Ca ≈ 0.19.
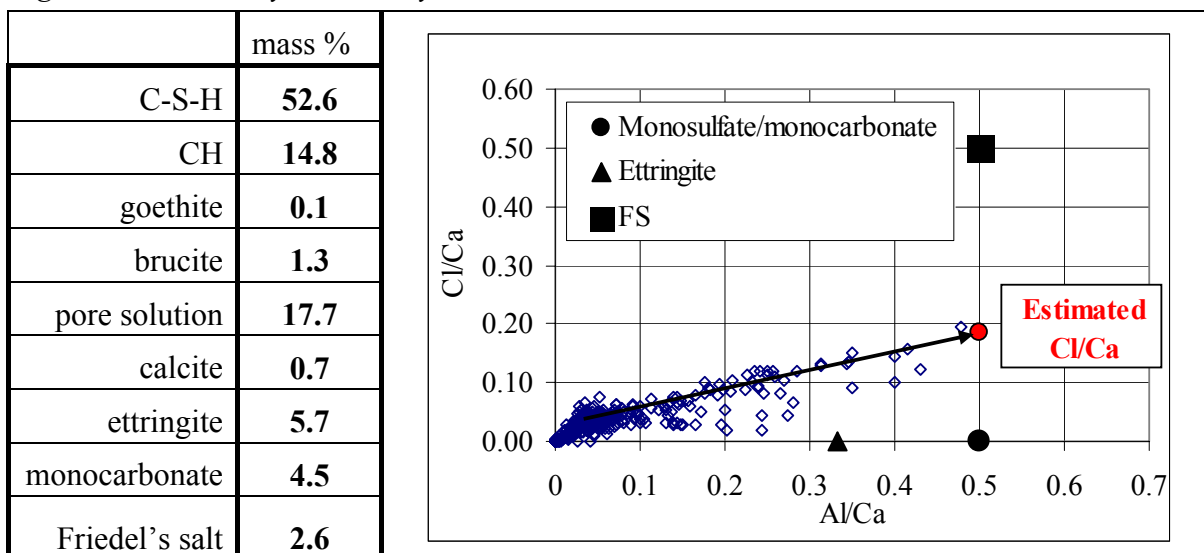
Hussain and Rasheeduzzafar [1994] reported a decreased chloride binding capacity in Portland cement pastes upon addition of sulfates. This is in agreement with the observations in **Fig. 4.1**, although more pronounced for the WPC(12) series than WPC(4). The decreased binding capacity by the pastes is due to the decreased amount of AFm phases able to bind chlorides, as these are converted to ettringite instead. Chloride bound initially by AFm phases will progressively be released upon addition of sulfates. The binding capacity of WPC(12), with a high content of Al_2O_3, is therefore affected more by the addition of sulfates than WPC(4) which has a lower content of Al_2O_3. The C-S-H appears to have the same binding capacity as that found in **Fig. 2.8**.

The observed behaviour found by **Xu [1997]** among others, that the addition of Na_2SO_4 results in a larger decrease in the chloride binding capacity of Portland cement pastes than $CaSO_4$, is solely due to the addition of alkalis to the paste, which increases the amount of free chloride in the pore solution (as was shown in **section 2.7**). **Table 4.c** compares the predicted assemblage in "WPC(4) 2.68 1.28 12.0" with the results of EDS-analyses (see **Table 4.d** for the predicted assemblage in "WPC(12) 2.68 3.83 12.0" and EDS-plots). It is observed that no AFm phases are present (not even Friedel's salt) and that there is a minor amount of ettringite compared to that of gypsum. Furthermore, C-S-H is still present with a composition similar to the described earlier in the thesis but with a higher content of SO_3. $Ca(OH)_2$ has not yet been used up (i.e. many more plots tending towards point (0,0) in the figure than can the explained by the content of $CaCO_3$, which also is plotted at the same coordinates). This suggests that Friedel's salt cannot coexist with gypsum, and therefore, any bound chloride when gypsum is present as a stable phase in the assemblage must be exclusively bound by the C-S-H. This suggests further that Al_2O_3 found as ettringite cannot react with chloride to form Friedel's salt. Furthermore, the possible phase assemblages in a PC system with CO_2 were assumed not to include Thaumasite ($3CaO.SiO_2.SO_3.CO_2.15H_2O$) at 20^oC. However, this phase was clearly indicated by EDS-analyses on WPC(12) at 12 mmol $MgSO_4$. The phase diagram in **Fig. 2.10** is therefore replaced by that in **Fig. 4.4** (from **Juel[2003]**). Note that MgO has been added, which is assumed to form MH (i.e. brucite).

Table 4.c: *Predicted assemblage in "WPC(4) 2.68 1.28 12.0" supported by EDS-analyses*

	mass-%
C-S-H	**49.0**
CH	**10.3**
goethite	**0.2**
brucite	**7.8**
pore solution	**10.1**
gypsum	**16.0**
ettringite	**2.7**
thaumasite	**4.0**
Friedel's salt	**0.0**
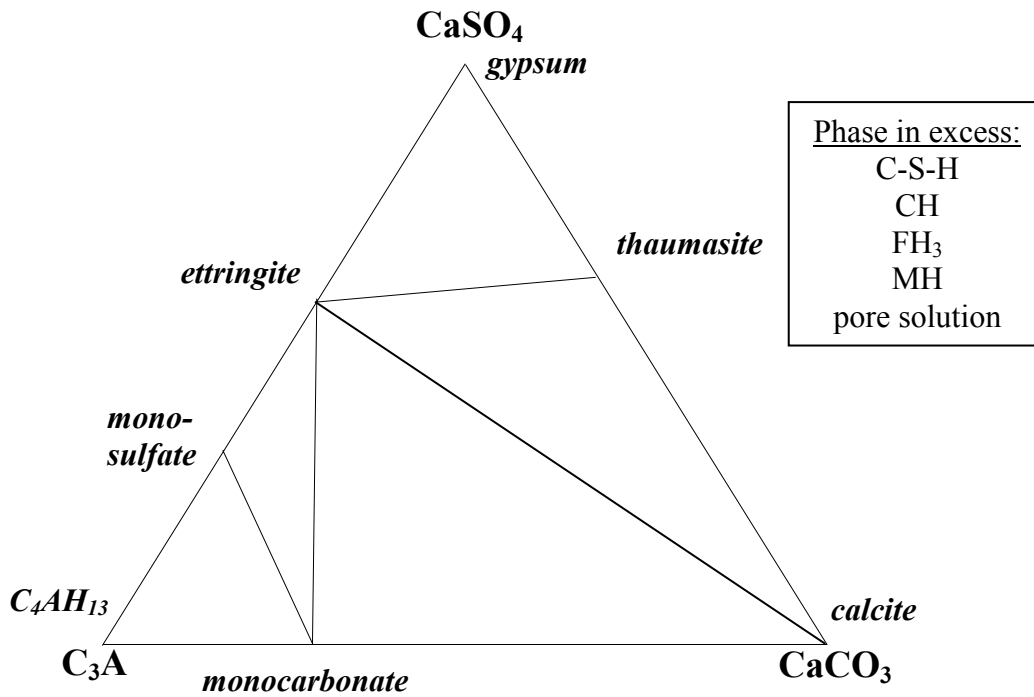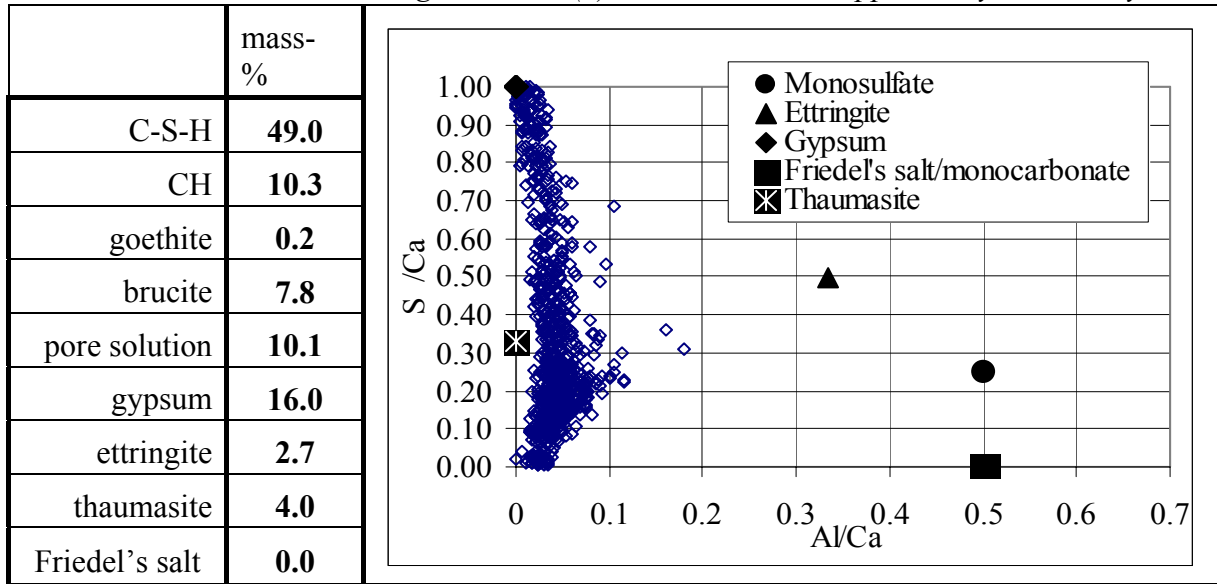
Fig. 4.4: *Phase diagram applying for the system CaO-SiO_2-Al_2O_3-SO_3-Fe_2O_3-CO_2-MgO-H_2O at $20^{o}C$ after Juel [2003].*

Table 4.d: *Predicted assemblage in "WPC(12) 2.68 3.83 12.0" supported by EDS-analyses*

	mass-%
C-S-H	**40.7**
CH	**5.8**
goethite	**0.1**
brucite	**7.3**
pore solution	**13.4**
gypsum	**7.9**
ettringite	**17.5**
thaumasite	**7.3**
Friedel's salt	**0.0**

Based on the observations in this section, the subsystem C_3A-$CaSO_4$-$CaCl_2$ dealt with earlier in the report appears to require some corrections. This is shown in **Fig. 4.5** where the diagram to the right is consistent with the incompatibility of Friedel's salt and gypsum. Although, more samples at increasing contents of sulfate and different levels of chloride addition should be tested to properly verify this.
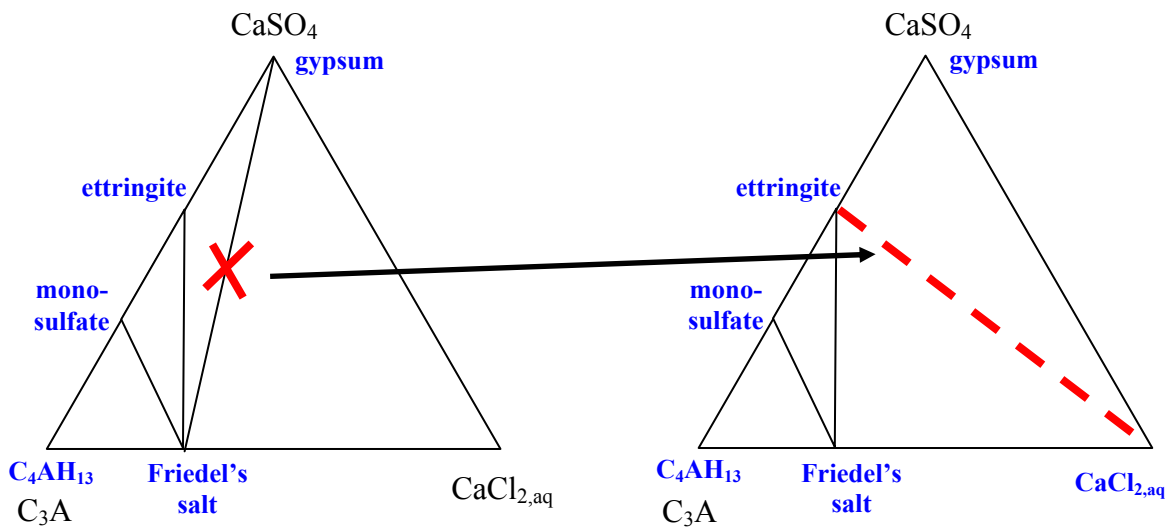
Fig. 4.5: *Illustration of the incompatibility in the initially proposed phase diagram for the C_3A-$CaSO_4$-$CaCl_2$ subsystem (left-hand side), and proposed phase diagram to account for the observed behaviour (right-hand side)*

Summarising the findings in this section, the possible phase assemblages found in a hydrated Portland cement paste exposed to chloride and sulfates are listed in **Table 4.e**. The relationships shown in **Table 2.g** still apply for the system when predicting the phase equilibria at varying contents of alkalis and chlorides.

Table 4.e: *Corrected phase assemblages in hydrated Portland cement pastes containing CO_2, exposed to chlorides and sulfates at 20^oC. System SiO_2-Al_2O_3-SO_3-Fe_2O_3-CaO-MgO-Na_2O-CO_2-$CaCl_2$-NaCl-H_2O*

No.	Phases in the subsystem C_3A-$CaSO_4$-$CaCO_3$-$CaCl_2$	Phases in excess	Degrees of freedom
1.	C_4AH_{13} + monosulfate + Friedel's salt – monocarbonate solid solution		3
2.	monosulfate + ettringite + Friedel's salt – monocarbonate solid solution	C-S-H	3
3.	ettringite + calcite + Friedel's salt – monocarbonate solid solution	CH FH_3 MH	3
4.	Friedel's salt + ettringite + calcite	Pore solution	3
5.	ettringite + calcite + thaumasite		3
6.	ettringite + thaumasite + gypsum		3

5   Phase equilibria in 25 year old Portland cement paste

During the project, the author had the chance to examine the phase equilibria in approximately 25 year old Portland cement pastes (w/p=0.60): a single limewater cured white Portland cement and two rapid hardening grey Portland cements exposed to 5 and 10 % NaCl solutions. The cross-section of the samples were approx. 3 x 5 mm. The composition of the white cement is the same as WPC(4) with only minor differences (i.e. same product from same manufacturer). The rapid hardening Portland cement had a composition similar to that given in **Table 5.a**. The content of CO_2 in the paste corresponded to approximately 1.0 mass % of cement (determined by TG-1000°C after 25 years).

Table 5.a: *Composition of the rapid hardening Portland cement in the 25 year old pastes*

SiO₂	Al₂O₃	Fe₂O₃	CaO	MgO	SO₃	K₂O	Na₂O	Na₂Oₑq	Cl
20.6	4.6	3.6	63.6	0.9	3.2	0.54	0.28	0.64	0.02

Although it is reported in the literature that the structure and composition of the C-S-H phase may change with time it is uncertain exactly how long this takes and the precise nature of the final stable phase. **Fig. 5.1** and **5.2** show 900 EDS-plots on the white Portland cement hydrated for 25 years, expressed in terms of S/Ca vs. Si/Ca and Al/Ca vs. Si/Ca, respectively, compared to a w/p 0.70 WPC(4) paste hydrated for 6 months. It is clearly observed that the Si/Ca ratio in the C-S-H is even closer to that assumed for the proposed thermodynamic model in this study, i.e. Si/Ca of 0.57, which again corresponds to a Ca/Si ratio of 1.75, as reported by several workers in the literature (e.g. **Famy et al. [2002]** and **Richardson [2000]**). The S/Ca ratio, however, has reduced from approx. 0.03 to 0.02, whilst the Al/Ca ratio in the C-S-H seems to have increased from approx. 0.04 to 0.05.
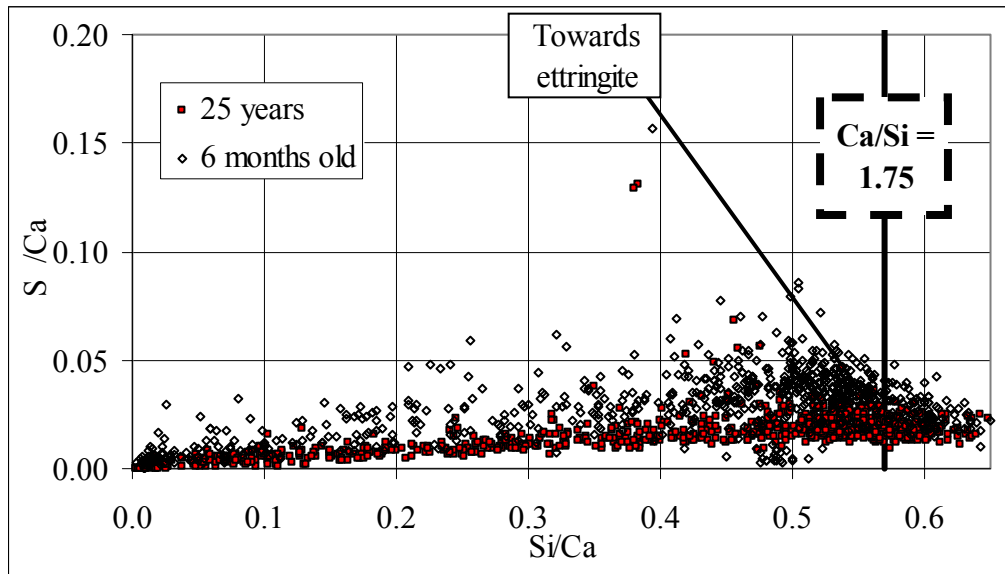
Fig. 5.1: *EDS-plots illustrating the difference in C-S-H composition in a white Portland cement at two maturities: 6 months (w/p = 0.70) and 25 years (w/p = 0.60). The composition is expressed in terms of S/Ca vs. Si/Ca*
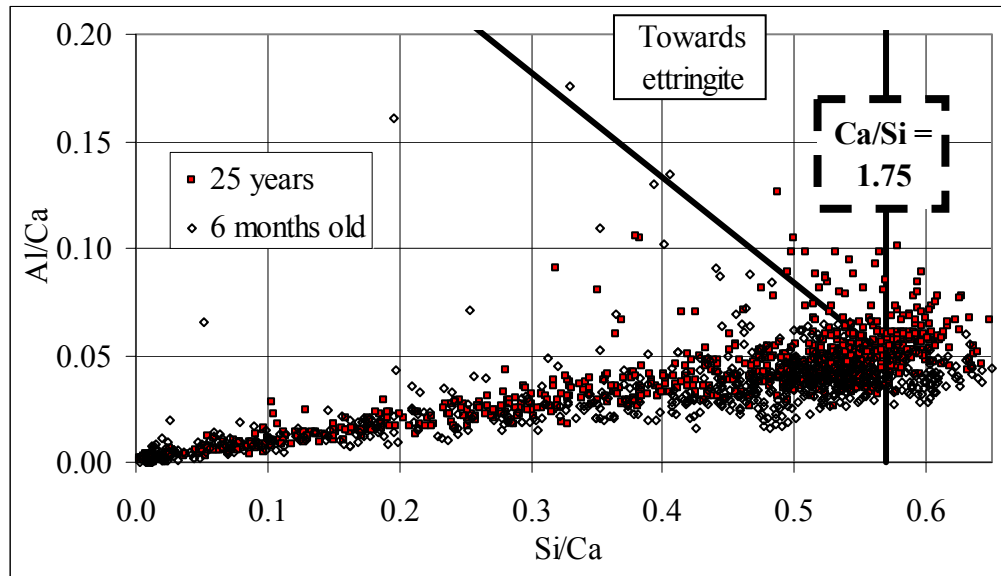
Fig. 5.2: *EDS-plots illustrating the difference in C-S-H composition in a white Portland cement at two maturities: 6 months (w/p = 0.70) and 25 years (w/p = 0.60). The composition is expressed in terms of Al/Ca vs. Si/Ca*

The predicted assemblages for the two white PC pastes at 6 months and 25 years (correcting for Al/Ca and S/Ca) include 1.1 and 0.5 vol-% ettringite, respectively. As only a few points tend toward the composition of ettringite, the air voids were examined for ettringite (significant amount of ettringite was observed to form in air voids by among others **Juel [2003]**) but without success. The reduced amount of SO_3 contained in the C-S-H at 25 years of maturity could imply a larger content of a sulfur-containing phase; and the most likely candidate would have been ettringite. However, upon chemical analysis of the powder, the total S/Si content was compared between the samples and showed that the 25 year old sample contained half as much SO_3 as the 6 months old, explaining the observed discrepancy in the figures: sulfur has leached from the 25 year old sample to the surrounding curing water, resulting in univariant conditions because of the undersaturation of the C-S-H phase with respect to sulphur, which can also explain the increase in Al_2O_3 of the C-S-H. This illustrates how easy incorrect conclusions could have been drawn.

The composition of the C-S-H in the grey PC paste exposed to 10% NaCl for 25 years was compared to an OPC paste at w/p 0.70 with a similar fraction of Friedel's salt in the solid solution phase. **Fig. 5.3** compares the two samples in terms of S/Ca vs. Si/Ca. It is observed that the S/Ca and Si/Ca ratio in the C-S-H of the two samples is similar, which suggests that the C-S-H reaches a stable composition already after 6 months of hydration (at least for the w/p-ratios studied). The same was observed when comparing the composition of the C-S-H in terms of Al/Ca vs. Si/Ca.
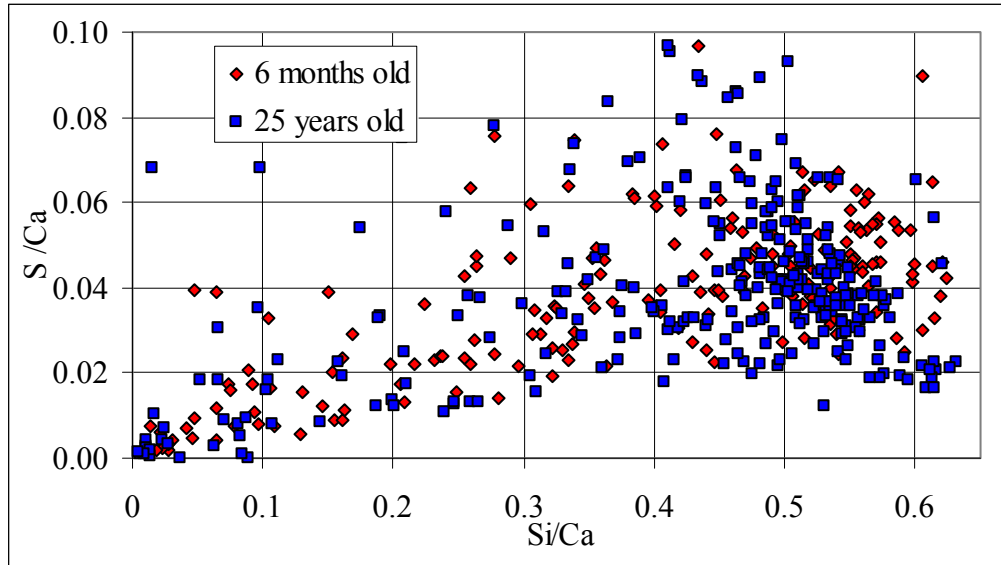
Fig. 5.3: *EDS-plots showing the composition of the C-S-H in the 6 months OPC paste (w/p=0.70) and the grey PC paste (w/p=0.60) exposed to 10% NaCl for 25 years. The composition is expressed in terms of S/Ca vs. Si/Ca*

As a first approximation, the model in **section 2.8** was used without any correction to predict the assemblage in the two w/p 0.60 chloride exposed 25 year old pastes of rapid hardening Portland cement. The concentration of Na and Cl in the exposure solution was measured, and the chloride and sodium contents of the cement paste were increased in the model until the predicted concentrations of Na and Cl were the same values as the measured. Then the measured Cl/Ca molar ratio in the solid solution phase and the measured total chloride content in the paste were compared with those predicted by the model.

Table 5.b: *Predicted phase assemblage and Cl/Ca vs. Al/Ca EDS-plots, for a w/p 0.60 Rapid-hardening Portland cement paste exposed to approx. 5 % NaCl for 25 years. Chloride and sodium have been added in the model until a [Cl⁻] of 927 mM and a [Na⁺] of 849 mM was reached, which were the concentrations determined experimentally in the surrounding exposure solution. **The measured chloride content of the paste was 1.70 mass %, against a predicted content of 1.80 mass%.** Remember that monocarbonate and Friedel's salt are present as a solid solution*

	mass %
C-S-H	49.6
CH	17.5
goethite	2.4
brucite	0.8
pore solution	14.5
calcite	0.8
ettringite	5.5
monocarbonate	3.3
Friedel's salt	5.6
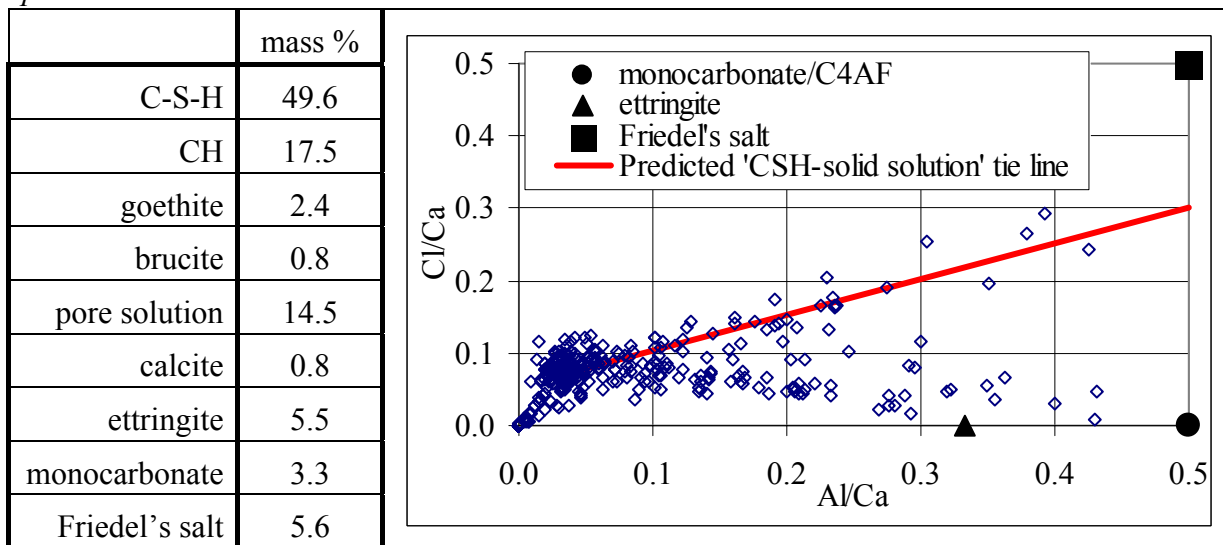
Table 5.b shows the predicted phase assemblage of the paste exposed to approx. 5% NaCl, as well as the predicted and experimentally determined Cl/Ca ratios in the solid solution phase. All

relevant predicted and measured properties of the paste are provided. **Table 5.c** shows the corresponding values for the paste exposed to approx. 10% NaCl.

Table 5.c: *Predicted phase assemblage and Cl/Ca vs. Al/Ca EDS-plots, for a w/p 0.60 Rapid-hardening Portland cement paste exposed to approx. 10 % NaCl for 25 years. Chloride and Sodium have been added in the model until a [Cl⁻] of 1875 mM and a [Na⁺] of 1736 mM was reached, which were the concentrations determined experimentally in the surrounding exposure solution.* **The measured chloride content of the paste was 2.60 mass %, against a predicted content of 2.53 mass%.** *Remember that monocarbonate and Friedel's salt are present as a solid solution*

	mass %
C-S-H	49.6
CH	17.5
goethite	2.4
brucite	0.8
pore solution	14.4
calcite	0.8
ettringite	5.5
monocarbonate	3.2
Friedel's salt	5.7
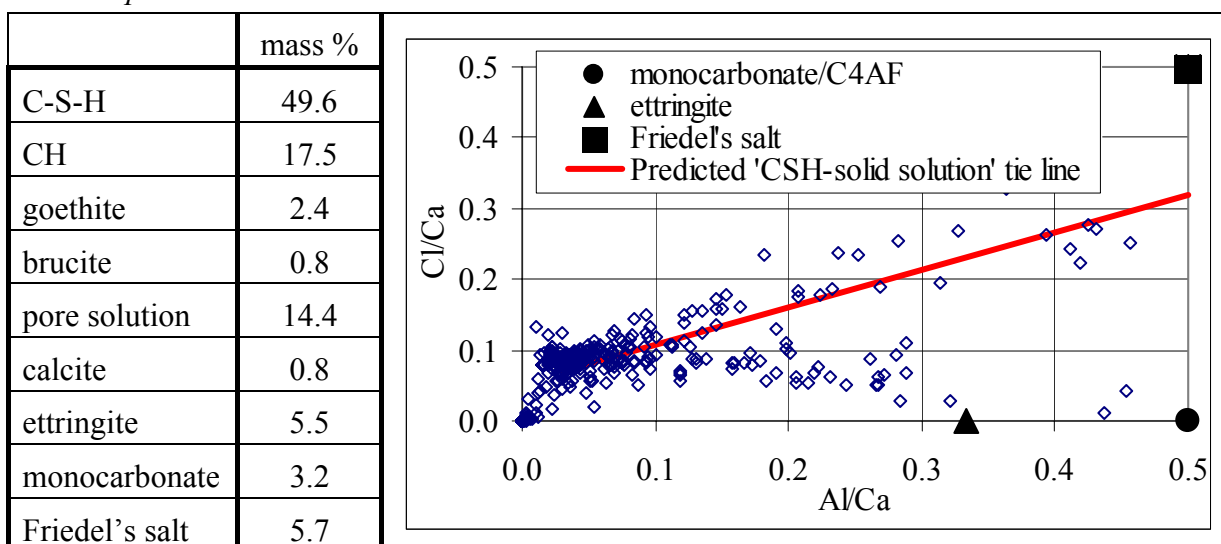
Both predicted Cl/Ca ratios in the solid solution phase and total chloride contents are in good agreement with the measured values. It is therefore concluded that the composition of the C-S-H after 25 years of hydration is similar to that after 6 months. The model in **section 2.8** succeeds in predicting the phase assemblage in the 25 year old pastes exposed to NaCl, indicating the long-term applicability of the model.

Note that the reason why the Cl/Ca ratio in the solid solution phase of the samples described in **Table 5.b** and **5.c** are so similar even though the concentration of chlorides in the exposure solution is very different is due to the large difference in sodium concentration.

For the EDS-plots shown in **Table 5.b** and **5.c** a few points tend towards the intersection point (0.5,0.0). This is not in agreement with the predicted assemblages in the tables, as monocarbonate is not present as an end-member phase, but instead as the solid solution phase with Friedel's salt. The composition at the mentioned intersection point also corresponds to that of unhydrated C_4AF, but also to that of monosulfate. In order to examine if C_4AF could be present in the assemblage of a 25 year old paste, the data was plotted in terms of Fe/Ca vs. Al/Ca, as shown in **Fig. 5.4** for the rapid hardening Portland cement paste exposed to 5% NaCl. Any clear trend of the data towards the intersection point (0.5,0.5) on that figure could be related to the presence of unhydrated C_4AF, which is undoubtedly observed in **Fig. 5.4**. The coloured, circles correspond to all the measured points with Al/Ca > 0.1 and Cl/Ca < 0.1 (i.e. tending toward the composition of ettringite and intersection point (0.5,0.0) in the figure in **Table 5.b**. It is observed in **Fig. 5.4** that these points tend towards either ettringite or the composition of C_4AF, which it is why it is not possible to exclude the possibility of unhydrated C_4AF being present in the examined paste even after 25 years of hydration. Unfortunately, there was not enough material to carry out XRD measurements to verify the above.
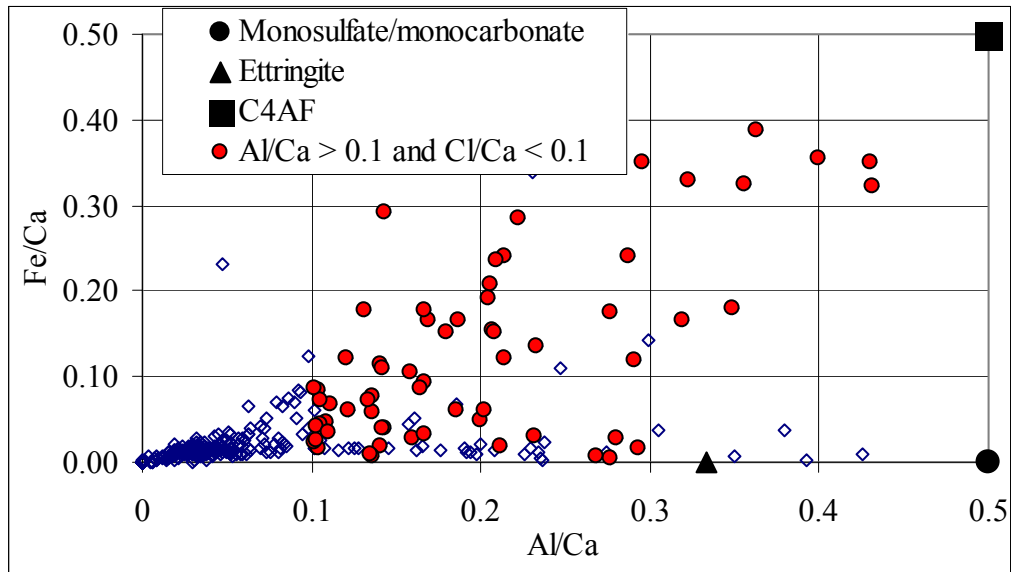
Fig. 5.4: *Fe/Ca vs. Al/Ca plot of the EDS-data for the w/p 0.60 25 year old rapid hardening Portland cement paste exposed to 5% NaCl, showing the presence of unhydrated C_4AF in the paste. Coloured, round plots correspond to points with Al/Ca > 0.1 and Cl/Ca < 0.1.*

6 Ingress of ions in hydrated Portland cement

The purpose of this section is to include the model described in **section 2.8** as part of a Finite Difference Model for simulating the ingress of chlorides in cement based materials. The FDM used is based on the model developed by **Truc [2000]** and the phase assemblage can now be predicted at each time and depth increment. Furthermore, the composite theory is applied at predicting the effective diffusion coefficients for the different ions in solution as a function of the predicted phase assemblage to avoid experimental calibration of the material dependent parameters.

6.1 Diffusion in multi-species solutions

The flux of a species "i" in a multi-species solution where no electrical field is applied can be described from the Nernst-Planck system of equations (**Truc [2000]**),

$$J_i(x,t) = -D_i \cdot \left(\frac{\partial c_i(x,t)}{\partial x} + z_i c_i(x,t) \frac{F}{RT} E(x,t) + \frac{c_i(x,t)}{\gamma_i(x,t)} \frac{\partial \gamma_i(x,t)}{\partial x} \right) \qquad \text{eq. 6.1}$$

where

$$
\begin{array}{ll}
J_i & \text{flux in mol / (m}^2\text{ s)} \\
D_i & \text{intrinsic diffusion coefficient of species i (m}^2\text{/s)} \\
c_i & \text{concentration of species i in solution (mol/m}^3\text{)} \\
\gamma_i & \text{activity coefficient of species i} \\
z_i & \text{valence number of species i} \\
T & \text{temperature (K)} \\
x & \text{depth (m)} \\
t & \text{time (s)} \\
F & \text{96484.6 (C/mol)} \\
R & \text{8.3143 (J/(mol K))}
\end{array}
$$

$E(x,t)$ is the electrical field, defined as follows (**Truc [2000]**)

$$E(x,t) = \frac{RT}{F} \frac{-\sum_i z_i D_i \frac{\partial c_i(x,t)}{\partial x}}{\sum_i z_i^2 D_i c_i(x,t)} \qquad \text{eq. 6.2}$$

The effect of the activity coefficient of the species in solution on the transport of ions, within the range of concentrations observed in concrete, is still not entirely known. Some authors (e.g. **Truc [2000]** and **Tang [1999]**) conclude from their investigations that it has negligible effect, while others consider it to have paramount effect (e.g. **Samson et al. [2001]**). In the following sections, the activity coefficients are set at 1 primarily because the concentrations of ions studied in this investigation are not high. **Eq. 6.1** can therefore be reduced to

$$J_i(x,t) = -D_i \cdot \left(\frac{\partial c_i(x,t)}{\partial x} + z_i c_i(x,t) \frac{F}{RT} E(x,t) \right) \qquad \text{eq. 6.3}$$

The intrinsic diffusion coefficient of each species (in this investigation, only Na^+, K^+, Cl^-, Ca^{2+} and OH^- are accounted for) can be calculated from the mobility of each of these at a certain temperature, according to the Einstein relation in **eq. 6.4**. **Table 6.a** shows the calculated intrinsic diffusion coefficients of the species considered, at 25 $^{\circ}$C.

$$D_i = \frac{u_i RT}{z_i F} \qquad \text{eq. 6.4}$$

Table 6.a: *Intrinsic diffusion coefficients for the species considered in this investigation*

Species, i	u_i in m²/(s V), at 298 K (from **Atkins [1998]**)	D_i in m²/s, at 298 K (According to Eq. 6.4)
Na^+	$5.19 \ 10^{-8}$	$1.33 \ 10^{-9}$
K^+	$7.62 \ 10^{-8}$	$1.96 \ 10^{-9}$
Cl^-	$7.91 \ 10^{-8}$	$2.03 \ 10^{-9}$
Ca^{2+}	$6.17 \ 10^{-8}$	$0.79 \ 10^{-9}$
OH^-	$20.6 \ 10^{-8}$	$5.30 \ 10^{-9}$

The mass conservation equation must be satisfied during the transport process. If no reactions occur between the ions in solution and any solids, the following equation must apply for each species.

$$p \frac{\partial c_i(x,t)}{\partial t} = - \frac{\partial J_i(x,t)}{\partial x}$$

eq. 6.5

"p" represents the volume fraction of porosity in the considered material where transport can take place.

However, if a reaction between the species in solution and the solids occur, the amount of species "i" bound over a certain time interval has to be added to the left hand of the equation.

The reaction rate of one species in solution with the solid phases of a cement paste is expected to differ from the reaction rate of the other species. This effect may be included by adjusting the mobility of each species (listed in **Table 6.a**) for any given material. **As will be shown in section 6.5, the intrinsic diffusion coefficients of Na^+ and K^+ were measured to be approximately 100 times lower than that given in Table 6.a.**

6.2   Effective diffusion coefficients in cementitious materials

The effective diffusion coefficients for each species in solution during transport through a hydrated Portland cement paste can be calculated by application of the composite theory. The procedure was already described in **paper VII (appendix A)**, but was applied to the more simplistic model proposed by Powers (see the paper for description) for the phase assemblage in hydrated Portland cements. Here the expressions are further developed to apply for the phase assemblage determined by application of the model described in **section 2.8**.

Jensen [1999] proposed, based on an equation from Maxwell for the diffusion coefficient of a composite, the application of the following equation for the diffusion coefficient of the gel matrix, D_{gm}. The gel matrix was defined as the total volume of solid 'gel' products, 'gel' water and unhydrated cement particles. Hence, the gel matrix according to the model described in **section 2.5** corresponds to the volume fraction occupied by all phases in the hydrated Portland cement paste, and therefore only excludes the volume fraction of capillary porosity. It was further assumed in **Jensen [1999]** that some of the phases are impenetrable for the transport of ions, namely calcium hydroxide and unhydrated cement particles, assumed furthermore to be present as inclusions in the so-called gel-proper, V_{gp}. The present author assumes furthermore that the transport through calcite, gypsum, goethite and brucite is non-existent, so expanding the expression proposed by **Jensen [1999]** gives the following,

$$D_{gm,i} = D_{gp,i} \frac{V_{gp}}{V_{gp} + \frac{3}{2}(V_{ce} + V_{CH} + V_{calcite} + V_{gypsum} + V_{goethite} + V_{brucite})}$$

eq. 6.6

where D_{gp} is the diffusion coefficient of the gel proper. As mentioned in **Jensen [1999]**, Garboczi has proposed a diffusion coefficient of chloride ions in the gel proper corresponding to 1/400 of the diffusion coefficient through water-filled capillaries, D_{cw} (i.e. the values listed in **Table 6.a**). It is assumed as a first approximation that the same relationships apply for all other species listed in **Table 6.a**.

Assuming phase symmetric crumbled foil composites, **Fuglsang-Nielsen [2004]** proposed the following equation for the diffusion coefficient through the cement paste, D_p,

$$D_{p,i} = D_{gm,i} \frac{n + 2\sqrt{n} \cdot (1 + c \cdot (n-1))}{n + 2\sqrt{n} - c \cdot (n-1)}$$

eq. 6.7

where n is defined by the ratio of D_{cw} to D_{gm}, i.e. 1/400, and c is the total volume fraction of capillary porosity. Finally, if the aggregates are impermeable, the effective diffusion coefficient, D_{eff}, through a mortar or concrete can be predicted by the following equation proposed by Maxwell (mentioned in e.g. **Jensen [1999]**),

$$D_i = D_{p,i} \frac{1}{1 + \varphi/2} (1 - \varphi)$$

eq. 6.8

where φ is the volume fraction of aggregates and air.

Finally, given the inhomogeneous pore structure of the cement paste, defects as e.g. microcracks, Interfacial Transition Zones between paste and aggregate, tortuosity, etc., the effective diffusion coefficient of a certain species "i" can be defined as,

$$D_{eff,i} = f_1 \cdot D_i$$

eq. 6.9

f_1 can be determined experimentally, by fitting to measured profiles (as done later in the report), if models for quantifying this effect are not available.

6.3 Finite Difference Model for the ingress of NaCl in cementitious materials

A Finite Difference Model was developed to simulate the ingress of NaCl in cementitious materials and is described in this section. The program was constructed on a Matlab-code, and is enclosed in the CD attached to the cover of this thesis. The codes are also attached in **appendix G**. The 'main.m' file constitutes the execution file where input is given and output is treated and plotted. This program calls on five different functions: 'initial.m' where the initial phase assemblage of the paste is calculated (based on the model in **section 2.5**), 'surf.m' where the phase assemblage at the surface is calculated based on the composition of the exposure solution (based on the model in **section 2.8**), 'equil.m' where the phase composition at a certain depth from the surface is calculated based on the content of alkalis, chloride and calcium at each time-step (based on the model in **section 2.8**), and 'MSing.m' where the diffusion of each species in the multi-component pore solution is calculated for each time-step (based on the theory in **sections 6.1** and **6.2**).

The concrete/mortar/paste is regarded as k number of nodes at the position x_k from the surface inwards, with a distance of Δx between each node. At any x_k and time t, following parameters are recorded: concentration of each species in the pore solution, phase assemblage, content of aggregates, air content and the total contents of alkali and chloride. These parameters are initially predicted by the function 'initial.m' at t = 0, but changed later at each time step Δt according to the advance in the transport process. Δt is defined to satisfy the following relation in order to ensure the stability of the numerical procedure (e.g. from **Jensen[1999]**, **Truc[2000]**),

$$0.5 < \frac{\Delta t \cdot D_{eff,max}}{\Delta x^2}$$

eq. 6.10

where $D_{eff,max}$ corresponds to the effective diffusion coefficient of the species with highest mobility; in this case, the coefficient for OH^- (see **Table 6.a**).

At each time step, the effective diffusion coefficients of the species (i.e. Na^+, K^+, Cl^-, Ca^{2+} and OH^-) in solution is calculated at each position x_k. From the concentration of each species at time t, the average diffusion coefficient between two consecutive nodes is applied to evaluate the concentration of each species at time $t + \Delta t$, by solving the following equation for each of the species considered (as done by function 'MSing.m').

$$\frac{c_i(x_k,t+\Delta t)-c_i(x_k,t)}{\Delta t} = -\frac{D_{eff,i}}{\Delta x}\left[\left[\frac{\frac{c_i(x_{k-1},t)-c_i(x_k,t)}{\Delta x}-...}{...-z_i\frac{c_i(x_{k-1},t)+c_i(x_k,t)}{2}\frac{\frac{1}{\Delta x}\sum_i z_i D_{eff,i}(c_i(x_{k-1},t)-c_i(x_k,t))}{\sum_i z_i^2 D_{eff,i}\frac{(c_i(x_{k-1},t)+c_i(x_k,t))}{2}}}+...\right. \\ \left. ...+\frac{\frac{c_i(x_k,t)-c_i(x_{k+1},t)}{\Delta x}-...}{...-z_i\frac{c_i(x_k,t)+c_i(x_{k+1},t)}{2}\frac{\frac{1}{\Delta x}\sum_i z_i D_{eff,i}(c_i(x_k,t)-c_i(x_{k+1},t))}{\sum_i z_i^2 D_{eff,i}\frac{(c_i(x_k,t)+c_i(x_{k+1},t))}{2}}}\right] \quad \text{eq. 6.11}$$

This numerical solution is obtained when combining **eq. 6.2**, **6.3** and **6.5**. To simplify the computation, the diffusion process is simulated assuming a porosity of 1 cm^3 at all times and depths (hence the non-appearance of the porosity p from **eq. 6.5**).

Once the concentration profiles for the different species at time $t +\Delta t$ are determined through the whole section of the concrete/mortar/paste, the added/removed amount of each species at each depth is scaled to the porosity of 1 cm^3 of paste + aggregate + air, in order to predict the phase assemblage and the corresponding new concentration of each species at each depth (according to function 'equil.m'). Notice that electroneutrality is maintained in the pore solution.

Once the new concentration profile for each species is predicted and the total content of chloride and alkalis at any depth is updated, a new diffusion step is simulated and followed again by the prediction of the phase assemblage as a function of depth. The iterations run until the computed time t equals the exposure time specified in the input section.

The boundaries at the surface node are set by application of function 'surf.m', where the phase assemblage in equilibrium with the exposure solution is predicted. The boundaries at the inner most node are defined assuming its properties to be identical with those in the second-last node. Hence the size of the specimen specified in the input section must be larger than the depth of ingress of the fastest species.

Besides the limitations of the phase equilibria model in **section 2.11**, following applies as well:

- leaching is only included until all Ca(OH)$_2$ is used up, i.e. no decalcification of the C-S-H phase, as reported elsewhere, is allowed.

- The program only accounts for the diffusion of Na^+, K^+, Cl^-, Ca^{2+} and OH^-.

- A decrease in pH from alkaline to neutral conditions is not considered to affect the phase and solubility diagrams in **chapter 2**. This is probably incorrect but is out of the scope of this investigation.

- The code, as provided in **appendix G**, is prepared to the cement compositions studied in this investigation, i.e. WPC(4), WPC(12), OPC and SRPC. However, other cements can fairly easy be added to the code.

6.4   Input and output parameters.

The user of the program is only to change the input parameters inside the file "main.m". Guidance on where to insert the different parameters is given inside the file within the section noted "input". **Fig. 6.1** illustrates the input area in file "main.m". Notice that the program is designed for the materials used in this investigation, and therefore, the powder composition has to be defined by selecting different weight percentages of the seven listed options.

```
%%%%%%%%%%%%%%%%%%%%%%%%%%%%%%%%%%%%%%%%%%%%%%%%%%%%%%%%%%%%%%%%%%%%%%%%%%%%%%%%%%%%%
%%%%%%%%%%%%%%%%%%%%%%%%%%%%%%%%%%%%%%%%%%%%%%%%%%%%%%%%%%%%%%%%%%%%%%%%%%%%%%%%%%%%%
%%%%%%%%%                           Input                          %%%%%%%%%%%%%%%%%%%
%%%%%%%%%%%%%%%%%%%%%%%%%%%%%%%%%%%%%%%%%%%%%%%%%%%%%%%%%%%%%%%%%%%%%%%%%%%%%%%%%%%%%
%%%%%%%%%%%%%%%%%%%%%%%%%%%%%%%%%%%%%%%%%%%%%%%%%%%%%%%%%%%%%%%%%%%%%%%%%%%%%%%%%%%%%

x       = 0.017;          % depth of specimen, in m
delta_x = 0.001;          % depth increment, in m
exp_time = 70*24*60*60;   % total exposure time, in seconds
trans_factor = 1;         % factor f1 in eq. 8.9

% Exposure conditions

exp_sol = [0.65 0.65 0.015 0.03 0.0];   % composition of the exposure solution in mmole/liter
                                        % respectively Cl, Na, Ca, OH, K

% Powder properties
% mass percent of each powder, note: the total sum has to be 100
HOCperc    = 99.00;    % wt.% low aluminate white PC, WPC(4)
RCIperc    = 00.00;    % wt.% high aluminate white PC, WPC(12)
OTCperc    = 00.00;    % wt.% ordinary PC, OPC
SACperc    = 00.00;    % wt.% low alkali sulfate resistant grey PC, SRPC
MKperc     = 00.00;    % wt.% metakaolin
SFperc     = 00.00;    % wt.% silica fume
KSperc     = 01.00;    % wt.% CaCO3

% Mix properties

waterpowder= 0.45;     % water-to-powder ratio
Vair       = 0.0;      % total volume fraction of air voids
Vagg       = 0.0;      % total volume fraction of aggregate
dagg       = 2.621;    % weighed average density of aggregate [g/cm3]
Rd_alkalis = 0.65;     % Initial distribution ration for alkalis in the C-S-H, Rd
```

Fig. 6.1: *Input area in file "main.m" and illustration of the guiding text inside the program. See* **appendix G** *for codes and functions called by "main.m".*

The output from the program is illustrated in four figures once the calculations are finished. The content in these is:

Figure nr. 1: Concentration of ions in the pore solution, in mol/l, as a function of depth.
Figure nr. 2: Total content of Cl, Na and K, in mass-% to dry sample, as a function of depth.
Figure nr. 3: Development of the phase assemblage as a function of depth, in mass-%.
Figure nr. 4: Ratio of Cl to OH in the pore solution as a function of depth.

Furthermore, relevant results are written to an Excel-compatible file for any eventual further treatment of data. The data has to be converted from text to columns, and the resulting matrix will have as many columns as depth increments, i.e. (1 + x/delta_x; values from **Fig. 6.1**).

The rows correspond to:

1. Content of C-S-H in g/cm^3 saturated sample
2. Content of CH in g/cm^3 saturated sample
3. Content of Brucite in g/cm^3 saturated sample
4. Content of Goethite in g/cm^3 saturated sample
5. Content of Pore solution in g/cm^3 saturated sample
6. Content of C_4AH_{13} in g/cm^3 saturated sample

7. Content of monosulfate in g/cm^3 saturated sample
8. Content of ettringite in g/cm^3 saturated sample
9. Content of gypsum in g/cm^3 saturated sample
10. Content of monocarbonate in g/cm^3 saturated sample
11. Content of calcite in g/cm^3 saturated sample
12. Content of Friedel's salt in g/cm^3 saturated sample (note that Friedel's salt is in solid solution with monocarbonate)
13. Concentration of Cl
14. Concentration of Na
15. Concentration of Ca
16. Concentration of OH
17. Concentration of K
18. Total content of Cl in mass-% to dry sample
19. Total content of K in mass-% to dry sample
20. Total content of Na in mass-% to dry sample
21. Dry density of sample in g/cm^3

As an example of output from the FDM, **Fig. 6.2** presents the 4 output-figures generated by Matlab when running the previously described Matlab program with the input data shown in **Fig. 6.1**. It should be remembered that monocarbonate and Friedel's salt are present as a single solid solution phase but it is chosen in the program to regard them as two separate phases for illustrative purposes.
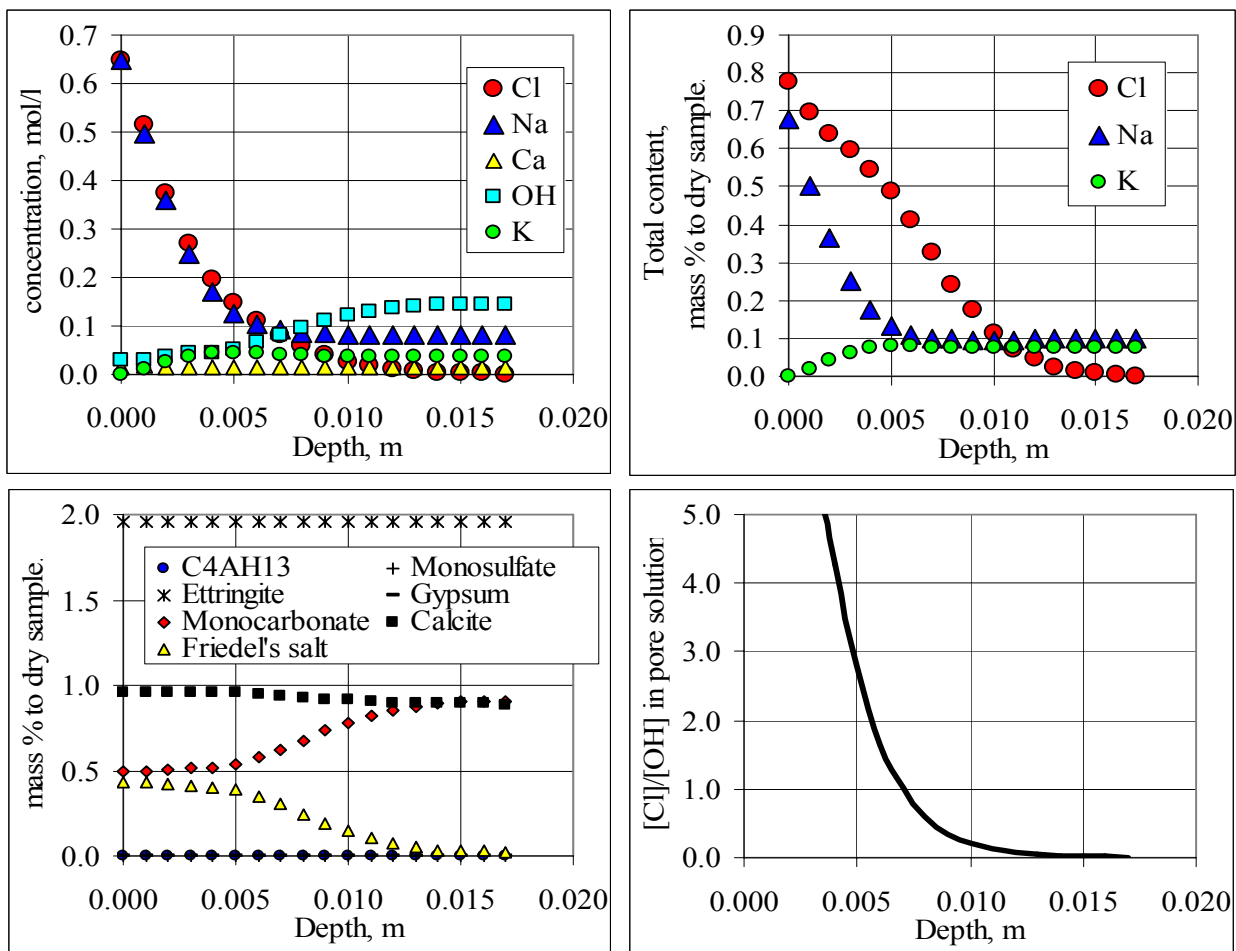
Fig. 6.2: *Output figures obtained when running the model described in* **section 6.3** *with the input data in* **Fig. 6.1**. Note: Friedel's salt and monocarbonate form a solid solution and are therefore only one phase.

6.5   Predicting the ingress of NaCl in Portland cement pastes

To test the applicability of the model described in **section 6.3** the ingress of NaCl in hydrated Portland cement pastes at w/p 0.45 was studied at a maturity of 4.5 months. The experimental procedure is thoroughly described in **appendix C**. Three types of Portland cement were tested (notations according to the specified in **appendix B**); WPC(4), WPC(12) and SRPC.

The samples were exposed to unidirectional ingress of a 650 mM NaCl solution for 70 days. The analyses on the samples were carried out by use of EDS-equipment. Three line-scans with spacing of approx. 4 mm, in direction perpendicular to the exposed surface, until a depth of 15 mm at step increments of 50 µm, were measured. Furthermore, at the depths of 2, 4, 6, 10 and 15 mm, line-scans of 200 to 600 randomly located points were measured parallel to the exposed surface, to study the phase assemblage as a function of depth. Rawdata from this measurements is provided in the files "profiles_WPC(4)_650mMNaCl, profiles_WPC(12)_650mMNaCl and profiles_SRPC_650mMNaCl" in the attached CD-ROM. Predicted assemblages are given in spreadsheet "predicted" and comparative plots in "comparison" in these Excel files.

The measured profiles for molar ratios of Cl to Si, Na to Si and K to Si were compared to those predicted by the model in **section 6.3**. Similarly, the molar ratio of Cl to Ca measured in the solid solution phase between monocarbonate and Friedel's salt at the depths of 2, 4, 6, 10 and 15 mm, was compared to that predicted by the model in **section 6.3**, to verify the assumption of instantaneous binding and the phase assemblage as a function of depth.

Surprisingly, the transport of alkalis is much slower than expected from the intrinsic diffusion coefficients given in **Table 6.a**. The ingress of Na in the Portland cement pastes was much slower than the ingress of Cl, which does not agree with that expected from the multi-species theory, where Cl and Na are expected to have similar ingress rates resulting from the electrical field between the ions in solution. The leaching of K was also observed to be much slower than initially expected from the model. Such observations are in accordance with that reported in **Volkwein [1995]**. The volume of exposure solution to volume of samples was high (approx. 36) and therefore, the pH of the exposure solution never exceeded 9.5, and the concentration of NaCl remained constant within ± 20 mmol/l.

As mentioned in **section 6.3**, the model does not by itself include the probable difference in reaction rate between the different species in solution and the hydrate phases in the cement. For example OH^- could be more readily available from dissolution of $Ca(OH)_2$ than absorption and desorption of alkalis in the C-S-H, resulting in a faster ingress of Cl^- compared to that of Na^+ due to fast leaching of OH^-. A good fit to the measured ingress profiles was obtained by reducing the intrinsic diffusion coefficient of alkalis by a factor of 100. This is included in the codes in **appendix G**.

The three left figures in **Table 6.b**, **6.c** and **6.d** compare the measured molar ratio profiles for Cl to Si, Na to Si and K to Si with the profiles predicted by the model in **section 6.3**. The intrinsic diffusion coefficients for alkalis were adjusted as mentioned above and the f_l factor in **eq. 6.9** was set to values ranging from 3.5 to 4.5 to include the effect of cracks or other defects expected (f_l values deduced by fitting to measured profiles). On the right side of these tables, the measured molar ratios of Cl to Ca in the solid solution phase are compared to the predicted by the model (illustrated by the red trend-lines), at the depths of 2, 4, 6 and 10 mm. Results from a depth of 15 mm are not presented here but can be seen in the Excel-files in the CD-ROM.

The scattering of plots for the ingress profiles (named "Average of 3 ingress profiles (EDS), in **Tables 6.b** to **6.d**") result from a combination of reduced measuring time on each point to 14 sec. instead of the 40 seconds applied for the phase equilibria measurements in **chapter 2**, and the fact that one points measured at a certain depth is not representative by itself as any combination of phases in the assemblage can have been measured. However, the plots can be used to visually compare the profiles, and combined with the far more accurate average Cl/Si, Na/Si and K/Si

ratios from 200/600 EDS-analyses at the depths of 2, 4, 6, 10 and 15 mm (named "Average of 200/600 EDS at depth x"), to conclude on the model's applicability. The comparison between measured and predicted Cl to Ca ratios (right hand figures in **Tables 6.b** to **6.d**) in the solid solution phase are far more accurate and serve as help for concluding on its accuracy.

An absolute verification of the model would require more samples, as here only one sample per cement type was examined. Parameters needing adjustment are e.g. f_l factor from eq. 6.9, and scaling of the intrinsic diffusion coefficients of Na^+ and K^+.

The predicted ingress profiles for Cl agree very well with the measured Cl to Si profiles and the Cl to Ca ratios in the solid solution phase as a function of depth, especially WPC(4) and WPC(12). A larger variation of SRPC is probably due to the presence of significant amounts of unreacted C_4AF, observed on the SEM. Good agreement is also found for the profiles of Na and K, but because of the scattering of the EDS-plots, it is difficult to define the appropriate ratio for reducing the intrinsic diffusion coefficient for alkalis with sufficient accuracy. However, the appropriate ratios must be at the applied level, because of the limited transport of alkalis that has occurred.

Because of the good agreement between predicted and measured Cl to Ca ratios in the solid solution phase, the assumption of quasi-instantaneous binding is justified. This assumption is made in most of the models for chloride ingress prediction (e.g. **Truc [2000]** and **Jensen et al. [2000]**).

The main advantage of the Finite Difference Model used for the prediction of NaCl ingress is that it allows judgement of the performance of different types of binder without having to carry out extensive and time consuming experiments for calibration purposes.

Generally, sulfate reactions result in a tightening of the surface region of the cementitious material which significantly slows the ingress of all other species from the environment, as well as the leaching of species from the pore solution of the cement paste (**Glasser [2001]**). Depending on the ability of the cement paste to withstand the expansive reactions (i.e. its sulfate resistance) spalling/cracking may occur after blocking of the surface region, which results in decreased durability. The process of sulfate attack is much more complex and was therefore not included in the finite element model.

Table 6.b: *Measured values vs. the predicted by the model in* **section 6.3** *for a w/p 0.45 WPC(4) paste with 1 mass % replacement of powder by calcite, and unidirectional exposure to 650 mM NaCl for 70 days at 20°C. Left-hand figures illustrate the ingress profiles of Cl, Na and K, while right-hand figures illustrate predicted (red line) and measured Cl to Ca in the solid solution phase. Note D_i for K and Na are adjusted by 1/100, $f_1 = 3.5$ (see eq. 6.9)*
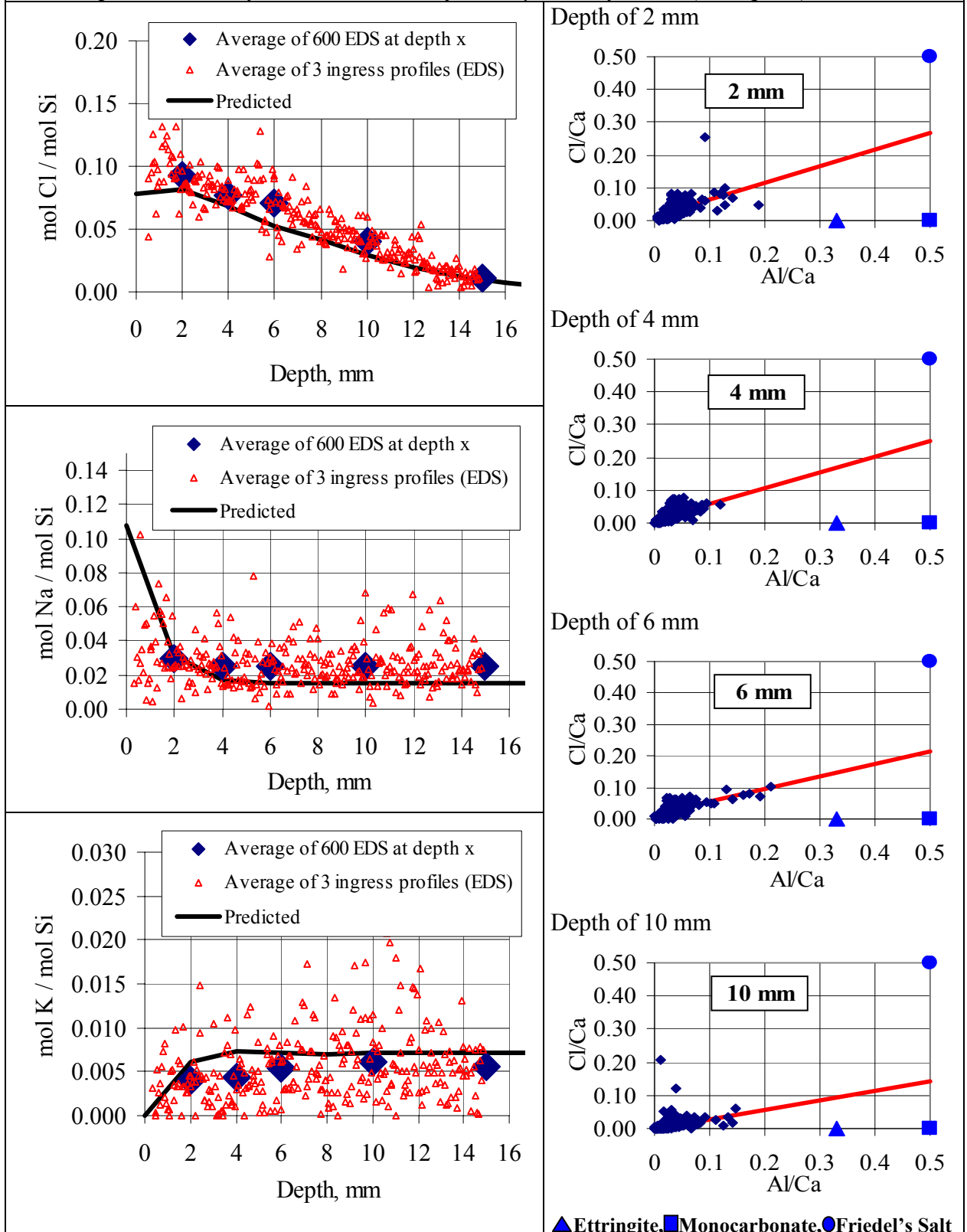
Table 6.c: *Measured values vs. the predicted by the model in* **section 6.3** *for a w/p 0.45 WPC(12) paste with 1 wt. % replacement of powder by calcite, and unidirectional exposure to 650 mM NaCl for 70 days at 20°C. Left-hand figures illustrate the ingress profiles of Cl, Na and K, while right-hand figures illustrate predicted (red line) and measured Cl to Ca in the solid solution phase. Note D_i for K and Na are adjusted by 1/100, f_1=4.5 (see eq. 6.9)*
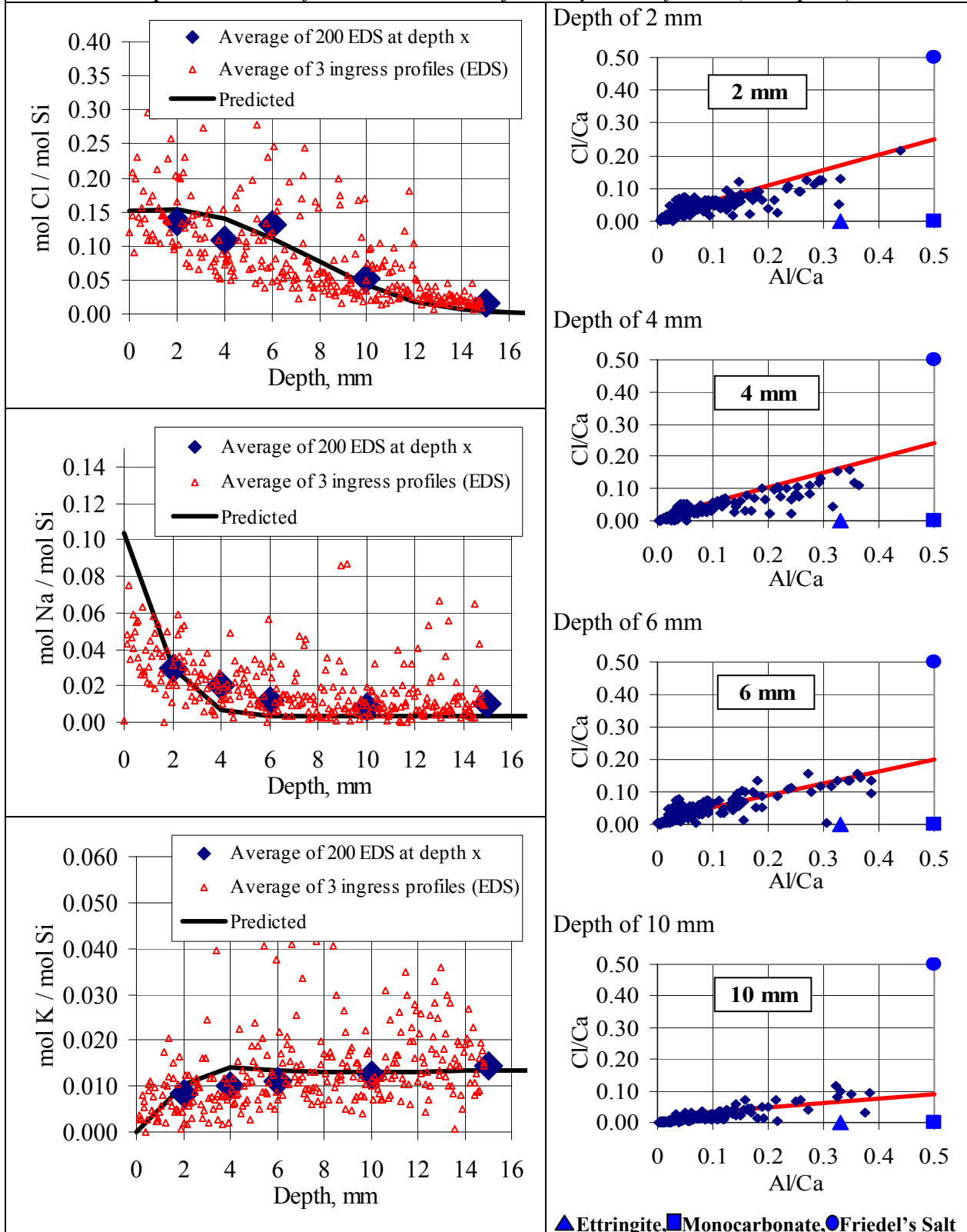
Table 6.d: *Measured values vs. the predicted by the model in* **section 6.3** *for a w/p 0.45 SRPC paste with 1 wt. % replacement of powder by calcite, and unidirectional exposure to 650 mM NaCl for 70 days at 20°C. Left-hand figures illustrate the ingress profiles of Cl, Na and K, while right-hand figures illustrate predicted (red line) and measured Cl to Ca in the solid solution phase. Note D_i for K and Na are adjusted by 1/100, f_1=3.5 (see eq. 6.9)*
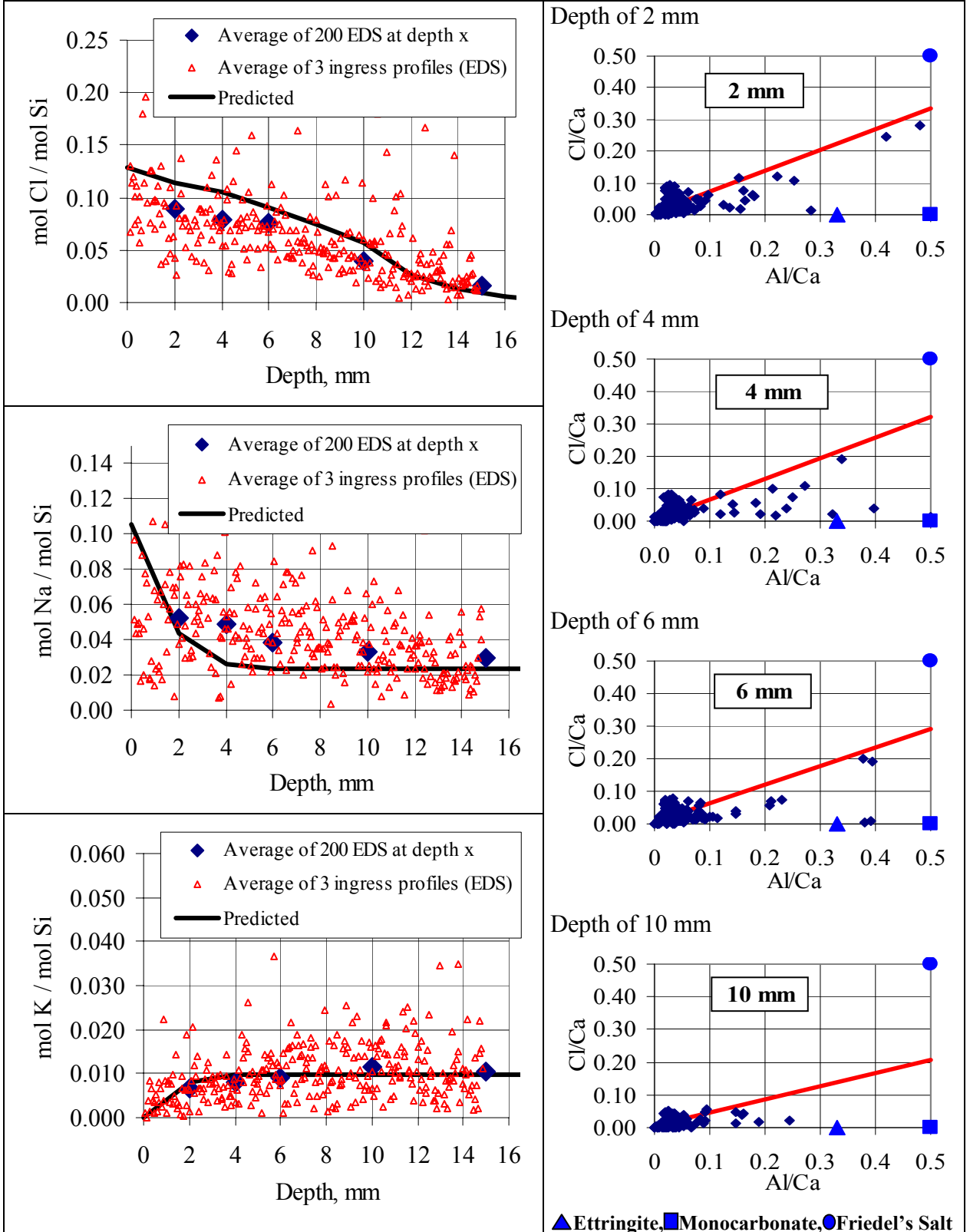
6.6 NaCl ingress in hydrated mortars

A set of experiments was carried out on fully hydrated mortar samples of WPC(4), WPC(12), OPC and SRPC to test the Finite Difference Model described earlier. However, polished thin-sections of the samples showed very poor adhesion between cement paste and aggregates, and extensive connexion of ITZ (Interfacial Transition Zone), most likely due to the improper selection of particle size distribution for the sand, where a higher amount of fine sand should have been used.

7 Practical implications

7.1 Chloride ingress and binding capacity

With regard to the selection of cement type, **ACI 222.3R-03** mentions that the effect of C_3A content in Portland cements "is not sufficiently clear to warrant selecting a chloride-reducing cement on the basis of the C_3A content. Further, other durability problems, such as sulfate attack, become more likely as the C_3A content is increased". This is confirmed by the findings of this study, where alkalis were found to play the major role on chloride binding, whilst the alumina content was found to have relatively minor effect.

Low-alkali Portland cements (Na_2O_{eq} lower than approx. 0.35) should be used in chloride rich environments as chloride binding is enhanced at reduced alkali content. As the ingress of external alkalis is much slower than that of chlorides, the amount of bound chlorides is increased at all total contents of chlorides, and the performance in terms of chloride threshold value is improved (i.e. the ratio of Cl^- to OH^- is reduced). The content of Al_2O_3 in a Portland cement paste has a relatively limited influence on its binding capacity, which is a clear advantage in marine environments, or other environments where both chlorides and sulfates are present, because a high binding capacity can be obtained while still ensuring high sulfate resistance of the Portland cement paste (i.e. by low contents of Al_2O_3). In environments where both sulfate and chloride are present, another argument for reducing the amount of Al_2O_3 in the binder is that the chloride binding capacity of a Portland cement paste is more severely reduced in pastes with high contents of alumina. The chloride binding properties of the C-S-H on the other hand remain unchanged, with sulfate attack only having a minor effect on chloride binding in pastes with low Al_2O_3.

ACI 222.3R-03 correctly states that "higher-alkali cements are effective in providing a higher pH environment around the steel in the presence of chloride ions" as at any given concentration of chlorides in the pore solution, better resistance is given by higher concentrations of hydroxyl ions. However, the statement can be interpreted incorrectly, as a high-alkali cement will bind less chlorides and therefore result in higher concentrations of chloride in the pore solution, compared to that for a low-alkali Portland cement, as discussed earlier in **section 2.10**.

Low alkali contents are common to most white Portland cements manufactured around the world, which is one reason why these should be considered as an alternative to conventional grey cements in chloride containing environment.

White Portland cements are also generally observed to have rapid strength development and high ultimate strength (i.e. dense matrix). The latter is due to the low iron content which in grey cements results in higher porosity: 1. because the C_4AF phase is slow to react and 2. because when it does react it results in high density, low volume iron oxide phases. High strengths are, of course, (once proper precautions are taken for the high early heat development during hydration) a desired property for many applications. As seen in **section 5** some C_4AF still remained unreacted, even after 25 years of hydration, which, all things equal, must suggest a higher capillary porosity of the cement paste.

The commonly used NaCl-binding isotherm for evaluation of the performance of a given cement paste in chloride environment or for implementation in service life prediction models by means of Langmuir or Freundlich equations, may be misleading. Because of the stoichiometric addition of NaCl, the chloride binding capacity of the paste is underestimated at alkali concentrations higher than the initial concentration in the pore solution, whilst the opposite applies for alkali concentrations lower than that initially present in the cement paste. In simple service life prediction models (where chloride binding cannot be predicted at each depth and time increments) a chloride binding isotherm at constant concentration of alkalis should be used

instead. The concentration of alkalis should be kept constant at a level corresponding to that initially present in the paste whereafter chloride can be added progressively by addition of e.g. $CaCl_2.2H_2O$.

Based on the observations and the theory behind the thermodynamic model, one should be careful when using procedures such as pore solution expression for determining the chloride binding isotherms of a cement paste. The assumption of equilibrium may be unjustified as soon as the pressure is changed dramatically in the concrete specimen for squeezing out the pore solution. The effect of applying such a procedure has not yet been thoroughly studied. When comparing chloride binding isotherms in the literature found by different experimental techniques, a clear difference is observed (in e.g. **Glass et al. [1997]**).

As was demonstated in this study, the model for the phase equilibria in hydrated Portland cement described in **section 2.5** and the chloride binding reactions covered in **section 2.8**, can be used for comparing the performance of different cements in any given aggressive environment. Without carrying out extensive experimental investigations, one can get a detailed picture of the performance of a Portland cement paste in terms of chloride binding, chloride threshold values, sulfate resistance, capillary porosity, etc. Furthermore, the model can be introduced to any finite element model for predicting the ingress of chloride into concrete.

Other processes, such as change in porosity due to e.g. leaching of $Ca(OH)_2$ and carbonation, can also be better understood and quantified by extending the phase equilibria model to decalcification of the C-S-H phase.

7.2   Service life prediction

The implementation of the model for the phase equilibria in hydrated Portland cements in Finite Difference Models for the ingress of chloride in multi-component solutions provides an accurate description of the process and can account for changes in porosity as a function of depth and time.

The common practise in Scandinavian countries for predicting the service life of a reinforced concrete structure for marine environment is based on the extrapolation of a chloride ingress profile determined by chloride ponding of the particular concrete for typically 35 days, at a maturity of 28 days. The error-function solution to Fick's 2. law of diffusion is fitted to the measured profile, thereby obtaining an apparent diffusion coefficient, which is used for the extrapolation upon factorisation to account for chloride binding, degree of hydration, exposure environments, etc (**HETEK53 [1996]**). The main disadvantage of such methods is that they cannot be accurately used to predict the performance of different binder types and mixing proportions without prior testing of the concretes. It is therefore a time consuming process.

As the design service life of structures in marine environments is normally over 50 years, and typically 100 years (as was minimum requirement for the Great Belt Bridge in Denmark) for marine structures, it appears reasonable to assume that the determining value for the diffusion coefficient of chlorides in the concrete after complete hydration applies. Furthermore, bridge piers and pylons are generally cast and cured for several weeks before use in the aggressive environment. For many cement types, the degree of hydration achieved at this time is relatively high. The effective diffusion coefficient for chlorides in the cement paste can be calculated by applying the composite theory in **section 6.2** to the phase assemblage calculated according to the phase equilibria model in **section 2.5**. The chloride binding capacity of the binder at any content of chloride can be predicted according to the relationships provided in **section 2.8**, and at the same time, the chloride threshold for initiation of chloride reinforced corrosion can be predicted. The use of Finite Difference Models is probably the most appropriate way of simulating the ingress of chlorides, however, they should be kept as simple as possible, e.g. in **chapter 6** it was observed that the ingress of alkalis has little influence on the overall transport process inside the concrete.

Some important factors still unresolved are the related to imperfections in the cement matrix (e.g. microcracks, cracks, connectivity of capillary pores), adhesion between paste and aggregate (i.e. size and connectivity of the so-called Interfacial Transition Zones) and densifying the surface region due to expansive reactions with sulfates, or formation of dense layers at the surface of the concrete from precipitation of dissolved ions in the exposure solution (good discussions on the last process are given in e.g. **Glasser [2001]** and **Buenfeld and Newman [1986]**).

The imperfections mentioned above may be accounted for by experimental calibration of the effective diffusion coefficient for chlorides in the concrete to measured chloride ingress profiles obtained from e.g. chloride ponding tests. However, if all effects are to be accounted for, it is of key importance that the exposure solution during such tests is close to that of the real exposure environment, and that the amount of exposure solution is high compared to the volume of exposed samples, as otherwise, the pH in the exposure solution will increase due to leaching, which undoubtedly changes the conditions for any eventual precipitation of minerals at the surface, such as e.g. aragonite, calcite or brucite (e.g. in **Buenfeld and Newman [1986]**). It should be noted that if a dense layer of a certain mineral precipitates at the surface of the concrete, which has a lower diffusivity than that of the concrete this will affect the chloride ingress profile by reducing the apparent surface chloride concentration as flow of these ions to the concrete is governed by the surface layer. Again, the effect of such a layer is easier to simulate by use of numerical routines.

Certainly many other important parameters play a significant role, such as the type of environmental load, as e.g. the ingress of chlorides in the splash zone of a concrete pylon will be more severe than in parts constantly submerged (**HETEK53 [1996]**), due to the drying and wetting of the surface, enhancing other faster transport processes such as capillary suction. Temperature is also a decisive parameter.

The transport of aggressive ions in concrete exposed to aggressive environments is very complex. A quantification of the influence of all different important parameters has still not been achieved and much further research has to be carried out.

8   Phase diagrams for Cl-binding in hydrated PC (20°C)

This chapter summarizes the phase diagrams applicable for hydrated Portland cement paste exposed to chlorides, sulfates and carbonate. These have been adjusted according to the findings during this investigation.

The subsystem CaO-SiO$_2$-H$_2$O is the same as that presented in **Fig. 2.1** (from **Taylor [1997]**).

Figs. 8.1 to **8.4** illustrate phase diagrams for relevant subsystems applicable to the system CaO-SiO$_2$-Al$_2$O$_3$-Fe$_2$O$_3$-SO$_3$-CaCl$_2$-CO$_2$-Na$_2$O-H$_2$O for hydrated Portland cement. The composition of the pore solution, as well as content of alkalis in the C-S-H, can be calculated from the relationships given in **Table 2.g**.

Fig. 8.1: *Subsystem C$_3$A-CaSO$_4$-CaCO$_3$ of the system SiO$_2$-Al$_2$O$_3$-SO$_3$-Fe$_2$O$_3$-CaO-MgO-Na$_2$O-CO$_2$-CaCl$_2$-NaCl-H$_2$O for hydrated Portland cement. C$_3$A does not refer to the normative content C$_3$A in the clinker, but to the total Al$_2$O$_3$*

CaSO₄
gypsum

ettringite

(+thaumasite)

Phase in excess:
C-S-H
calcium hydroxide
goethite
brucite
pore solution

*mono-
sulfate*

(+calcite)

C₄AH₁₃

C₃A   *Friedel's salt +
monocarbonate
(solid solution)*   **CaCl₂₍aq₎**

Fig. 8.2: *Subsystem C₃A-CaSO₄-CaCO₃ of the system SiO₂-Al₂O₃-SO₃-Fe₂O₃-CaO-
MgO-Na₂O-CO₂-CaCl₂-NaCl-H₂O for hydrated Portland cement. C₃A does not
refer to the normative content C₃A in the clinker, but to the total Al₂O₃*

CaCO₃
calcite

Phase in excess:
C-S-H
calcium hydroxide
goethite
brucite
pore solution

monocarbonate   **(+ettringite)**

(+ettringite)

*Solid
solution*

C₃A

*C₄AH₁₃+monosulfate
or
monosulfate+ettringite*   *Friedel's
salt*   **CaCl₂ ₍aq₎**
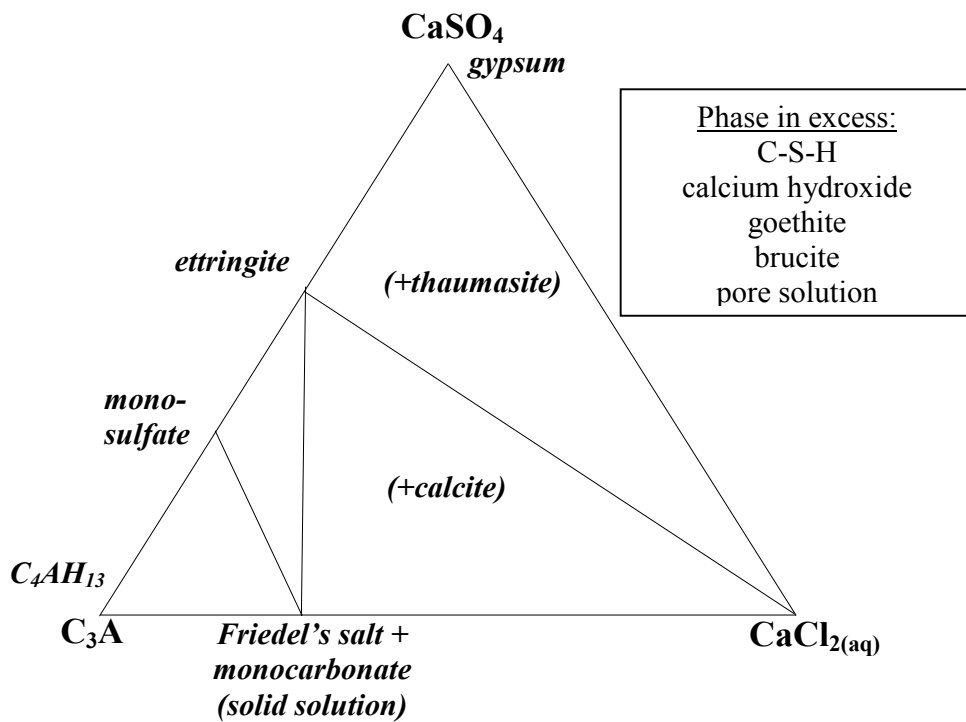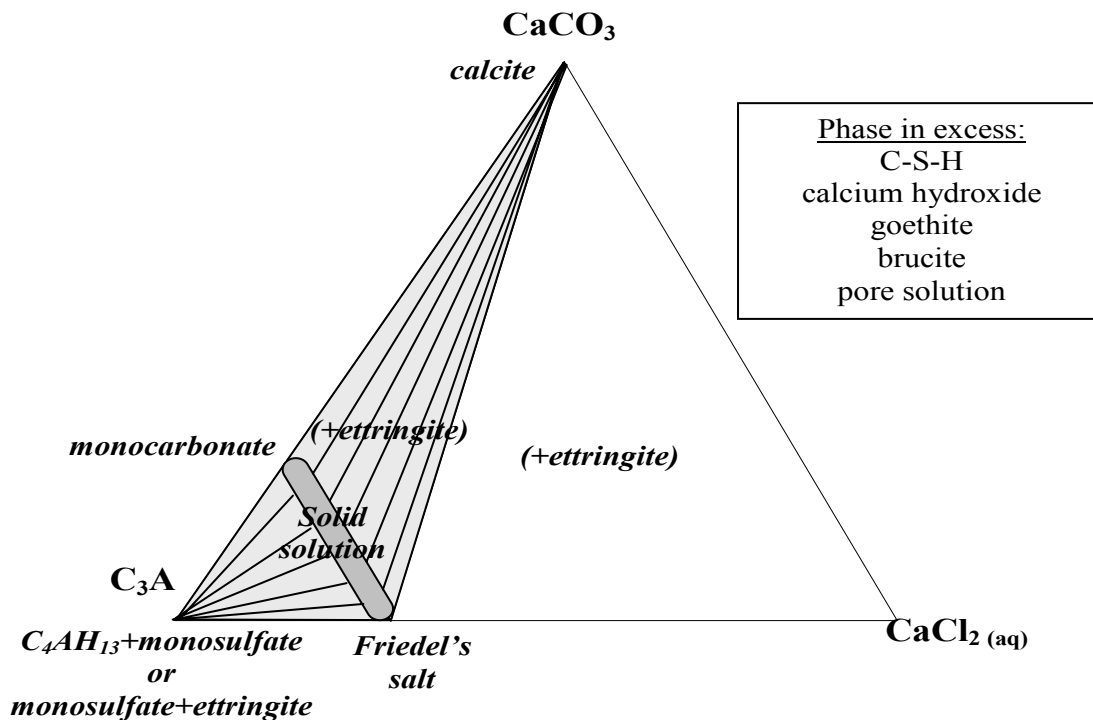
Fig. 8.3: *Subsystem C₃A-CaCl₂-CaCO₃ of the system SiO₂-Al₂O₃-SO₃-Fe₂O₃-CaO-MgO-
Na₂O-CO₂-CaCl₂-NaCl-H₂O for hydrated Portland cement. C₃A does not refer
to the normative content C₃A in the clinker, but to the total Al₂O₃*
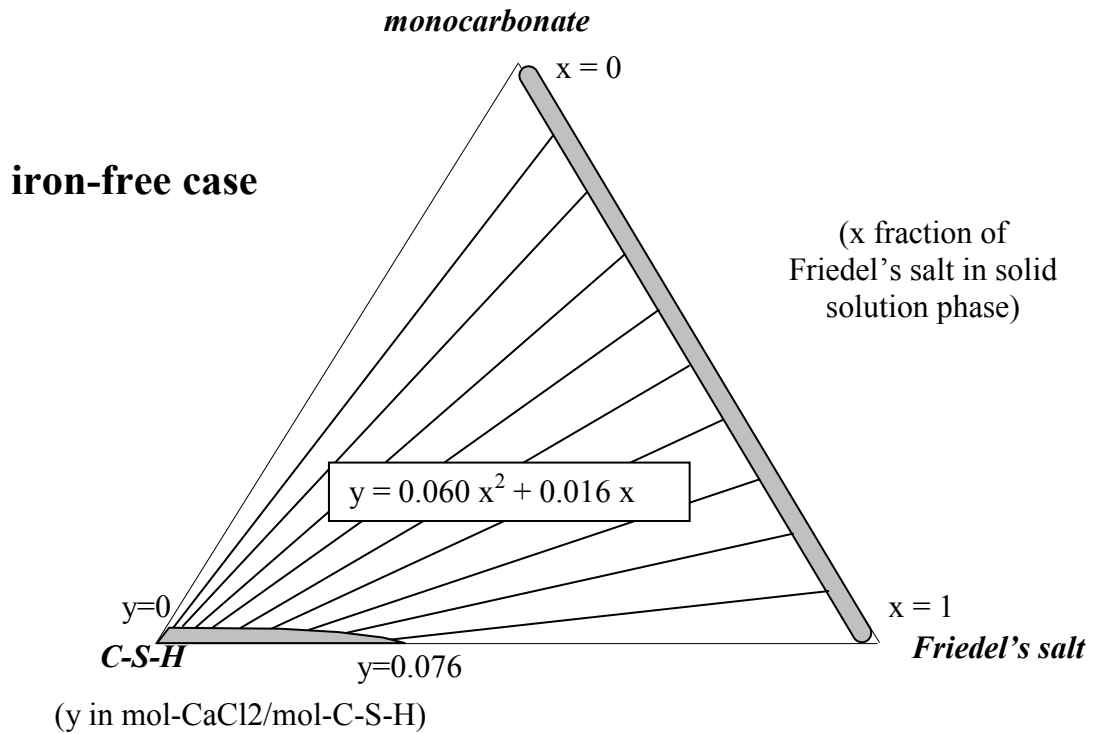
Fig. 8.4: *Pseudo ternary subsystem for "C-S-H – monocarbonate- Friedel's salt" in the SiO_2-Al_2O_3-SO_3-Fe_2O_3-CaO-MgO-Na_2O-CO_2-$CaCl_2$-NaCl-H_2O system for hydrated Portland cement (notice: iron-free case; i.e. white Portland cement). C-S-H corner is not-to-scale*

9 Conclusions

An equilibrium model for predicting the stable or metastable phase assemblage in hydrated Portland cement pastes has been proposed. The model was verified through EDS-analyses and measurements of evaporable water (upon drying at $105^{\circ}C$) and non-evaporable water (loss of ignition at $1000^{\circ}C$) of pastes of three different types of Portland cement at different w/p ratios. From the chemical composition of the Portland cement and the mix proportions with water, the phase assemblage can be predicted without any further experimental calibration.

The model was further developed to allow the prediction of the stable or metastable phase assemblage at any addition of chlorides, alkalis, carbonate and sulfates, including the composition of the pore solution. The resulting model gave a very good correlation between predicted and experimentally determined values. Furthermore, the model was verified against available data in the literature, as well as on a few Portland cement pastes exposed to NaCl for 25 years, again giving excellent agreement between predictions and experimental results. An Excel spreadsheet including this model is provided in the CD attached to the cover of this thesis. The model could successfully be applied for predicting the phase assemblage in Portland cement pastes with supplementary cementitious materials such as silica fume and slag, but should include corrections for decalcification of the C-S-H phase at high silica contents.

During the development of this model, the following partial conclusions were drawn,

- The Ca/Si, Al/Ca, S/Ca of the C-S-H in hydrated white Portland cement pastes was found to be 1.75, 0.04 and 0.03, respectively. The water saturated density of the phase was found to be approximately 2.10 g/cm^3 and 19 mass % of the phase is weakly bound water that can evaporate at temperatures around $100^{\circ}C$.
- The incorporation of iron in the structure of the C-S-H (corresponding to Fe/Ca = 0.02) affects also the incorporation of Al and S. The Al/Ca and S/Ca molar ratios in hydrated grey Portland cement was observed to be 0.06 and 0.05, respectively.
- A solid solution between Friedel's salt and monocarbonate has been confirmed, which governs the relationship between free and bound chlorides.
- Significant amounts of chloride are bound by the C-S-H phase, with a well-defined distribution between the three phases; AFm solid solution phase of Friedel's salt and monocarbonate, the pore solution and the C-S-H at any given total content of alkali.
- Binding of chlorides in a cement paste appears to be a reversible process as described in **section 2.9**. Differences observed between absorption and desorption chloride binding isotherms are the result of changing the content of alkalis in the system.
- The incorporation of iron in the structure of the C-S-H reduces its chloride binding capacity. Worth noting is that a significant amount of unhydrated C_4AF grains appeared to be present even after 25 years of hydration. The investigations carried out suggest that the reaction product for Fe_2O_3 is FH_3.
- The content of alkalis is the main governing parameter for the chloride binding capacity of a Portland cement paste; the higher the content of alkalis the lower chloride binding capacity at any given total content of chlorides. As alkalis ingress much slower than chlorides, low alkali cements should be used in chloride containing aggressive environments in order to enhance chloride binding.
- Reduction in Na_2O_{eq} content of Portland cements below approx. 0.35% results in better protection against reinforcement corrosion, as the ratio of chloride to hydroxyl ions in solution is effectively reduced due to the enhanced chloride binding, even though this reduced the initial concentration of hydroxyl ions in the pore solution.
- The content of Al_2O_3 has a relatively limited effect on the chloride binding capacity of a Portland cement paste when compared to the effect of alkalis. At high contents of

alumina more chloride is bound by the solid solution phase, whilst more chlorides are bound by the C-S-H in low alumina cements. This allows the production of concrete with a high sulfate resistance (i.e. very low content of Al_2O_3) whilst maintaining a high chloride binding capacity (i.e. low alkali Portland cement).

- The effect of sulfate addition to a Portland cement paste on chloride binding can be predicted by the model as well. The addition of sulfates reduces the amount of bound chloride at any content of chlorides, but the effect is more severe at higher sulfate contents. At extreme additions, i.e. when gypsum can form, only the C-S-H contributes to the binding of chlorides, as apparently, Friedel's salt cannot coexist in a stable assemblage with gypsum. This gives one more reason for the use of low aluminate Portland cements in aggressive sulfate containing environments, as the amount of C-S-H would generally become higher.

- Thaumasite was observed to form at 20^oC and the possible phase assemblages in the system SiO_2-Al_2O_3-SO_3-Fe_2O_3-CaO-MgO-Na_2O-CO_2-$CaCl_2$-$NaCl$-H_2O are as follows

No.	Phases in the subsystem C_3A-$CaSO_4$-$CaCO_3$-$CaCl_2$	Phases in excess	Degrees of freedom
1.	C_4AH_{13} + monosulfate + Friedel's salt – monocarbonate solid solution		3
2.	monosulfate + ettringite + Friedel's salt – monocarbonate solid solution	C-S-H CH FH$_3$ MH Pore solution	3
3.	ettringite + calcite + Friedel's salt – monocarbonate solid solution		3
4.	Friedel's salt + ettringite + calcite		3
5.	ettringite + calcite + thaumasite		3
6.	ettringite + thaumasite + gypsum		3

The model for the phase equilibria in hydrated Portland cement pastes was introduced into an already existing numerical routine found in the literature, for simulating the diffusion of chlorides in the multi-component pore solution of Portland cement pastes. The activity coefficient of the ions was set to 1.0. The effective diffusion coefficients for the different species were predicted from the calculated phase assemblage by using an existing composite theory. The resulting model was able to predict the ingress of chlorides from a 650 mM NaCl solution into hydrated Portland cement pastes of three types of Portland cement. Profiles of chloride, sodium and potassium measured by EDS were compared to the predicted profiles, and the fraction of Friedel's salt in the AFm solid solution phase was controlled as a function of depth. Excellent agreement was found between the experimentally determined values and those predicted by the model. The model can be applied as a basic service life prediction model for reinforced concrete submerged in aggressive environments as the ratio of chloride to hydroxyl ions in solution is computed at all depths and time-increments. The advantage of the model is that it can predict the ingress of chlorides in the Portland cement pastes, without any prior experimental calibration, and the performance of different Portland cement types in a certain environment can be compared.

Complete verification of the Finite Difference Model is still to be carried out as the number of experimental tests was limited and the prepared mortars for verification purposes proved to be of very poor quality.

Following partial conclusions were drawn during the development of the ingress model,

- Alkalis are transported (both from ingress and leaching) at a much lower rate than predicted from the intrinsic diffusion coefficients. The predicted effective diffusion coefficients of alkali ions have to be scaled down approx. 20 fold. The reason for this was not studied, but it could be a consequence of hydroxyl ions (from dissolution of $Ca(OH)_2$) being readily available for balancing the charge of the solution when chloride ingresses, whilst reactions of alkalis with the C-S-H may be a slow process.

- The predicted phase assemblage as a function of depth when assuming quasi-instantaneous reaction rates is in agreement with those measured on the exposed Portland cement pastes.

- The presence of sulfates in the chloride containing exposure solution had a positive effect by reducing the ingress of chlorides in the WPC(4) Portland cement paste, due to its high sulfate resistance. However, it was not possible to include the reactions of sulfates in the Finite Element Model as it is unknown what occurs once all capillary porosity is taken up by reaction products; can reactions no longer occur? Is it necessary to introduce fracture mechanics to simulate crack formation? Is the dominant mechanism a slow but progressive dissolution of the surface of the concrete? This should be studied further because it may have a large effect on the service life of structures in marine environments, where sulfates are always present.

10 Topics for further research

The following investigations are recommended:

- Further verification of phase equilibria model, especially with supplementary cementitious materials.

- Further development of the phase equilibria model to for use in pastes with low w/p-ratio, incomplete hydration, and the capillary porosity is significantly reduced or non-existent. Pressure may change and lead to extra degree of freedom.

- Effect of temperature on the applicable phase diagrams.

- Mineralogical studies on the composition of the C-S-H, special interest on solid solutions with other components, e.g. Na_2O, K_2O, Al_2O_3, SO_3, Fe_2O_3, MgO, and the effect that the incorporation of these ions has on the alkali binding properties of the C-S-H.

- Study on the expansion due to sulfate exposure as a function of the cement paste's potential ettringite formation against the initial volume of paste, when accounting for the degree of hydration of C_4AF in grey Portland cements. Can the sulfate resistance of a Portland cement paste be evaluated from such a relationship?

- Prediction of the effect of sulfate attack. Research on reactions taking place at the surface layer of the concrete, among others, precipitation of gypsum and brucite. What is the effective diffusivity of such layers and how can they best be implemented in a service life prediction model.

- Quantification of the effect of ITZ (Interfacial Transition Zone) between the cement paste matrix and aggregate and their connectivity, microcracks, and pore size distribution and connectivity of pores, as a function of particle size distribution of all constituents of the concrete and composition of the cement.

- The study of the transport of alkalis into cementitious materials. Why do the effective diffusion coefficients need to be adjusted?

- Study of the chloride binding at high sulfate contents where gypsum is formed. As gypsum and Friedel's salt appear to be incompatible phases, what are the possible phase assemblages are high sulfate contents?

11 References

ACI 222.3R-03

    ACI Committee 222, ACI 222.3R-03: Design and construction practices to mitigate corrosion of reinforcement in concrete structures. American Concrete Institute, Farmington Hills, Michigan, 2003.

Al-Amoudi [1995]

    Al-Amoudi, O.S.B., Performance of 15 reinforced concrete mixtures in magnesium-sodium sulfate environments. Construction and Building Materials (9) no. 3, pp. 149-158, 1995.

Atkins [1998]

    Atkins, P.W., Physical Chemistry 6th edition. Oxford University Press, Oxford, 1998.

Bentz [1997]

    Bentz, D.P., Three-dimensional computer simulation of Portland cement hydration and microstructure development. Journal of the American Ceramic Society (80), pp. 3-21, 1997.

Birnin-Yauri and Glasser [1998]

    Birnin-Yauri, U.A. and Glasser, F.P. Friedel's salt, $Ca_2Al(OH)_6(Cl,OH)$. $2H_2O$: Its solid solution and their role in chloride binding. Cement and Concrete Research (28), pp. 1713-1723, 1998.

CRC Handbook [1982]

    CRC Handbook of Chemistry and Physics, 63rd edition, edited by Weast, R.C., CRC Press, Roca Raton, Florida, 1982.

Damidot and Glasser [1993]

    Damindot, D. and Glasser, F.P., Thermodynamic investigation of the $CaO-Al_2O_3-CaSO_4-H_2O$ system at 25°C and the influence of Na_2O. Cement and Concrete Research (23) no. 6, pp. 221-238, 1993.

Damidot and Glasser [1995]

    Damidot, D. and Glasser, F.P., Thermodynamic investigation of the $CaO-Al_2O_3-CaSO_4-CaCO_3-H_2O$, Advances in Cement Research (27), pp. 129-134, 1995.

Famy et al. [2002]

    Famy, C., Scrivener, K.L., Atkinson, A. and Brough, A.R., Effects of an early or a late heat treatment on the microstructure and composition of inner C-S-H products of Portland cement mortars. Cement and Concrete Research (32), pp. 269-278, 2002.

Famy et al. [2003]

    Famy, C., Brough, A.R., Taylor, H.F.W., The C-S-H gel of Portland cement mortars: Part I. The interpretation of energy-dispersive X-ray microanalyses from scanning electron microscopy, with some observations on C-S-H, AFm and AFt phase compositions. Cement and Concrete Research (33), pp. 1389-1398, 2003.

Fuglsang-Nielsen [2004]

    Fuglsang-Nielsen, L., Composite materials- mechanical and physical behaviour as influenced by phase geometry. Dep. of Civil Engineering, Technical University of Denmark, expected to 2004.

Fukuhara et al [1981]

    Fukuhara, M., Goto, S., Asaga, K., Daimon, M. and Kondo, R., Mechanisms of C_4AF hydration with gypsum, Cement and Concrete Research (11), pp. 407-414, 1981.

Glass et al. [1997]

Glass, G.K., Hassanein, N.M. and Buenfeld, N.R., Neural network modelling of chloride binding, Magazine of Concrete Research (49) No. 181, pp. 323-335, 1997

Gollop and Taylor [1996]

Gollop, R.S. and Taylor, H.F.W., Microstructural and Microanalytical Studies of Sulfate Attack. V. Comparison of Different Slag Blends. Cement and Concrete Research (26) no. 7, pp. 1029-1044, 1996.

Glasser [2001]

Glasser, F.P., Role of chemical binding in diffusion and mass transport. In: Ion and mass transport in cement-based materials, pp. 129-180, Edited by: Hooton, R.D., Thomas, M.D.A., Marchand, J. and Beaudoin, J.J. Materials Science of Concrete, Special volume. The American Ceramic Society, United States of America, 2001.

Herfort and Juel [2001]

Herfort,D and Juel,I.A., The mineralogy of sulfate and sea water attack on concrete interpreted from EPMA analysis. Proceedings of the 23rd International Conference on Cement Microscopy, Albuquerque, New Mexico, 2001.

HETEK53 [1996]

HETEK report no. 53, Chloride Penetration into Concrete, State of the Art. Nilson, L.-O., Poulsen, E., Sandberg, P., Sørensen, H.E. and Klinghoffer, O. The Danish Road Directorate, 1996.

HETEK83 [1997]

HETEK report no. 83, A system for prediction of chloride ingress into concrete, Theoretical background. Nilson, L.-O., Sandberg, P., Poulsen, E., Tang, L., Andersen, A. and Frederiksen, J.M. The Danish Road Directorate, 1997.

Hong and Glasser [1999]

Hong, S.-Y. and Glasser, F.P., Alkali binding in cement pastes. Part I. The C-S-H phase. Cement and Concrete Research (29), pp. 1893-1903, 1999.

Hong and Glasser [2002]

Hong, S.-Y. and Glasser, F.P., Alkali sorption by C-S-H and C-A-S-H gels. Part II. Role of alumina. Cement and Concrete Research (32), pp. 1101-1111, 2002.

Hussain and Rasheeduzzafar [1994]

Hussain, S.E. and Rasheeduzzafar, A.S., Influence of sulfates on chloride binding in cements. Cement and Concrete Research (24), pp. 8-24, 1994.

Jensen et al. [2000]

Jensen, O.M., Korzen, M.S.H., Jakobsen, H.J. and Skibsted, J., Influence of cement constitution on chloride binding in cement paste. Advances in Cement Research (12-2), pp. 57-64, 2000.

Jensen et al. [1999]

Jensen, O.M., Chloride Ingress in Cement Paste and Mortar measured by Electron Probe Micro Analysis. Dept. of Civil Engineering. Technical University of Denmark. Series R No.51, Lyngby, 1999.

Juel and Herfort [2002a]

Juel,I.A. and Herfort,D. The durability of concrete to sulfate and seawater attack. Proceedings of the XVIII Symposium on Nordic Concrete Research, Helsingør, Denmark, June 2002.

Juel and Herfort [2002b]

Juel,I.A. and Herfort,D. The mineralogy of chloride attack on concrete containing limestone filler. Proceedings of the 24th International Conference on Cement Microscopy, San Diego, California, 2002.

Juel [2003]

Juel, I.A. Mineralogical and Thermodynamic Porcesses by Sulfate and Seawater Attack of Danish Concrete. Danish Industrial Ph.D. project, EF-816 Durability in cooperation between Research and Development Centre, Aalborg Portland A/S, and Gaological Institute, University of Copenhagen, Copenhagen 2003.

Korzen [1998]

Korzen, M.S.H. Chloride binding in cement paste (in Danish). Master Thesis at the Department of Civil Engineering, Technical University of Denmark, Lyngby, Denmark, 1998.

Kurtis et al. [2000]

Kurtis, E.K., Monteiro, P.J.M., and Madanat, S.M., Empirical models to predict concrete expansion caused by sulfate attack, ACI Materials Journal (97-M20), pp. 156-161, 2000.

Kuzel and Pöllmann [1991]

Kuzel, H.-J. and Pöllmann, H., Hydration of C_3A in the presence of $Ca(OH)_2$, $CaSO_4.2H_2O$ and $CaCO_3$, Cement and Concrete Research (21), pp. 885-895, 1991.

Lea [1970]

Lea, F.M., The chemistry of cement and concrete, 3rd edition, Edward Arnold Ltd Press, 1970.

Lindvall [2001]

Lindvall, A., Probabilistic, Performance-Based Service Life Design of Concrete Structures: Environmental Actions and Response. In: Ion and mass transport in cement-based materials, pp. 323-340, Edited by: Hooton, R.D., Thomas, M.D.A., Marchand, J. and Beaudoin, J.J. Materials Science of Concrete, Special volume. The American Ceramic Society, United States of America, 2001.

Mason [1978]

Mason, R., Petrology of the metamorphic rocks, Vol. III. George Allen & Unwin (publishers) Ltd., London, 1978.

Palecki and Setzer [2001]

Palecki, S. and Setzer, M.J., Life-time prediction of high performance concrete with respect to durability (CONLIFE). Proceedings: Workshop on Durability of Exposed Concrete Containing Secondary Cementitious Materials, November 21-23 Hirtshals. Denmark, 2001.

Patzias [1991]

Patzias, T., 'The development of ASTM Method C1012 with Recommended Acceptance Limits for Sulfate Resistance of Hydraulic Cements', Cement, Concrete, and Aggregates, CCAGDP, Vol. 13, No.1, pp. 50-57, 1991.

Putnis and McConnell [1980]

Putnis, A. and McConnell, J.D.C., Principles of mineral behaviour. Elsevier, New York, 1980.

Richardson [2000]

Richardson, I.G., The nature of C-S-H in hardened cements. Cement and Concrete Research (29), pp. 1131-1147, 1999.

Samson et al [2001]

Samson, E., Marchand, J. and Maltais, Y., Modelling Ionic Diffusion Mechanisms in Saturated Cement-Based Materials-An Overview. In: Ion and mass transport in cement-based materials, pp. 97-112, Edited by: Hooton, R.D., Thomas, M.D.A., Marchand, J. and Beaudoin, J.J. Materials Science of Concrete, Special volume. The American Ceramic Society, United States of America, 2001.

Saremi and Mahallati [2002]

Saremi, M. and Mahallati, E., A study of chloride induced depassivation of mild steel in simulated concrete pore solution, Cement and Concrete Research (32), pp. 1915-1921, 2002.

Tang and Nilsson [1993]

Tang,L. and Nilsson,O. Chloride binding capacity and binding isotherms of OPC pates and mortars, Cement and Concrete Research (23), pp.247-253, 1993.

Tang [1996]

Tang,L., Electrically accelerated methods for determining diffusivity in concrete current development, Magazine of Concrete Research (48) No. 176, 1996

Tang [1999]

Tang,L., Concentration dependence of diffusion and migration of chloride ions. Part 2. Experimental evaluations, Cement and Concrete Research (29), pp.1469-1474, 1999.

Taylor [1997]

Taylor, H.F.W., Cement Chemistry, 2nd Edition. Thomas Telford Services Ltd., London, 1997.

Taylor and Newbury [1984]

Taylor, H.F.W, and Newbury, D.E., An electron microprobe study of a mature cement paste, Cement and Concrete Research (14), pp. 565-573, 1984.

Teoreanu et al [1979]

Teoreanu, I., Filoti, G., Hritcu, C., Bucea, L., Spânu, V., Ciocanel, S. and Ivascu, M., Interaction mechanism of $2CaO.Fe_2O_3$ and $4CaO.Al_2O_3.Fe_2O_3$ with water, at various pressures and temperatures, Il Cemento, Vol. 76, pp. 19-28, 1979.

Truc [2000]

Truc, O., Prediction of chloride penetration into saturated concrete – Multi-species approach, Doctoral Thesis, publication P-00:4, Department of Building Materials, Chalmers University of Technology, Göteborg, Sweden, 2000.

Tuutti [1982]

Tuutti, K. Corrosion of Steel in Concrete. Swedish Cement and Concrete Research Institute, Stockhom. Report No. CBI Research FO 4:82, 1982.

Volkwein [1995]

Volkwein, A., Penetration of chlorides into concrete – Phenomena and consequences. Points of view based on 20 years research and site experience with deicing salts. Proceedings of the International RILEM workshop on Chloride penetration into concrete, St-Rémy-lès-Chevreuse, France, 1995.

Xu [1997]

Xu, Y., The influence of sulfates on chloride binding and pore solution chemistry. Cement and Concrete Research (27), pp. 1841-1850, 1997.

APPENDICES

Appendix A: Publications

Paper I:
The durability of white Portland cement to chloride and sea water attack
Paper II:
Effect of solid solution of AFm phases on chloride binding
Paper III:
Phase equilibria in hydrated Portland cement
Paper IV:
Binding of chloride and alkalis in Portland cement systems
Paper V:
Performance of white Portland cement in aggressive environments
Paper VI:
Chloride binding in the CaO-SiO_2-Al_2O_3-Fe_2O_3-SO_3-Na_2O-CO_2-H_2O system for PC
Paper VII:
Chloride diffusion in partially saturated cementitious material

Appendix B: Materials

Phase equilibria

Non-steady state ingress of aggressive ions

Appendix C: Experimental procedures

Appendix D: Properties of phases selected for the model

Appendix E: Data for equilibria in PC systems at varying chloride and alkali content

Appendix F: Data for equilibria in PC systems at varying MgSO$_4$ content

Appendix G: Matlab codes for the FDM for chloride ingress

Main program "main.m"

Code of function "initial.m"

Code of function "initial.m"

Code of function "surf.m"

Code of function "MSing.m"

Code of function "equil.m"

Appendix A:

Paper I: The durability of white Portland cement to chloride and sea water attack

Nielsen, E.P., Herfort, D., and Geiker, M.R.

NCR - Workshop Proceedings No.3. Nordic Miniseminar – Durability of exposed concrete containing secondary cementitious materials. Hirtshals, November 21-23, 2001.

ABSTRACT

A PhD-project is described which is designed to test the hypothesis that white Portland cement significantly improves the durability of concrete to selected types of attack, including chlorides which is the main focus of the study. This hypothesis is mainly based on the premise that white Portland cement results in a lower porosity and permeability than can be achieved with conventional grey Portland cements. In order to test this hypothesis the rate of chloride ingress and sulfate attack over a range of composition is studied, particularly with regard to the aluminate content which plays a major role in binding both chlorides and sulfates.

Key words: white Portland cement, chlorides, durability, phase rule.

INTRODUCTION

Durability concerns play a major role in the design of reinforced concrete structures in aggressive environments, for example where de-icing salts are used or in marine environments.

It is generally agreed that when chlorides penetrate into concrete they become partially fixed by the hydrate phases by one or more processes collectively referred to as binding. The mechanisms are still not entirely clear [1] but it is assumed that it is mainly the aluminium-bearing hydration products that react chemically with the chloride ions and form Friedel's salt or solid solutions which include Friedel's salt. Competition for the aluminates by the sulfate and carbonate ions will affect the capacity of the system to bind chlorides. The very high specific surface area of the C-S-H phase is often believed to substantially contribute to binding through physical absorption, although evidence that it plays little or no role is also convincing [2]. Binding is also influenced by temperature [1].

Some authors have found good agreement between experimental data and theoretical models which assume that the binding of chloride ions occurs spontaneously [3], whilst others have measured periods of up to a week before chloride binding in Ordinary Portland Cement pastes reaches equilibrium [4], with the rate of diffusion depending on the experimental conditions in question. Since binding is a key factor in controlling the rate of ingress, this topic is in need of thorough investigation.

Among existing models, a numerical routine developed at Chalmers University [5] predicts the rate of diffusion-based ingress of chloride ions in fully saturated material by taking into account the interaction with other ions in the transport process. The effect of the microstructural development and moisture content on transport is not included in this model.

One of the parameters relevant for service life design and reassessment of concrete structures which has not been fully addressed, is the effect of the degree of saturation and the state of moisture on the ingress of chlorides into reinforced concrete structures. Except in fully submerged parts of marine structures, concrete is rarely completely saturated when exposed to chlorides or other deteriorating agents.

Some empirical models (e.g. [9]), which include the degree of saturation, are available. A theoretical approach was proposed in [6,7], where the diffusion coefficients of ions were calculated by combining the composite theory [3] with Powers' model for the phase composition [8]. A similar approach has recently been proposed, but without distinguishing between the rate of diffusion in the capillary and 'gel' pores [12,13], and without taking into account the microstructural changes due to reactions within the system. Compared to an earlier empirical model, which includes the effect of relative humidity on the rate of diffusion [9], better agreement between experimental and theoretical results have been obtained by [6,7]. The method still needs verification, and further development is needed to improve the model for percolation through the capillary pores, and to increase the field of application for different cement types.

Preliminary investigations at Aalborg Portland predict non-pozzolanic systems based on white Portland cement to have a significantly lower capillary porosity (after all of the cement has reacted) than comparable systems containing grey cement; and assuming that pore distributions and connectivity remain unaffected, to have lower permeability. At equal porosity, the sulfate resistance of white Portland cement from Aalborg Portland is expected to be significantly greater than that of most grey sulfate resisting cements owing to its lower Al_2O_3 content, of only 1.9%. The low alkali content of white Portland cement, which is generally in the region of 0.2 $Na_2O_{,equivalent}$, can be safely assumed to involve lower risks of both alkali aggregate reaction, and delayed ettringite formation from heat curing or excessive heat of hydration.

Areas which could suggest poorer durability of concrete produced from white Portland cement include excessive heat of hydration, since most white Portland cements are rapid hardening, and may facilitate early age cracking, and lower chloride binding due to lower Al_2O_3 contents, particularly of the white Portland cement from Aalborg Portland's plant in Denmark. An obvious solution to this would be to add an Al_2O_3 rich pozzolan such as granulated blast furnace slag which, apart from increasing chloride binding and lowering the heat of hydration, is predicted to further reduce permeability as a result of lower capillary porosities. The effect of silica fume, on the other hand, is less clear. Although it clearly reduces capillary porosity, its effect on chloride binding is open to debate. According to models which rely solely on the binding of the aluminate bearing hydrate phases [10], silica fume should have no effect despite several reports to the contrary such as in [11]. Our explanation for silica fume's apparent effect is that, at levels of replacement sufficiently high for all portlandite to be exhausted, higher ratios of Si/Ca result in the C-S-H phase which can then accommodate higher levels of alkali by adsorption. This in turn results in lower concentrations of both alkalis and chloride in the pore solution.

MODELS

The aim of the project is to develop a model for diffusion based ingress of chloride ions in presence of sulfate, carbonate and alkali ions to be used for service life prediction. Different degrees of saturation are to be included to the model. The service life prediction model will result from the combination of two separate models, i.e. phase equilibria and ingress, as described below.

Phase Equilibria and microstructure

The model will be based on the hydrate phase assemblages, and the relative contents of phases within the assemblages, calculated from the chemical composition of the anhydrous cementitious constituents plus water. The calculations will assume thermodynamically stable or metastable equilibrium, and therefore strict observance with the phase rule. As a first approximation, the model will assume invariant assemblages at constant temperature (and pressure), containing the maximum number of phases, i.e. where the number of phases is equal to the number of chemical components.

The relative contents of phases in weight % within the system can be calculated by solving 'n' equations for 'n' unknowns, where 'n' is the number of components and phases. This can be performed on a 'n x n' matrix where the determinant corresponds to the chemical composition of the system and the known chemical compositions of the phases are entered into the matrix. The result can be recalculated to volume % from the phase densities. Account will then be taken of the possibility of solid solution of phases such as Friedel's salt with the other AFm phases, and variable alkali contents, both of which would introduce degrees of freedom which among other things allow variability in the concentration of free chlorides in the pore solution. The above calculations will be used to determine the relative contents of all phases with increasing additions of chlorides, sulfates and alkalis in addition to the theoretical capillary porosity. An attempt will also be made to model the permeability of the cement matrix based on the size and spatial distribution of pores calculated from the distributions of the anhydrous material at different water/cement ratios.

Kinetic model

In addition to the phase equilibria model kinetic variables responsible for diffusion will also be taken into account. This will primarily involve modelling the relationship between the rate of ingress and porosity, pore size distribution and the extent of physical adsorption, e.g. at the surface of the C-S-H phase. A "multi-species" approach, as the described in [5], will be used for simulating the diffusion of ions within the pore solution.

Combined model

A combined model will be obtained by combining the phase equilibria and kinetic models to determine the effective diffusion coefficient in the cement matrix, i.e. by combining the intrinsic diffusion coefficients of free chloride ions through the capillary and 'gel' pores, and the distribution of chlorides between the hydrate phases and the pore solution as a function of the mineralogical composition. Finally, the effect of different degrees of saturation will be included towards the end of the project by applying the model proposed in [6,7].

EXPERIMENTAL

The experimental procedure designed to test the above models will essentially involve testing of paste specimens covering a range of compositions listed below:

Low-alumina white PC (4.5% C_3A) + GBFS (0, 30%) + SF (0,10,30%)

High-alumina white PC (12% C_3A)

Ordinary PC + GBFS (0, 30%).

The three cements are EN 197-1 CEM I 52.5 N.

The pastes will be prepared at a high water cement ratio to allow rapid reaction before subsequent exposure: water cement ratios of 0.70 and 0.45 are used for microstructure and transport, respectively.

Paste mineralogy

Once hydration has essentially gone to completion, the paste specimens will be immersed in solutions of $CaCl_2$ and $MgSO_4$ at three different levels of alkali-concentration, over a range of concentrations allowing progressively higher degrees of reaction or binding to take place (i.e. Cl binding isotherms etc.). Once equilibrium is obtained, the mineral phases in the paste will be identified by a combination of EPMA and XRD analysis, whilst the pore solution will be analysed by ICP (Inductively Coupled Plasma Atomic Emission Spectrometry) and AA (Atomic Absorption) for all major components, by analysing the above solutions after removal of the paste specimens. The experimental set-up for the exposure of specimens is shown in fig.1.
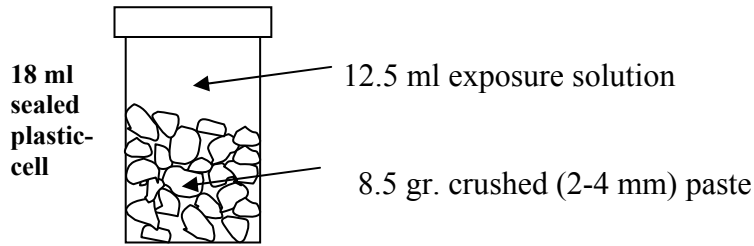
Figure 1: Experimental set-up for the chloride binding-isotherms.

Paste porosity

The capillary porosity, air content, pore size distribution and water sorption isotherms of pastes with similar compositions will be determined by vacuum- and pressure saturation, low-temperature microcalorimetry and RH-conditioning (RH ranging from 11% to 98%), respectively, at lower water cement ratios than those used above for the mineralogical analysis, i.e. 0.45.

Ingress of ions

A series of tests on mortars and/or pastes will be performed with the primary goal of verifying the combined model; i.e. by determining rates of ingress, particularly of chlorides, as a function of the two sets of variables, i.e. mineralogy and paste porosity.

The water powder ratio for the samples will be 0.45. Similar procedures will be carried out in order to determine the rate of sulfate diffusion and the phase development, in addition to seawater where the combined diffusion of both chlorides and sulfate are involved.

In-situ testing

A series of large concrete slabs will be placed in a marine exposure site on the west coast of Jutland to study the performance of the concrete when exposed to real-life conditions and to verify and further develop the service life model. This study will, of course, extend beyond the completion date for the PhD project described here. The concrete compositions chosen will allow the effect of different alumina and silica contents to be studied at the same porosity and the effect of variable porosity to be studied at the same alumina and silica contents.

REFERENCES

1. O.M.Jensen, M.S.H. Korzen, H.J.Jakobsen and J.Skibsted, Influence of Cement Paste Constitution and Temperature on Chloride Binding in Cement Paste. Advances in Concrete Research 12 No.2, April 2000.
2. Lambert, P., Page, C.L. and Short, N.R., Pore solution chemistry of the hydrated system Tricalcium silicate/Sodium chloride/water. Cement and Concrete Research, Vol.15, 1985.
3. O.M.Jensen, Chloride Ingress in Cement Paste and Mortar Measured by Electron Probe Micro Analysis, Dept. of Structural Engineering and Materials, Technical University of Denmark. Series R No. 51, 1999.
4. Tang L. and L.-O.Nilsson, Chloride Binding Capacity and Binding Isotherms of OPC Pastes and Mortars, Cement and Concrete Research, Vol.23, 1993.
5. Olivier Truc, Prediction of Chloride Penetration into Saturated Concrete- Multi-Species Approach. Ph.D thesis at the Department of Building Materials, Chalmers University of Technology, Göteborg, Sweden 2000.
6. E.P.Nilsen, Transport Mechanisms in Cementitious Materials. MSc thesis, BYG·DTU, April 2001.
7. E.P.Nielsen and M.Geiker, Transport of Moisture and Chlorides in partially Saturated Cementitious Material, submitted for publication in Cement and Concrete Research.

8. T.C.Powers and T.L.Brownyard, Studies of physical properties of hardened portland cement paste. Jour. Amer. Concr. Inst., Vol. 43 or Portland Cem. Ass. Bull. No. 22, 1946-47)

9. A.V.Saetta, R.V.Scotta, and R.Vitalini, Analysis of Chloride Diffusion into Partially Saturated Concrete. ACI Materials Journal, Vol.90, M47. Sept-Oct 1993.

10. U.A.Birnin-Yauri and F.P.Glasser, Friedel's salt, Ca2Al(OH)6(Cl,OH).2H2O: Its solid solution and their role in chloride binding, Cement and Concrete Research, Vol.28, No.12, pp.1713-1723, 1998

11. T.Yamato, M.Soeda and Y Emoto, Chemical resistance of concrete containing condensed silica fume. In:Proceedings of the 3rd International Congress on fly ash, silica fume, slag, and natural pozzolans in concrete, Trondheim, 1989. ACI Special publication 114;vol.Iipp.897-913.

12. T.Ishida, An integrated computational system of mass/energy generation, transport and mechanics of materials and structures, PhD thesis, University of Tokyo, 1999 (in Japanese), referred to in [12].

13. K.Maekawa and T.Ishida, Service life evaluation and durability design system for self-compacting concrete. In Proceedings of 2nd International Symposium on self-compacting concrete, Tokyo, 2001. Edt. by K.Ozawa and M.Ouchi.

Paper II: Effect of solid solution of AFm phases on chloride binding

Nielsen, E.P., Herfort, D., Geiker, M.R and Hooton, R.D.

Proceedings of the 11th International Congress on the Chemistry of Cement, Durban, South Africa, 11-16 May 2003.

ABSTRACT:

The phase rule has been applied to model the binding of chlorides in hydrated Portland cements. The model predicts the solid solution of at least two AFm phases. It was tested in the laboratory on cement pastes prepared from white Portland cements containing 4 and 12% C_3A, and a grey Portland cement containing 7% C_3A. 1% calcite was added to all cements. The pastes were stored in solutions of different Cl (from $CaCl_2$) and Na (from NaOH) concentrations. When equilibrium was reached the mineralogy of the pastes was investigated by XRD and EDS analysis on the SEM. The solution was also analysed for Cl in addition to all other major components. The distribution of chloride between the solution and the solid phases was found to be controlled by an AFm solid solution phase consisting of monocarbonate and Friedel's salt. Higher contents of Friedel's salt in this solid solution phase corresponded to in higher concentrations of Cl in the aqueous solution. Chloride was also bound by the C-S-H phase, but this too was governed by the content of Friedel's salt in the solid solution phase. All of the results obtained can be predicted by applying the phase rule and assuming equilibrium conditions.

INTRODUCTION

The harshest conditions that concrete can be subjected to usually involve some form of attack by chlorides. These include marine environments, roads and bridges exposed to de-icing salt, etc. In the case of reinforced concrete, the time it takes for the chlorides to migrate to the reinforcement is the main parameter used to predict the service life of the concrete.

It is generally agreed that when chlorides migrate into concrete they become partially fixed by the hydrate phases through one or more processes collectively referred to as binding. The binding capacity of the cement paste system has a significant effect on the service life of reinforced concrete, where only chlorides in solution can be transported towards the reinforcement where at some critical concentration they initiate corrosion.

The mechanisms that result in binding of chloride ions are still not entirely clear [1], but it is assumed that it is mainly the aluminium-bearing hydration products that react chemically with the chloride ions to form Friedel's salt, or solid solutions which include Friedel's salt [3]. Competition for the aluminates by the sulfate and carbonate ions will affect the capacity of the system to bind chlorides. The very high specific surface area of the C-S-H phase is often believed to substantially contribute to binding through physical adsorption [7], although evidence that it plays little or no role is also convincing [4].

The binding process is normally examined by determining the contents of chlorides bound in cement paste as a function of the concentration of chlorides in an external solution over a wide range of total chloride contents. The results are then expressed by means of the so-called Langmuir or Freundlich isotherms [5], depending on which of these provides the best fit over the range of concentrations examined. In this paper we describe a thermodynamic model based on the phase rule for predicting the stable or metastable equilibrium phase assemblages in cement paste. The model is specifically applied to binding of chloride ions in presence of carbonates at constant alkalis contents. The model is then tested experimentally in the laboratory.

THERMODYNAMIC MODEL BASED ON THE PHASE RULE

Although the 'Phase Rule' is valid for all chemical systems in equilibrium, only a handful of workers have used it to describe hydrated cement [2,8,9]. The rule states that the number of *phases (P)* plus the *degrees of freedom (F)* in a system is equal to the number of *components (C)* plus *n*. In the standard form *n* is equal to 2, but at constant temperature and pressure *n* can be reduced to 0, so that the phase rule becomes $P + F = C$.

The main components in hydrated Portland cement are CaO, SiO_2, Al_2O_3, Fe_2O_3, SO_3 and H_2O. The maximum number of phases that can form in the fully hydrated system (for the invariant assemblage where F=0) is, therefore, six. For a typical Portland cement these phases would be the C-S-H phase, portlandite, monosulfate, ettringite, an iron oxide phase (possibly FH_3) and the pore solution. From the chemical composition of the system, and standard chemical compositions of the individual hydrate phases, the contents of phases in wt. % within any invariant system can be calculated by solving 'n' equations for 'n' unknowns, where 'n' is the number of components and phases. As a first approximation the composition of the pore solution is set to that of pure H_2O. This is valid as long as the weight fraction of components dissolved is negligible compared to the weight fraction that has reacted to form solid phases.

The introduction of chloride and carbonate adds two extra components to the system allowing up to eight phases at constant temperature and pressure. At small additions of these components the two additional phases would normally be the AFm phases, monocarbonate, and Friedel's salt. For convenience, $CaCl_2$, $CaCO_3$, $CaSO_4$ and C_3A are chosen as components in this paper rather than Cl, CO_2, SO_3, and Al_2O_3. This is valid as long as these components occur as stoichiometric units in all hydrate phases. The presence of sodium (or potassium) introduces a degree of freedom rather than an extra phase, except at very high concentrations, but this can be disregarded when the alkali content is held constant. When $CaCO_3$ and $CaCl_2$ (and additional $CaSO_4$) are introduced to the 6-component system for hydrated Portland cement, all of the changes in phase assemblages (except at very high contents) take place within the subsystem for C_3A-$CaSO_4$-$CaCl_2$-$CaCO_3$. The other phases (i.e. C-S-H, $Ca(OH)_2$, FH_3, pore solution) occur as excess phases which participate in all phase assemblages, and as long as invariant conditions prevail remain constant in composition within any given assemblage. The 4-component sub-system C_3A-$CaSO_4$-$CaCl_2$-$CaCO_3$ is illustrated in fig.1 by means of the two 3-component sub-systems for chloride attack (fig 1a), and carbonate addition (fig.1b).
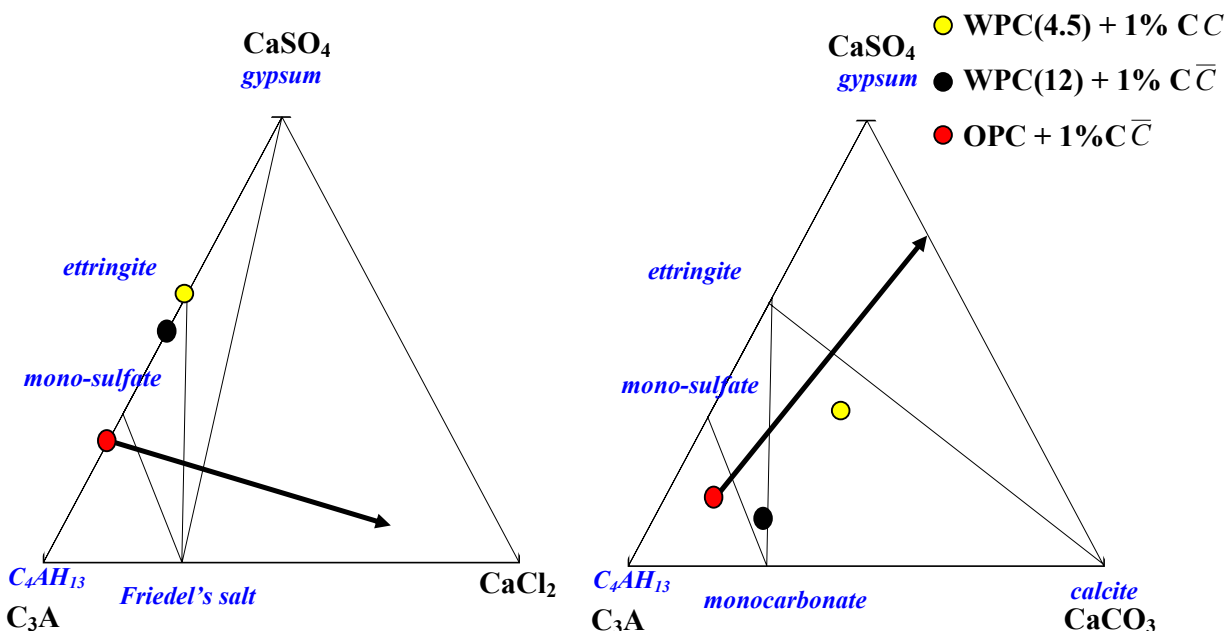
Figure 1a. sub-system for C_3A-$CaSO_4$-$CaCl_2$ Figure 1b. sub-system for C_3A-$CaSO_4$-$CaCO_3$.

Arrow schematises the change in phase contents with increased CaCl₂. Filled circles indicate initial composition for all three pastes examined (see table 2) before chloride addition.

The addition of $CaCl_2$ to an under-sulfated Portland cement consisting of hydroxy AFm and monosulfate shown in fig. 1a for the sub-system C_3A-$CaSO_4$-$CaCl_2$ would initially form Friedel's salt. Further addition results in a exhaustion in the hydroxy AFm phase until it is eventually exhausted. Ettringite can only form at this point and continues to form along side Friedel's salt with further addition of $CaCl_2$. In all, four different 3-phase assemblages are possible with increasing $CaCl_2$ contents. Four 3-phase assemblages are also possible in the C_3A-$CaSO_4$-$CaCO_3$ shown in fig 1b. By combining the two diagrams, addition of $CaCl_2$ to a system starting out with a mixture of monosulfate, hydroxy AFm and monocarbonate, should result in the sequence of five 4-phase assemblages shown in table 1.

Table 1. Predicted sequence of phase assemblages resulting from $CaCl_2$ addition to hydrated Portland cement with relative high C_3A/$CaSO_4$ ratio.

1.	Hydroxy-AFm, Monosulfate, Monocarbonate and Friedel's salt	
2.	Monosulfate, Ettringite, Monocarbonate and Friedel's salt	Phases in excess: C-S-H, Calcium hydroxide, Goethite and Pore solution
3.	Ettringite, Calcite, Monocarbonate and Friedel's salt	
4.	Ettringite, Calcite, Gypsum and Friedel's salt	
5.	Calcite, Gypsum, Friedel's salt, + degree of freedom (i.e. ↑ of Cl in PS)	

According to the phase rule, no degrees of freedom are possible in assemblages 1 to 4 since each assemblage consists of eight components and the maximum number of phases (i.e. eight). An important constraint imposed by this invariance is that the composition of all phases must remain constant within each assemblage. However, once the total binding capacity is exhausted, i.e. when all the ettringite has reacted to form gypsum and Friedel's salt (assemblage no.5), only seven phases exist giving one degree of freedom. This degree of freedom would allow the $CaCl_2$ concentration to increase in the pore solution upon further addition, until it eventually becomes saturated with respect to $CaCl_2.2H_2O$.

A $CaCl_2$-binding isotherm for the sequence of reactions described above, at a constant level of alkalis, would be expected to develop as illustrated in figure 2. The small increases in concentration of free chloride ions are the result of probable differences in the composition of the pore solution between assemblages.
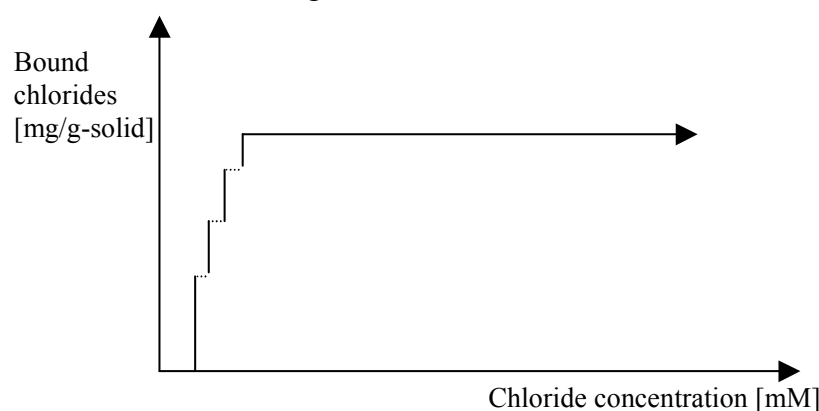
Figure 2. Schematised development of a $CaCl_2$ binding isotherm in an invariant system.

Significantly, this hypothetical isotherm for $CaCl_2$ has not been reported in the literature. Instead, the relationship between bound and free chlorides is invariably described as a

continuous curve best described by the Langmuir or Freundlich models [2,6]. This implies either non-equilibrium conditions, which in our view is unlikely, or solid solution between two or more phases. The latter would reduce the number of phases and, therefore, provide one or more degrees of freedom, which would allow the chloride concentration to increase in the pore solution as a function of the total chloride content in the system. In the absence of sulfate and carbonate, a likely candidate for this solid solution would be the hydroxy-AFm - Friedel's salt solid solution phase reported in [3]. In the presence of carbonate, a solid solution between monocarbonate and Friedel's salt has also been reported [10,11], and this, in our view, would be the most likely phase to occur in realistic systems which must always contain some carbonate. The possible solid solution of monocarbonate and Friedel's salt forms the basis of the model which is tested in this study.

EXPERIMENTAL

Three Portland cement pastes were examined: two white Portland cements with Bogue-C_3A contents of approx. 4 and 12%, and a grey ASTM type II Portland cement. All the pastes were prepared at a w/s ratio of 0.70 after replacement of the cement by 1.0 wt. % calcite (note that all of the cements already contain some CO_2, present of course as carbonate). Compositions of the cements (determined by XRF) are shown in table 2.

Table 2. Composition of the Portland cements tested

Cement	SiO_2	Al_2O_3	Fe_2O_3	CaO	SO_3	MgO	Na_2O	K_2O	CO_2[*]
WPC(4)	24.8	1.87	0.33	68.9	2.20	0.52	0.16	0.11	0.14
WPC(12)	23.6	4.49	0.21	65.9	2.38	0.97	0.03	0.20	0.72
OPC	21.0	4.90	3.64	65.1	3.00	0.89	0.30	0.41	0.08
* Determined by DTG.									

Cement id.	C_3S	C_2S	C_3A	C_4AF
WPC(4)	72.2	16.8	4.4	1.0
WPC(12)	51.7	28.6	11.5	0.6
OPC	59.1	15.6	6.8	11.1

The cement pastes were cast in 2 cm³ centrifuge tubes, sealed and kept at a constant temperature of 20°C for one month. The samples were then de-moulded and crushed to between 2-4 mm in size. The crushed paste of approximately 8.25 g was then weighed before being placed in 12.5 ml. solution for 5 months at 20°C. For each type of cement paste, the specimens were exposed to solutions of increasing $CaCl_2$ concentration, allowing progressively higher degrees of reaction, but at a constant alkali content. WPC(4) was stored at a sodium concentration (by addition of NaOH) of either 250 or 550 mM, whilst the OPC specimens were stored at 550mM and the WPC(12) specimens at 250mM.

After six months when the pastes had fully reacted with the solutions to equilibrium, the phase equilibria was exaimined by a combination of EDS (Energy Dispersive Scanning, at 15keV, 25μA and measuring time of 40 s.) and XRD (X-Ray Diffraction) analysis, and analysis of the solutions by titration (chloride and pH), ICP (Inductively Coupled Plasma Atomic Emission Spectrometry) and AA (Atomic Absorption) for all major components, after removal of the solid phases by filtration.

RESULTS AND DISCUSSION

The Al/Ca and S/Ca ratios were found by EDS analysis to be fairly constant in the C-S-H at approximately 0.04 and 0.03, respectively.

A combination of XRD and EDS analysis verified the sequence of phase assemblages 1, 2 and 3, listed in table 1, except that Friedel's salt and monocarbonate occurred in solid solution, instead of as two separate phases. As predicted, the initial assemblage to form at low contents of $CaCl_2$ in the paste prepared from the low C_3A white cement (WPC(4)), was ettringite + calcite + monocarbonate + Friedel's salt (assemblage no. 3 in table 1), or more correctly ettringite + calcite + AFm_{ss}, where the solid solution phase is a mixture of monocarbonate and Friedel's salt. The initial assemblage formed from the high C_3A white PC, (WPC(12)) corresponds to assemblage no. 2 in table 1. Assemblage no. 3 formed at higher concentrations. The initial assemblage formed at small contents of $CaCl_2$ in the paste prepared from the grey Portland cement (OPC) corresponds to assemblage no. 1 in table 1. Assemblage no. 2 followed by assemblage no. 3 formed at higher $CaCl_2$ contents for this cement. In no case was the content of $CaCl_2$ high enough to form assemblage nos. 4 and 5, although preliminary results not included here indicate that these assemblages form as well.

Solid solution was found between Friedel's salt and monocarbonate for all of the specimens examined. This is illustrated by plotting the Cl/Ca vs. Al/Ca ratios determined from EDS analysis shown in figure 3. Only two data sets are plotted here, i.e. for the low C_3A white PC (WPC(4)) with Na =550mM, at two different Cl contents. Figure 4 shows the same data, but plotted as S/Ca vs. Al/Ca. Since assemblage no 3 persisted at all chloride contents investigated for this cement, neither monosulfate nor Kuzel's salt were identified. Monosulfate was identified in assemblages 1 and 2 for the two other cements, where it invariably occurred as a pure phase without forming a solid solution with any of the other AFm phases.
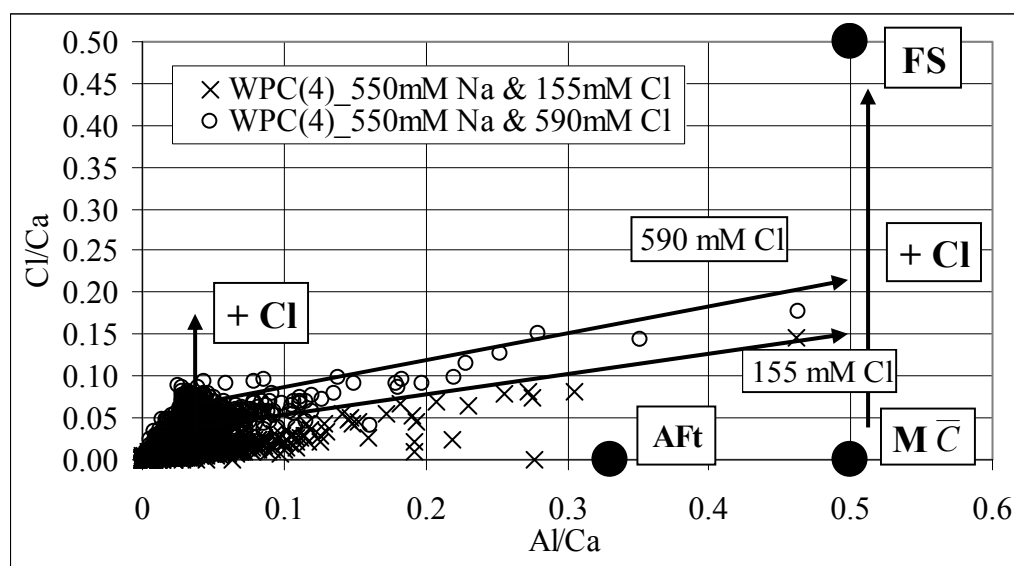
Figure 3. EDS-data illustrating the development of Cl/Ca in the AFm_{ss} phase between monocarbonate (M$\hat{C}$) and Friedel's salt (FS) and in C-S-H, at increasing Cl additions.
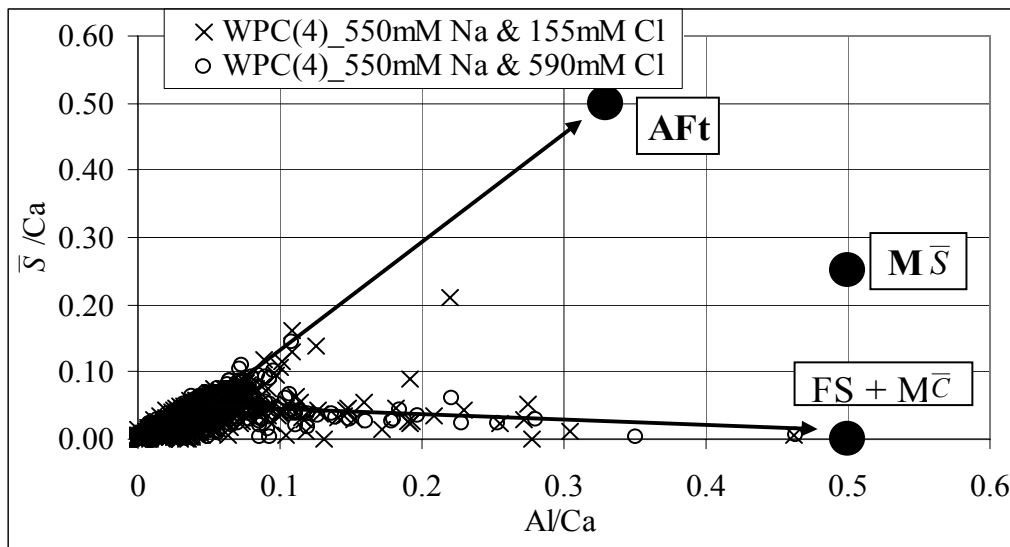
Figure 4. S/Ca vs. Al/Ca from EDS analyses. Plots are the same as the presented in figure 3.

XRD-patterns for the pastes examined confirmed the assemblages described above (not shown). For the AFm$_{ss}$ phase, the same type of ordered stacking of layers of monocarbonate and Friedel's salt described in [11] was observed.

The solid solution of Friedel's salt and monocarbonate introduces a degree of freedom to the system. This permits the relative content of Friedel's salt to increase in the AFm solid solution, along with a concomitant increase in the concentration of chloride ions in both the pore solution and in the C-S-H phase. The phase rule is satisfied as long as a single relationship exists for the distribution of Cl between all three phases regardless of C$_3$A and C-S-H contents. That such a relationship exists at constant alkali content for the two white cements can be seen in figs. 5 and 6 where, despite a marked difference in C$_3$A contents (as well as C-S-H contents due to the significant difference in C$_3$S contents in the clinker) almost exactly the same distribution is found between all three phases at the constant alkali content of 250 mM Na. Lower concentrations are found in the C-S-H phase and AFm$_{ss}$ phase at the higher concentration of 550mM Na in the solution. The difference in binding in the AFm$_{ss}$ and C-S-H phase between the white and grey cements is possibly due to the presence of iron in the grey cement which adds an extra degree of freedom to the system. The relationship between the concentration of Cl in the C-S-H phase and the AFm$_{ss}$ phase (fig.6) appears to be independent of the alkali content.
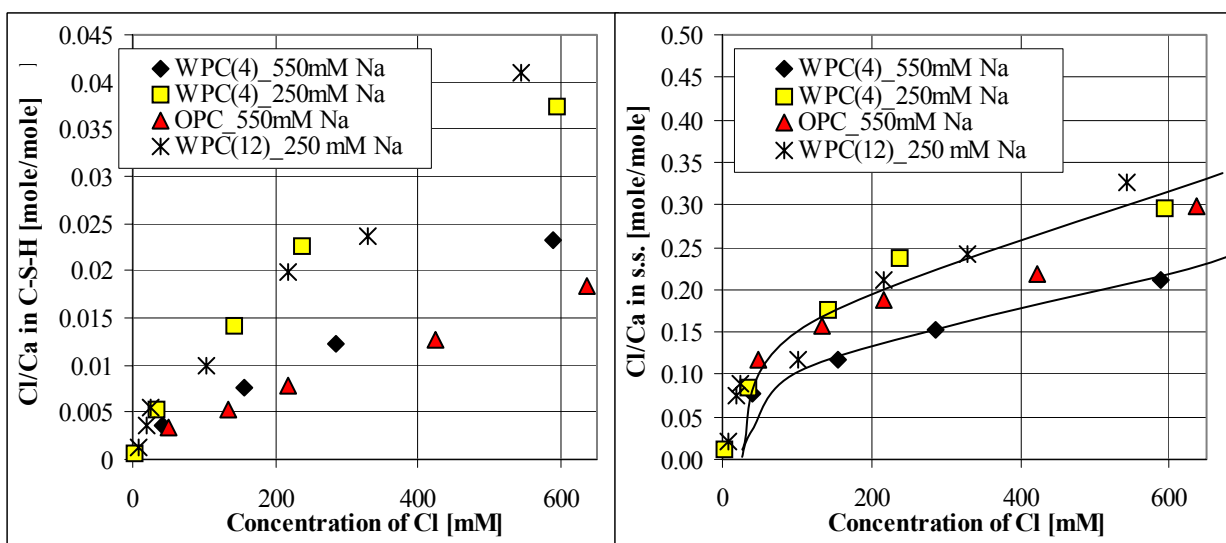
Figure 5. Cl/Ca ratio in the C-S-H and AFm$_{ss}$ phases versus the concentration of Cl$^-$.
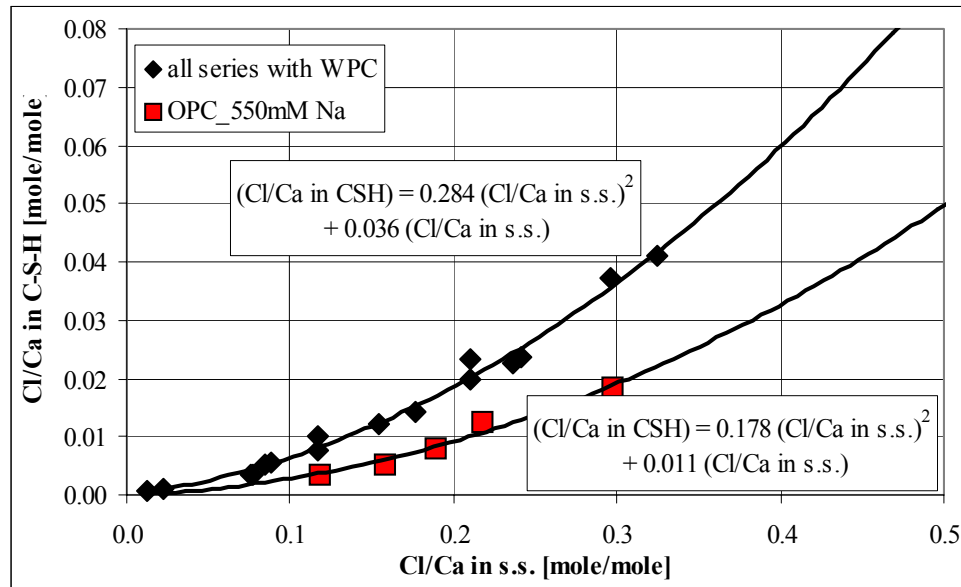
Figure 6. Cl/C ratio in the C-S-H versus the Cl/Ca ratio in the AFm$_{ss}$ phase for all cements and alkali contents.

The above relationships apply to the distribution of chloride between the individual phases, but not to the ratio of total bound and free chlorides, since this will of course vary depending on cement composition (i.e. C_3A content etc.). This is clear from the traditional Cl isotherm shown in figure 7 (for the same data used in figs. 5 and 6) where different isotherms clearly exist for the two white cements.
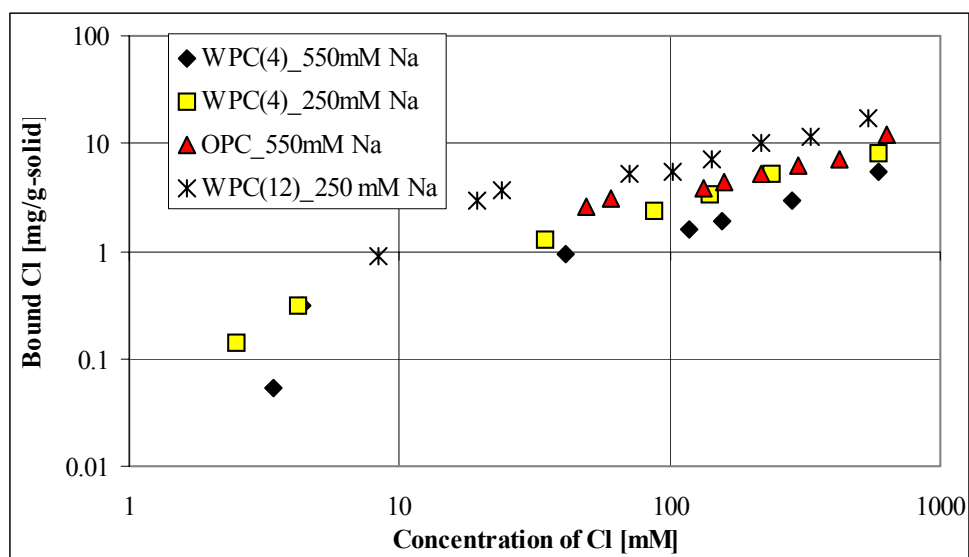
Figure 7. Chloride binding isotherms for the same data shown in figs 5 and 6.

The above relationship can be understood more readily from the ternary subsystem shown in fig.8 which is constructed from figs. 5 and 6. This diagram should apply to any white Portland cement in which the concentration of Na in the pore solution is fixed at 250 mM. At higher alkali contents, concentrations of Cl (or Friedel's salt) in the AFm$_{ss}$ phase and C-S-H phase will be lower for the same concentration of Cl in the pore solution. The same relationship should apply regardless of the relative content of C_3A, C-S-H, sulfate, carbonate and pore solution. The relationship can be used to calculate the overall binding capacity, i.e. the relationship between the free and bound chlorides, from the overall hydrate phase assemblage (which can in turn be calculated quantitatively from the chemical composition of the cement and water cement ratio as described above for the thermodynamic model).
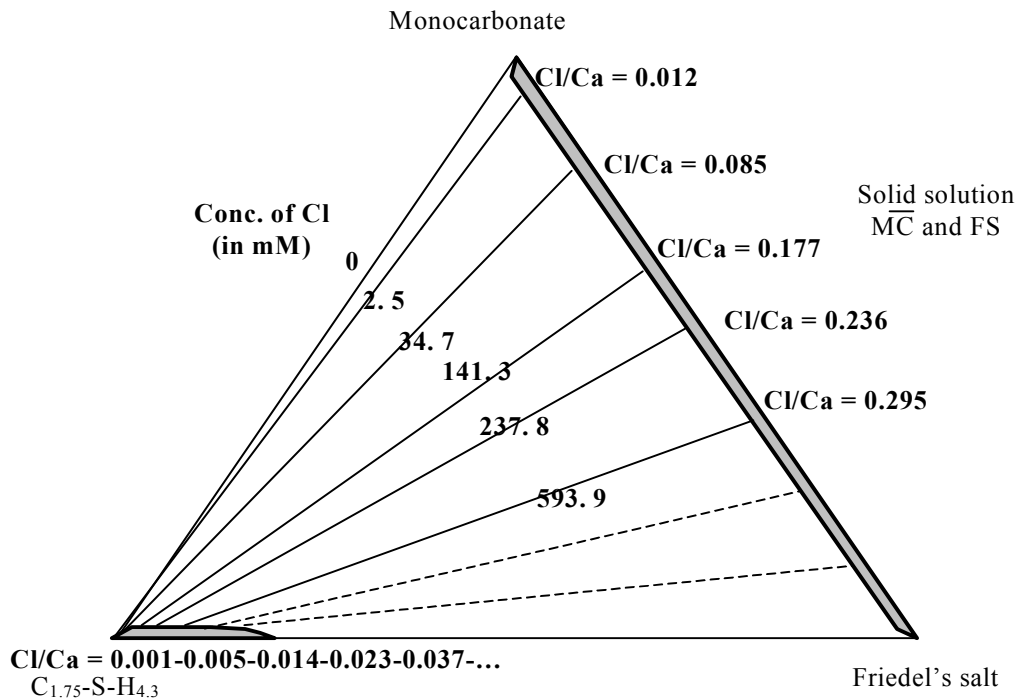
Figure 8: Pseudo ternary system for 'C-S-H'-Friedel's salt-Monocarbonate at a constant Na concentration in solution of 250 mM. Solid tie lines and corresponding chloride concentrations were determined in this study. The dashed lines are extrapolated from this.

The above relationship predicts that for a given aluminate content, low sulfate contents and high carbonate contents should be beneficial to binding since both would effectively increase the content of monocarbonate and therefore lower the mole fraction of Friedel's salt in the AFm_{ss} phase. Lower contents of Friedel's salt in the AFm_{ss} phase are beneficial because they lower the concentration of Cl in the pore solution (and C-S-H phase). Sulfate which invariably accompanies chloride intrusion from sea water, effectively lowers the mole fraction of monocarbonate in the AFm_{ss} phase, increasing the mole fraction of Friedel's salt and the chloride concentration in the pore solution. The reduction in binding capacity caused by sulfate attack, however, can be mitigated by the presence of carbonates which have the opposite effect.

CONCLUSION

Solid solution between Friedel's salt and monocarbonate reported elsewhere has been confirmed for hydrated Portland cement containing 1% calcite and different contents of C_3A.

The relationship between free and bound chlorides is governed by this solid solution.

Chlorides are also bound by the C-S-H phase, with a well defined distribution of chloride between all three phases (i.e. the AFm solid solution phase, the pore solution and the C-S-H phase) at any given alkali content. This relation is dependent on the iron content of the system.

Higher alkali and sulfate contents reduce the binding capacity of hydrated Portland cement. Carbonates increase the binding capacity.

All these results can be predicted by applying the phase rule.

REFERENCES

Books

[1]   Glasser,F.P. Role of Chemical Binding in Diffusion and Mass Transport. In Ion and Mass Transport in Cement-Based Materials, Materials Science of Concrete, Ed. R.D.Hooton M.D.A Thomas, J.Marchand, J.J.Beaudoin. Pub. The American Ceramic Society, pp.129-154, 2001

[2]   Glasser, F.P., "Application of the Phase Rule to Cement Chemistry", Chapter 5 in Refractory Materials Volume 6-II, Ed. Allen M. Alper, pub. Academic Press, 1970.

Journal articles

[3]   Birnin-Yauri, U.A. and Glasser, F.P. Friedel's salt, $Ca_2Al(OH)_6(Cl,OH). 2H_2O$: Its solid solution and their role in chloride binding. Cement and Concrete Research, vol.28, pp. 1713-1723, 1998

[4]   Lambert, P., Page, C.L. and Short, N.R. Pore solution chemistry of the hydrated system Tricalcium silicate/Sodium chloride/water. Cement and Concrete Research, vol.15, 1985.

[5]   Martin-Perez,B, Zibara,H., Hooton,R.D. and Thomas,M.D.A. A study of the effect of chloride binding on service life predictions. Cement and Concrete Research, vol.30, 200, p. 1210-1223.

[6]   Tang,L. and Nilsson,O. Chloride binding capacity and binding isotherms of OPC pates and mortars, Cement and Concrete Research, vol.23, pp.247-253, 1993.

Conferences

[7]   Yamato, T., Soeda, M. and Emoto, Y. Chemical resistance of concrete containing condensed silica fume. In: ACI Special Publication 114: Proceedings of the 3rd International Congress on fly ash, silica fume, slag, and natural pozzolans in concrete, ACI, Trondheim, 1989, p.897-913.

[8]   Herfort , D., Porsborg, A.T., Grundvig, S., Jakobsen, H.J. and Skibsted, J. Hydrate Phase Assemblages of Portland Cement Pastes Stored at 5 and 20°C. Proceedings of the 20th IOM Cement and Concrete Science Conference. Sheffield, 2000.

[9]   Juel,I., Herfort,D, Gollop,R, Konnerup-Madsen,J, Jakobsen,H.J. and Skibsted,J. A thermodynamic model for predicting the stability of thaumasite. Proceedings of the 1st international conference on thaumasite in cementitious materials. Building Research establishment UK, 2002.

[10]   Herfort,D and Juel,I.A., The mineralogy of sulfate and sea water attack on concrete interpreted from EPMA analysis. Proceedings of the 23rd International Conference on Cement Microscopy, Albuquerque, New Mexico, 2001.

[11]   Juel,I.A. and Herfort,D. The mineralogy of chloride attack on concrete containing limestone filler. Proceedings of the 24th International Conference on Cement Microscopy, San Diego, California, 2002.

Paper III: Phase equilibria in hydrated Portland cement

Nielsen, E.P., Herfort, D. and Geiker, M.R.

ABSTRACT

A model is described for predicting the equilibrium phase assemblage in hydrated Portland cement, and for calculating the relative contents and composition of phases present in the assemblage, from the chemical composition of the cement and the water/cement ratio. The method is also used to calculate the content of capillary pores using the best available data for the densities for each of the phases.

These calculations were carried out on three different Portland cements (two white Portland cements and one grey) at water/cement ratios of 0.70. EDS analysis on the SEM was used to verify the presence of all phases predicted by the model. A density for the C-S-H phase of approx. 2.10 g/cm^3 and an evaporable water content in the C-S-H of approx. 19 % provided the best agreement between the predicted values of chemical shrinkage, loss of ignition and content of evaporable water, and experimental data. Other results included compositional data on the C-S-H phase corresponding to molar ratios of Al/Ca = 0.04 and S/Ca = 0.03 in all cements investigated, and Fe/Ca = 0.02 in the grey Portland cement.

INTRODUCTION

In Powers' model (Ref. [1]) the hydrated Portland cement is assumed to consist of a single hydrate phase with properties corresponding to the average of all phases present. This fails to take into account the true multi-phase nature of hydrated Portland cement.

More appropriate mathematically derived models (in e.g. Refs. [2,3,4]) have been used to describe the hydration of cement over time, and as a function of the degree of hydration of the clinker phases. Although these models are clearly an improvement on the more simplistic Powers' model, they do not generally satisfy Gibb's Phase Rule which applies to all chemical systems at equilibrium.

For hydrated Portland cement pastes it is reasonable to assume that equilibrium conditions apply after two or threes months of hydration, because reaction of the unhydrated clinker proceeds very slowly at this stage (e.g. Ref. [5]). The validity of this assumption is, however, dependent on the composition of the cement and the hydraulic reactivity of the anhydrous phases, the water-to-cement ratio, the presence of supplementary cementitious materials, etc.

In the present paper a method is described for predicting the metastable or stable phase assemblage in hydrated Portland cement systems from the chemical composition of the cement, and for calculating the relative contents of phases present. The predictions were subsequently tested experimentally as part of extensive studies on concrete durability by the present authors. Parts of the model have already been described in earlier publications (e.g. Refs. [6,7,8]), but further development has occurred since then and the model has been modified accordingly.

PHASE EQUILIBRIA

As noted above, the 'Phase Rule' applies to all chemical systems in equilibrium. Even though the formulation of the rule is very simple it has rarely been applied to hydrated cement systems (e.g. in Ref.[9]). The rule states that the number of *phases* plus the *degrees of freedom* equals the number of *components,* plus a constant *n*, which is dependent on the history of the system with respect to pressure and temperature. If the process is kept under isobaric or isothermal

conditions n is 1, if neither n is 2, and if both n is 0 (Ref. [10]). At constant temperature and pressure the rule takes the form P + F = C.

In a fully hydrated Portland cement, which as a first approximation is invariant at constant temperature and pressure, the relative contents of phases of known composition present can be calculated by solving 'n' equations for 'n' unknowns, where 'n' is the number of components and phases. Since the system is invariant, the composition of each of the phases must remain constant. As an example, the amount of each of the six phases in an invariant six-component system can be calculated by solving the six by six matrix in Eq. (1).

$$\begin{bmatrix} W_{C1}^{P1} & W_{C1}^{P2} & W_{C1}^{P3} & W_{C1}^{P4} & W_{C1}^{P5} & W_{C1}^{P6} \\ W_{C2}^{P1} & W_{C2}^{P2} & W_{C2}^{P3} & W_{C2}^{P4} & W_{C2}^{P5} & W_{C2}^{P6} \\ W_{C3}^{P1} & W_{C3}^{P2} & W_{C3}^{P3} & W_{C3}^{P4} & W_{C3}^{P5} & W_{C3}^{P6} \\ W_{C4}^{P1} & W_{C4}^{P2} & W_{C4}^{P3} & W_{C4}^{P4} & W_{C4}^{P5} & W_{C4}^{P6} \\ W_{C5}^{P1} & W_{C5}^{P2} & W_{C5}^{P3} & W_{C5}^{P4} & W_{C5}^{P5} & W_{C5}^{P6} \\ W_{C6}^{P1} & W_{C6}^{P2} & W_{C6}^{P3} & W_{C6}^{P4} & W_{C6}^{P5} & W_{C6}^{P6} \end{bmatrix} \begin{bmatrix} P_{1,total} \\ P_{2,total} \\ P_{3,total} \\ P_{4,total} \\ P_{5,total} \\ P_{6,total} \end{bmatrix} = \begin{bmatrix} C_{1,total} \\ C_{2,total} \\ C_{3,total} \\ C_{4,total} \\ C_{5,total} \\ C_{6,total} \end{bmatrix} \quad (1)$$

where $P_{m,total}$ is the total content of phase "m" in the system in weight %, W_{Cj}^{Pm} is the weight fraction of the component "j" in phase "m", and $C_{j,total}$ is the total content of the component "j" in the system in weight %.

A fully hydrated Portland cement paste has typically six major components (i.e. SiO_2, Al_2O_3, CaO, Fe_2O_3, SO_3, H_2O), and can form a maximum of six phases (five hydrate phases and the pore solution) at constant temperature and pressure. For a typical Portland cement paste, these phases are assumed to be: C-S-H, calcium hydroxide (CH), monosulfate ($C_3A.C\bar{S}.H_{12}$), ettringite ($C_3A.3C\bar{S}.H_{32}$), iron oxide (probably FH_3), and pore solution.

Alkalis are disregarded in this paper as they do not form any solid phases within the range of concentrations observed in Portland cement pastes (Ref. [11]). A significant portion of the alkalis appears to be incorporated in the structure of the C-S-H whilst remainder is present in solution at well defined distribution ratios between the two phases (Refs. [11,12]). The inclusion of alkalis in the model is described in Ref. [13].

Poorly crystalline calcium silicate hydrate, C-S-H, and calcium hydroxide are the main hydrate phases in Portland cement systems, formed by hydration of C_3S and C_2S. Different compositions of the C-S-H in Portland cement systems have been proposed, but $C_{1.75}SH_4$ appears to be the most frequently reported (in e.g. Ref. [5,6,8]). Al and S are typically observed to be incorporated in the C-S-H, corresponding to Al/Ca = 0.04 and S/Ca = 0.03 (Refs. [8,14], determined by EDS-analysis on different mature Portland cement pastes wet cured at 20^oC). The density of the phase under saturated conditions has been reported at values ranging from 1.95 g/cm^3 to 2.45 g/cm^3 (Ref. [5]), with most values at the lower end, and contents of evaporable water around 18-20% (Refs. [5,11]).

Depending on the Al_2O_3/SO_3-ratio (Ref. [5,15,16]), a hydroxy-AFm phase may replace ettringite, or gypsum may replace monosulfate, as seen on the C_3A-$CaSO_4$ binary side of the diagram for the ternary subsystem C_3A-$CaSO_4$-$CaCO_3$ shown in Fig. 1. For convenience, $CaCO_3$, $CaSO_4$, and C_3A are chosen as components rather than CO_2, SO_3, and Al_2O_3. This is valid as long as these components occur as stoichiometric units in all hydrate phases. The other phases (i.e. C-S-H, CH, FH_3, and pore solution) occur as excess phases in most assemblages formed from normal Portland cement.
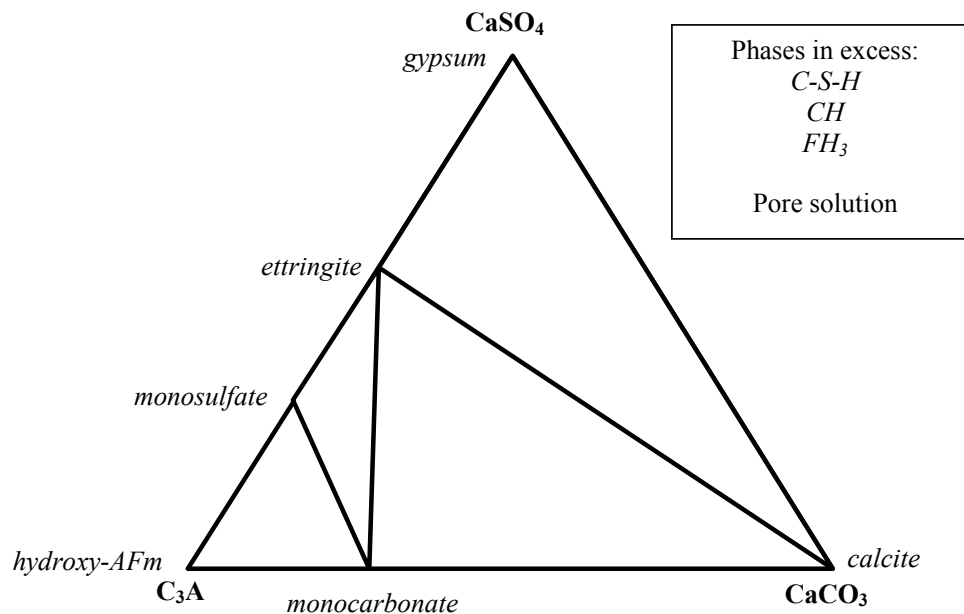
Fig. 1: Ternary subsystem C_3A-$CaSO_4$-$CaCO_3$ assumed for the thermodynamic model.

If solid solution phases where anionic substitution of e.g. SO_4^{2-} or CO_3^{2-} in AFm or AFt phases occur in a system, these should be easily detectable by EDS analysis or similar techniques, as molar ratios of e.g. Cl/Ca and S/Ca in such phases would change following the degree of anionic substitution. In this study ettringite and monosulfate, when present, were invariably found as pure end-member phases. Distinction between monocarbonate, hemicarbonate and hydroxy-AFm phases, or a solid solution between these, is difficult to make by this method but can be performed by other methods such as X-ray diffraction.

At ages less than about one year the composition of the hydroxy-AFm is most likely to be C_4AH_{13} (e.g. in Ref. [5]) or C_4AH_{18} (e.g. in Ref. [16]), but in older pastes the more stable phase hydrogarnet, C_3AH_6, is likely to be present instead (Refs. [5,15]).

Kuzel and Pöllmann (Ref. [16]) who studied the CaO-Al_2O_3-$CaSO_4$-$CaCO_3$-H_2O system, found that in relatively young pastes (hydrated for less than a month), the phases formed were hemicarbonate ($C_3A.\frac{1}{2}C\overline{C}.\frac{1}{2}CH.H_{11.5}$), monocarbonate ($C_3A.C\overline{C}.H_{12}$), monosulfate, ettringite, and calcium hydroxide. At increasing contents of $CaCO_3$ the amount of monocarbonate was found to increase relative to hemicarbonate, and the content of monosulfate was reduced. Such a phase assemblage does not satisfy the phase rule as there is one phase too many (i.e. the solution itself is also a phase), and equilibrium conditions can therefore not apply. Damidot and Glasser (Ref. [15]) concluded that hemicarbonate is only stable at low concentrations of carbonate and sulfate, and high concentrations of calcium, whilst monocarbonate is stable over a wider range of concentrations, and suggested that it forms preferentially in systems containing alkalis. The reason for this was attributed to the common ion effect, which reduces the concentration of calcium, whilst increasing the concentration of sulfate, aluminate and carbonate.

As mentioned in Ref. [5], several investigators have noted that the Fe/Ca ratio in the hydrate phases tends to be higher than that of the ferrite phase in the clinkers, and have concluded that an iron (III) oxide gel or hydroxide is formed. Teoreanu et al. (Ref. [17]) concluded that the hydration products at ordinary temperatures included FH_3, in agreement with Fukuhara et al. (Ref. [18]). They based their conclusions on measurements of heat of hydration by conduction calorimetry and suggested that the hydration of C_4AF resulted in the formation of ettringite containing some iron (composition $C_3(A_{0.75}F_{0.25}).3CaSO_4.31H_2O$) and FH_3. According to Taylor and Newbury (Ref. [19]) the tendency to form iron oxide gel or iron hydroxide may be related to the ability of Al^{3+} to migrate relatively easily through the paste, whilst Fe^{3+}, owing to its lower

solubility, cannot, and is therefore, largely confined to the space originally occupied by the anhydrous ferrite phase.

After calculating the relative contents of hydrate phases in weight %, the best available data on the densities of the hydrate phases can be used to calculate the relative contents in volume % (e.g. in Refs. [5,20]).

EXPERIMENTAL

Three Portland cement pastes were examined: two white Portland cements with Bogue-C_3A contents of approx. 4 and 12%, and a grey Portland cement with a Bogue-C_3A content of 7%. The compositions of these cements are shown in table 1.

Table 1. Composition of the Portland cements tested

Cement id.	SiO_2	Al_2O_3	Fe_2O_3	CaO	SO_3	Na_2O	K_2O	CO_2[*]
WPC(4)	24.8	1.87	0.33	68.9	2.20	0.16	0.11	0.14
WPC(12)	23.6	4.49	0.21	65.9	2.38	0.03	0.20	0.72
OPC	21.0	4.90	3.64	65.1	3.00	0.30	0.41	0.08
* Determined by DTG.								

Cement id.	C_3S	C_2S	C_3A	C_4AF
WPC(4)	72.2	16.8	4.4	1.0
WPC(12)	51.7	28.6	11.5	0.6
OPC	59.1	15.6	6.8	11.1

All the pastes were prepared at a w/p ratio of 0.70 after replacement of the cement by 1 wt. % finely ground calcite (specific surface area higher than 1000 m^2/kg). The powder was mixed for 5 minutes in a Hobart mixing machine, before addition of one third of the water and mixing for 3 minutes, followed by a further 3 minutes mixing with the remaining water. The pastes were cast in 2 cm^3 centrifuge tubes, sealed and slowly rotated for two days to avoid bleeding. After de-moulding, series of three 2 cm^3 specimens were placed in 12 ml de-carbonated water, then sealed and stored at 20°C for six months, which was ample time for the hydrated cement to reach equilibrium and for the composition of the solution to remain constant. The solution is to all extents and purposes identical to pore solution albeit at a much lower alkali content which is diluted by an order of magnitude.

After six months, the specimens were examined by EDS (Energy Dispersive Spectroscopy, at 15keV, 25μA and measuring time of 40 s. per point, calibrated against relevant standards). The evaporable water content upon drying at 105°C was determined followed by the determination of the loss of ignition at 1000°C.

RESULTS

The compositions of the three cement pastes after addition of limestone and water are given in Table 2.

Table 2: Components in the w/s 0.70 'wet' mixes (i.e the three cement pastes)

System id.	SiO_2	Al_2O_3	Fe_2O_3	CaO	SO_3	CO_2	H_2O
WPC(4)_070	24.62	1.86	0.33	68.70	2.18	0.56	70.00
WPC(12)_070	23.37	4.45	0.21	65.75	2.36	1.13	70.00
OPC_070	20.79	4.86	3.61	65.00	2.97	0.50	70.00

Before calculating the relative contents of phases in each of the three hydrated cement pastes, analyses were performed, to determine the composition of the hydrate phases, and the contents of unreacted clinker. Hydration of the ferrite phase can be neglected in the case of the white Portland cements, due to their very low iron content. Fig. 2 shows the results of 350 EDS individual spot analyses on the hydrated OPC pastes plotted as Fe/Ca vs. Al/Ca (molar ratios).
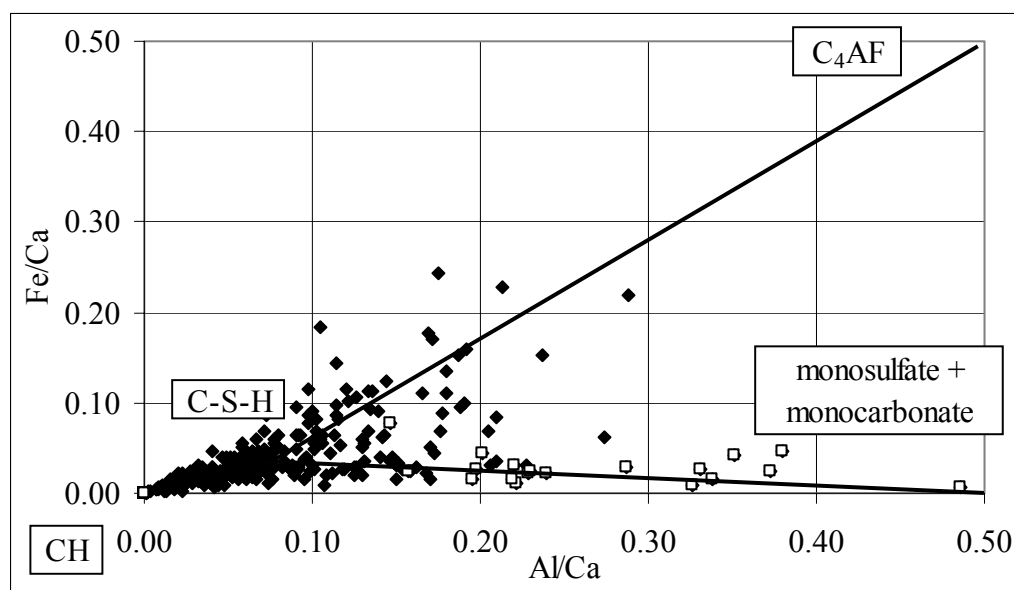
Fig. 2: 350 EDS analyses on OPC_070 plotted as Fe/Ca vs. Al/Ca (squares indicate plots with S/Ca > 0.10).

Some plots show trends in the direction of the composition for C_4AF, indicating that not all of the ferrite has reacted. Some plots correspond to higher Fe/Ca molar ratios than the anhydrous phases (i.e. plots above the C-S-H – C_4AF tie-line), indicating the presence of iron hydroxide intimately mixed with the other hydrates. The trends towards the monosulfate phase (i.e. 'squares' in Fig. 2, which have a S/Ca > 0.10) indicates little or no iron in this phase.

The region bound by the C-S-H – monosulfate/monocarbonate - C_4AF tie-lines in Fig. 2 can be regarded as a type of phase diagram with each plot representing the chemical composition of a volume of paste, the size of which depends on the conditions of analysis on the SEM (generally a few μm^3). All the plots within this region can be projected onto the C-S-H - C_4AF tie-line by tracing a line from the monosulfate composition, through each plot to where it intersects the tie-line. The average Fe/Ca ratio of the mixture of C-S-H and C_4AF can then be used to calculate the volume ratio of C-S-H to C_4AF. The composition of the C-S-H used here assumed some solid solution of iron corresponding to a Fe/Ca ratio of 0.02 (see Fig. 2). For the OPC paste examined, the average Fe/Ca ratio was 0.405, corresponding to a C_4AF/C-S-H volume ratio of approx. 0.03, equivalent to a C_4AF content of 2.20 % by weight of solid phases. This corresponds to a degree of hydration for C_4AF of approx. 75%, which is in agreement with the data in Refs. [5,20]. This was confirmed by point counting of a polished section (2600 counts) which gave a C_4AF content of 0.7 vol. % of the total paste.

Refs. [5,20] reported a degree of reaction of the belite phase after 6 months hydration of approx. 80%. The alite and aluminate phases are almost completely hydrated (Ref. [5]), and therefore the degree of hydration of these is assumed to be 95%. For the systems examined, the overall degree of hydration is predicted to be 88-92 %, based on the Bogue composition in Table 1. Parrott et al. (Ref. [21]) found the degree of hydration of a white Portland cement (the same as WPC(4) in the present investigation) at 100 days of maturity to be approx. 90 % for a w/s ratio of 0.71 by QXRD analysis. They also carried out measurements on an ordinary Portland cement with similar composition and properties to the OPC cement in this investigation, and found a degree of hydration of approx. 85 % at a maturity of 100 days.

According to the ternary subsystem in Fig. 1, four assemblages are possible as shown in Table 3. The relative compositions and densities of the hydrate phases are given in Table 4. Only one of these assemblages is possible for each of the cements when solving the 7 x 7 simultaneous equations.

Table 3: Possible phase assemblages from the ternary subsystem in Fig. 1.

1.	C_4AH_{13}, monosulfate, monocarbonate +	Phases in excess: C-S-H, CH, FH_3 and pore solution
2.	monosulfate, ettringite, monocarbonate +	
3.	ettringite, calcite, monocarbonate +	
4.	ettringite, calcite, gypsum +	

Table 4: Phase compositions and densities. Data from Refs. [5,20].

Component Phase	SiO_2	Al_2O_3	Fe_2O_3	CaO	SO_3	CO_2	H_2O	Density [g/cm^3]
C-S-H	25.24	1.49		41.23	1.77		30.27	1.95-2.45
CH				75.69			24.31	2.24
FH_3			89.76				10.24	4.28
Pore solution							100.0	1.00
Gypsum				32.57	46.50		20.93	2.32
Ettringite		8.12		26.81	19.14		45.93	1.77
Monosulfate		16.38		36.03	12.86		34.73	2.01
C_4AH_{13}		18.19		40.02			41.79	2.05
Monocarbonate		17.94		39.46		7.74	34.86	2.01
Calcite				56.03		43.97		2.72

The assemblages predicted from the cement compositions in Table 2 are shown in Table 5, with the relative contents of phases given in weight-% of the water saturated system. Note that the amount of pore solution assumes water saturated conditions in which the volume produced from chemical shrinkage is taken up by the absorption of additional water.

Table 5: Phase contents calculated for each cement, in weight-% to water saturated paste.

	WPC(4)_070	WPC(12)_070	OPC_070
Assemblage no.	3	3	2
$C_{1.75}SH_4$	50.8	47.2	42.9
CH	19.2	14.6	16.5
FH_3	0.2	0.1	1.8
Pore solution	22.3	21.4	22.7
Monosulfate	---	---	6.3
Ettringite	1.9	2.8	0.8
Monocarbonate	0.4	8.4	3.7
Calcite	0.7	0.0	---
C_3S	1.8	1.2	1.5
C_2S	2.6	3.9	2.1
C_3A	0.1	0.3	0.2
C_4AF	0.1	0.1	1.6
Density of C-S-H [g/cm^3]	2.11	2.09	2.10
Evaporable water in C-S-H (wt. %)	18.5	19.0	19.0
Chemical shrinkage [ml/100g cement]	5.8 (5.5-6.0)	5.7 (5.5-6.0)	5.9 (5.5-6.0)
Volume-% capillary porosity	38.5	36.9	39.1
Evaporable water [wt.% to sat. paste]	31.5 (31.0)	30.7 (30.5)	31.0 (31.0)
L.O.I [wt% to dry paste]	18.8 (18.6)	20.6 (20.4)	20.6 (20.8)

The evaporable water is predicted as the sum of pore solution and evaporable water in the C-S-H in mass-%, which is considered to be weakly bound water that evaporates on drying at 105°C (in e.g. Refs. [5,11]). The chemically bound water in the other phases is assumed to be non-

evaporable water, which is not entirely correct as particularly the ettringite and hydroxy-AFm phases, and to a lower extent other AFm phases, will lose considerable amounts of water on drying at 105°C (Ref. [5]). For the cements studied here, however, this does not affect the above assumption because none of the pastes contain hydroxy-AFm, and the amount of ettringite is very low. The loss of ignition is predicted by adding all the non-evaporable water in the system to the amount of CO_2, which is released on ignition at 1000°C.

The density of the C-S-H phase and its content of evaporable water were the uncertain input data used for the calculations. These properties have a major effect on the chemical shrinkage of the paste and the loss of ignition, respectively, allowing therefore adjusting them separately. The evaporable water content of the paste is affected by both properties. Table 5 shows the actual density that gave the best fit for predicted parameters (chemical shrinkage, loss of ignition, and evaporable water) and those determined experimentally (also included in the table, in parenthesis). Note that the chemical shrinkage measurements were not carried out in this study, but were determined elsewhere on similar cements (Refs. [21,22]). The density of the C-S-H is approximately 2.10 g/cm^3 and the evaporable water content of the C-S-H is approx. 19%. No significant difference was observed between the white and grey cements, which suggests that the densities used for the phases are correct, and the assumption that all iron not incorporated in the C-S-H is found as an iron hydroxide is valid.

Fig. 3 shows 1,500 EDS-plots, for S/Ca vs. Al/Ca determined for the hydrated cement WPC(4)_070. A large number of measurements were needed owing to the low contents of alumina and sulfur in this cement. Most of the AFm phases and ettringite are intimately mixed with the C-S-H phase. However, the plots clearly show the presence of ettringite and confirm the absence of monosulfate. The trend towards the point (Al/Ca,S/Ca) = (0.5,0.0) indicates the presence of either C$_4$AF and/or an AFm-phase without sulphur. Given the absence of C$_4$AF and an aluminate content insufficient to form the hydroxy AFm-phase, it is concluded that these plots must represent a mixture of monocarbonate and C-S-H. Observations on the ESEM also confirmed that a considerable amount of the calcite remained as a stable phase, as predicted by the model. The calcite had fully reacted in the pastes prepared from the high aluminate cements WPC(12)_070 and OPC_070, again as predicted by the model.
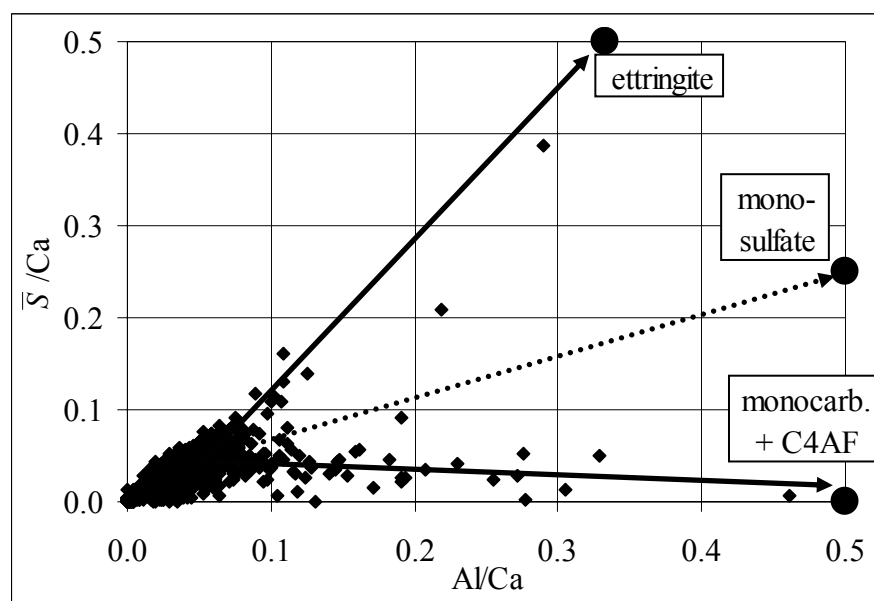
Fig. 3: 1,500 EDS-plots from WPC(4)_070, as S/Ca vs. Al/Ca

The hydrated cement WPC(12)_070 has a high content of alumina and about twice as much CO_2 as the two other cements (see Table 2). The composition of the paste is close to the monocarbonate-ettringite tie-line on Fig.1, and the amount of calcite or monosulfate is therefore

low. The dominant aluminate-containing phase in this hydrated cement is monocarbonate, which is confirmed by the plots in Fig. 4. The plots above the C-S-H-monosulfate tie-line indicate the presence of ettringite.
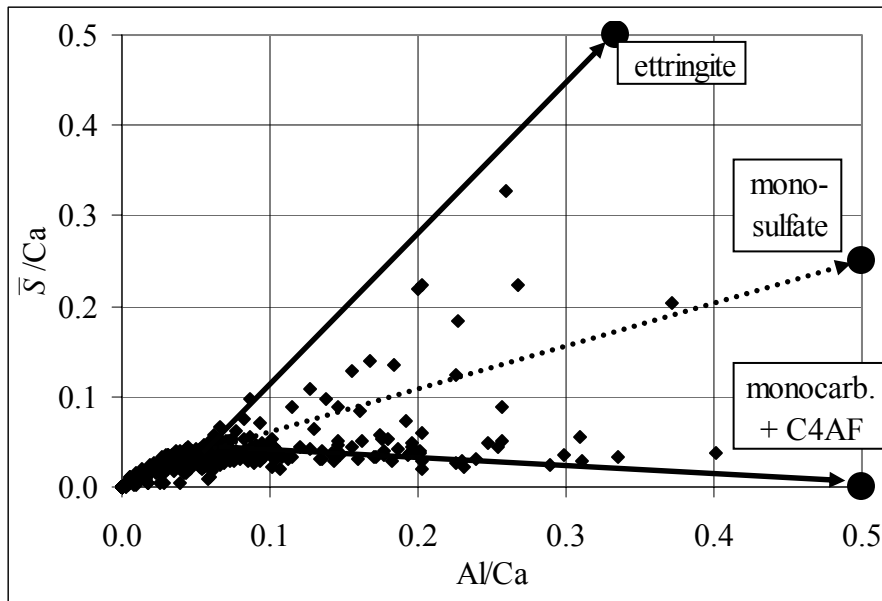
Fig. 4: 350 EDS-plots from WPC(12)_070, as S/Ca vs. Al/Ca.

Fig. 5 shows 350 EDS-plots for the hydrated cement OPC_070 and confirms that the stable phases here are monocarbonate and monosulfate. No clear tendency towards ettringite is observed, but a low content was also predicted by the model. It should be noted that some of the plots close to the C-S-H-monocarbonate tie-line include some of the unreacted C_4AF clinker phase.
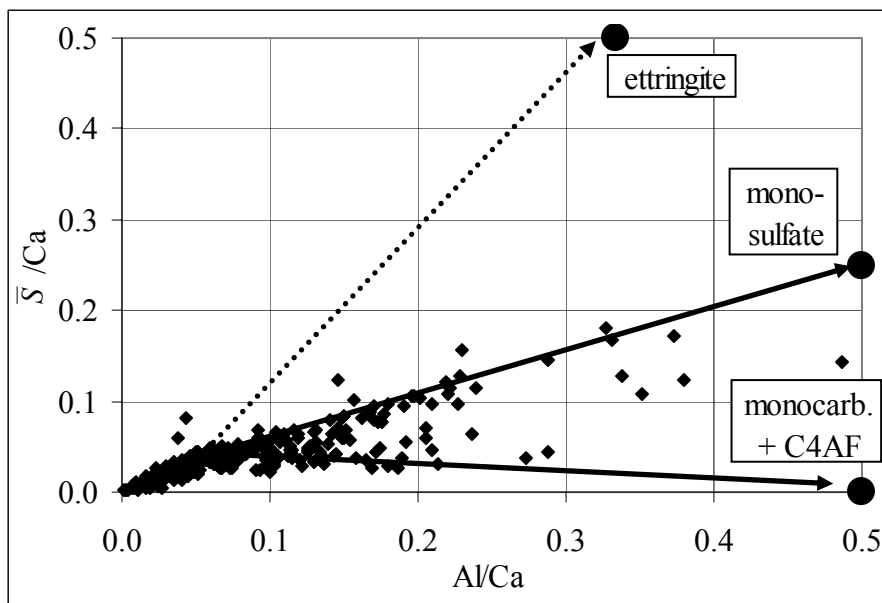
Fig. 5: 350 EDS-plots form OPC_070, as S/Ca vs. Al/Ca.

CONCLUSION

The accuracy of a method based on the phase rule for predicting the phase assemblage and calculating the relative contents of phases was tested by EDS analysis. The stability, and relative contents of monosulfate, monocarbonate and ettringite are consistent with the predictions for

each of the three cements tested. Composition of the C-S-H was $C_{1.75}SH_4$ with Al/Ca = 0.04, S/Ca = 0.03 and Fe/Ca = 0.02 (only in the grey cement).

The results indicated that approximately ¾ of the ferrite phase had reacted after 6 months, and apart from some solid solution of iron and aluminium in the C-S-H phase, the aluminate exclusively formed AFm phases and ettringite, and all the available iron formed a hydrous iron phase presumably FH_3.

The model was also used to calculate the capillary porosity. The density of the C-S-H phase, as well as its content of evaporable water, needed in this calculation was adjusted until agreement was reached between the values for chemical shrinkage, loss of ignition and evaporable water content predicted by the model and those determined experimentally. The C-S-H phase densities determined in this way were 2.11, 2.09, 2.10 g/cm^3 in the three cement pastes studied, suggesting the true density of the C-S-H in water saturated Portland cement to be approximately 2.10 g/cm^3. The evaporable water content of the water saturated C-S-H was 19 weight-%.

REFERENCES

[1] T. C. Powers and T. L. Brownyard, Studies of the Physical Properties of Hardened Portland Cement Paste. Journal of the ACI 18 (8) Part 9, 1947.

[2] Bentz, D.P., Three-dimensional computer simulation of Portland cement hydration and microstructure development, Journal of the American Ceramic Society (80), pp. 3-21, 1997.

[3] Bentz, D.P., CEMHYD3D: A three-dimensional cement hydration and microstructure development modeling package. Version 2.0, Internal report NISTIR 6485, Building and Fire Research Laboratory, NIST, 2000.

[4] K. van Breugel: Simulation of hydration and formation of structure in hardening cement-based materials. 2nd ed. 1997.

[5] Taylor, H.F.W., Cement Chemistry, 2nd edition. Thomas Telford Services Ltd., London, 1997.

[6] Herfort,D and Juel,I.A., The mineralogy of sulfate and sea water attack on concrete interpreted from EPMA analysis. Proceedings of the 23rd International Conference on Cement Microscopy, Albuquerque, New Mexico, 2001.

[7] Juel,I.A. and Herfort,D. The mineralogy of chloride attack on concrete containing limestone filler. Proceedings of the 24th International Conference on Cement Microscopy, San Diego, California, 2002.

[8] Nielsen, E.P., Herfort, D., Geiker, M.R. and Hooton, R.D., Effect of solid solutions of AFm phases on chloride binding. Proceedings of the 11th International Congress on the Chemistry of Cement, Durban, South Africa, May 2003.

[9] Glasser, F.P., Application of the Phase Rule to Cement Chemistry. Chapter 5 in Refractory Materials Volume 6-II, Ed. Allen M. Alper, Academic Press, New York, 1970.

[10] Putnis, A. and McConnell, J.D.C., Principles of mineral behaviour. In: Geoscience Texts Vol.I, Blackwell Scientific Publications, p. 82, 1980.

[11] Hong, S.-Y. and Glasser, F.P., Alkali binding in cement pastes. Part I. The C-S-H phase. Cement and Concrete Research (29), pp. 1893-1903, 1999.

[12] Hong, S.-Y. and Glasser, F.P., Alkali sorption by C-S-H and C-A-S-H gels. Part II. Role of alumina. Cement and Concrete Research (32), pp. 1101-1111, 2002.

[13] Nielsen, E.P., Herfort, D. and Geiker, M.R., Binding of chlorides and alkalis in Portland cement systems, Cement and Concrete Research **(XX), pp. Xx-xx, 200x**

[14] Famy, C., Scrivener, K.L., Atkinson, A. and Brough, A.R., Effects of an early or a late heat treatment on the microstructure and composition of inner C-S-H products of Portland cement mortars. Cement and Concrete Research (32), pp. 269-278, 2002.

[15] Damidot, D. and Glasser, F.P., Thermodynamic investigation of the CaO-Al$_2$O$_3$-CaSO$_4$-CaCO$_3$-H$_2$O, Advances in Cement Research (27), pp. 129-134, 1995.

[16] Kuzel, H.-J. and Pöllmann, H., Hydration of C$_3$A in the presence of Ca(OH)$_2$, CaSO$_4$.2H$_2$O and CaCO$_3$, Cement and Concrete Research (21), pp. 885-895, 1991.

[17] Teoreanu, I., Filoti, G., Hritcu, C., Bucea, L., Spânu, V., Ciocanel, S. and Ivascu, M., Interaction mechanism of 2CaO.Fe$_2$O$_3$ and 4CaO.Al$_2$O$_3$.Fe$_2$O$_3$ with water, at various pressures and temperatures, Il Cemento, Vol. 76, pp. 19-28, 1979.

[18] Fukuhara, M., Goto, S., Asaga, K., Daimon, M. and Kondo, R., Mechanisms of C$_4$AF hydration with gypsum, Cement and Concrete Research (11), pp. 407-414, 1981.

[19] Taylor, H.F.W. and Newbury, D.E., An electron microprobe study of a mature cement paste, Cement and Concrete Research (14), pp. 565-573, 1984.

[20] Lea, F.M., The chemistry of cement and concrete, 3rd edition, Edward Arnold Ltd Press, 1970.

[21] Parrott, L.J., Geiker, M., Gutteridge, W. and Killoh, D., Monitoring Portland cement hydration: comparison of methods, Cement and Concrete Research (20), pp. 919-926, 1990.

[22] Geiker, M.R, Studies of Portland cement hydration by measurements of chemical shrinkage and a systematic evaluation of hydration curves by means of the dispersion model, doctoral thesis. Institute of Mineral Industry, Technical University of Denmark, Lyngby, 1983.

Paper IV: Binding of chloride and alkalis in Portland cement systems

Nielsen, E.P., Herfort, D. and Geiker, M.R.

ABSTRACT

A thermodynamic model for describing the binding of chloride and alkalis in hydrated Portland cement pastes has been developed. The model is based on the phase rule, which for cement pastes in aggressive marine environment predicts multivariant conditions, even at constant temperature and pressure. The effect of the chloride and alkalis has been quantified by experiments on cement pastes prepared from white Portland cements containing 4 and 12% C_3A, and a grey Portland cement containing 7% C_3A. One weight-% calcite was added to all cements. The pastes prepared at w/s ratio of 0.70 were stored in solutions of different Cl ($CaCl_2$) and Na (NaOH) concentrations. When equilibrium was reached the mineralogy of the pastes was investigated by EDS analysis on the SEM. A well-defined distribution of chloride was found between the pore solution, the C-S-H phase, and an AFm solid solution phase consisting of Friedel's salt and monocarbonate. Partition coefficients varied as a function of iron and alkali contents. The lower content of alkalis in WPC results in higher chloride contents in the C-S-H phase. High alkali contents result in higher chloride concentrations in the pore solution.

INTRODUCTION

Increasingly, "multi-species" approaches (as in e.g. Refs. [1,2]) are being used to improve service life prediction models for the onset of corrosion of steel reinforcement. These take into account the electrical interaction between diffusing ions and the concentration of each of these, which strongly influence the rate of diffusion of each ion in a multi-component solution.

The rate of transport is also highly dependent on the interaction of each of the species with the solid phases in the cement paste, as well as the concentration gradient for each of the species. This appears to result in significantly higher penetration rates for chlorides than alkalis, as observed in the profiles in Ref. [3], as well as unpublished data by the present authors.

Given today's still incomplete understanding of the fundamental processes involved, chloride binding isotherms need to be measured for each new binder composition, using procedures as described in Refs. [4,5]. These procedures are time consuming and the result is highly dependent on the source of chlorides; e.g. NaCl, which in contrast to $CaCl_2$, results in progressively higher levels of sodium as the chloride concentration is increased.

Models predicting the phase equilibria of cementitious binder systems, and the diffusion of each of the species in these systems would provide a powerful means of identifying the optimum binder composition in a given service environment.

Studies on the mineralogy of chemical attack (mainly from seawater) and ionic transport in Portland cement pastes, with and without supplementary cementitious materials, are presently being carried out by the present authors. A thermodynamic model for calculating the phase assemblage in Portland cement pastes was presented in Ref. [6]. The model was applied in Ref. [7] to quantify the distribution of chloride between the solid solution phase of Friedel's salt and monocarbonate, and chloride incorporated in the C-S-H phase. In the present paper this model is developed further to include the effect of alkalis.

PHASE EQUILIBRIA

As described in Ref. [6], the phase rule applies to all chemical systems in equilibrium. It states that the number of phases (P) plus the degrees of freedom (F) of a system must equal the number of components (C) at constant temperature and pressure.

A fully hydrated Portland cement paste has six major components (i.e. SiO_2, Al_2O_3, CaO, Fe_2O_3, SO_3, H_2O) and can form a maximum of six phases (five hydrate phases and the pore solution). For a typical Portland cement paste, the phases initially formed would be (Ref. [6]): $C_{1.75}$-S-H_4, calcium hydroxide, monosulfate, ettringite, iron hydroxide (FH_3) and the pore solution. Depending on the Al_2O_3/SO_3-ratio, an hydroxy-AFm phase may occur instead of ettringite, or gypsum instead of monosulfate.

In aggressive environments, concrete structures are often subjected to attack by sulfates, carbon dioxide, chloride, and alkalis. The phase assemblages which form are of course dependent on the composition of the system, in addition to temperature and pressure, regardless of whether the components have an external or internal origin. Depending on the relative content of CO_2, calcite and/or monocarbonate will be present in the stable assemblage (see Ref. [6]).

As reported in Refs. [7, 8, 9, 10], a complete solid solution exists between monocarbonate and Friedel's salt in Portland cement pastes. The relationship between the amount of chloride incorporated in the C-S-H and chloride in the solid solution phase (expressed as fraction of Friedel's salt in the solid solution phase) was found to be strongly dependent on the iron content, as shown in Fig.1, owing to the solid solution of iron in the C-S-H phase, reported in Ref. [6].
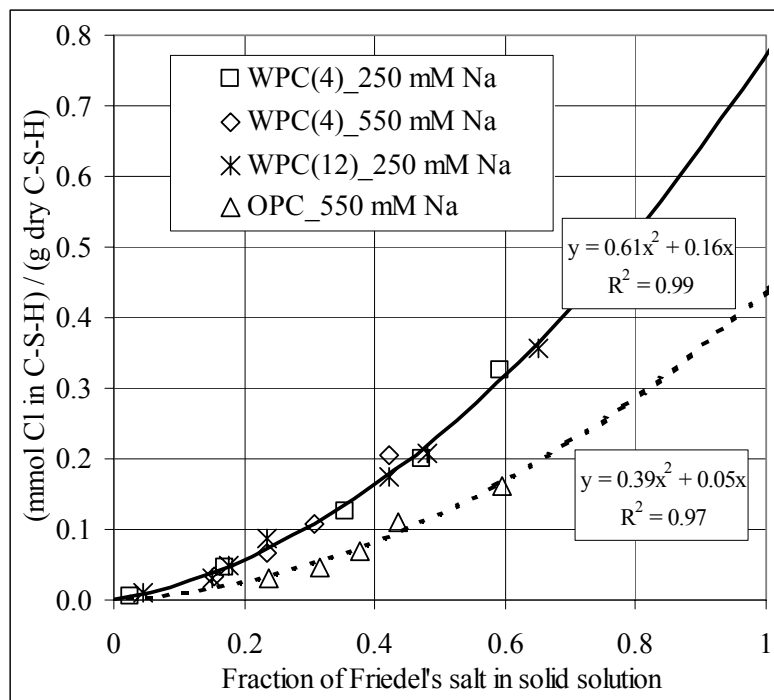
Fig. 1: Chloride content in the C-S-H vs molar fraction of Friedel's salt in the AFm solid solution phase. Dashed curve corresponds to OPC pastes. The solid curve corresponds to the two WPCs.

The presence of sodium in a hydrated Portland cement which already contains chloride must be defined by at least two additional components. The choice of Na_2O as a component is sufficiently to describe the incorporation of Na in the solid phases (essentially C-S-H), whilst both Na_2O an NaCl are needed to account for the presence of both NaCl and NaOH in the pore solution. At low concentrations of chloride, the composition of the pore solution can be

expressed by relative contents of NaCl, Na_2O, and H_2O. Once all the sodium is balanced by chlorides, any further addition of chlorides can be expressed by the increase in $CaCl_2$ concentration, where Ca^{2+} is released from the solid phases.

Hong and Glasser (Refs. [11,12]) investigated the incorporation of alkalis (both sodium and potassium) up to equilibrium concentrations of 300 mM in artificially prepared C-S-H and determined the distribution ratio, R_d, defined by the concentration of sodium or potassium in the C-S-H phase divided by the concentration in the pore solution, expressed as ml/g ([mmol alkali in C-S-H / g-dry C-S-H] / [mmol alkali in solution / ml solution]). The R_d value was found to be independent of the content of alkalis in the system, but strongly dependent on the Ca/Si ratio of the C-S-H.

In aggressive environments, at least four additional components are introduced to the system, i.e. CO_2, $CaCl_2$, Na_2O, and NaCl (note that Na_2O is the only alkali considered at this stage, and that sulfate was already listed among the components in Portland cement paste).

All systems of fully hydrated Portland cement pastes exposed to aggressive marine environment have therefore at least three degrees of freedom (i.e. P + F = C ; 7 + F = 10); one degree of freedom made possible by the solid solution of Friedel's salt and monocarbonate (Ref. [7]), and the remaining two by the presence of alkalis. The presence of MgO is not considered in this paper and the system is therefore restricted to the following ten components: CaO, SiO_2, Al_2O_3, Fe_2O_3, Na_2O, NaCl, $CaCl_2$, SO_3, CO_2, and H_2O

EXPERIMENTAL

Three Portland cement pastes were examined: two white Portland cements with Bogue-C_3A contents of approx. 4 (WPC(4)) and 12% (WPC(12)), and a grey (OPC) Portland cement with a Bogue-C_3A content of 7%. The compositions of these cements are shown in table 1.

Table 1. Composition of the Portland cements tested

Cement id.	SiO_2	Al_2O_3	Fe_2O_3	CaO	SO_3	Na_2O	K_2O	CO_2[*]
WPC(4)	24.8	1.87	0.33	68.9	2.20	0.16	0.11	0.14
WPC(12)	23.6	4.49	0.21	65.9	2.38	0.03	0.20	0.72
OPC	21.0	4.90	3.64	65.1	3.00	0.30	0.41	0.08
* Determined by DTG.								

Cement id.	C_3S	C_2S	C_3A	C_4AF
WPC(4)	72.2	16.8	4.4	1.0
WPC(12)	51.7	28.6	11.5	0.6
OPC	59.1	15.6	6.8	11.1

All the pastes were prepared at a w/s ratio of 0.70 after replacement of the cement by 1.0 wt. % calcite, and cast in 2 cm^3 centrifuge tubes, sealed and kept at 20°C for one month. The samples were then de-moulded, crushed to 2-4 mm in size, weighed (to approximately 8.3 g) and stored in 12.5 ml. solution for 5 months at 20°C. For each cementtype, the samples were stored in solutions of different $CaCl_2$ concentrations, resulting in different degrees of binding (note that a different specimen was used in each case) at constant alkali content. WPC(4) was stored at sodium contents of both 250 and 550 mM Na (by addition of NaOH to the initial solution), whilst the OPC specimens were stored in solutions of 550 mM Na, and the WPC(12) specimens in 250 mM Na.

After six months, when the specimens were judged to have essentially attained equilibrium, the hydrated phases were examined by EDS (Energy Dispersive Spectroscopy, at 15keV, 25μA and analysis time of 40 s. per point), and analysis of the solutions by titration (chloride and pH), ICP (Inductively Coupled Plasma Atomic Emission Spectrometry) and AA (Atomic Absorption) for all major elements, after removal of the solid phases by filtration.

RESULTS AND DISCUSSION

Table 2 shows the predicted phase assemblages for the three hydrated Portland cement pastes examined (see Ref. [6] for details of the calculations and assumptions regarding degree of hydration). Chloride was introduced to the system as a single additional component (i.e. $CaCl_2$) which resulted in the formation of Friedel's salt in solid solution with monocarbonate. EDS evidence of this solid solution can be found in [7,8] and XRD evidence in [9,13].

Table 2. Assemblages predicted for each cement paste, in weight-%.

	WPC(4)_070	WPC(12)_070	OPC_070
Assemblage no.	3	3	2
$C_{1.75}SH_4$	50.8	46.8	42.6
CH	19.2	14.4	16.4
FH_3	0.2	0.1	1.7
Pore solution	22.2	21.9	23.1
Monosulfate	---	---	6.2
Ettringite	1.9	2.8	0.8
Monocarbonate	0.4	8.4	3.7
Calcite	0.7	0.0	---
Friedel's salt	0.0	0.0	0.0
C_3S	1.8	1.3	1.6
C_2S	2.6	3.9	2.1
C_3A	0.1	0.3	0.2
C_4AF	0.1	0.1	1.6

The concentrations of the major components in the solution are shown in Fig. 2 for the WPC(4) cement (at 550 mM Na) at increasing contents of total chloride. Similar trends are observed for the other cements, albeit at two different levels of Na. The Cl^- concentration increases at the expense of OH^- due to the common ion effect in which Ca^{2+} (the chloride is added to the system as $CaCl_2$) removes OH^- from solution by precipitating the more insoluble portlandite phase (reaction 1 in Table 3). The Cl^- concentration is seen to increase slightly more than can be explained by the reduction in OH^- concentration. This discrepancy is balanced by a corresponding increase in Na^+ concentration.
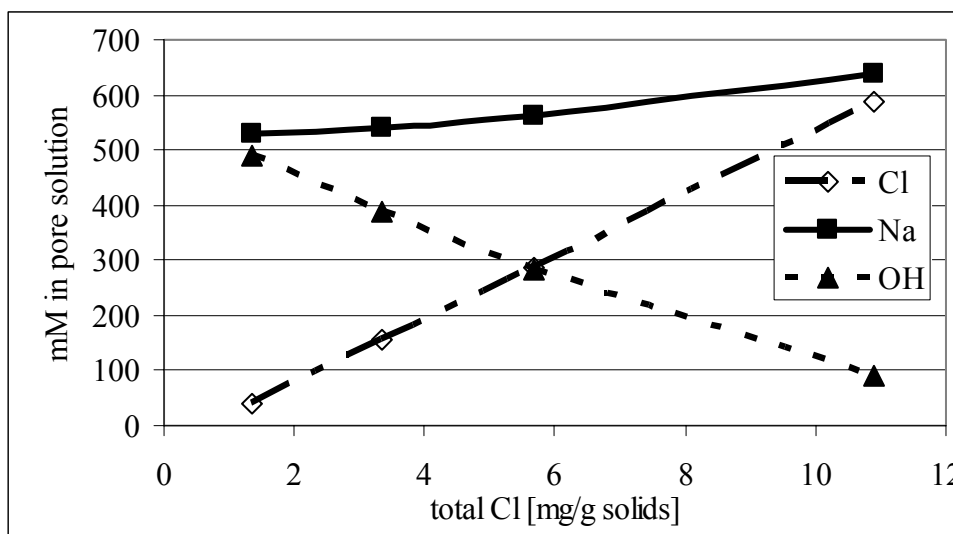
Fig. 2: Cl^-, Na^+ and OH^- concentration in the WPC(4) paste at 550 mM Na as a function of the total chloride content.

Table 3. Reactions involved deduced for the binding of $CaCl_2$ in the WPC(4) paste at 550 mmol/l sodium

Reaction 1	Common ion effect	$2NaOH_{(aq)} + CaCl_{2(aq)} \rightarrow$ $Ca(OH)_{2(s)} + 2NaCl_{(aq)}$
Reaction 2	a. Exchange in C-S-H containing alkalis	$5\ CaCl_{2(aq)} + 6\ NaOH_{(C\text{-}S\text{-}H)} \rightarrow$ $6\ NaCl_{(aq)} + 2\ CaCl_{2(C\text{-}S\text{-}H)} + 3\ Ca(OH)_{2(s)}$
	b. Exchange with alkali-free C-S-H	$Ca(OH)_{2(C\text{-}S\text{-}H)} + CaCl_{2(aq)} \rightarrow$ $CaCl_{2(C\text{-}S\text{-}H)} + Ca(OH)_{2(s)}$
Reaction 3	Binding by AFm	$C_3A.CaCO_3.11H_2O_{(s)} + x\ CaCl_{2(aq)} \rightarrow$ $C_3A.CaCO_{3(1-x)}.CaCl_{2(x)}.11H_2O_{(s)} + x\ CaCO_{3(s)}$

Assuming that all of the Na not present in solution is bound by the C-S-H phase (a reasonable assumption based on the results of Hong and Glasser in Refs. [11,12]), the contents of Na in the C-S-H phase can be calculated as shown in Fig 3. The Cl content bound by the C-S-H phase determined by EDS analysis is included in the same diagram. The Cl contents in the C-S-H phase can also be back calculated from the concentrations in solution in the same way as described for Na, by subtracting the chloride bound by the AFm solid solution phase (also determined by EDS analysis, see Fig. 1) to give essentially identical results. The Cl bound in the AFm phase does not affect the relationships in Figs. 2 and 3 because the $CaCl_2$ added to the system is stoichiometrically incorporated into the AFm phase as shown by reaction 3 in Table 3. The reaction which explains the 2:3 exchange of Cl^- for Na^+ in the C-S-H phase in the WPC(4) paste at 550 mmol/l sodium is given by reaction 2.a (at low chloride contents, i.e. alkali-containing C-S-H) in Table 3.
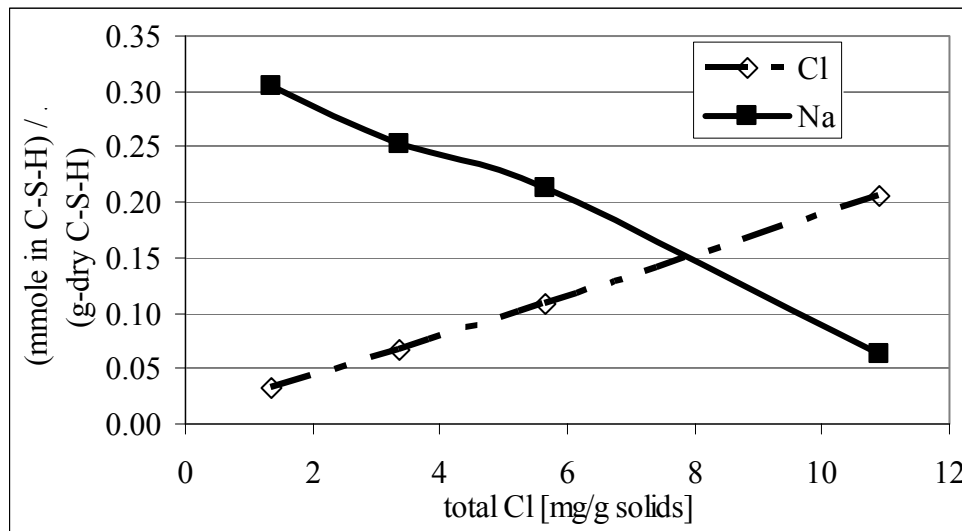
Fig. 3: Chloride and sodium content in the C-S-H, in the WPC(4) paste at 550 mM Na, as a function of the total chloride content.

This relationship will of course break down as the supply of Na from the C-S-H phase is exhausted. Continued addition of $CaCl_2$ leads to a 1:1 replacement of $Ca(OH)_2$ in the C-S-H by $CaCl_2$ (as shown by reaction 2.b in Table 3) and a 20:1 relation for $CaCl_2$ in solution and $CaCl_2$ in the C-S-H, deduced from similar figures for WPC(4) and WPC(12) pastes both at 250 mmol/l sodium. This explains the increase in Ca^{2+} concentration in the solution at high chloride contents shown in Fig. 4.
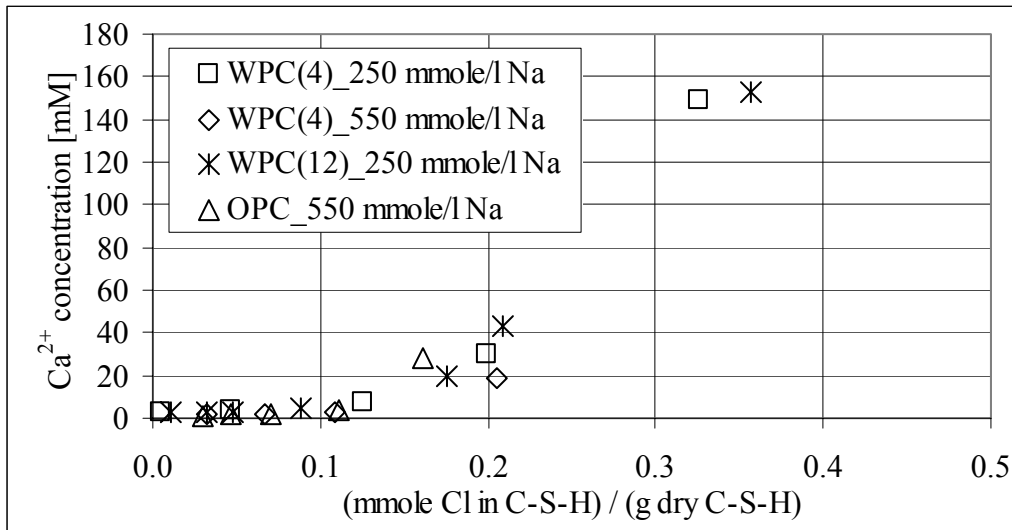
Fig. 4: Ca^{2+} concentration in the pore solution as a function of the chloride content in the C-S-H.

The data is presented in a more general way in Figs. 5 and 6, which are applicable to all comparable hydrated Portland cement pastes at water-to-powder 0.70, regardless of Na contents. Fig. 5 shows that the distribution coefficient for alkalis, Rd, between the pore solution and the C-S-H phase is not constant (as would be the case in a univariant system at constant T and P in which the sole degree of freedom corresponds to the Na content), but is inversely proportional to the Cl content in the C-S-H phase. For all of the cements the Na is completely removed from the C-S-H phase at a Cl content in the C-S-H phase of 0.24 mmol / g dry C-S-H. Fig. 6 shows the distribution of Cl between the pore solution and C-S-H phase for the pastes studied.
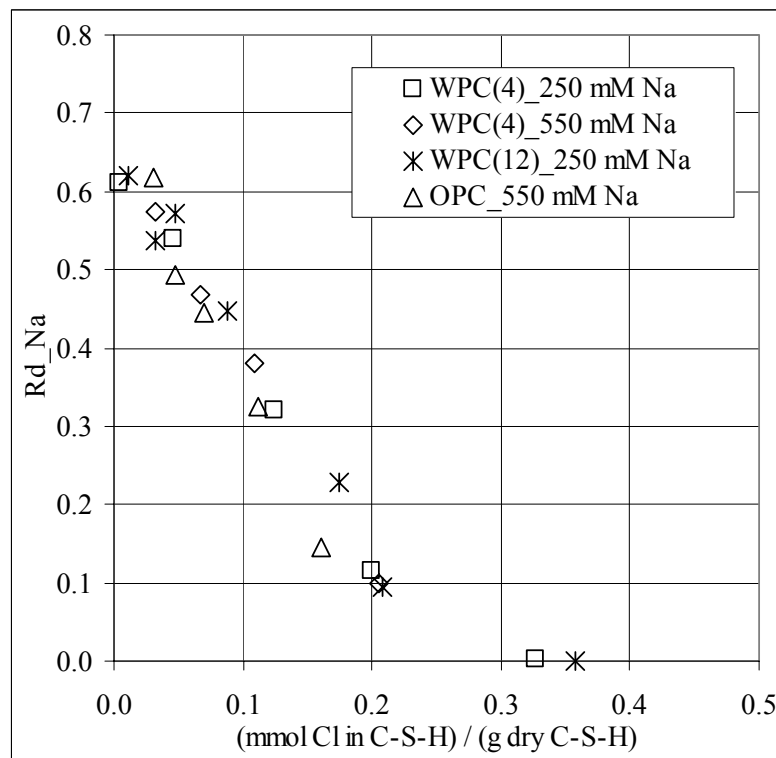
Fig. 5: Distribution ratio for alkalis, R_d, as a function of the chloride content in the C-S-H. Note: Applies only for w/p 0.70 Portland cement pastes.
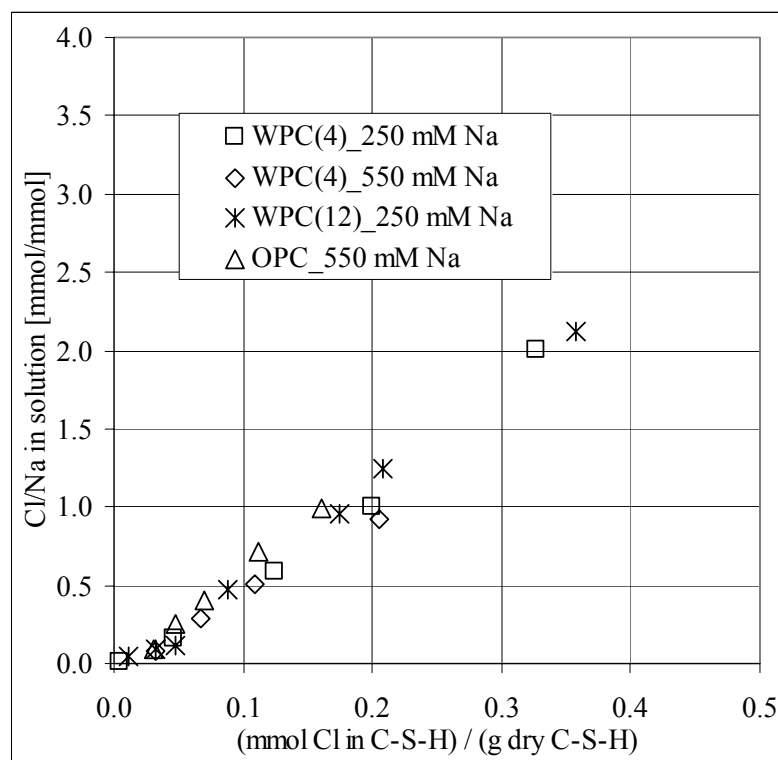
Fig. 6: Molar ratio of chloride to sodium in the pore solution as a function of the chloride content in the C-S-H. Note: Applies only for w/p 0.70 pastes.

For the calculations carried out in this work it was assumed that the part of the water in the C-S-H structure held by a weaker binding strength (see Ref. [6]), corresponding to 19 mass-% of the saturated phase, was not available for the solution of ions. This lead to R_d values close to 0 for Cl contents in the C-S-H higher than approximately 0.24 [mmol / g dry C-S-H]. If, on the other hand, it was assumed that this water did form part of the pore solution, negative values of R_d (approx. −0.20) would have been obtained, which is physically impossible. It is the authors' view that this so-called weakly bound water is not different from the remaining water bound by the C-S-H and is simply an artifact of the methods by which it is determined.

It should be noticed that the results presented in Figs. 2, 3, 4, 5 and 6 are dependent on the amount of solution relative to the solid phases. Only the distribution ratio for alkalis in the chloride free case, Rd of 0.65, is a global value, independent of the amount of solution. By further treatment of the data in Figs. 5 and 6, the overall global reactions taking place in hydrated Portland cement pastes upon addition of chloride were deduced, and are presented in Table 4.

Table 4. Global complete reaction describing the binding of chloride by the C-S-H and AFm phases, and the composition of the pore solution.

---

1. Chloride binding in Portland cement pastes in which some Na is present in the C-S-H
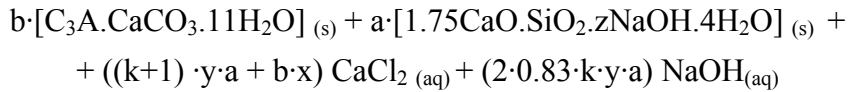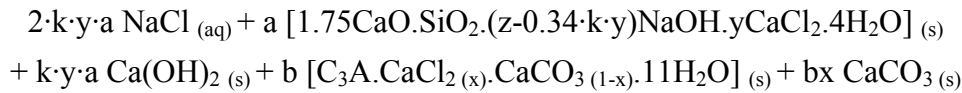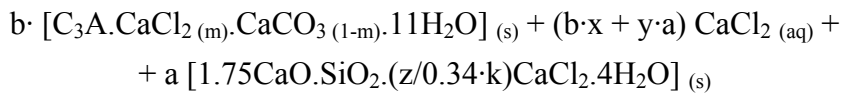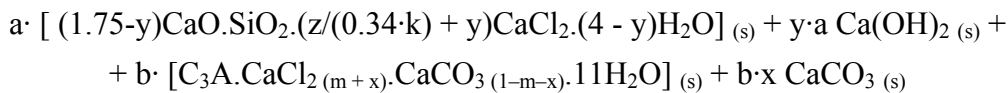
$$b \cdot [C_3A.CaCO_3.11H_2O]_{(s)} + a \cdot [1.75CaO.SiO_2.zNaOH.4H_2O]_{(s)} +$$
$$+ ((k+1) \cdot y \cdot a + b \cdot x)\, CaCl_{2\,(aq)} + (2 \cdot 0.83 \cdot k \cdot y \cdot a)\, NaOH_{(aq)}$$
$$\downarrow$$
$$2 \cdot k \cdot y \cdot a\, NaCl_{(aq)} + a\, [1.75CaO.SiO_2.(z-0.34 \cdot k \cdot y)NaOH.yCaCl_2.4H_2O]_{(s)}$$
$$+ k \cdot y \cdot a\, Ca(OH)_{2\,(s)} + b\, [C_3A.CaCl_{2\,(x)}.CaCO_{3\,(1-x)}.11H_2O]_{(s)} + bx\, CaCO_{3\,(s)}$$

2. Chloride binding in Portland cement pastes with alkali-free C-S-H

$$b \cdot [C_3A.CaCl_{2\,(m)}.CaCO_{3\,(1-m)}.11H_2O]_{(s)} + (b \cdot x + y \cdot a)\, CaCl_{2\,(aq)} +$$
$$+ a\, [1.75CaO.SiO_2.(z/0.34 \cdot k)CaCl_2.4H_2O]_{(s)}$$
$$\downarrow$$
$$a \cdot [\,(1.75-y)CaO.SiO_2.(z/(0.34 \cdot k) + y)CaCl_2.(4 - y)H_2O]_{(s)} + y \cdot a\, Ca(OH)_{2\,(s)} +$$
$$+ b \cdot [C_3A.CaCl_{2\,(m+x)}.CaCO_{3\,(1-m-x)}.11H_2O]_{(s)} + b \cdot x\, CaCO_{3\,(s)}$$

Note: in eq.2, for each mol of $CaCl_2$ bound by the C-S-H, (PS/a)/75 mol $CaCl_2$ remain in solution, where PS denotes the amount of solution in millilitre (i.e. pore solution + exposure solution, if applicable).

Notes:

- 'x' denotes the fraction of Friedel's salt in the AFm solid solution phase; 'y' denotes the content of $CaCl_2$ in the C-S-H, in mol/mol, and is related to 'x' as follows,

In the iron-free case (white Portland cement)

$y = 0.0601\, x^2 + 0.0164\, x$

In the iron-containing case (grey Portland cement)

$y = 0.0376\, x^2 + 0.0046\, x$

- 'a' is the content of C-S-H, in mol; 'b' is the initial content of monocarbonate, in mol.

- 'z' is the molar ratio of NaOH in the chloride-free C-S-H to C-S-H, i.e. in mol/mol. This can be calculated from the initial Rd, i.e. 0.65 (see the text), which is a general value, independent of water to powder ratio.

- 'k' is defined as

$k = z \cdot (PS/a) \cdot 25 / (0.83 \cdot 0.81 \cdot M_{w,C-S-H} \cdot Rd_0) = z \cdot (PS/a) \cdot 0.2354$, where PS is the amount of solution in milliliter (i.e. pore solution + exposure solution, if applicable).

- 'm' denotes the fraction of Friedel's salt in the solid solution phase at the chloride content where all alkalis have been released to the pore solution from the C-S-H.

The model can be used to predict the phase assemblage, including contents and compositions of the phases present in any Portland cement paste at equilibrium, at any known total alkali and chloride content, solely on the basis of the chemical composition of the system. As a first approximation, potassium can be assumed to behave similarly to sodium, which was observed by Hong and Glasser (Ref. [11]). Fig. 7 illustrates the values measured for the WPC(4) pastes at 250 and 550 mmol/l sodium compared to those predicted by the described model (i.e. using the reactions in Table 4). The model was applied to chloride binding data available in the literature

(see Ref. [14]) where excellent agreement was found between the measured and predicted results from both absorption and desorption determinations.
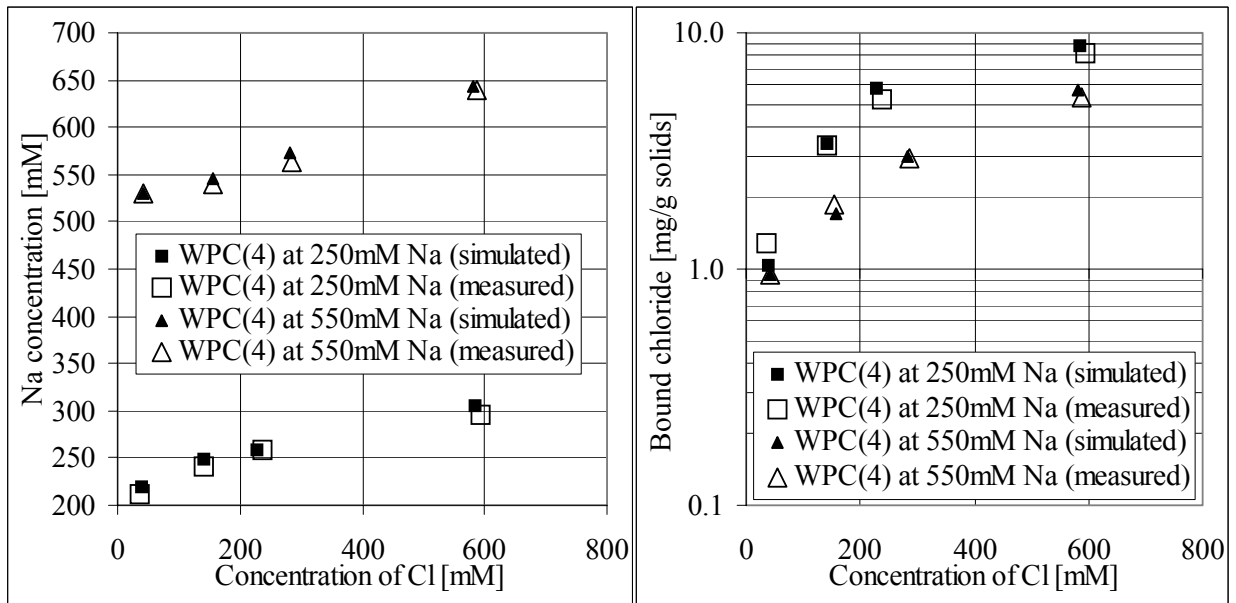
Fig. 7: Comparison between the values measured and those simulated according to the reactions in Teble 4, for the pastes WPC(4) at both 250 and 550 mmol/l Na.

In carbonate free systems (which do not exist in real concrete), the same type of binding is expected, as the monosulfate phase is likely to form a similar solid solution with Friedel's salt. This hypothesis is presently being tested. Furthermore, the addition of supplementary cementitious materials, such as silica fume, metakaolin and slag will not affect the model, as long as $Ca(OH)_2$ is still present in the system, or where the C-S-H is not decalcified by leaching or attack by $MgSO_4$.

Conventional chloride binding isotherms for same specimens described above are shown in Fig. 8 at two different levels of Na^+ concentration in the pore solution (250 and 550 mM for WPC(4), 250 mM for WPC(12), and 550 mM for OPC).
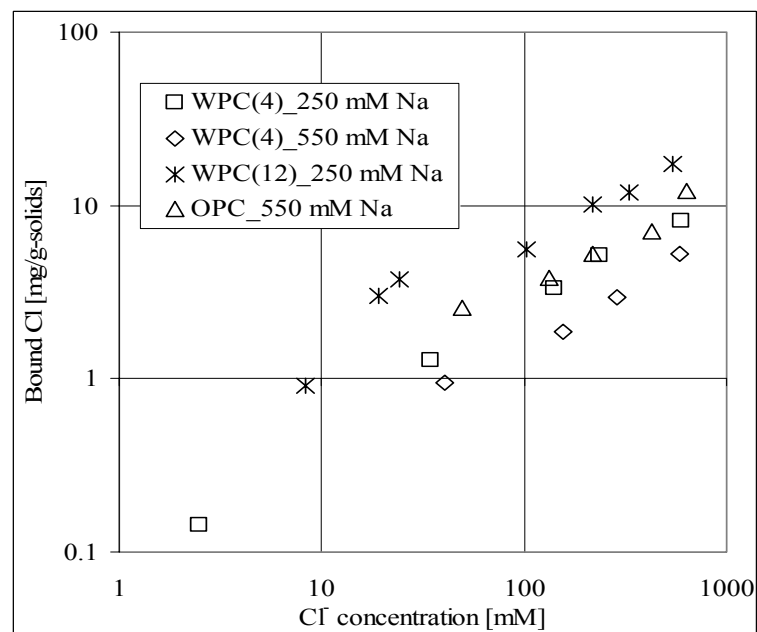
Fig. 8: Chloride binding isotherms determined for the cement pastes examined. Each isotherm is measured at a constant equilibrium concentration of Na^+.

These concentrations are typical for the normal range of alkalis in the pore solution in normal concretes (except for WPC(4) at 550 mM Na^+). It is observed that the binding of chlorides in WPC(4) paste at 250 mM Na^+ is similar to that in the OPC paste, even though the content of Al_2O_3 is approx. 3 times higher in OPC. The WPC(12) paste at 250 mM Na^+ has the greatest chloride binding over the range of chloride contents studied, even though it has a slightly lower content of Al_2O_3 than OPC. The maximum binding capacity of the AFm phases in the OPC cement is predicted to be slightly higher, but this is of little value in Portland cements containing alkalis given that the chloride concentration of sea water rarely exceeds 600 mM Cl^- (given as the average chloride concentration in sea water in Ref.[15]), hindering thereby the exhaustion of the binding capacity by aluminate phases.

CONCLUSION

A thermodynamic model for calculating the phase assemblage and the pore solution composition in fully hydrated Portland cement pastes has been presented. The model describes the distribution of alkalis and chloride in the solid phases and the pore solution, predicted from the chemical composition of system. The model can be used to predict the performance of different types of Portland cement under different conditions of exposure.

Alkalis have a negative impact on the binding of chlorides because they increase the concentration of chlorides in solution.

The absence of iron in white Portland cement is beneficial to chloride binding owing to significant increase in the content of Cl bound by the C-S-H phase compared to conventional Portland cement.

ACKNOWLEDGEMENTS

REFERENCES

[1] Truc, O., Prediction of Chloride Penetration into Saturated Concrete – Multi-Species Approach. Doctoral Thesis. Department Of Building Materials, Chalmers University of Technology, Göteborg, Sweden 2000.

[2] Samson, E., Marchand, J. and Maltais, Y., Modeling ionic diffusion mechanisms in structured cement-based materials – an overview. In: Ion and mass transport in cement-based materials, pp. 97-112, Edited by: Hooton, R.D., Thomas, M.D.A., Marchand, J. and Beaudoin, J.J. Materials Science of Concrete, Special volume. The American Ceramic Society, United States of America, 2001.

[3] Volkwein, A., Penetration of chlorides into concrete – Phenomena and consequences. Points of view based on 20 years research and site experience with deicing salts. Proceedings of the International RILEM workshop on Chloride penetration into concrete, St-Rémy-lès-Chevreuse, France, 1995.

[4] Tang, L. and Nilson, L-O., Chloride binding capacity and binding isotherms in of OPC pastes and mortars. Cement and Concrete Research 23 (1993) 247-253.

[5] Jensen, O.M., Korzen, M.S.H., Jakobsen,H. J. and Skibsted, J., Influence of cement constitution on chloride binding in cement paste, Advances in Cement Research 12 (2) (2000) 57-64.

[6] Nielsen, E.P., Herfort, D., Geiker, M.R., Phase equilibria of hydrated Portland cement, Accepted for publication in Cement and Concrete Research in march 2004.

[7]   Nielsen, E.P., Herfort, D., Geiker, M.R. and Hooton, R.D., Effect of solid solutions of AFm phases on chloride binding. Proceedings of the 11th International Congress on the Chemistry of Cement, Durban, South Africa, 2003.

[8]   Herfort,D and Juel,I.A., The mineralogy of sulfate and sea water attack on concrete interpreted from EPMA analysis. Proceedings of the 23rd International Conference on Cement Microscopy, Albuquerque, New Mexico, 2001.

[9]   Juel,I.A. and Herfort,D. The mineralogy of chloride attack on concrete containing limestone filler. Proceedings of the 24th International Conference on Cement Microscopy, San Diego, California, 2002.

[10]   Pöllmann, H., Solid solution of complex calcium aluminate hydrates containing Cl^-, OH^- and CO_3^{2-} -anions. Proceedings of the 8th International Congress on the Chemistry of Cement, Rio de Janeiro, Brazil, 1986

[11]   Hong, S.-Y. and Glasser, F.P., Alkali binding in cement pastes. Part I. The C-S-H phase. Cement and Concrete Research 29 (1999) 1893-1903.

[12]   Hong, S.-Y. and Glasser, F.P., Alkali sorption by C-S-H and C-A-S-H gels. Part II. Role of alumina. Cement and Concrete Research 32 (2002) 1101-1111.

[13]   Juel, I.A., Mineralogical and thermodynamic processes by sulfate and seawater attack of Danish concrete. Industrial Ph.D. thesis, EF-816 Durability, Geological Institute, University of Copenhagen, Copenhagen, 2004.

[14]   Nielsen,E.P., Herfort, D. and Geiker, M.R., Chloride binding in the CaO-SiO_2-Al_2O_3-SO_3-Na_2O-CO_2-H_2O system for Portland cement. Proceedings of the International Symposium on Advances in Concrete through Science and Engineering, Northwestern University, Evanston, Illinois, 2004.

[15]   Glasser, F.P., Role of chemical binding in diffusion and mass transport. In: Ion and mass transport in cement-based materials, pp. 129-180, Edited by: Hooton, R.D., Thomas, M.D.A., Marchand, J. and Beaudoin, J.J. Materials Science of Concrete, Special volume. The American Ceramic Society, United States of America, 2001.

Paper V: Performance of white Portland cement in aggressive environment.

Nielsen, E.P., Thrysøe, J., Herfort, D. and Geiker, M.R.

ABSTRACT

This paper presents a discussion of the main mechanisms involved in the binding of chlorides in Portland cement pastes, as well as their overall effect on the ingress of chlorides from the surrounding environment. The discussion is based on experimental studies on chloride ingress in both mortars and concretes.

Chloride binding is enhanced in Portland cements with low iron and alkali content. The low iron content results in a higher binding capacity of chloride by the C-S-H phase, and the reduced alkali content results in a larger part of the chloride being bound at any total content of chloride. Compared to the effect of these two parameters the total content of alumina has a minor influence on the binding capacity, as extremely high concentrations of chlorides are required in alkali containing environments to achieve the maximum chloride binding capacity of the AFm phases.

Since the ingress of alkalis from an external solution is remarkably lower than the ingress of chlorides, low alkali Portland cements are expected to result in better performance in chloride containing environments. This, as well as the fact that the uptake of chlorides by the C-S-H is enhanced in systems with low iron content makes white Portland cement an appropriate candidate for such environments. In aggressive environments, where both chlorides and sulfates are present, low aluminate white Portland cements will result in fine performance.

INTRODUCTION

White Portland cement enjoys only a small share of the global market for Portland cement. White Portland cement clinker differs from other Portland cement clinker by having a much lower iron content, which makes it much harder to burn. White Portland cement is a specialised product, which today generally is used to applications where colour is a primary objective.

An often overlooked advantage of the much lower iron content in white Portland cement is the improved durability that this can be expected to result in. Since iron forms the high density, low volume FH_3 phase, a lower content of iron should result in a higher relative volume of hydrate phases, and therefore a lower capillary porosity. This, in part, results in higher strengths and lower permeability. Some of the iron in Portland cements is incorporated in the structure of the C-S-H reducing thereby its chloride binding capacity. The binding capacity of the C-S-H in white Portland cements (i.e. low iron content) is therefore higher. Furthermore, white Portland cements have a low content of alkalis, which not only reduces the risk of alkali silica reaction but also results in higher degrees of chloride binding at any total chloride content (see next section).

Thus, structures built of concretes with low-alkali Portland cements with low iron content (i.e. white Portland cements) are expected to result in prolonged service life in chloride rich environments, compared to structures made from comparable grey Portland cements. Since sulfates are always present in marine environments, sulfate-resistant white Portland cements are expected to result in similar or better performance than comparable grey sulfate-resistant Portland cements.

Since durability concerns play a major role in the design of reinforced concrete structures in aggressive environments, for example in aggressive marine environments and where de-icing

salts are used, the performance of white cements in such environments is presently studied at Aalborg Portland A/S. This paper deals with the effect of binding mechanisms on chloride ingress.

BACKGROUND

It is generally agreed that when chlorides penetrate into concrete they become partially fixed by the hydrate phases by one or more processes collectively referred to as binding. Part of the ingressing chloride ions are thereby removed from the pore solution, delaying the time to reach a critical content at the reinforcement level.

Chlorides are bound in both AFm phases and in the C-S-H. The total binding capacity of all types of Portland cement pastes is nearly impossible to achieve in 'real' exposure environments because of the presence of alkalis, requiring extremely high concentration of chlorides in solution (Ref. [1]). Thus, the total amount of AFm phases formed does normally not control the binding capacity in actual concrete structures.

Nielsen et al. [2] found a relation between the content of chloride in the C-S-H and that in the AFm solid solution phase (monocarbonate-Friedel's salt). The relation applies for all mature Portland cement pastes, but is dependent on the total iron content. The binding capacity of the C-S-H in white Portland cements is approximately twice as high as in ordinary grey Portland cements.

The studies in [2] served as background for developing a model for calculating the phase assemblage (including the composition of the pore solution) in mature Portland cement pastes, at varying contents of alkalis, chloride, and carbonate (in [1]). The distribution of alkalis between the pore solution and the C-S-H was found highly dependent on the content of chloride in the paste. The findings in [1] are summarized in Fig. 1.

In a Portland cement paste with a given total content of alkalis and chlorides, further addition of chloride (upper-left in Fig. 1) will result in part of the alkalis in the C-S-H going into solution, part of the chloride becoming bound by the solid phases, and a larger part of the introduced chloride remaining in solution, as the ratio of chloride to alkalis in the pore solution increases for increasing total content of chlorides. The inverse (upper-right in Fig. 1) is observed upon removal of chlorides.
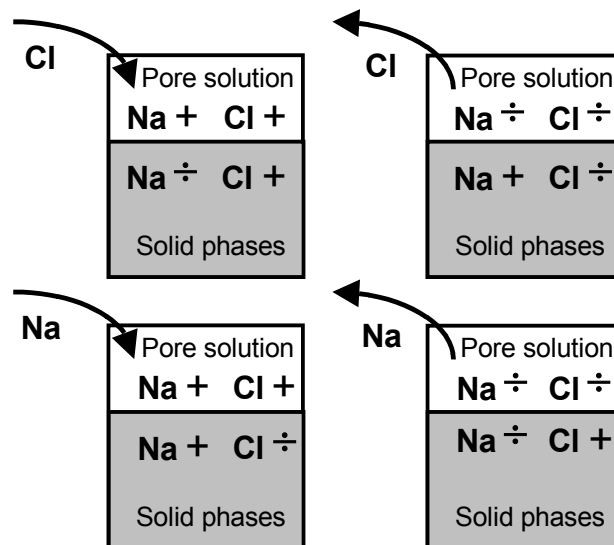
Figure 1: Chloride and alkali binding in Portland cement ('+' for increase, '÷' for decrease, arrows for addition/extraction of Cl or Na)

The addition/extraction of alkalis (lower-left/lower-right in Fig. 1) to a Portland cement paste with a constant content of chlorides will result in a change in the ratio between chlorides in solution and chlorides bound by solid phases.
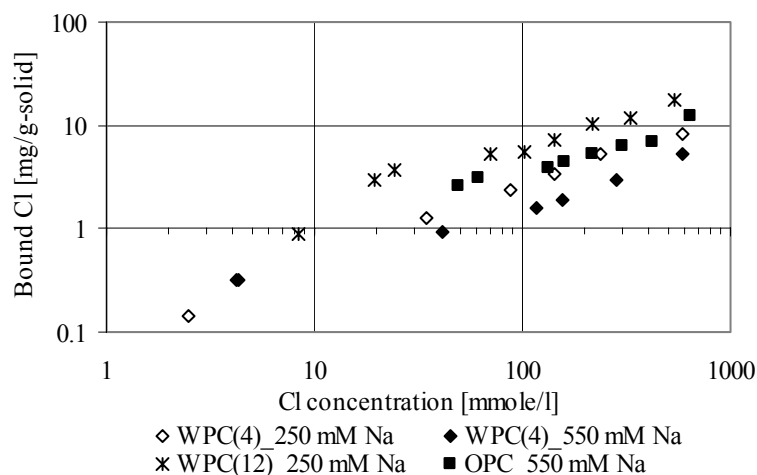
Figure 2: Chloride binding isotherms at varying alkali contents for the cements examined (from Ref.[2]).

The chloride binding isotherms measured in [2] are shown in Fig. 2 (The terminology applied for the cement pastes corresponds to the cements listed in Table a, accompanied with the equilibrium concentration of sodium in the pore solution, in mmol/l). Each isotherm was measured at constant alkali concentration but varying chloride content.

The concentration of alkalis for the measured binding isotherms corresponds to that expected in a w/c 0.45 cement paste of the respective cements prior to chloride addition, except for WPC(4)_550 mM Na which was prepared for comparison with the system OPC_550 mM Na.

It is noticed that the binding isotherms are highly dependent on the content of alkalis (see WPC(4)_250 mM Na against WPC(4)_550 mM Na).

Volkwein [3] observed that the ingress of alkalis is much slower than that of chlorides. Therefore, low alkali cements should be used in aggressive environments thereby enhancing the chloride binding of the cement paste. A white Portland cement is expected to further enhance the chloride binding of the concrete due to increased uptake in the C-S-H.

In Portland cement pastes, the ratio of Al_2O_3 to SO_3 is the most important controlling parameter with regard to sulfate resistance. High Al_2O_3/SO_3-ratio results in expansive reactions, due to the conversion of hydroxy-AFm to monosulfate, and hence to ettringite upon exposure to sulfate.

EXPERIMENTAL

The investigations cover mortars and concretes prepared in two parallel research projects at Aalborg Portland. Due to this some variations in age at testing and duration of testing occur.

The cements examined are listed in Table a, as well as relevant compositional properties.

Table a: Relevant properties of the cements examined.

Id.	ASTM-type	Corrected Bogue composition						Na_2O_{eq}
		C_3S	C_2S	C_3A	C_4AF	$CaSO_4$	Lime	
WPC(4)	V (white)	64.9	22.4	4.5	1.0	3.6	2.15	0.23
WPC(12)	I (white)	41.2	36.6	11.5	0.6	4.0	2.6	0.21
OPC	II (grey)	51.3	22.1	6.5	11.2	4.7	1.49	0.54
SRPC	V (grey)	52.8	29.8	3.9	7.0	3.5	1.24	0.39

The development of strength for the cements examined is presented in Table b, measured according to EN-196.

Table b: Strength development of the cements (EN-196), in MPa.

	1 day	2 days	7 days	28 days
WPC(4)	18.2	30.8	52.3	71.6
WPC(12)	12.0	23.9	44.9	66.1
OPC	17.0	27.5	46.7	66.7
SRPC	9.1	17.4	35.2	57.2

Mortar mixes

Mortars were prepared following the recipes in Table c. 1 wt.% of calcite was added to the powder to enhance the binding properties of the cements (see [2] for more information).

Table c. Design mixes for the mortars, in kg/m^3

Id. of mix	WPC(4)	WPC(12)	OPC
Cement		445.5	
Calcite (fine ground)		4.5	
Water		214	
Quartz-sand (0.25-1)		511	
Quartz-sand (1-4)		1193	

The mortars were cast into 150·100·100 mm moulds, de-molded after 2 days, sealed in plastic bags with limited amount of surrounding water, and cured for 3 months at 20^{0}C before surface-sealing, cutting and exposure of specimens for 70 days in either a 650 mM NaCl solution, or a 650 mM NaCl + 30 mM MgSO$_4$ solution.

Sulfate resistance of the cements was measured according to ASTM C1012.

Concrete mixes

Concretes were prepared following the recipes in Table d, having a water-to-powder ratio of 0.45. Notice that no calcite was added to these specimens.

Table d. Design mixes for the concretes, in kg/m^3

Id. of mix	WPC(4)_5%SF	SRPC_5%SF	WPC(4)	WPC(12)	OPC
Cement id.	WPC(4)	SRPC	WPC(4)	WPC(12)	OPC
Cement	316		333		
Silica fume	17		---		
Water	150				
Sand (0-2 mm)	686				
Stone (2-8 mm)	235				
Stone (8-16 mm)	885				

The concrete specimens were casted in blocks of 200·200·200 mm and cured at 20°C for 28 days for the concretes with silica fume, and 180 days for concretes without silica fume, prior to exposure to a 16.5 wt.% NaCl solution. The exposure times were 35 and 180 days for concretes with silica fume, and 35 and 70 days for concretes without silica fume.

Chloride diffusion coefficients according to NT BUILD 492 (migration test) was measured on concrete cylinders at a maturity of 28 and 180 for specimens with silica fume, and 180 days for specimens without silica fume.

Analyses after exposure

Chloride, sodium, and calcium profiles were determined on each specimen after exposure. Dust samples were ground parallel to the cut ingress surface of the concretes/mortars in layers of each about 1 mm, down to a depth of 8 mm, and in layers of 2 mm down to approximately 18-20

mm. The material from each layer was dried at $105^{o}C$ and analysed for Cl, Na_2O and CaO contents.

CHLORIDE AND ALKALI INGRESS

The chloride and sodium ingress profiles measured on the mortar samples exposed to a 650 mM NaCl solution for 70 days, are presented in Fig. 3.

The depths of chloride ingress in the three mortars are similar at the exposure times examined even though the composition of the cements differs remarkably. This is consistent with the expectations, as the lack of binding capacity in AFm phases in WPC(4) due to the low aluminate content is counteracted by the high binding capacity of the C-S-H phase in white cements (due to the low iron content). OPC has a higher binding capacity by AFm phases due to the higher alumina content but has significantly lower capacity to bind chlorides in calcium silicate hydrate phase due to the high iron content. The total binding capacity of all types of Portland cement pastes is nearly impossible to achieve in 'real' exposure environments because of the presence of alkalis, requiring extremely high concentration of chlorides in solution.
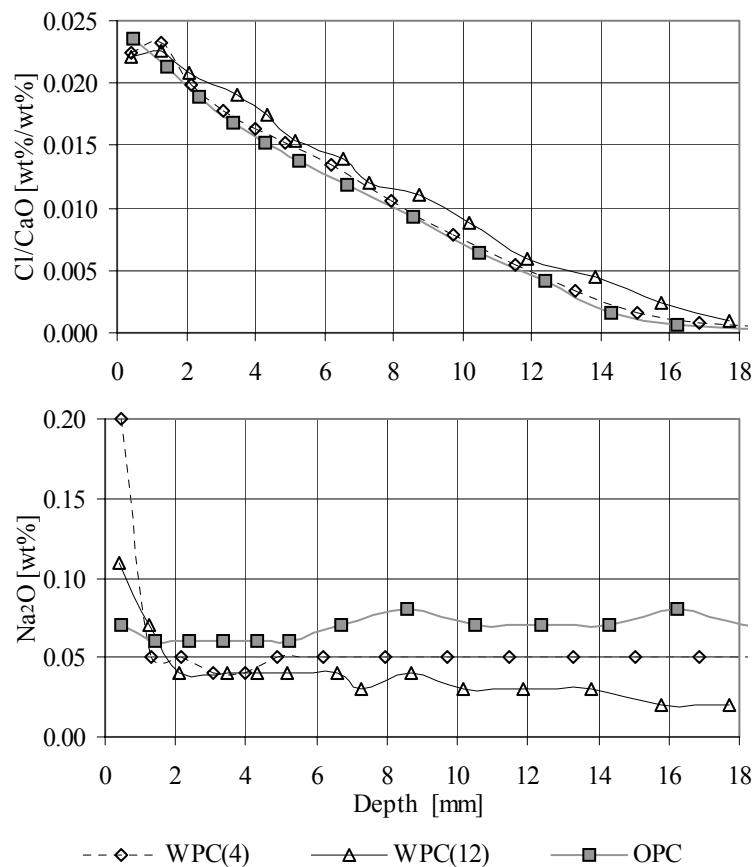
Figure 3: Cl/CaO- and sodium profiles in mortars specimens exposed to 650 mM NaCl for 70 days.

The ingress of chlorides in the WPC(12) mortar was expected to be lower than the other mixes. However, similar ingress depth was obtained which is likely to result from lesser amount of ettringite (i.e. low density) being formed than for the OPC mortar, counteracting the beneficial effect of the lack of high density phases in WPC(12).

The ingress of alkalis from the external solution is remarkably slower than that of chlorides (Fig. 3). Therefore, the content of alkalis as a function of depth is the corresponding to that of each of the cements, except at the near surface regions. The chloride binding isotherms in Fig. 2 can be used (except for WPC(4)_550 mM Na), as an approximation, for deducing the difference in chloride concentration in the pore solution at a certain total chloride content, for the cements

WPC(4), WPC(12) and OPC. However, note that the isotherms in Fig.2 were measured at equilibrium with constant sodium concentration, but not constant content of sodium, as the distribution of alkalis between C-S-H and pore solution is dependent on the content of chloride. As shown in Fig.1 this will result in a larger increase in chloride concentration in the pore solution in cements with high alkali content upon addition of chlorides.

Even though the chloride ingress depth for WPC(12) is slightly higher than for the two other systems, this cement presents the highest binding capacity at any total content of chloride, and hence, the concentration of chlorides in the pore solution is lowered. The chloride binding isotherm for WPC(4) at 250 mM Na and OPC at 550 mM Na are similar, allowing thereby to deduce that the chloride threshold is found approximately at the same depth on the chloride profiles.
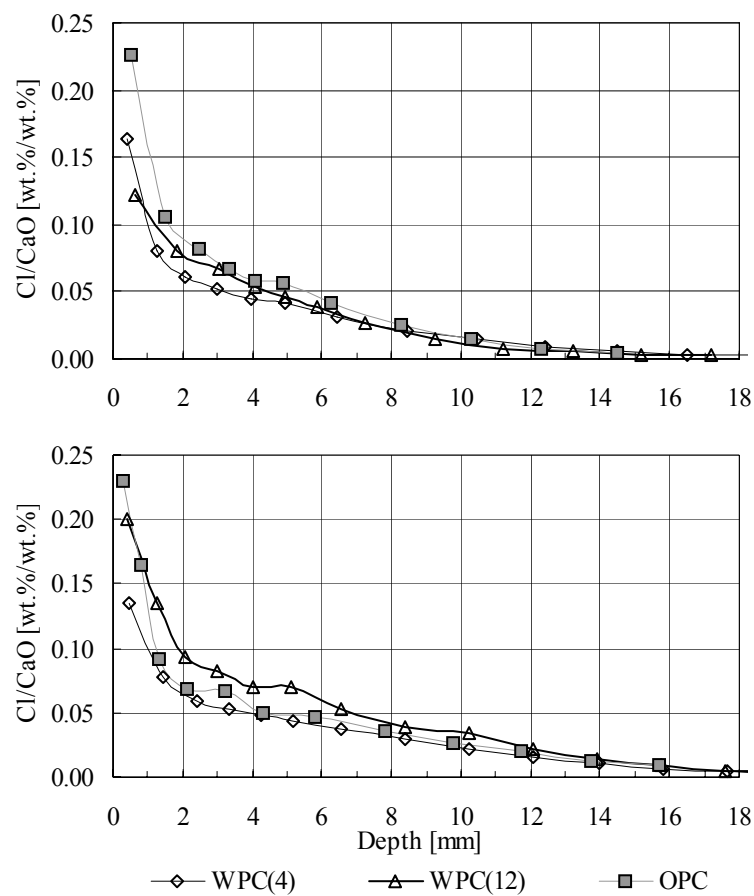
Figure 4: Cl/CaO profiles in concretes cured for 180 days prior to exposure to a 16.5 wt.% NaCl solution for 35 (upper figure) and 70 (lower figure) days.

Fig. 4 shows the chloride profiles obtained in concretes WPC(4), WPC(12) and OPC cured for 180 days prior to exposure for 35 and 70 days to a 16.5 % NaCl solution. The same trends as in Fig. 3 are found for these profiles.

The chloride ingress profiles for WPC(4)_5%SF and SRPC_5%SF cured for 28 days prior to exposure for 35 and 180 days to a 16.5 wt.% NaCl solution are resented in Fig. 5.
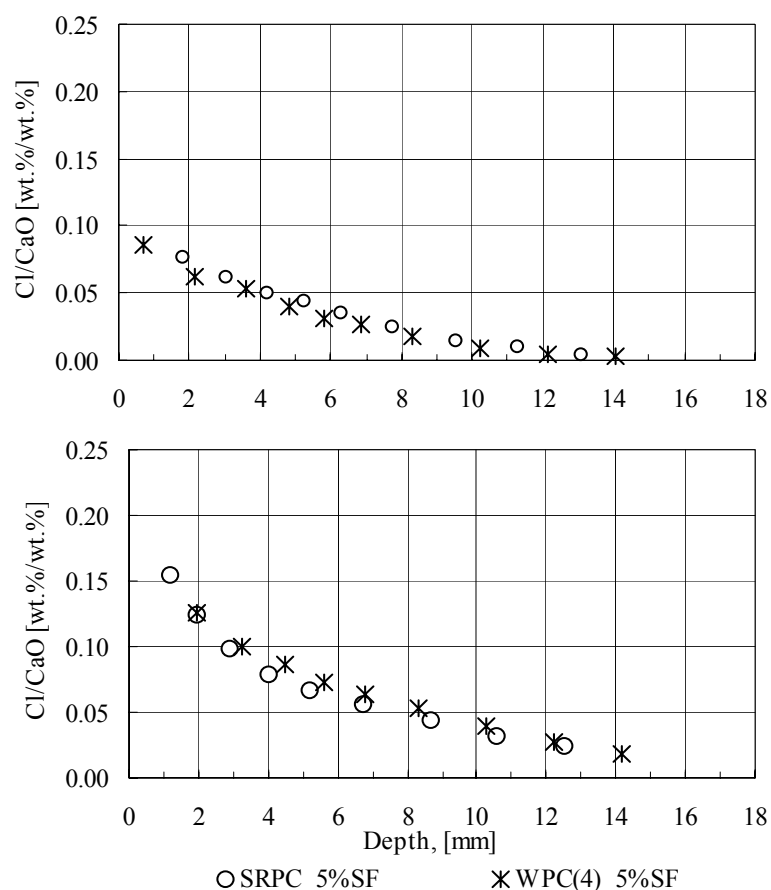
Figure 5: Cl/CaO-profiles in concretes WPC(4)_5%SF and SRPC_5%SF after 35 (upper) and 180 (lower) days of exposure.

Even though the concrete based on WPC(4)_5%SF contains far less aluminate the chloride ingress and the penetration depth is at the same level as for the concrete based on SRPC_5%SF. SRPC_5%SF is a concrete mixture having a powder composition similar to the one used for the construction of the "Oeresund link" bridge connecting Denmark and Sweden.

Chloride diffusion coefficients determined according to NT BUILD 492 on concretes are shown in Table e.

Table e: Chloride diff. coeff. [m^2/s] according to NT BUILD 492.

Days of maturity	28	180
SRPC_5%SF	9.9	2.7
WPC(4)_5%SF	5.7	3.1
WPC(4)	---	10.0
RCI(4)	---	9.6
OPC	---	9.6

As observed for the chloride ponding tests, the chloride migration test shows that concrete based on white Portland cement (WPC(4)) with silica fume develops a resistance against chloride penetration, expressed by the chloride diffusion coefficient, at the same level as for the concrete based on sulfate resistant Portland cement with silica fume. However, as expected from the strength development data in Table e, WPC(4)_5%SF densifies much faster than the SRPC_5%SF concrete, which is an advantage upon exposure at early hydration times. The resistance against chloride penetration in the concretes without silica fume is similar.

SULFATE RESISTANCE

Fig. 6 illustrates the results obtained following ASTM C1012 on the cements WPC(4), WPC(12) and OPC. The measurements are compared to a reference Type V Portland cement from Ref. [4], which is considered to be a sulfate-resistant Portland cement by the authors of [4].

WPC(4) presents a high sulfate resistance due to the low expansion over time. Surprisingly, OPC also exhibits less expansion than the reference cement. This is probably due to slower hydration of the ferrite phase in the cement, which results in an initially reduced Al_2O_3/SO_3-ratio and a reduced amount of ettringite being formed at later stages of hydration. WPC(12) is, as expected, not sulfate resistant.
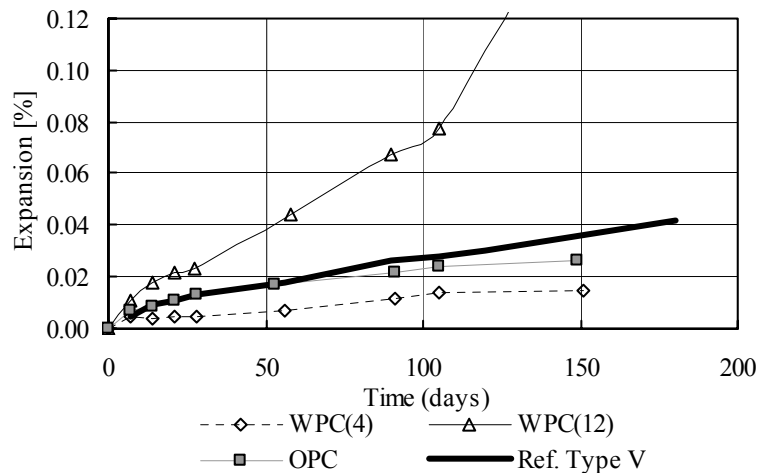
Figure 6: Average expansion of mortar specimens subjected to a 350 mM Na_2SO_4 solution, following the procedure in ASTM C1012.

COMBINED INGRESS OF CHLORIDES AND SULFATES

Fig. 7 shows the results Cl/CaO- and sodium profiles in mortars exposed to 650 mM NaCl and 30 mM $MgSO_4$ for 70 days.

In contrast to the results in Fig. 4, a clear difference in the chloride ingress profiles is observed when sulfates are present in the solution. The exposure to sulfates is expected to tighten, to some extent, the surface region due to formation of ettringite, gypsum and brucite (as observed in Ref. [5], and confirmed by EDS analysis of the surface region of the samples), lowering thereby the capillary porosity of the paste. This should reduce the rate of ingress of external ions in solution, which is observed in the mortar WPC(4) (when comparing to the corresponding profile in Fig. 4). However, the depth of ingress for WPC(12) and OPC is similar to that in the sulfate-free environment, which can be related to possible formation of cracks at the near-surface region, because of the lower sulfate resistance, and therefore limited available porosity to allow the reaction of the solids with the ingressing sulfates.
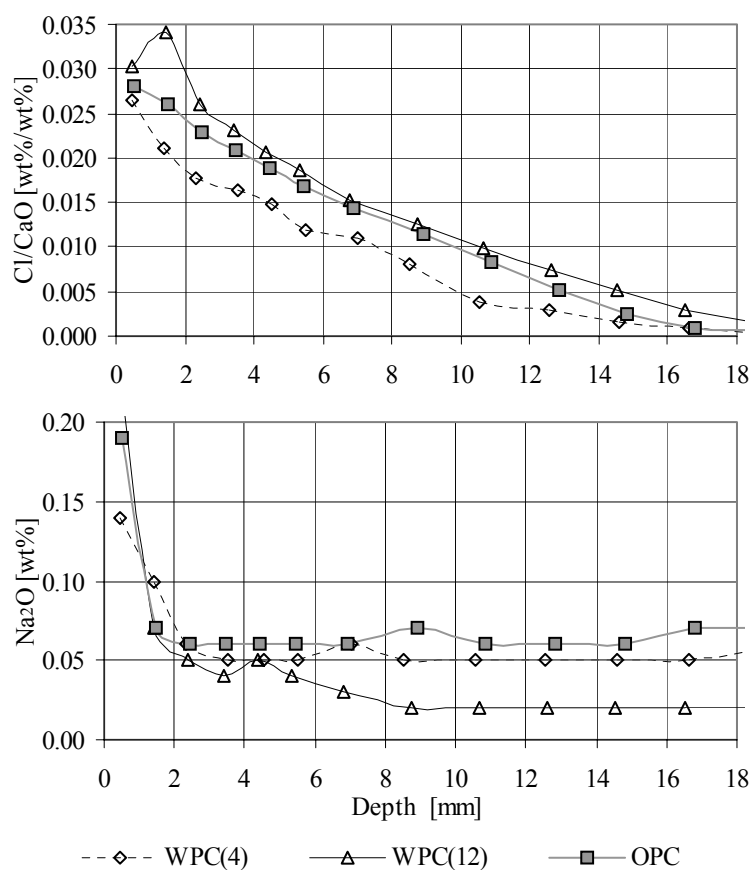
Figure 7: Cl/CaO- and sodium ingress profiles in mortars exposed to 650mM NaCl + 30 mM $MgSO_4$ for 70 days.

Similar results as those in Figs. 6 and 7, but on a mortar based on the cement SRPC will be available for the presentation at the conference.

CONCLUSION

Low-alkali Portland cements should be used in chloride containing environment thereby enhancing the chloride binding capacity. Due to the much slower rate of ingress of alkalis long-term binding is facilitated.

An increased chloride binding capacity of C-S-H is observed in white Portland cements.

The chloride binding capacity is enhanced in white Portland cements and is therefore expected to result in better performance in chloride containing environment, than comparable grey cements.

Low-aluminate white Portland cements will perform satisfactorily in marine environments (i.e. both chlorides and sulfates in the environment), due to combined enhanced chloride binding and the sulfate resistance of the cement.

The fast rate of strength development in the e.g. WPC(4) cements will result in a fast densification of the cement paste matrix, and hence low ingress rates already at early ages.

REFERENCES

[1]   Nielsen, E.P., Herfort, D. and Geiker, M.R., Binding of chlorides and alkalis in Portland cement, submitted in may 2003 for publication in Cement and Concrete Research.

[2]   Nielsen, E.P., Herfort, D., Geiker, M.R. and Hooton, R.D., Effect of solid solutions of AFm phases on chloride binding. Proceedings of the 11th International Congress on the Chemistry of Cement, Durban, South Africa, May 2003.

[3]   Volkwein, A., Penetration of chlorides into concrete – Phenomena and consequences. Points of view based on 20 years research and site experience with deicing salts. Proceedings of the International RILEM workshop on Chloride penetration into concrete, St-Rémy-lès-Chevreuse, France, 1995.

[4]   Patzias, T., 'The development of ASTM Method C1012 with Recommended Acceptance Limits for Sulfate Resistance of Hydraulic Cements', Cement, Concrete, and Aggregates, CCAGDP, Vol. 13, No.1, Summer 1991, pp. 50-57.

[5]   Glasser, F.P., Role of chemical binding in diffusion and mass transport. In: Ion and mass transport in cement-based materials, pp. 129-180, Edited by: Hooton, R.D., Thomas, M.D.A., Marchand, J. and Beaudoin, J.J. Materials Science of Concrete, Special volume. The American Ceramic Society, United States of America, 2001.

Paper VI: Chloride binding in the CaO-SiO_2-Al_2O_3-Fe_2O_3-SO_3-Na_2O-CO_2-H_2O system for Portland cement.

Nielsen, E.P., Herfort, D. and Geiker, M.R.

Proceedings of the International Symposium on Advances in Concrete through Science and Engineering organised by RILEM and ACBM on March 21-24, 2004, Evanston, Illinois.

ABSTRACT

A model for predicting the phase assemblage in hydrated Portland cements at different contents of chlorides and alkalis, including calculations of the relative contents and compositions of the phases present was described in [1,2]. Additional data on the accuracy and verification of the model is presented in this paper, including calculations of the threshold values for chloride induced corrosion as a function of cement composition. The Al_2O_3 and Fe_2O_3 contents of Portland cements are shown to have limited effect on the overall chloride binding capacity compared to the effect of alkalis, with high alkali contents significantly reducing the chloride binding capacity. Lower alkali contents, although resulting in a lower pH of the pore solution, are shown to lower the Cl/OH-ratio of the pore solution, therefore reducing the risk of corrosion. Practical applications of the model are also discussed.

INTRODUCTION

Durability is an important consideration in the design of reinforced concrete structures exposed to aggressive environments, e.g. sea water or de-icing salts. In such environments, the time taken to the initiation of chloride induced reinforcement corrosion is the major criterion for predicting the service life of the concrete.

When chlorides penetrate into concrete they become partially fixed by the hydrate phases through one or more processes collectively referred to as binding, which is generally agreed to have a significant effect on service life. Only free chlorides in the pore solution can be transported towards the reinforcement and initiate corrosion.

Attempts to predict the service life of a concrete structure without including the chloride binding capacity of the binder will result in spurious results, since different cements are known to perform differently. Furthermore, the service life predictions should also include both the concentration of free chlorides in the pore solution necessary to initiate corrosion, and the predicted rate of ingress.

The mechanisms involved in the binding of chloride ions are still not entirely understood [3], but it is believed by most workers to be related to reaction of chlorides in the pore solution with the aluminate rich hydrate phases to form Friedel's salt or AFm solid solutions which include Friedel's salt [4]. Competition for the aluminates by the sulfate and carbonate ions will affect the capacity of the system to bind chlorides. In addition to the aluminate phases, the very high specific surface area of the C-S-H phase is often believed to substantially contribute to binding through physical adsorption [5], although other studies have shown it to play little or no part [6].

Binding is normally quantified by determining the ratio at equilibrium of bound to free chlorides over a range of total chloride contents. The results are then expressed in terms of Langmuir or Freundlich equations (e.g. in [3]), depending on which of these provides the best fit over the range of concentrations examined. Alkalis will significantly affect these results (as found in [7]) and care should therefore be taken when comparing results obtained by this method that this is done at constant alkali contents. Chloride isotherms have been used by numerous workers to identify the key cement properties responsible for the binding capacity. Other methods for this

have included statistical analysis of the large amount of data found in the literature using a neural network [8].

The authors of the present paper have developed a model for predicting the equilibrium phase assemblage and contents and compositions of phases present for most Portland cement types [1,2]. The distribution of chlorides and alkalis between the pore solution and the solid phases is included. The model is described in this paper, and its accuracy is tested against independent data in the literature. The model is also used to predict the effect of cement composition on chloride threshold values, and examples of the practical applications of this are discussed.

MODEL FOR CHLORIDE AND ALKALI BINDING IN PORTLAND CEMENT PASTE

The 'Phase Rule' applies for all systems at equilibrium and is equally applicable under stable (lowest free energy) and metastable conditions. It states that for non-reacting systems (in e.g. [9]) the number of Phases plus the Degrees of Freedom equals the number of Components plus a constant n, which is dependent on the state of the system with respect to pressure and temperature. At constant temperature and pressure n is 0.

The main components of a hydrated Portland cement are CaO, SiO_2, Al_2O_3, Fe_2O_3, SO_3 and H_2O. A fully hydrated Portland cement paste will therefore form a maximum of six phases in an invariant phase assemblage [1], normally C-S-H, calcium hydroxide, monosulfate, ettringite, iron hydroxide and the pore solution. Depending on the Al_2O_3/SO_3-ratio, an hydroxy-AFm phase may occur instead of ettringite, or gypsum instead of monosulfate.

The relative contents of phases in weight % in a system of known composition (e.g. cement composition and water/cement ratio) can be calculated by solving 'n' equations for 'n' unknowns (where 'n' is the number of components and phases), and assuming fixed compositions of the hydrate phases. The contents in volume % can be calculated from the standard densities of the hydrate phases (given in e.g. [10]).

In aggressive environments, concrete structures are often subjected to attack by carbon dioxide, sulfates, chloride, and alkalis. Depending on the relative content of CO_2, calcite and/or monocarbonate will form in the invariant hydrate assemblage. The addition of sulfates to this invariant assemblage does not change the composition of the phases present, including the pore solution [11], but does change the relative content of the aluminate hydrate phases, and therefore indirectly affects chloride binding.

Alkalis do not form solid phases but are distributed between the pore solution and the C-S-H phase which can be defined by a distribution coefficient, R_d (in [12]). The distribution is similar for both sodium and potassium. The presence of alkalis in a Portland cement paste must therefore introduce at least one degree of freedom (since no additional phase is formed). Furthermore, it was shown in [1,7,11] that the addition of chloride to partially carbonated Portland cement paste results in a solid solution between Friedel's salt and monocarbonate, which also introduces a degree of freedom.

The contents of phases in the multivariant assemblage containing alkalis and chloride can also be calculated by initially assuming invariant conditions. Subsequently, the distribution of chlorides and alkalis can be included by applying the experimentally determined relationships found in [2]. An example of this is given in Table 1, which applies to a hydrated white Portland cement paste (i.e. negligible content of Fe_2O_3), with an initial assemblage consisting of C-S-H, CH, monosulfate, ettringite, monocarbonate and pore solution before chloride addition, to levels below that needed to release all alkalis from the C-S-H phase.

Table 1: Reaction taking place in iron-free Portland cement pastes initially consisting of C-S-H, CH, pore solution, monosulfate, ettringite and monocarbonate, with addition of chlorides at levels lower than that required to release all the alkali from the C-S-H (from [2]).

Chloride binding in PC pastes in which Na is still present in the C-S-H, and AFm phases other than monocarbonate are present

$$\mathbf{b} \cdot [C_3A.CaCO_3.11H_2O]_{(s)} + \mathbf{a} \cdot [1.75CaO.SiO_2.\mathbf{z}NaOH.4H_2O]_{(s)} +$$
$$+ \ ((\mathbf{k+1}) \cdot \mathbf{y} \cdot \mathbf{a} + \mathbf{b} \cdot \mathbf{x}) \ CaCl_{2 \ (aq)} + \mathbf{2 \cdot 0.83 \cdot k \cdot y \cdot a} \ NaOH_{(aq)}$$
$$\downarrow$$

$$\mathbf{2 \cdot k \cdot y \cdot a} \ NaCl_{(aq)} + \mathbf{a} \ [1.75CaO.SiO_2.(\mathbf{z-0.34 \cdot k \cdot y})NaOH.\mathbf{y}CaCl_2.4H_2O]_{(s)}$$
$$+ \ \mathbf{k \cdot y \cdot a} \ Ca(OH)_{2 \ (s)} + \mathbf{(b+bx)} \ [C_3A.CaCl_{2 \ (x)}.CaCO_{3 \ (1-x)}.11H_2O]_{(s)}$$
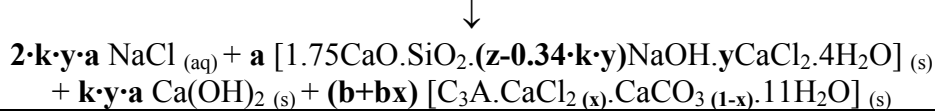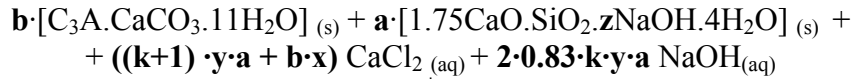
- '**x**' mole fraction of Friedel's salt in the solid solution phase; '**y**' content of $CaCl_2$ in C-S-H, in mol/mol, related to each other as follows,

$\mathbf{y} = 0.0601 \ \mathbf{x}^2 + 0.0164 \ \mathbf{x}$ **(iron free system, i.e. white PC)**

- '**a**' is the content of C-S-H, in mol; '**b**' is the initial content of monocarbonate, in mol.
- '**z**' is the molar ratio of NaOH, in the chloride-free C-S-H, to C-S-H, i.e. in mol/mol. This is calculated from the initial Rd, i.e. 0.65.
- '**k**' is defined as $\mathbf{k} = \mathbf{z} \cdot (\mathbf{PS/a}) \cdot 0.24$, where **PS** is the amount of pore solution in milliliters.

Chloride ions are distributed between the C-S-H (with a very high binding capacity), the monocarbonate-Friedel's salt solid solution, and the pore solution. The binding of chloride by the C-S-H results in a significant release of alkalis to the pore solution. Furthermore, the pH of the solution decreases with increasing chloride content (see Table 1). A well-defined distribution was found between the content of chloride bound by the C-S-H and that bound by the solid solution phase. This distribution was the same for all alkali contents but was shown to be dependent on the iron content of the cement ([2]; Table 1 is for iron-free systems).

As an indication of the accuracy of the model, the experimentally determined concentrations of chloride and sodium in the isotherm solution (essentially pore solution) for the different cement types tested to develop the model are plotted against the concentrations calculated by the model [2] in Figure 1. The composition of the Portland cements are shown in Table 2.
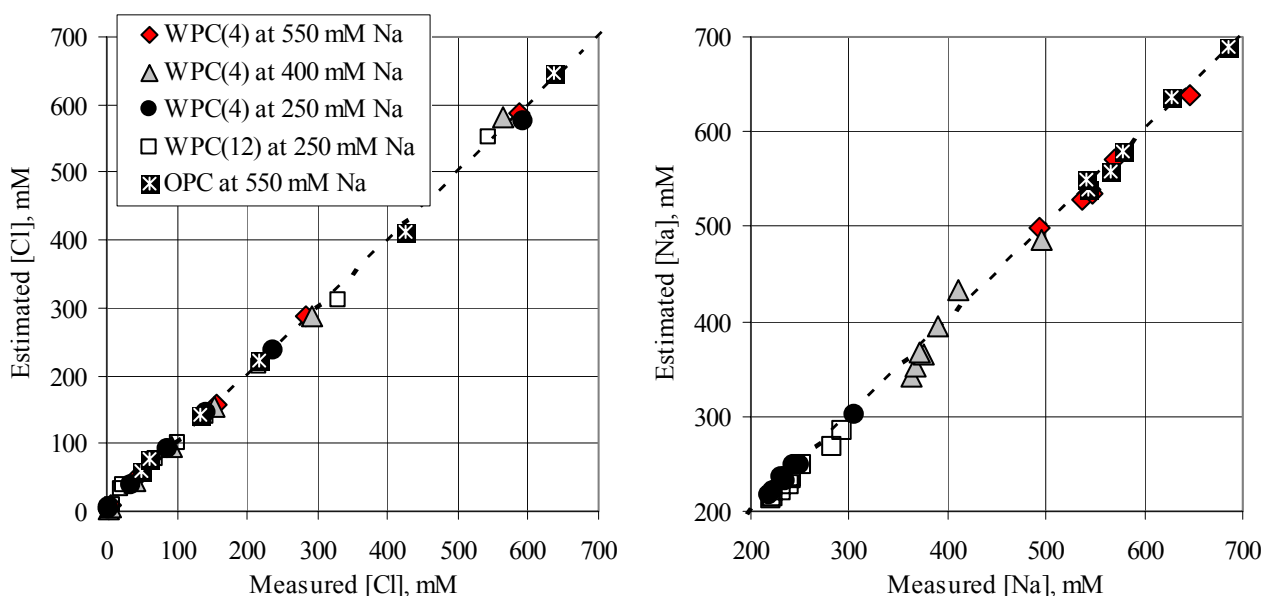
Fig. 1: Chloride and alkali concentration experimentally determined for the series examined in this investigation, plotted against the predicted by the model in [2].

Table 2: Composition of the Portland cements examined.

Id.	C_3S	C_2S	C_3A	C_4AF	$CaSO_4$	Lime	Na_2O_{eq}
WPC(4)	64.9	22.4	4.5	1.0	3.6	2.15	0.23
WPC(12)	41.2	36.6	11.5	0.6	4.0	2.6	0.21
OPC	51.3	22.1	6.5	11.2	4.7	1.49	0.54

The model briefly summarized in this section can be used to predict the chloride binding of any Portland cement paste, at any content of alkalis and chlorides. The composition of the pore solution can also be calculated to give the chloride threshold value of any concrete produced from a given cement type.

COMPARISON WITH DATA FROM THE LITERATURE

To successfully apply the above model to data published elsewhere, detailed documentation of the materials used (e.g. chemical composition of the cement, including alkali and CO_2 content, mixing properties), and the experimental conditions (e.g. total amounts of cement paste and exposure solution), are needed. Unfortunately, such detailed documentation is rarely provided. The results found in [13] (some of them published in [3]) is an exception and includes all the necessary data. In this study, the chloride binding isotherms were determined for different Portland cement pastes at different w/c ratios and temperature. The chloride source was NaCl and the amount of storage solution, both initial and after equilibrium, was documented for each sample, in addition to the equilibrium composition of the solution, the content of anhydrous cement, and the content of hydrated cement paste.

Figure 2.a compares the chloride concentrations in the pore solution obtained by the model described here and the equilibrium concentrations determined in [13] for w/c 0.50 pastes at 20^oC. Unfortunately, the concentration of alkalis was not measured in [13] and could therefore not be compared. The effect of desorption was also investigated in [13] by replacing 2.2 ml of the equilibrium storage solution with 8 ml lime-saturated water. Figure 2.b compares the results obtained in [13] with the results obtained by the model.
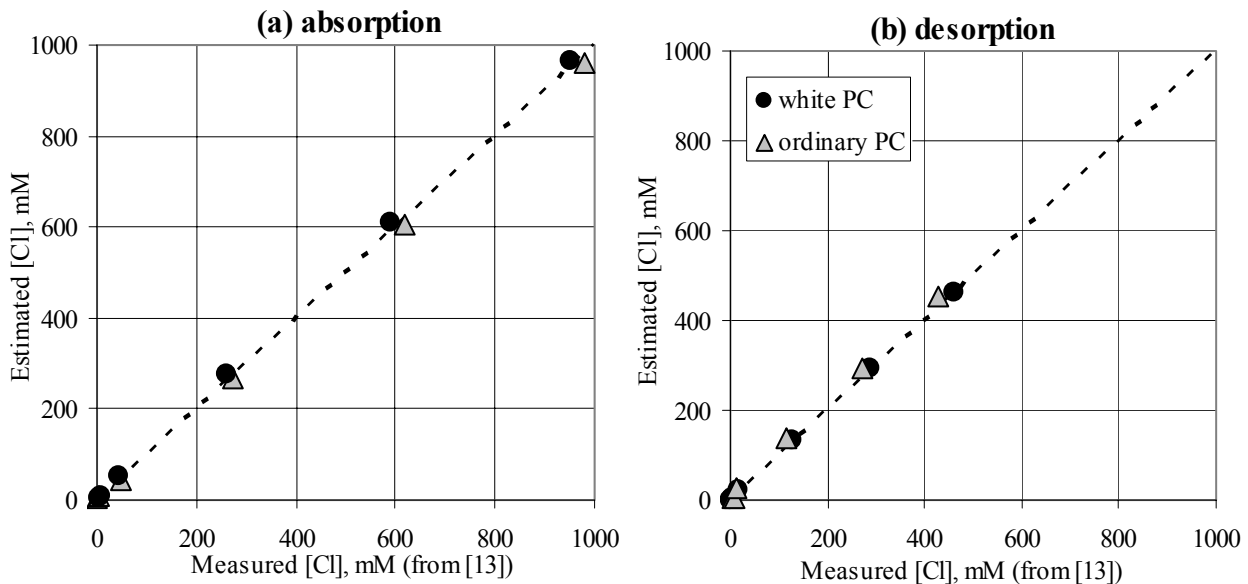
Fig. 2: Comparison of chloride concentrations calculated from the model in Table 1, and those measured in [13]; after chloride absorption (a) and chloride desorption (b).

The chloride isotherms for the white Portland cement, both for absorption and desorption, are plotted in Figure 3. It is a common observation elsewhere that the relative content of bound chloride, is higher after desorption than absorption. Some authors have suggested (e.g. [3]) that a significant portion of the chloride is bound to the high specific surface area of the C-S-H phase

by a process of physical adsorption, and that these forces are strong enough to fix the chloride ions to the surface of the C-S-H during leaching of chlorides.
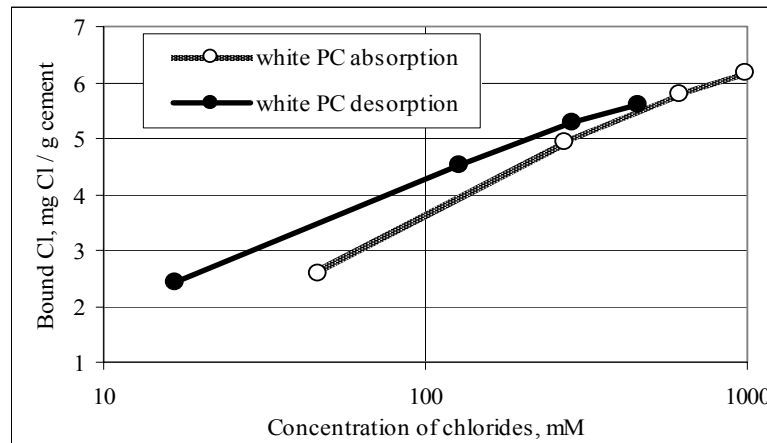
Fig. 3: Chloride binding isotherms for the white PC during absorption and desorption based on the data measured in [13].

After applying the model described in this paper it is clear that this explanation is unnecessary, and the desorption isotherm is purely a result of re-equilibration in response to a reduction in the alkali content of the system.

For reasons discussed elsewhere [8], there is considerable concern that the results obtained from pore expression analyses do not represent equilibrium conditions at normal temperature, pressure and water saturated conditions, and data obtained by this method is therefore not considered.

EFFECT OF ALKALI AND ALUMINA CONTENT ON CHLORIDE BINDING

The model can be used to calculate the effect of combined changes to the alkali and alumina contents on chloride binding. Figure 4.a shows the concentration of chloride in the pore solution in a white Portland cement paste with a w/c ratio of 0.45 (WPC(4) in Table 2) and a total content of chloride corresponding to 3.5 mg/g cement, as a function of the total content of Al_2O_3 and Na_2O_{eq} of the cement.
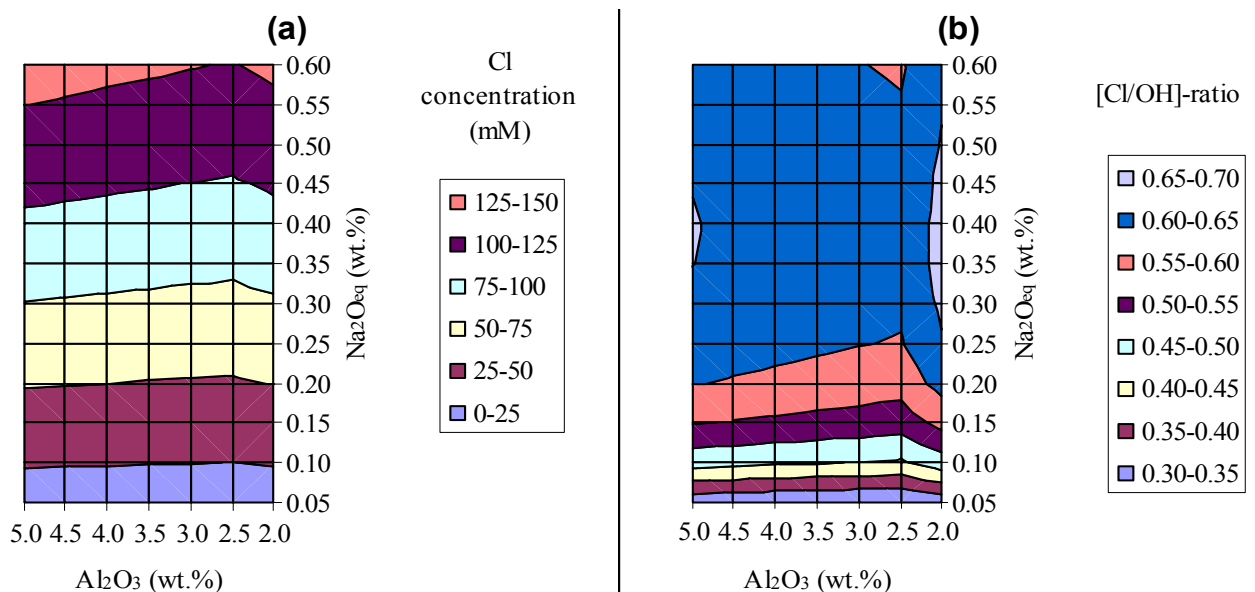
Fig. 4: Variation in chloride concentration (a) and ratio of chloride to hydroxyl ions (b) in the pore solution of a WPC(4) paste at w/p 0.45 with constant chloride content at 3.5 mg/g cement, as a function of Al_2O_3 and Na_2O_{eq} contents.

It is observed that the content of Al_2O_3 (5 % corresponds to 13% C_3A) in the cement does not significantly affect its binding capacity. This is largely due to the high binding capacity of the C-S-H, as shown in Table 1. The content of Na_2O_{eq} on the other hand has a very significant impact on the binding capacity. The higher the content of alkalis, the lower the chloride binding capacity.

The positive effect that lowering the alkali content has on the binding capacity of chlorides, however, must be evaluated in conjunction with the negative effect that the lower pH is known to have on the risk of corrosion. Figure 4.b shows the calculated [Cl/OH]-ratios in the pore solution of a paste corresponding to that shown in Figure 4.a. The reduction in the total Na_2O_{eq} content below 0.4% is seen to significantly reduce the [Cl/OH]-ratio and should therefore significantly reduce the risk of corrosion for a given total content of chloride.

POSSIBLE APPLICATIONS

Figure 5 shows chloride ingress profiles determined in 6 months pre-cured w/c 0.45 concretes exposed to a 16.5 % NaCl solution for 70 days at 20^oC. The cements are the same as those listed in Table 2.
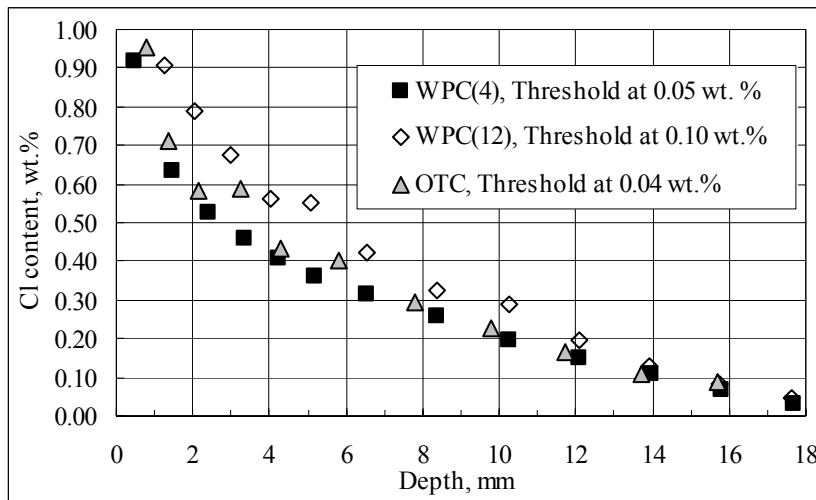
Fig. 5: Chloride ingress profiles and chloride threshold values, in 6 months old w/p 0.45 concretes exposed to 16.5 % NaCl solution for 70 days at 20^oC (cement content 333 kg/m^3).

The model can be used to calculate the threshold content of chloride by weight of the concrete for each cement type (see legends in Figure 5), assuming in this case that the critical [Cl/OH]-ratio for initiating corrosion is 0.6. For the results shown in Figure 4, the depth at which the threshold contents of chloride occur are 17 mm for both the WPC(4) and OPC cements and 14.4 mm for the WPC(12) cement.

Given that the composition of the pore solution can be calculated for any content of chloride and alkalis, the model can be included in so-called finite element models for chloride ingress (as in [15, 16]) of any Portland cement based system, at all time-steps, to accurately predict the rate determining concentration gradient in the pore solution. Figure 6 shows the calculated concentration profiles for chloride, alkalis, hydroxyl ions and calcium, corresponding to the ingress profiles in the OPC in concrete in Figure 5. It is assumed that the alkalis do not migrate (consistent with evidence from [17, 18] where the alkalis were observed to ingress at a very low rate), and therefore, the changes in alkali concentration in the pore solution result solely from the release of alkalis from the C-S-H due to binding of chloride. The lowest value for [OH$^-$] is 30 mM consistent with the equilibrium solubility of $Ca(OH)_2$ [2], and the assumption that depth at which $Ca(OH)_2$ is leached is much less than the depth of chloride ingress.
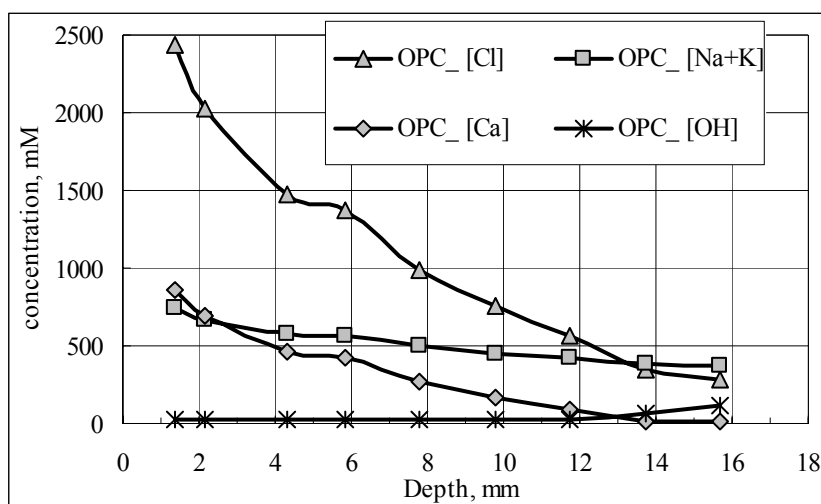
Fig. 6: Predicted composition of the pore solution in concrete OPC in Figure 4, after 70 days of exposure to 16.5 % NaCl solution.

CONCLUSION

The thermodynamic model for chloride binding in hydrated Portland cement described in [2] has been verified. The model shows excellent reproducibility and has been successfully applied to independent data in the literature.

The difference in chloride binding isotherms observed during absorption and desorption of chlorides are solely the result of leaching of alkalis, and are unrelated to strong surface adsorption forces of the C-S-H that has been proposed by other workers.

The alkali content of Portland cement has a much greater effect on chloride binding than its content of Al_2O_3.

Low alkali contents increase chloride binding, and lower the ratio of chloride to hydroxyl ions in the pore solution.

REFERENCES

1. Nielsen, E.P., Herfort, D. and Geiker, M.R. Phase equilibria of hydrated Portland cement. Submitted for publication in Cement and Concrete Research in june 2003.

2. Nielsen, E.P., Herfort, D. and Geiker, M.R. Chloride and alkali binding in Portland cement systems. Submitted for publication in Cement and Concrete Research in june 2003.

3. Jensen, O.M., Korzen, M.S.H., Jakobsen, H.J. and Skibsted, J. Influence of Cement Paste Constitution and Temperature on Chloride Binding in Cement Paste, Advances in Concrete Research **12** (2) (2000).

4. Birnin-Yauri, U.A. and Glasser, F.P. Friedel's salt, Ca2Al(OH)6(Cl,OH). 2H2O: Its solid solution and their role in chloride binding. Cement and Concrete Research **28** (12) (1998).

5. Yamato, T., Soeda, M. and Emoto, Y. Chemical resistance of concrete containing condensed silica fume. In: ACI Special Publication 114: Proceedings of the 3rd International Congress on fly ash, silica fume, slag, and natural pozzolans in concrete, Trondheim, 1989 (ACI, 19898) 897-913.

6. Lambert, P., Page, C.L. and Short, N.R. Pore solution chemistry of the hydrated system Tricalcium silicate/Sodium chloride/water. Cement and Concrete Research **15** (1985).

7. Nielsen, E.P., Herfort, D. and Geiker, M.R., Hooton, R.D. Effect of solid solution of AFm phases on chloride binding. In: Proceedings of the 11th International Congress on the Chemistry of Cement 11-16 May 2003 (Durban, South Africa).

8. Glass, G.K., Hassanein, N.M. and Buenfeld, N.R., Neural network modelling of chloride binding. Magazine of Concrete Research **49** (181) (1997), pp. 323-335.

9. Putnis, A. and McConnell, J.D.C. Principles of mineral behaviour. In: Geoscience Texts Vol.I, Blackwell Scientific Publications, 1980.

10. Taylor, H.F.W., Cement Chemistry, 2nd edition. (Thomas Telford Services Ltd., Great Britain, 1997).

11. Juel, I.A., Mineralogical and thermodynamic processes by sulfate and seawater attack in Danish concrete. Industrail Ph.D. thesis, EF-816-Durability, Geological Institute, University of Copenhagen, Denmark (2003).

12. Hong, S.-Y. and Glasser, F.P., Alkali binding in cement pastes. Part I. The C-S-H phase. Cement and Concrete Research **29** (1999), pp. 1893-1903.

13. Korzen, M.S.H. Chloride binding in cement paste (in Danish). Master Thesis at the Department of Civil Engineering, Technical University of Denmark, Lyngby, Denmark, 1998.

14. Saremi, M. and Mahallati, E., A study of chloride induced depassivation of mild steel in simulated concrete pore solution, Cement and Concrete Research (32),, 2002.

15. Marchand,J., Samson, E., Maltais, Y., Lee,R.J. and Sahu,S., Predicting the performance of concrete structures exposed to chemically aggressive environment-field validation, Materials and Structures **35**, pp. 623-631, 2002.

16. Truc, O., Prediction of Chloride Penetration into Saturated Concrete – Multi-Species Approach. Doctoral Thesis. Department Of Building Materials, Chalmers University of Technology, Göteborg, Sweden, 2000

17. Nielsen, E.P., Thrysøe, J., Herfort, D. and Geiker, M.R., Performance of white Portland cement in aggressive environment. Proceedings of the 7th International Conference of Concrete in Hot and Aggressive Environments. Bahrain, 13-15 October, 2003

18. Volkwein, A., Penetration of chlorides into concrete – Phenomena and consequences. Points of view based on 20 years research and site experience with deicing salts. Proceedings of the International RILEM workshop on Chloride penetration into concrete, St-Rémy-lès-Chevreuse, France, 1995.

Paper VII: Chloride diffusion in partially saturated cementitious material

Nielsen, E.P. and Geiker, M.R.

ABSTRACT

The paper proposes a combined application of composite theory and Powers' model for microstructural development for the prediction of the diffusion coefficient as a function of the moisture content of a defect free cementitious material. Measurements of chloride diffusion in mortar samples (440 kg/m^3 rapid hardening Portland cement, w/c=0.5, maturity min. 6 months) stored at 65 % and 85 % RH, as well as in vacuum saturated mortar samples, illustrate the applicability of the method.

INTRODUCTION

Durability aspects are increasingly determining for the design of reinforced concrete structures in aggressive environment, e.g. structures exposed to seawater or de-icing salts. Except in submerged parts of marine structures, concrete is rarely saturated when exposed to chlorides. Therefore, models for the ingress of chloride into partly saturated concrete are relevant for the service life design and reassessment of reinforced concrete structures.

Both capillary suction of chloride contaminated water and diffusion of chloride ions are likely transport mechanisms for chlorides in partly saturated concrete. Capillary suction will be dealt with in a separate paper.

An equation for the effect of relative humidity on the rate of diffusion of ions in cementitious materials has been proposed by Saetta et al. [1]. However, as the diffusion coefficient is expected to be dependent on the amount of moisture available for the diffusing substance, a model taking this parameter into account is expected to provide more accurate predictions. Such an approach is proposed in the present paper, where the diffusion coefficient is calculated by combining the composite theory with Powers' model for the development of the microstructure in cement paste. Jensen [2] has applied a similar approach for simulating the ingress in saturated cement paste and mortar. A similar approach has recently been applied to partly saturated cementitious materials, but without distinguishing between the rate of diffusion in the capillary and gel pores [3,4], which causes an overprediction of the diffusion coefficient at low degrees of moisture saturation.

In contrast to the proposed approach, existing models are semi-empirical and require extensive calibration.

The present paper is, with some modifications, based on recent studies of diffusion in partly and fully saturated cementitious material given in [5].

THEORY

Diffusion

Diffusion is the transport of ions caused by differences in concentration. Descriptions of the mechanism can be found elsewhere, e.g. [6,7]. For the calculations presented in the present paper two solutions to Fick's 2nd law of non-steady state diffusion are applied: the 'instant plane source' solution for an instantaneous limited supply of ions [8],

$$c(x,t) = \frac{m_{Cl}}{\sqrt{\pi Dt}} \exp\left(-\frac{x^2}{4Dt}\right)$$

(1)

and the commonly used error function solution for constant supply of diffusing substance [7],

$$c(x,t) = C_s - (C_s - C_i) \cdot erf \frac{x}{\sqrt{4 \cdot t \cdot D}} \tag{2}$$

where $c(x,t)$ is the total content of chlorides at a depth x and exposure time t, m_{Cl} is the total mass of diffusing ions, C_s is the chloride content at the surface, and C_i is the total background chloride content . D is the chloride ion diffusion coefficient of the porous material assuming no interaction between the ions and the material.

For service life design and re-design, D in Eq.1 and 2 is generally substituted by D_{app}, which is the 'apparent' diffusion coefficient fitted by the least sum of squares method and including the interaction of the ions with the solids.

Saetta et al. [1] have proposed that the diffusion coefficient of chloride ions at a given relative humidity, RH, relative to the diffusion coefficient at 100 % RH can be given as,

$$\left(1 + \frac{(1 - RH)^4}{(1 - RH_c)^4} \right)^{-1} \tag{3}$$

where RH_c is the RH at which $D(RH_c) = \frac{1}{2}D(100\ \%)$.

<u>Numerical modeling of chloride diffusion</u>

The following numerical solution to Fick's 2nd law of diffusion (see e.g. [2]) is adopted in the present paper,

$$c_f(x,t) = c_f(x,t-\Delta t) + D \frac{\Delta t}{(\Delta x)^2} \left[c_f(x-\Delta x, t-\Delta t) + c_f(x+\Delta x, t-\Delta t) - 2(c_f(x,t-\Delta t)) \right] \tag{4}$$

where $c_f(x,t)$ denotes the concentration of chlorides at the depth x from the surface at the exposure time t, and D is the chloride ion diffusion coefficient of the porous material assuming no interaction between the ions and the material.

The boundary conditions for the simulation can be adjusted for each time step, when the concentration of chloride ions in the environment as a function of time is known and, when the depths considered is high enough to ensure that the chloride concentration in the inner-most part of the sample remains unchanged during the exposure time.

To ensure stability of the numerical procedure, the Fourier steps should be maximum 0.5 (see e.g.[2]), thereby obeying the relation

$$0.5 < \frac{\Delta t \cdot D}{\Delta x^2} \tag{5}$$

A considerable amount of the chloride ions may become fixed in the hydrate phases through processes collectively referred to as binding. The mechanisms are still not fully described [9], but it is assumed that it is mainly the aluminum-bearing hydration products that react chemically with the chloride ions and form Friedel's salt or solid solutions, which include Friedel's salt [10].

The binding process is normally quantified by measuring the amount of bound chlorides in equilibrium with a chloride-containing exposure solution, for increasing concentrations of chlorides. The results are commonly expressed by means of the so-called Freundlich or Langmuir isotherms [2,9], depending on which provides the best correlation to the data. Considering the Freundlich isotherm, the equilibrium between bound, c_b [mg Cl/ g-gel], and free chloride ions, c_f [mol Cl/l pore solution] is expressed by,

$$c_b = \alpha \cdot c_f^{\beta} \tag{6}$$

where α and β are constants (regression parameters) with no physical meaning. When the binding capacity becomes exhausted, any further addition of chlorides will result in an increase in the concentration of free chlorides in the pore solution.

There is no clear information available on whether binding is an instantaneous process or if a binding rate should be introduced. Instantaneous binding is easy to compute as quasi-instantaneous by for each time increment recalculating the binding equilibrium at each depth. Following this procedure, Jensen [2] found satisfying correlation between measured and calculated chloride profiles in cement pastes. Therefore, instantaneous binding is assumed for the later calculations.

<u>Chloride diffusivity in cementitious materials</u>

Powers and Brownyard [11] carried out a thorough investigation on, among others, the porosity of Portland cement systems. The so-called Power's model (due to this authors later work) provides an approximation of the volume fraction of the different phases (characterised as cement, capillary (free) water, gel solid, gel water, and capillary water from chemical shrinkage, i.e. empty or refilled capillary pores) that constitute the cement paste throughout the hydration process.

Before presenting the model, two constants, which are characteristic of the cement paste examined, are calculated: $k=0.23(C_3S)+0.32(C_2S)+0.32(C_3A)+0.37(C_4AF)$, and the initial porosity, $p = (w/c)/(w/c + \rho_w/\rho_c)$, where w/c is the water-to-cement ratio, and ρ_w and ρ_c are the density of water and cement. For a cement paste composed of the investigated rapid hardening Portland cement (Bogue composition $C_3S=50$ %, $C_2S=24$ %, $C_3A=7$ %, and $C_4AF=11$ %) with $w/c=0.50$, k and p become 0.26 and 0.61, respectively.

According to [11], the total volume of gel water in a cement paste can be calculated from $0.9 \cdot n_l \cdot k \cdot w_n$, where n_l is the number of monolayers of water that are physically adsorbed to the gel solid, and w_n is the loss of ignition for the given paste at the actual degree of hydration. According to [12], the fourth monolayer can be regarded as free water, i.e. capillary water, i.e. $n_l=3$. Hence, the volume fraction of gel water, V_{gw}, as a function of the degree of hydration (loss of ignition of approx. 22 % at 100 % hydration, predicted from [13,14]) in a Portland cement paste with the clinker composition mentioned above, can be written as,

$$V_{gw} = 0.48 \cdot (1 - p)\alpha \tag{7}$$

where α is the degree of hydration, ranging from 0 to 1.

The volume fraction of empty or refilled capillary pores generated by the chemical shrinkage, V_{cs}, is according to [12] given by following equation,

$$V_{cs} = 0.2 \cdot (1 - p)\alpha \tag{8}$$

Power's and Brownyard [11,15] found that the volume of capillary water unconsumed during hydration was $w_o-0.75\cdot(1+3\cdot k)\cdot w_n$, where w_o is the initial amount of water in the system. The volume fraction of capillary water, V_{cw}, in a paste of the actual cement can be expressed

$$V_{cw} = p - 1.14 \cdot (1 - p)\alpha \tag{9}$$

The volume fraction of the unreacted cement, V_{ce}, at a certain degree of hydration can be calculated as,

$$V_{ce} = (1 - p)(1 - \alpha) \tag{10}$$

The volume fraction of solid products of reaction, V_{gs}, can be calculated by subtracting Eq.7, 8, 9, and 10 from 1.0, i.e.

$$V_{gs} = 1.46(1 - p)\alpha \tag{11}$$

In cement paste, diffusion through both the solid gel products and the unhydrated cement is essentially nonexistent. Transport can, therefore, only take place through the pore system of the paste. The volume fraction of the pore system in a paste (the capillary porosity, $V_{cw}+V_{cs}$, and gel porosity, V_{gw}) at a given degree of hydration can be described according to the equations listed above.

Powers and Brownyard [11] concluded that 'capillary water does not exist at pressures below about $0.45 \cdot p_s$', where p_s is the saturated vapor pressure, as well as that 'at vapour pressures greater than $0.45 \cdot p_s$ and less that p_s, the capillary water is present'. Based on that, it will be assumed in the present paper that there exists a threshold vapour pressure (i.e $0.45 \cdot p_s$) where all gel pores are water-filled, and all capillary pores are empty. This assumption has been validated by comparing values calculated by Eq.7, 8, and 9 with a measured desorption isotherm of a 5 years old w/c=0.45 rapid hardening Portland cement paste [16] (similar clinker composition as the used for the present experiments). The moisture content of that paste in equilibrium with $0.45 \cdot p_s$ was 15 wt. %, while the gel water content calculated according to Eq.7 was 17 wt. % of the sample.

Jensen [2] has, based on an equation proposed by Maxwell for the diffusion coefficient of a composite, applied the following equation for the diffusion coefficient of the gel matrix (i.e. $V_{gs}+V_{gw}+V_{ce}$), D_{gm}. It is assumed that the cement and calcium hydroxide exist as inclusions in the so-called gel proper, V_{gp} (i.e. $V_{gs}+V_{gw}-V_{CH}$),

$$D_{gm} = D_{gp} \frac{V_{gp}}{V_{gp} + \frac{3}{2}(V_{ce}+V_{CH})} \tag{12}$$

where D_{gp} is the diffusion coefficient of the gel proper. V_{CH} can be predicted from the reactions taking place and the degree of hydration. As mentioned in [2], Garboczi has proposed the following value for the diffusion coefficient of chloride ions $D_{gp}= 4.6 \cdot 10^{-12}$ m^2/s, corresponding to 1/400 of the diffusion coefficient through water-filled capillaries, $D_{cw}=1.81 \cdot 10^{-9}$ m^2/s.

Assuming phase symmetric crumbled foil composites, Nielsen [17] proposed the following equation for the diffusion coefficient through the cement paste, D_p,

$$D_p = D_{gm} \frac{n + 2\sqrt{n} \cdot (1 + c \cdot (n-1))}{n + 2\sqrt{n} - c \cdot (n-1)} \tag{13}$$

where $n=D_{cw}/D_{gm}$, and $c= V_{cw}+V_{cs}$.

Finally, if the aggregates are impermeable, the diffusion coefficient, D, through a mortar or concrete can be predicted by the following equation proposed by Maxwell (e.g. in [2]),

$$D = D_p \frac{1}{1+\phi/2}(1-\phi) \tag{14}$$

where ϕ is the volume fraction of aggregates and air.

MATERIALS AND EXPERIMENTS

A mortar with w/c ratio of 0.5 was selected for the experiments. The mix composition is given in Table 1. The cement used was rapid hardening Portland cement with the clinker composition mentioned in section 2.3.

Table 1: Mix composition of the mortar (dry density 2075 [kg/m^3])

Component	Unit	Amount
Rapid hardening portland cement	kg/m^3	440
Water	kg/m^3	220
Sand (0-4 mm)	kg/m^3	1575
Air content	vol. %	4

Beams (300·100·100 mm^3) were cast and stored for one day at 20 ^{0}C in moulds. After demoulding the beams were cured in saturated lime curing tanks at 20 ^{0}C for 4 days and subsequently at 50 ± 4 ^{0}C until a maturity of 4.6 months was achieved. The maturity is the equivalent age at 20 ^{o}C, based on the maturity function given in [18] and activation energy at 33,500 J/mole.

At 4.6 maturity months the beams were conditioned at 65 ± 2 % RH (22.5 ± 1 ^{0}C) for 20 days, when approx. 85 % RH was measured in the centre of the samples. Some beams were then transferred to 85 ± 1 % RH (20 ^{0}C), while others were left at 65 % RH.

At a maturity of approx. 6 months, the beams were cut or split (see dimensions below) and conditioned to 65 % and 85 % RH until constant weight.

The moisture content was determined for the different conditionings applied, see Table 2. Due to the applied conditioning procedures, the equilibrium of the samples conditioned at 65 % RH was achieved by desorption, whilst the equilibrium of the samples conditioned at 85 % RH was reached by desorption at the centre, but absorption at the surface. Absorption and desorption curves in the range from 65 to 95% RH indicated negligible hysteresis for the examined material, why any effect of such phenomenon has been disregarded in the present paper.

Table 2: Moisture content

Conditioning	Moisture content [mass%]	Degree of saturation [%]	
		Capillary	Vacuum
65 % RH	4.9	66.2	53.8
85 % RH	5.4	73.0	59.4
Capillary saturation	7.4	100	81.3
Vacuum saturation	9.1		100

All experiments were carried out on samples more than six maturity-months old. At this age the influence of changes in the maturity of the paste on the diffusion properties is assumed to be negligible [7]. The degree of hydration is predicted to be 80-85 % based on data presented in [19] from the development of non-evaporable water in RPC-pastes and a maximum non-evaporable water content at 22 % for the actual cement predicted according to [13, 14].

Chloride diffusion in partly saturated mortar was measured on four samples. The near surface region of two times two samples (70·100·100 mm^3) conditioned at 65 % and 85 % RH, respectively, was contaminated by chlorides and subsequently returned to the conditioning rooms for 60 days. The chloride contamination was obtained by immersion of the samples in a 26 mass % NaCl solution for two hours followed by drying the surface with a hair drier (avoiding excessive heating) until the samples reached the weight prior to chloride exposure. Chloride profiles were determined 4 days after immersion and revealed background concentration at 5 mm or less.

The chloride diffusion in saturated mortar was measured on two samples (60·100·100 mm^3), which originally were conditioned at 85 % RH and subsequently vacuum saturated and left for three days in tap water before being submerged in a 3 mass % NaCl solution for 30 days.

The chloride profiles were determined by profile grinding in 2 mm steps and potentiometric titration of the powder samples. Prior to titration, the samples were prepared according to the NT Build 208 method [7], except that the powder was not sieved, and the amount of HNO_3 was reduced to 5 ml (enough to reduce the pH to 1).

RESULTS AND DISCUSSION

Chloride profiles in samples preconditioned and stored for 60 days at 65 and 85 % RH after a limited exposure to chlorides, are given in Fig.1 and 2 (circles). Fig.3 illustrates the chloride profile obtained in a vacuum saturated mortar after 30 days of exposure to a 3 wt. % NaCl solution (circles). By fitting Eq.1 to the two first mentioned profiles, and Eq.2 to the last (dotted curves), the apparent diffusion coefficients, D_{app}, given in Table 3 are obtained. The best fit was obtained by the least sum of squares method.
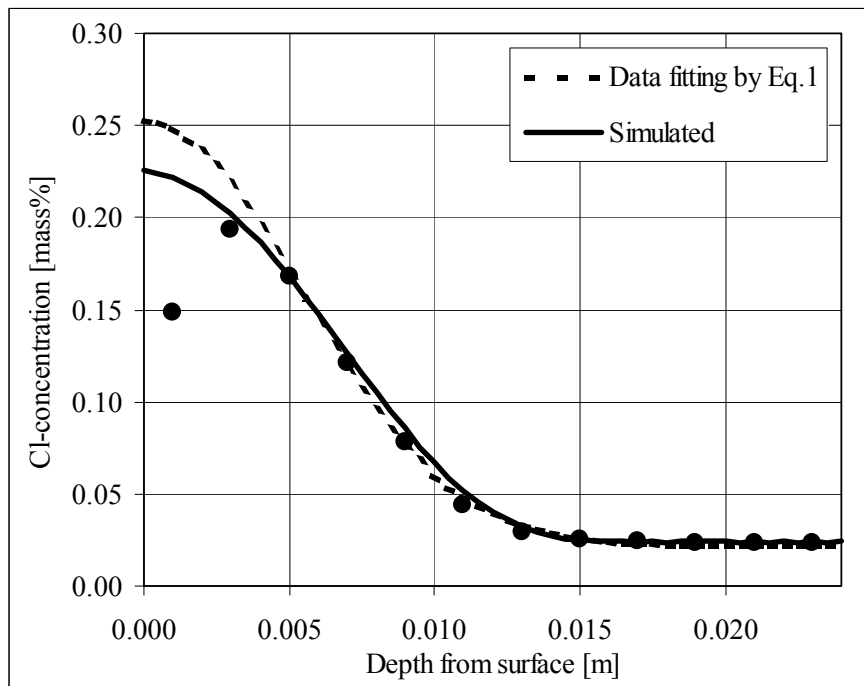
Figure 1: Chloride profile (circles) after 60 days of exposure for a limited supply of ions. Degree of vacuum saturation 0.53. Dotted curve: best fit by Eq.1 with $D_{app} = 2.7 \cdot 10^{-12}$ m^2/s and $m_{Cl} = 1.53$ g. Straight curve: simulated ingress by the numerical procedure with $D = 5.5 \cdot 10^{-12}$ m^2/s, calculated with the suggested approach (Eq.7-14).
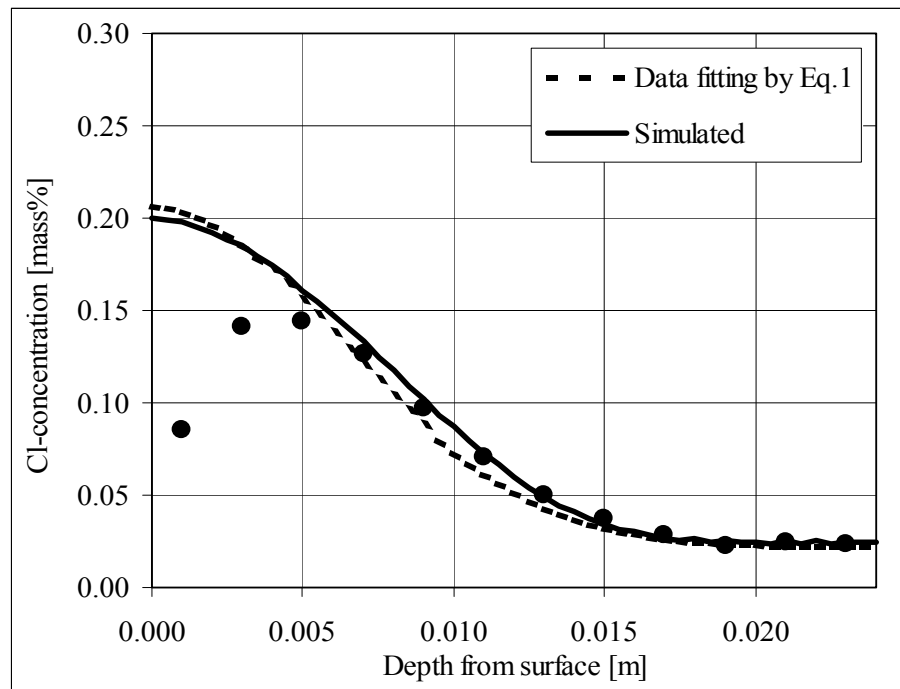
Figure 2: Chloride profile (circles) after 60 days of exposure for a limited supply of ions. Degree of vacuum saturation 0.60. Dotted curve: best fit by Eq.1 with $D_{app} = 3.8 \cdot 10^{-12}$ m^2/s and $m_{Cl} = 1.45$ g. Straight curve: simulated ingress by the numerical procedure with $D = 7.9 \cdot 10^{-12}$ m^2/s, calculated with the suggested approach (Eq.7-14).
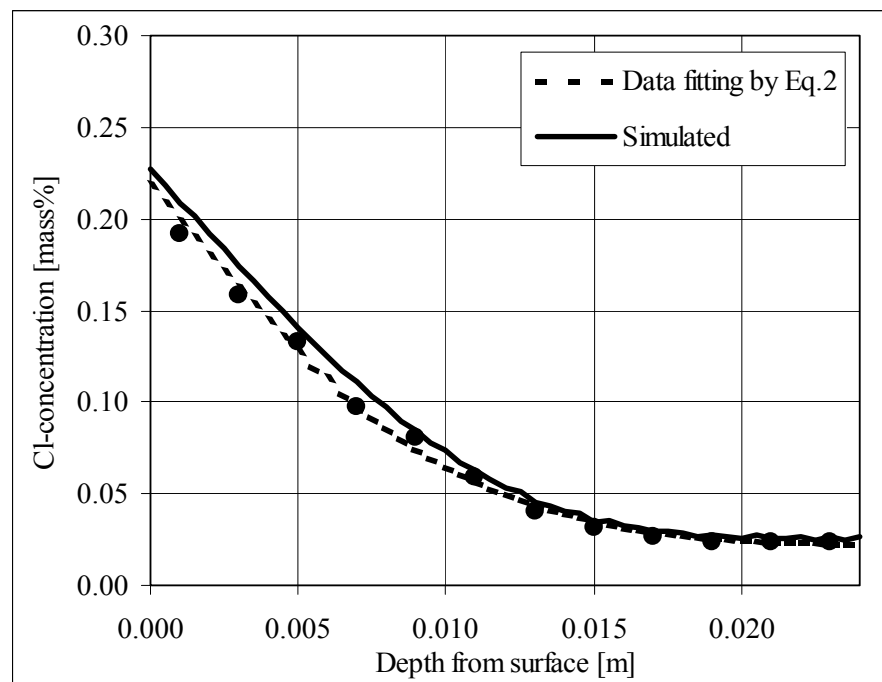
Figure 3: Chloride profile (circles) after 30 days of exposure to a 3% NaCl solution. Degree of vacuum saturation 1.0. Dotted curve: best fit by Eq.2 with $D_{app} = 12.9 \cdot 10^{-12}$ m^2/s and $C_s = 0.218$ wt. %. Straight curve: simulated ingress by the numerical procedure with $D = 20.2 \cdot 10^{-12}$ m^2/s, calculated with the suggested approach (Eq.7-14).

Table 3: Exposure conditions, apparent diffusion coefficients, D_{app}, determined from experiments and simulated diffusion coefficients, $D_{simulated}$, using the proposed approach

Conditioning	Exposure	D_{app} [m²/s]·10^{12}	$D_{simulated}$ [m²/s]·10^{12}
65 % RH	26.4 % NaCl for 2h followed by drying and 65 % RH	2.7	5.5
85 % RH	26.4 % NaCl for 2h followed by drying and 85 % RH	3.8	7.9
Vacuum-saturation	Immersed in 3 % NaCl	12.9	20.2

The applicability of Eq.3 is illustrated in Fig.4. The calculations are carried out by applying Eq.3 to the apparent diffusion coefficients (D_{app} in Table 2) and fitting by the least sum of squares method in order to find the best value for RH_c. Eq.3 appears to underestimate the transport by factor of approx. 5-10 on the diffusion coefficients at 65 % RH. The fit would become slightly poorer if the diffusion coefficient at 100 % RH was lower, as expected if the diffusion coefficient for 100 % capillary saturation (81% vacuum saturation, according to Table 2) was applied.
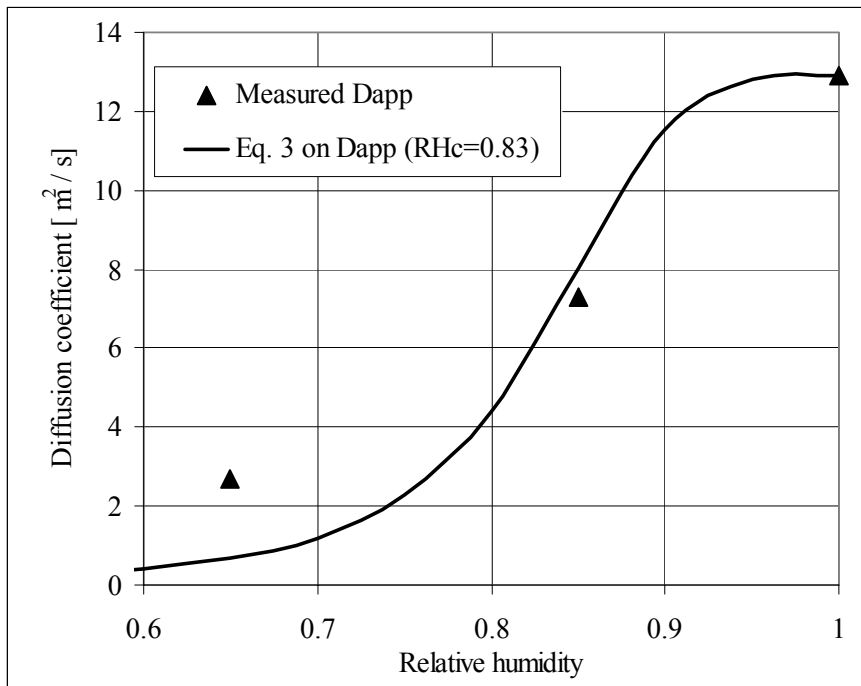
Figure 4: Application of Eq. 3 on apparent diffusion coefficients, with RH_c selected in order to offer the best fit by the method of least sum of squares. Y-axis denotes the diffusion coefficient independent of type, and the x-axis denotes the relative humidity of the sample.

The composite theory has been applied on volume fractions predicted by Powers' model (see Section 2.3) to derive the dependency of the diffusion coefficients on the degree of vacuum saturation of the material. It is assumed that 100 % vacuum-saturation is the degree of saturation at which all of the capillary pores are water-filled. Furthermore, it is assumed that air voids remain empty.

The degree of saturation where only gel water exists is assumed to be 45 % vacuum saturation, see Section 2.3, i.e. $V_{gw}=0.45 \cdot (V_{cw}+V_{cs}+V_{gw})$. The assumption is supported by extrapolation of desorption isotherms for the investigated mortar measured in the range from 100 to 65 % RH.

Based on the above, the predicted amount of water in the capillary pores of the actual material varies linearly from 0 to 0.30 cm^3/cm^3 ($V_{cs}+V_{cw}$, calculated from Eq.7 and 8) in the range from 45 to 100 % vacuum saturation.

Following the procedure described in section 2.3, the effective diffusion coefficient of the examined mortar is calculated to $5.5 \cdot 10^{-12}$, $7.9 \cdot 10^{-12}$ and $20.2 \cdot 10^{-12}$ [m^2/s] (see Table 2) for degrees of vacuum saturation at 0.54, 0.60 and 1.0.

The chloride adsorption isotherm for a rapid hardening Portland cement paste is given in [9]. α and β in Eq.6 are determined to 7.036 and 0.499 by fitting by the least sum of squares method. The maximum binding capacity of the cement paste is 6.8 mg Cl/g-gel (deduced from [9]).

The ingress curves in Fig.1, 2, and 3 are obtained (i.e. straight curves) when using the numerical routine in Section 2.2 and the approach defined previously for predicting the diffusion coefficients at different degrees of saturation. For the simulations in Fig.1 and 2 it is assumed that the total chloride in the sample is distributed within the outermost 2 mm at time 0.

The correlation between the simulated ingress in partly saturated material, according to the suggested approach and the measured profiles supports the application of the approach.

By the proposed approach, the dependency of the diffusion coefficient on the degree of saturation can be predicted for any cementitious material if Powers' model for the phase composition in the paste is applicable for the cementitious materials used, and the degree of hydration can be determined.

CONCLUSION

An application of the composite theory on volume fractions of the microstructural phases predicted by Powers' model for deriving the dependency of the diffusion coefficients on the degree of saturation has been proposed. The approach is based on the assumption that diffusion in porous material is dependent on the moisture content. Initial experimental verification shows agreement between measured and simulated chloride profiles in mortar samples (rapid hardening Portland cement, w/c = 0.5) conditioned at 65 and 85 % RH, and vacuum saturated. The model takes into account the composition and degree of hydration of the actual cementitious material.

ACKNOWLEDGEMENTS

REFERENCES

[1]   A. V. Saetta, R. V. Scotta and R. V. Vitaliani, Analysis of Chloride Diffusion into Partially Saturated Concrete. ACI Materials Journal 90 (M47) (1993), pp. 441-451.

[2]   O. M. Jensen, Chloride Ingress in Cement Paste and Mortar measured by Electron Probe Micro Analysis. Dept. of Civil Engineering. Technical University of Denmark. Series R No.51, Lyngby 1999.

[3]   T. Ishida, An integrated computational system of mass/energy generation, transport and mechanics of materials and structures, PhD thesis, University of Tokyo, 1999 (in Japanese), referred to in [4].

[4]   K. Maekawa and T. Ishida, Service life evaluation and durability design system for self-compacting concrete. In Proceedings of 2nd International Symposium on self-compacting concrete. Edt. by K. Ozawa and M. Ouchi. Tokyo, 2001.

[5]   E. P. Nielsen, Transport Mechanisms in Cementitious Materials, MSc thesis at the Dept. of Civil Engineering, Technical University of Denmark, Lyngby, 2001.

[6]   J. Kropp, H. K. Hilsdorf, H. Grube, C. Andrade and L-O. Nilsson, Transport Mechanism and Definitions. Chapter 2 in RILEM report 12: Performance Criteria for Concrete Durability. T.J.Press Ltd. UK, 1995.

[7]   L.-O. Nilsson, E. Poulsen, P. Sandberg, H. E. Sørensen, O. Klinghoffer and J. M. Frederiksen, Chloride Penetration into Concrete, State of the Art. Transport Processes, Corrosion Initiation, Test Methods and Prediction Models. HETEK Report No.53. Road Directorate, 1996.

[8]   M. A. Climent, G. de Vera, J. López, C. García and C. Andrade, Transport of Chlorides through non-saturated Concrete after an Initial Limited Chloride Supply. 2nd. Int RILEM, Workshop on "Testing and Modelling the Chloride Ingress into Concrete". Paris, 11-12 September 2000.

[9]   O. M. Jensen, M. S. H. Korzen, H. J. Jakobsen and J. Skibsted, Influence of Cement Constitution and Temperature on Chloride Binding in Cement Paste. Advances in Concrete Research 12 (2) (2000).

[10]   U. A. Birnin-Yauri and F. P. Glasser, Friedel's salt, $Ca_2Al(OH)_6(Cl,OH).2H_2O$: Its solid solution and their role in chloride binding. Cem Concr Res 28 (12) (1998).

[11]   T. C. Powers and T. L. Brownyard, Studies of the Physical Properties of Hardened Portland Cement Paste. Journal of the ACI 18 (8) Part 9 (1947).

[12]   P. F. Hansen, Hærdeteknologi-1. Portlandcement, Aalborg Portland & BKF-centralen, 1978

[13]   H. F. W. Taylor, Cement Chemistry, 2nd edition. Thomas Telford Services Ltd., London, 1997.

[14]   F. M. Lea, The chemistry of cement and concrete, 3rd edition. Edward Arnold Ltd. Press, 1970

[15]   T. C. Powers, The Non-Evaporable Water Content of Hardened Portland-Cement Paste – Its Significance for Concrete Research and Its Method of Determination, Research Laboratories of the Portland Cement Association, PCA, Bulletin 29, Chicago 1949.

[16]   A.M. Kjeldsen and P.V. Nygaard, Udtørring af betongulve (Drying of concrete floors). Mid-term project at the Department of Civil Engineering, Technical University of Denmark, 2000.

[17]   L. Fuglsang-Nielsen, Composite materials- mechanical and physical behaviour as influenced by phase geometry. Dep. of Civil Engineering, Technical University of Denmark, expected to 2002.

[18]   CEB-Design guide: Durable Concrete Structures. Task Group 20: Durability and Service Life of Concrete. Thomas Telford Services Ltd., 1992

[19]   G. Verbeck, Energetics of the Hydration of Portland Cement. Proceedings of the Fourth International Symposium on Chemistry of Hydration of Portland Cement in Washington (Paper IV-3). U.S. Department of Commerce, 1960.

Appendix B: Materials

The materials used for the experiments in the present work are listed in the following.

<u>Low-aluminate White Portland cement (abbreviated as WPC(4))</u>

This ASTM Type V Portland cement is produced at the Aalborg Portland A/S plant in Denmark. The chemical composition of the batch used is presented in the following table.

SiO_2	Al_2O_3	Fe_2O_3	CaO	MgO	SO_3	K_2O	Na_2O	Na_2O_{eq}	Cl
24.83	1.87	0.33	68.86	0.52	2.2	0.11	0.16	0.232	0.002

Relevant physical properties:
   Blaine Fineness: 370 m^2/kg
   Density: 3170 kg/m^3
   Loss of ignition   0.67 %
   CO_2-content   0.14 %

The Bogue composition of the cement is the following.

	C_3S	C_2S	C_3A	C_4AF	$CaSO_4.2H_2O$	Free CaO
Excl. free CaO	72.2	16.8	4.4	1.0	3.7	---
Incl. free CaO	62.1	24.4	4.4	1.0	3.7	2.49

Characteristic strength development (EN-196)

	1 day	2 days	7 days	28 days
Strength, MPa	18.2	30.8	52.3	71.6

<u>High-aluminate White Portland cement (abbreviated as WPC(12))</u>

This ASTM Type I Portland cement is produced at the Aalborg White Asia plant in Malaysia. The chemical composition of the batch used is presented in the following table.

SiO_2	Al_2O_3	Fe_2O_3	CaO	MgO	SO_3	K_2O	Na_2O	Na_2O_{eq}	Cl
23.57	4.49	0.21	65.88	0.97	2.38	0.2	0.03	0.162	0.005

Relevant physical properties:
   Blaine Fineness: 400 m^2/kg
   Density: 3150 kg/m^3
   Loss of ignition   2.3   %
   CO_2-content   0.72 %

The Bogue composition of the cement is the following.

	C_3S	C_2S	C_3A	C_4AF	$CaSO_4.2H_2O$	Free CaO
Excl. free CaO	51.7	28.6	11.5	0.6	4.0	---
Incl. free CaO	41.2	36.6	11.5	0.6	4.0	2.6

Characteristic strength development (EN-196)

	1 day	2 days	7 days	28 days
Strength, MPa	12.0	23.9	44.9	66.1

<u>Ordinary Portland cement (abbreviated as OPC)</u>

This ASTM Type II Portland cement is produced at the Aalborg Portland A/S plant in Denmark. The chemical composition of the batch used is presented in the following table.

SiO_2	Al_2O_3	Fe_2O_3	CaO	MgO	SO_3	K_2O	Na_2O	Na_2O_{eq}	Cl
20.96	4.9	3.64	65.12	0.89	3	0.41	0.3	0.57	0.011

Relevant physical properties:
   Blaine Fineness: 380 m^2/kg
   Density: 3190 kg/m^3
   Loss of ignition   0.57 %
   CO_2-content   0.08 %

The Bogue composition of the cement is the following.

	C$_3$S	C$_2$S	C$_3$A	C$_4$AF	CaSO$_4$.2H$_2$O	Free CaO
Excl. free CaO	59.1	15.6	6.8	11.1	5.1	---
Incl. free CaO	52.9	20.3	6.8	11.1	5.1	1.51

Characteristic strength development (EN-196)

	1 day	2 days	7 days	28 days
Strength, MPa	17.0	27.5	46.7	66.7

Sulfate Resisting Portland cement (abbreviated as SRPC)

This ASTM Type V Portland cement is produced at the Aalborg Portland A/S plant in Denmark. The chemical composition of the batch used is presented in the following table.

SiO$_2$	Al$_2$O$_3$	Fe$_2$O$_3$	CaO	MgO	SO$_3$	K$_2$O	Na$_2$O	Na$_2$O$_{eq}$	Cl
24.23	2.92	2.30	66.52	0.75	2.06	0.15	0.24	0.34	0.003

Relevant physical properties:

    Blaine Fineness: 341 m^2/kg

    Density: 3190 kg/m^3

    Loss of ignition 0.54 %

    CO$_2$-content 0.11 %

The Bogue composition of the cement is the following.

	C$_3$S	C$_2$S	C$_3$A	C$_4$AF	CaSO$_4$.2H$_2$O	Free CaO
Excl. free CaO	57.8	26.0	3.9	7.0	3.5	---
Incl. free CaO	52.8	29.8	3.9	7.0	3.5	1.24

Characteristic strength development (EN-196)

	1 day	2 days	7 days	28 days
Strength, MPa	9.1	17.4	35.2	57.2

High alumina granulated blastfurnace slag

Finely ground Norwegian granulated blastfurnace slag from NESC. The chemical composition of the batch used is

SiO$_2$	Al$_2$O$_3$	Fe$_2$O$_3$	CaO	MgO	SO$_3$	K$_2$O	Na$_2$O	Na$_2$O$_{eq}$	Cl
34.24	12.34	0.50	40.97	7.57	2.23	0.33	0.26	0.48	0.067

Physical properties of interest are:

    Blaine Fineness: 1300 m^2/kg

    Density: 2960 kg/m^3

    Loss of ignition 0.54 %

    CO$_2$-content 1.33 %

White silica fume

White silica fume from ELKEM. The chemical composition of the batch used is presented in the following table.

SiO$_2$	Al$_2$O$_3$	Fe$_2$O$_3$	CaO	MgO	SO$_3$	K$_2$O	Na$_2$O	Na$_2$O$_{eq}$	Cl
95.91	0.15	0.12	0.17	0.10	0.20	0.07	0.26	0.31	---

Physical properties of interest are:

    Density: 2250 kg/m^3

    Loss of ignition 0.60 %

Calcite

Fine graded calcite from drying of chalk slurry from the Aalborg Portland A/S plant. The chemical composition of the batch used is presented in the following table.

SiO$_2$	Al$_2$O$_3$	Fe$_2$O$_3$	CaO	MgO	SO$_3$	K$_2$O	Na$_2$O	Na$_2$O$_{eq}$	Cl
3.52	0.42	0.18	52.89	0.40	0.07	0.07	0.06	0.11	0.008

Physical properties of interest are:

Blaine fineness   1300 m^2/kg
Density: 2739 kg/m^3
CO_2-content   41.71%

Sand

Quartz-sand with three different grading curves were combined for the preparation of mortars and concretes. The particle size data, as well as density and absorption is presented in the following table (according to DS 405.9).

Sieve, [mm] Sand id.	4.0	2.0	1.0	0.5	0.25	0.125	0.075	Dry density [kg/m^3]	Absorption %
'0 – 2 mm'	100.0	98.4	88.8	48.1	11.2	3.5	0.8	2621	0.50
'0.25 – 1 mm'	100.0	100.0	100.0	80.0	0.0	0.0	0.0	2621	0.37
'1 – 4 mm'	100.0	44.0	1.0	0.0	0.0	0.0	0.0	2596	0.80

Stone

Granite stone with two different grading curves were combined for the preparation of the concretes. The particle size data, as well as density and absorption, is presented in the following table (according to DS 405.9).

Sieve, [mm] Stone id.	16.0	8.0	4.0	2.0	1.0	0.5	0.25	0.125	0.075	Dry dens. [kg/m^3]	Absorp. %
'2 – 8 mm'	100.0	95.5	33.1	6.8	4.3	3.6	3.2	2.8	2.2	2619	0.69
'8 – 16 mm'	88.6	12.4	4.5	4.5	4.5	4.5	4.5	4.5	4.5	2608	0.61

Appendix C: Experimental procedures

<u>'Phase equilibria'</u>

This chapter describes the experimental procedure adopted to examine the phase equilibria in hydrated Portland cement pastes. The results are presented in **Appendix E** and **F**.

Mixing, casting and curing

Cement pastes of w/p 0.70 with 1 mass % replacement of powder by calcite were prepared according to the following mix (amounts are given in gram). The water used was de-aired, de-mineralized water.

Paste id.	Cementtype	Cement	Calcite	Silica fume	Slag	Water
WPC(4)	WPC(4)	594.0	6.0	---	---	420.0
WPC(12)	WPC(12)	594.0	6.0	---	---	420.0
OPC	OPC	594.0	6.0	---	---	420.0
WPC(4)_10%SF	WPC(4)	534.6	6.0	59.4	---	420.0
WPC(4)_30%SL	WPC(4)	415.8	6.0	---	178.2	420.0
OPC_30%SL	OPC	415.8	6.0	---	178.2	420.0

The powder was mixed for 5 minutes in a Hobart mixing machine before addition of one third of the water and mixing for 3 minutes, followed by a further 3 minutes mixing with the remaining water. The pastes were cast in 2 cm^3 centrifuge tubes, sealed, slowly rotated for two days to avoid bleeding, and stored at 20°C for one month.

Exposure

After 1 month of curing the samples were de-molded, crushed to 2-4 mm in size, weighed (to approximately 8.3 g) and placed in 12.5 ml. solution for 5 months at 20°C. For each paste, the samples were stored in solutions of different $CaCl_2$ concentrations, resulting in different degrees of binding (note that a different specimen was used in each case) at constant alkali content. WPC(4) was stored at sodium contents of both 250 and 550 mM Na^+ (by addition of NaOH to the initial solution), whilst the OPC specimens were stored in solutions of 550 mM Na, and the WPC(12) specimens in 250 mM Na^+.

During exposure, the specimens were kept in desiccators evacuated from air and refilled with N_2 (pressure in equilibrium with atmospheric air), in order to avoid carbonation through diffusion of CO_2 through the plastic. The plastic containers were not completely tight which is why the amount of exposure solution after exposure varies from the 12.5 ml initially supplied. The resulting amount of exposure solution was used for all calculations regarding phase equilibria.

Five months was ample time for the cement to achieve a degree of hydration at which metastable conditions are safely assumed to apply, and fully equilibrate with the solution, which, making allowance for the dilution of alkalis can be regarded as pore solution.

Some additional samples were exposed to solutions of varying contents of $MgSO_4$ and NaCl, in order to examine the phase equilibria in sulfate-exposed pastes and the effect on chloride binding.

The composition of each exposure solution before and after exposure is listed in the tables of **appendix E** and **F**.

Analyses

The specimens were examined randomly over a period of 3-4 months in order to avoid temporary systematic errors during the analyses in the laboratories.

The hydrated phases were examined by EDS (Energy Dispersive Spectroscopy, at 15 keV, 25 μA and analysis time of 40 s. per point) analysis on carbon-coated polished sections. The elements included were Ca, Si, Al, S, Fe, Cl, Na, K, Mg, Zn and P. A total amount of 900 randomly chosen points were analyzed on the WPC(4) and 1100 on WPC(4)_10%SF pastes because of the low content of aluminate and sulfate reducing the chance of detecting AFm and

AFt phases, whilst 300 points for the remaining pastes. The name of the data files for each paste is given on the tables in **appendix E** and **F**.

The calculated normalized weight percentage of each element was not used during the interpretation of the results, as these are dependent on the total amount of material analyzed and the number of elements the material is assumed to consist of. The molar ratio between the elements was used instead, avoiding thereby unnecessary sources of error. The technique is schematized in **Figure C.1**.
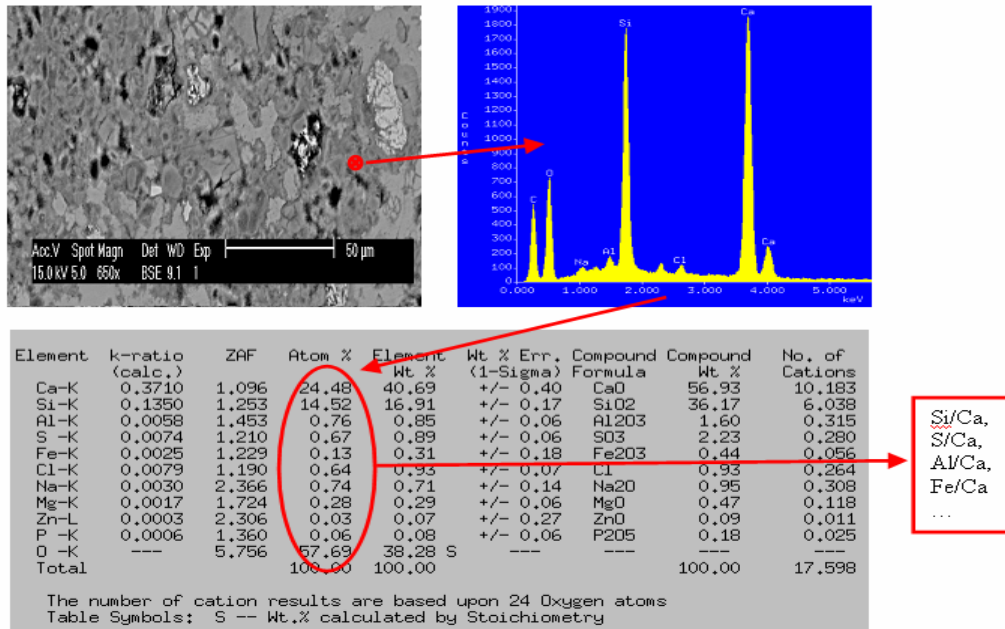
Fig. C.1: *Schematization of data sampling from EDS-analysis of a single point*

		S/Si	Al/Si	Fe/Si	Ca/Si
WPC(4)	Average composition of samples, mol/mol	**0.084**	**0.219**	**0.009**	**2.334**
	Std. Deviation between samples, mol/mol	0.005	0.020	0.002	0.179
	Expected from chemical composition, mol/mol	**0.076**	**0.224**	**0.007**	**2.990**
	Coefficient of Variance from expected, %	5	1	14	12
	Total samples included	**13**			
	EDS-spotanalyses per sample	**~900**			
		S/Si	Al/Si	Fe/Si	Ca/Si
WPC(12)	Average composition of samples, mol/mol	**0.074**	**0.085**	**0.011**	**2.482**
	Std. Deviation between samples, mol/mol	0.005	0.004	0.001	0.085
	Expected from chemical composition, mol/mol	**0.066**	**0.089**	**0.010**	**3.014**
	Coefficient of Variance from expected, %	5	2	5	10
	Total samples included	**7**			
	EDS-spotanalyses per sample	**~300**			
		S/Si	Al/Si	Fe/Si	Ca/Si
OPC	Average composition of samples, mol/mol	**0.112**	**0.241**	**0.106**	**2.641**
	Std. Deviation between samples, mol/mol	0.017	0.044	0.010	0.164
	Expected from chemical composition, mol/mol	**0.107**	**0.275**	**0.132**	**3.350**
	Coefficient of Variance from expected, %	2	7	11	12
	Total samples included	**5**			
	EDS-spotanalyses per sample	**~300**			

Fig. C.2: *Accuracy of EDS measurements while adopting standardless technique*

Fig. C.2 is meant to illustrate the accuracy of the EDS measurements as the technique was used standardless due to the vaste amount of analyses. 13 WPC(4), 7 WPC(12) and 5 OPC pastes were used for this purpose, and the accuracy of the technique is tested by comparison of measured S/Si, Al/Si, Fe/Si and Ca/Si against the expected from the chemical composition in **appendix B** (i.e. 'Expected from chemical composition' in **Fig. C.2**). 'Average composition of samples' refers to the total average composition from all samples calculated as the mean value of the average of each sample. 'Std. Deviation between samples' refers to the standard deviation of 'Average composition of samples' between samples. 'Coefficient of Variance' expresses the percentage variation between expected and measured values. The values for standard deviation are low (less than 10-15% of average value) and the Coefficient of Variance against expected values is also low for S/Si and Al/Si ratios (less than 7%), little higher for Fe/Si and Ca/Si ratios (but less than 14%). However, the fact that measured Ca/Si ratios are lower than the expected is consistent with the leaching of $Ca(OH)_2$ during exposure and is therefore not related to an inaccurate measurement. Furthermore, the standard deviation on Ca/Si ratios is lower than 6% which suggests an excellent agreement between the chemical composition measured on each sample. It is concluded that the use of a standardless technique leads to satisfactory accuracy for the purpose of this investigation.

The equilibrium solution was analyzed by titration ([Cl^-] and pH), ICP (Inductively Coupled Plasma Atomic Emission Spectrometry for [SO_4^{2-}], [Al^{3+}], [Si^{4+}] and [Ca^{2+}]) and AA (Atomic Absorption for [Na^+] and [K^+]), after removal of the solid phases by filtration.

The evaporable water content upon drying at 105^oC was determined followed by the determination of loss of ignition at 1000^oC, in order to calibrate the densities of the phases applied in the phase equilibria model.

XRD analyses were planned for all of the cement pastes examined, but were impeded by technical problems with the equipment. The time to complete installation of the new device was too long to allow storing of the samples for later study, as the samples could become affected by carbonation, drying or moisture absorption, etc, leading to unrepresentative data.

'Non-steady state ingress of aggressive ions'

The following chapter describes the experimental procedures adopted to examine the ingress of aggressive substances in cement-based materials.

Pastes and mortars

Mixing, casting and curing

Cement pastes of w/p 0.45 with 1 mass % replacement of powder by calcite were prepared according to the following mix (amounts are given in gram). De-aired, de- mineralized water was used for the preparation of the specimens.

Paste id.	Cementtype	Cement	Calcite	Water
WPC(4)	WPC(4)	1775	18	807
WPC(12)	WPC(12)	1775	18	807
SRPC	SRPC	1775	18	807

The powder was mixed for 5 minutes in a Hobart mixing machine, before addition of one half of the water and mixing for 3 minutes, followed by a further 3 minutes mixing with the remaining water. The pastes were cast in 150 mm x Ø70 mm cylinders, sealed, slowly rotated for approximately 24 hours to avoid bleeding. The samples were then de-molded, cut into 2 specimens of 60 mm x Ø70 mm, sealed in plastic bags with minimum surrounding water to reduce leaching, and stored at 20^oC for 4.5 months.

Mortars were prepared at w/p 0.48 (corrected for absorption by aggregates) with 1 mass % replacement of powder by calcite, according to the following mix (amounts are given in kg/m^3). De-aired, de-mineralized water was used for the preparation of the specimens.

Mortar id.	Cementtype	Cement	Calcite	Sand 0.25 - 1.0	Sand 1.0 - 4.0	Water
WPC(4)	WPC(4)	445.5	4.5	511.2	1192.7	214.0
WPC(12)	WPC(12)	445.5	4.5	511.2	1192.7	214.0
OPC	OPC	445.5	4.5	511.2	1192.7	214.0
SRPC	SRPC	445.5	4.5	511.2	1192.7	214.0

Sand and powder was mixed for 5 minutes, before addition of one half of the water and mixing for 3 minutes, followed by 3 minutes mixing with the remaining water. The mortars were cast in 600 x 100 x 100 mm^3 molds, sealed and de-molded after 2 days. The bars were cut in specimens of 130 x 100 x 100 mm^3, each of them sealed in plastic bags with minimum surrounding water to reduce leaching, and stored at 20°C for 4.5 months. Thus, the samples were kept saturated.

Exposure

After curing, the paste and mortar specimens were surface dried for 1.5 hours in a 45°C oven prior to immersion in special molds filled with Epoxy. The molds were selected as small as possible in order to minimize the amount of Epoxy needed for covering the specimens, reducing thereby the heat development during its hardening. After 24 hours, the Epoxy was completely hardened and the samples were cut in halves, immersed in the curing water from the plastic bags for 2 hours to saturate the region near the cut surface, and exposed to the following environments (20°C),

    a. 650 mM NaCl
    b. 650 mM NaCl + 30 mM $MgSO_4$ (only mortar specimens)

The specimens were extracted from these solutions after 35 (mortars) and 70 (mortars and pastes) days of exposure for analyses.

Analyses

The mortar samples were studied for ingress of aggressive substances by chemical analysis of ground profiles, and by mapping and spot-analysis by EDS. The pastes were only examined through EDS analysis.

Profile grinding: Dust was ground off the specimens at depth increments of 2 mm and dried at 105°C to constant weight. Thereafter, the content of acid soluble Cl, Na, K and Ca was determined allowing the tracement of concentration profiles as a function of depth.

EDS-analyses of mortars: 40 x 20 x 20 mm^3 specimens were cut out from the exposed samples and dried at 45°C for two days prior to Epoxy impregnation and preparation of polished thin-sections with a thickness of 1 mm. These were introduced to the ESEM and two forms of EDS-analyses were conducted,

- Element mapping of the surface region to reveal layering at the surface region
- Line-scans (300 single spot analyses for alumina-rich cements, and 900 single spot analyses for the aluminate-poor cement points per line) at different depths (at 1, 2, 3, 4, 6, 8, 10, 13 and 16 mm, and additionally 19 and 22 for samples exposed for 70 days) to study the phase assemblage as a function of depth.

EDS-analyses of pastes: Polished thin-sections were prepared from the surface region of the exposed samples. The specimens extracted covered an area of approx. 1.5 cm of the exposed surface and 2 cm inwards. The samples were introduced in the ESEM and two forms of EDS-analyses were conducted,

- Ingress/Leach profiles for relevant ions by line-scanning at steps of 50 μm from the surface inwards until a depth of 15 mm. 3 parallel line-scans were measured on each sample, placed at least 4 mm from each other.
- Linescans (300 single spot analyses for alumina-rich cements, and 900 single spot analyses for the aluminate-poor cement points, per line) at different depths (at 2, 4, 6, 10 and 15 mm) to study the phase assemblage as a function of depth.

Concretes

Mixing, casting and curing

Concretes were prepared at w/p 0.45 (corrected for absorption of aggregates), according to the following design mix (amounts are given in kg/m^3).

Concrete id.	Cementtype	Cement	Sand 0 – 2.0	Stone 2.0 – 8.0	Stone 8.0 – 16.0	Water
WPC(4)	WPC(4)	333	680	232	876	160
WPC(12)	WPC(12)	333	680	232	876	160
OPC	OPC	333	680	232	876	160

Aggregate and powder were mixed for 5 minutes, before addition of one half of the water and mixing for 3 minutes, followed by a further 3 minutes mixing with the remaining water. The concretes were cast in 200 x 200 x 200 mm^3 molds, de-molded after 24 hours, and stored in curing tanks at 20°C for 6 months.

Exposure

Each cube was halved and immersed in a 16.5 mass % NaCl-solution for 35 and 70 days. The cut surfaces constituted the exposure surface for later analyses.

Analyses

After exposure, dust was ground off the concrete specimen from the exposure surface inwards at steps of 1 mm (at the surface region) or 2 mm (at the inner part of the profile). The dust samples were dried at 105°C to constant weight and the content of acid soluble Cl and Ca was determined. Hence the concentration profiles as a function of depth could be traced.

Appendix D: Properties of phases selected for the model

The compositional data for the phases used in the developed model are listed in the following. The data has mainly been extracted from **Taylor [1997]** and **Lea [1970]**.

Table D.1: *Phase compositions and densities*

Component Phase	SiO_2	Al_2O_3	Fe_2O_3	CaO	SO_3	CO_2	MgO	$CaCl_2$	H_2O	Density [g/cm^3]
C-S-H	25.24	1.49		41.23	1.77				30.27	2.10 *[1]
CH (calcium hydroxide)				75.69					24.31	2.24
FH$_3$ (goethite)			89.76						10.24	4.28
MH (brucite)							69.09		30.91	2.39
Pore solution									100.0	1.00 *[2]
Gypsum				32.57	46.50				20.93	2.32
Ettringite		8.12		26.81	19.14				45.93	1.77
Monosulfate		16.38		36.03	12.86				34.73	2.01
C$_4$AH$_{13}$		18.19		40.02					41.79	2.05
Monocarbonate		17.94		39.46		7.74			34.86	2.01
Calcite				56.03		43.97				2.72
Thaumasite	9.7			27.0	12.9	7.1			43.3	2.1
Friedel's Salt		18.1		30.0				19.8	32.1	2.08

*[1] See Paper III for the description of how this value was obtained, as well as for the non-evaporable content of the C-S-H (i.e. 19 wt. %), and Al_2O_3 and SO_3 contents.

*[2] The density of the pore solution is throughout the report assumed to be 1.00 g/cm^3, corresponding to that of pure water. Small variations in density because of the ions dissolved in the pore solution are neglected (the error induced by this ranges from 0 to approx. 3 %)

Appendix E: Data for equilibria in PC systems at varying chloride and alkali content

In the following, an example on how the phase equilibria calculations were carried out for the specimens listed in this appendix and **appendix F**, is given. It is based on sample no. 27 (see later in this appendix) with EDS file WPC(12)_27.

From the amount of paste (with known chemical composition) prior to exposure and the total weight of the specimen (paste+exposure solution) at equilibrium, the phase assemblage in the paste without externally added ions can be predicted (using the model in **section 2.5**).

<div align="center">

Total weight of sample prior to exposure = 8.25 g

Total weight of sample + exposure solution = 18.22 g (at equilibrium)

</div>

C-S-H	4.66
CH	1.32
Goethite	0.01
Brucite	0.07
Pore solution	1.55
calcite	0.01
ettringite	0.18
monocarbonate	0.76
Friedels salt	0.00

- Total weight of saturated paste = 8.56 g (incl. imbibed water)

- Amount of pore solution = 1.55 g (incl. imbibed water)

- Amount of exposure solution = 9.65 g (corrected for imbibed water)

- Total weight of dry sample = 6.13 g (excl. pore solution and 'gelporosity', corresponding to 19 mass-% of C-S-H)

Based on the total amount of Cl and Na added to the exposure solution, the chemical composition of the paste and the chemical composition of the exposure solution at equilibrium, the distribution of Cl and Na between solid phases and the solution can be calculated.

	Total added	From paste	**Total**
	mmol	mmol	**mmol**
Na	2.70	0.05	**2.75**
Cl	4.22	0.01	**4.22**

Exposure solution	
mmol/l	
Na+K	227.6
Cl	216.7

	Amount in solids	Amount in solution
	mmol	mmol
Na+K	0.20	2.55
Cl	1.79	2.43

The amount of bound alkalis can be expressed directly as wt.% to dry C-S-H (as all bound alkali is found in the C-S-H),

<div align="center">

Na content in C-S-H = 100 * (0.20*23/1000) / (4.66*.81) = 0.12 wt.%

</div>

Bound Cl is distributed between C-S-H and the AFm solid solution phase. The amount of chloride in solids can then iteratively be distributed between these two phases until the content of chloride in the AFm solid solution phase is similar to that measured with the EDS equipment. A fine match is found for the following assemblage,

C-S-H	4.70
CH	1.32
Goethite	0.01
Brucite	0.07
Pore solution	1.52
calcite	0.05
ettringite	0.18
monocarbonate	0.44
Friedel's salt	0.31

Cl/Ca in C-S-H = 0.0199 (mol/mol)

→ corresponding to a Cl/Ca ratio in the monocarbonate-Friedel's salt solid solution at = 0.21 (mol/mol)

The EDS results plotted in terms of molar ratios of Cl/Ca vs. Al/Ca for this particular sample is shown in the following figure. The tie-line predicted from the assemblage above is also included in the figure.
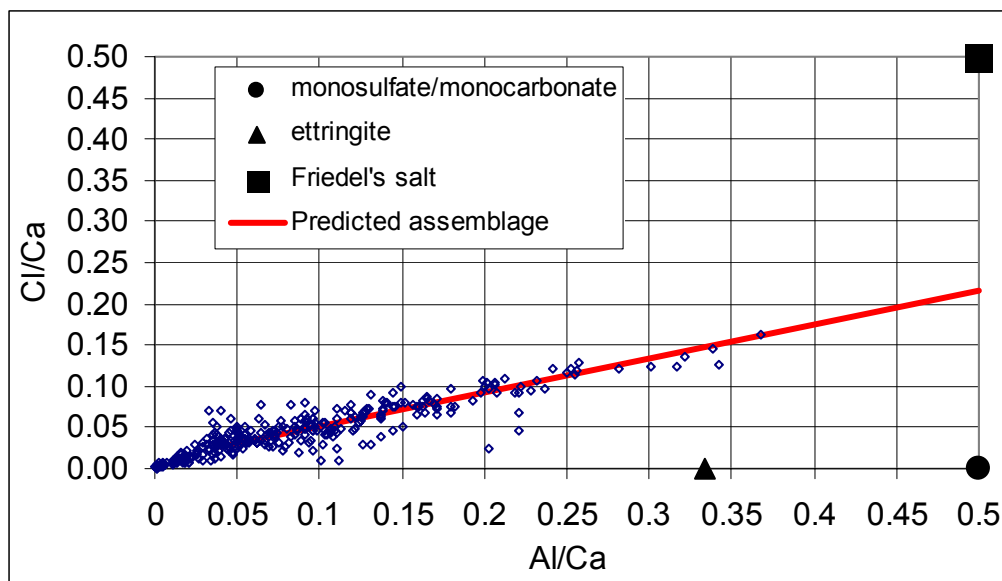
It must be noticed that upon sample preparation for EDS-analysis, the sample is dried at 40^oC prior to Epoxy impregnation. This results in the precipitation of the originally dissolved ions on the surface of the solid phases. For this paste, the average increase in Cl/Ca molar ratio due to that fact corresponds to 0.006. This has negligible effect on the Cl/Ca ratio in the solid solution phase between monocarbonate and Friedel's salt, but has a significant effect on the Cl/Ca ratio in the C-S-H (approx. 30% increase). The value at 0.006 was added to the tie-line between the C-S-H and the solid solution in the figure above, obtaining a fine match with the EDS-plots.

All data from phase equilibria in hydrated PC systems at varying contents of chlorides and alkalis are presented below.

1-6: WPC(4)_550 mM Na 7-13: WPC(4)_400 mM Na 14-20: WPC(4)_250 mM Na

no.	Exposure solution [g]	Pore solution [g]	Dry weight of solids [g]	Dry weight of C-S-H [g]	Composition of pore solution [mmol/l]								Total bound Cl	Bound Cl in C-S-H	Bound Cl in AFm	Bound Na in C-S-H	Fraction of FS in solid solution	Total addition to the system [mmoles]				EDS-file
					Na^+	K^+	Cl^-	pH	Ca^{2+}	Si^{4+}	Al^{3+}	SO_4^{2-}	[wt-% to total solids]			[wt.% to C-S-H]		Na	Cl	Ca	OH	
1	10.39	1.63	5.96	3.96	487.3	6.4	3.4	13.5	1.9	0.0	0.8	3.2	0.01			0.80		6.984	0.050	0.025	6.987	
2	9.26	1.63	5.96	3.96	539.1	6.5	4.4	13.6	1.5	0.0	0.9	3.3	0.03			0.80		6.987	0.100	0.050	6.987	
3	9.74	1.62	6.00	3.98	530.2	6.7	40.9	13.5	2.0	0.0	0.9	3.1	0.09	0.07	0.02	0.80	0.15	6.984	0.625	0.313	6.987	WPC(4)_3
4	10.20	1.62	5.96	3.96	540.2	6.8	154.9	13.5	1.8	0.0	1.0	2.3	0.18	0.15	0.03	0.58	0.23	7.040	2.117	0.045	5.016	WPC(4)_4
5	9.91	1.62	5.97	3.97	562.6	7.0	284.9	13.3	3.0	0.0	0.7	1.9	0.29	0.25	0.04	0.49	0.31	7.080	3.776	0.132	3.571	WPC(4)_5
6	9.61	1.61	6.00	4.00	638.9	7.6	588.1	12.9	18.7	0.0	0.8	0.5	0.53	0.48	0.05	0.15	0.42	7.170	7.494	0.304	0.287	WPC(4)_6
7	10.82	1.63	5.97	3.96	357.2	6.7	3.0	13.4	2.1	0.0	0.5	1.3	0.01			0.40		4.835	0.050	0.025	4.837	
8	10.43	1.63	5.97	3.96	360.0	6.6	5.1	13.5	1.8	0.0	0.5	1.6	0.02			0.43		4.835	0.100	0.050	4.837	
9	10.13	1.62	5.97	3.95	369.8	6.8	39.5	13.4	2.0	0.0	0.5	1.2	0.10	0.08	0.02	0.43	0.11	4.841	0.626	0.163	4.544	WPC(4)_9
10	10.45	1.62	5.98	3.97	365.4	6.8	92.4	13.4	2.5	0.0	0.5	1.1	0.16			0.40		4.859	1.382	0.072	3.622	
11	9.83	1.62	5.98	3.96	384.7	5.8	154.4	13.3	3.2	0.0	0.8	0.3	0.21	0.18	0.03	0.42	0.24	4.876	2.118	0.000	2.757	WPC(4)_11
12	9.35	1.62	5.96	3.97	404.5	6.9	291.1	13.1	6.8	0.0	0.8	0.0	0.35	0.31	0.04	0.42	0.36	4.908	3.780	0.000	1.055	WPC(4)_12
13	9.14	1.57	6.08	4.02	487.7	8.3	563.4	12.6	64.2	0.0	0.6	0.0	0.82	0.76	0.06	0.40	0.51	4.926	7.437	1.307	0.106	WPC(4)_13
14	8.94	1.62	5.96	3.95	227.4	6.9	2.5	13.3	3.0	0.0	0.4	0.0	0.01	0.01	0.00	0.32	0.02	2.699	0.050	0.011	2.673	WPC(4)_14
15	9.53	1.63	5.98	3.96	215.7	6.3	4.2	13.2	3.4	0.0	0.6	0.0	0.03			0.32		2.699	0.100	0.050	2.700	
16	10.17	1.62	5.98	3.97	212.0	6.3	34.7	13.2	3.7	0.0	0.4	0.5	0.13	0.11	0.02	0.26	0.17	2.703	0.626	0.126	2.331	WPC(4)_16
17	9.62	1.62	5.97	3.97	225.3	6.5	87.4	13.1	5.1	0.0	0.4	0.3	0.24			0.25		2.711	1.381	0.107	1.545	
18	9.39	1.62	5.98	3.98	241.8	7.1	141.3	12.9	8.0	0.0	1.1	0.2	0.33	0.29	0.04	0.09	0.35	2.718	2.115	0.154	0.912	WPC(4)_18
19	10.50	1.60	6.04	4.00	237.1	6.9	237.9	12.7	29.8	0.0	1.0	0.0	0.52	0.47	0.05	0.06	0.47	2.726	3.763	0.595	0.155	WPC(4)_19
20	8.51	1.53	6.15	4.01	296.2	8.7	593.9	12.4	149.2	0.0	1.4	0.0	0.82	0.76	0.06	0.00	0.59	2.726	7.375	2.385	0.123	WPC(4)_20

was added as NaOH and $CaCl_2$, centrifuged, the pH was measured, 12.5 ml were extracted and the concentration of the ions was corrected due to the common ion effect, which results in the precipitation of $Ca(OH)_2$

21-29: WPC(12)_250 mmole/l Na

30-35: OPC_550 mmole/l Na

no.	Exposure solution [g]	Pore solution [g]	Dry weight of solids [g]	Dry weight of C-S-H [g]	Composition of pore solution [mmol/l]								Total bound Cl	Bound Cl in C-S-H	Bound Cl in AFm	Bound Na in C-S-H [wt-% to C-S-H]	Fraction of FS in solid solution	Total addition to the system [mmoles]				EDS-file
					Na⁺	K⁺	Cl⁻	pH	Ca²⁺	Si⁴⁺	Al³⁺	SO₄²⁻	[wt-% to total solids]					Na	Cl	Ca	OH	
21	9.75	1.53	6.12	3.77	199.9	21.3	8.3	13.3	2.9	0.0	0.2	0.0	0.09	0.02	0.07	0.29	0.04	2.674	0.250	0.125	2.675	WPC(12)_21
22	9.04	1.54	6.17	3.79	216.0	23.6	19.2	13.3	2.6	0.0	0.2	0.5	0.30	0.07	0.23	0.27	0.15	2.676	0.726	0.272	2.496	WPC(12)_22
23	9.85	1.53	6.15	3.78	201.2	21.9	24.1	13.2	3.2	0.0	0.1	0.2	0.38	0.11	0.27	0.27	0.18	2.677	0.926	0.316	2.384	WPC(12)_23
24	9.92	1.54	6.17	3.80	208.0	22.2	70.6	13.2	4.2	0.0	1.0	0.7	0.52	■	■	0.22	■	2.688	1.709	0.183	1.346	■
25	9.34	1.54	6.14	3.79	218.1	24.1	101.9	13.1	5.1	0.0	1.0	0.7	0.55	0.19	0.36	0.22	0.23	2.692	2.064	0.152	0.933	WPC(12)_25
26	9.86	1.53	6.15	3.80	217.8	23.5	142.3	13.0	8.5	0.0	0.5	0.4	0.72	■	■	0.16	■	2.698	2.876	0.297	0.418	■
27	9.69	1.52	6.20	3.81	227.6	24.4	216.7	12.8	10.0	0.0	0.5	0.4	1.02	0.38	0.64	0.12	0.42	2.700	4.215	0.880	0.246	WPC(12)_27
28	8.54	1.50	6.22	3.81	264.1	29.2	329.2	12.6	42.9	0.0	0.7	0.1	1.18	0.45	0.73	0.06	0.48	2.700	5.378	1.423	0.170	WPC(12)_28
29	9.33	1.48	6.26	3.83	256.1	27.1	543.9	12.4	153.2	0.0	0.7	0.0	1.75	0.78	0.97	0.00	0.65	2.701	8.966	3.178	0.091	WPC(12)_29
30	10.49	1.68	6.11	3.24	510.5	32.6	48.9	13.5	1.4	0.0	1.0	5.0	0.25	0.06	0.19	0.68	0.24	6.749	1.029	0.007	5.736	OPC_30
31	10.29	1.63	6.09	3.32	507.7	32.5	60.8	13.5	1.6	0.0	1.0	4.9	0.31	■	■	0.75	■	6.746	1.254	0.186	5.867	■
32	10.35	1.63	6.10	3.32	531.2	34.0	133.9	13.5	1.6	0.0	0.4	4.0	0.38	0.09	0.29	0.60	0.32	6.762	2.264	0.370	5.242	OPC_32
33	10.27	1.63	6.09	3.32	543.6	34.7	216.3	13.4	1.6	0.0	0.5	3.8	0.52	0.14	0.38	0.56	0.38	6.807	3.469	0.113	3.568	OPC_33
34	9.76	1.62	6.10	3.32	589.2	37.6	424.0	13.2	3.6	0.0	0.5	1.8	0.70	0.22	0.48	0.44	0.44	6.874	6.034	0.098	1.039	OPC_34
35	9.41	1.52	6.25	3.33	644.9	41.5	636.8	12.7	27.9	0.0	0.8	0.0	1.21	0.31	0.90	0.21	0.60	6.895	9.100	0.239	1.530	OPC_35

was added as NaOH and CaCl₂, centrifuged, the pH was measured, 12.5 ml were extracted and the concentration of the ions was corrected

due to the common ion effect, which results in the precipitation of Ca(OH)₂

WPC(4)_250 mM Na

WPC(4)_550 mM Na
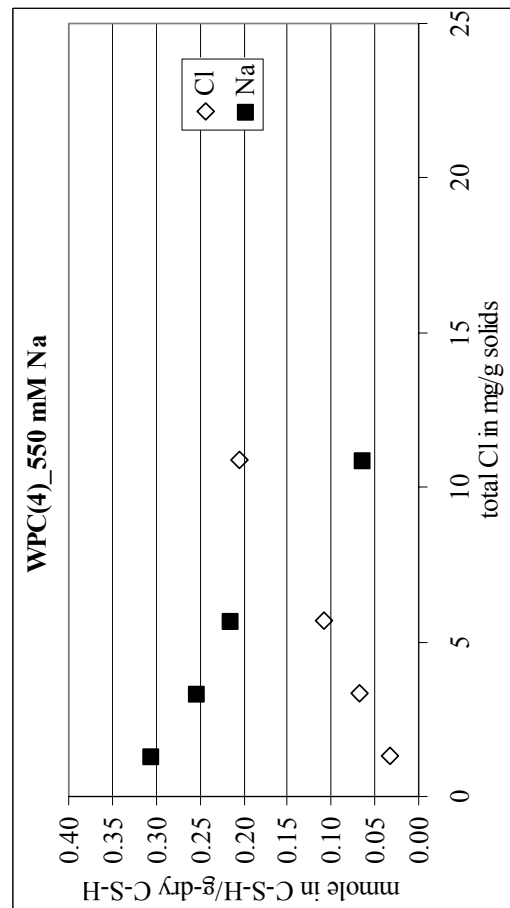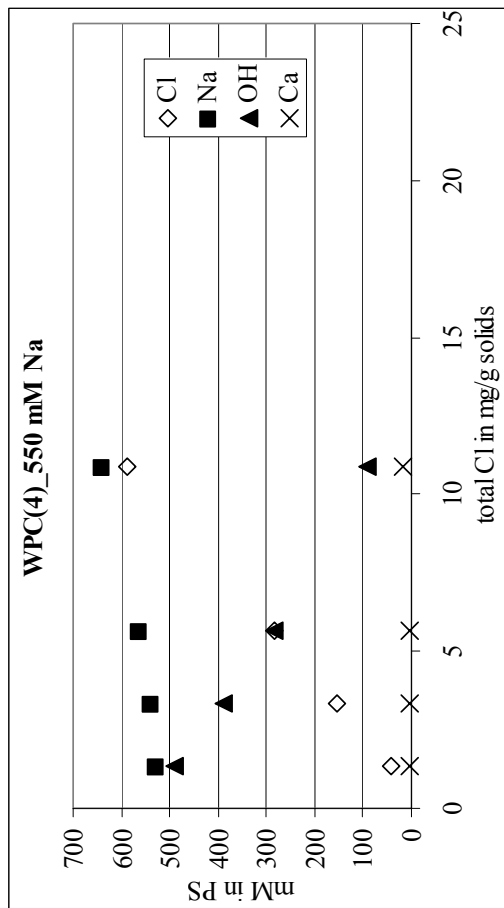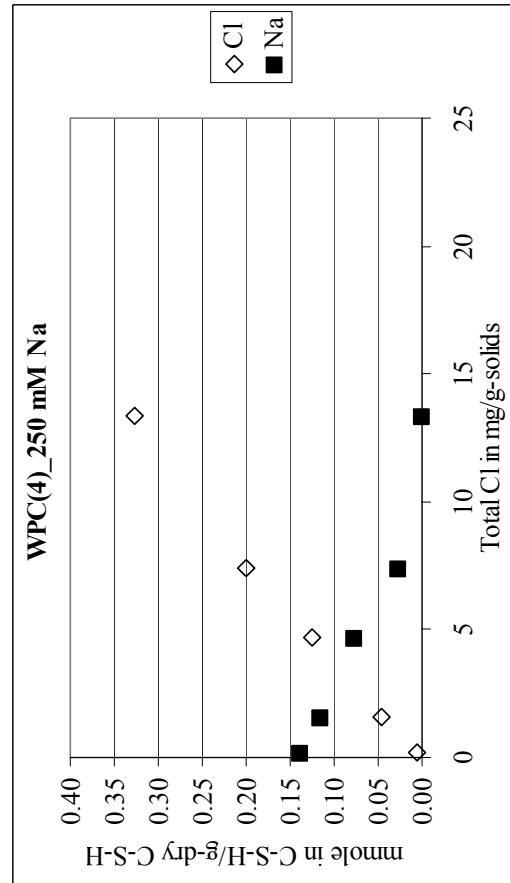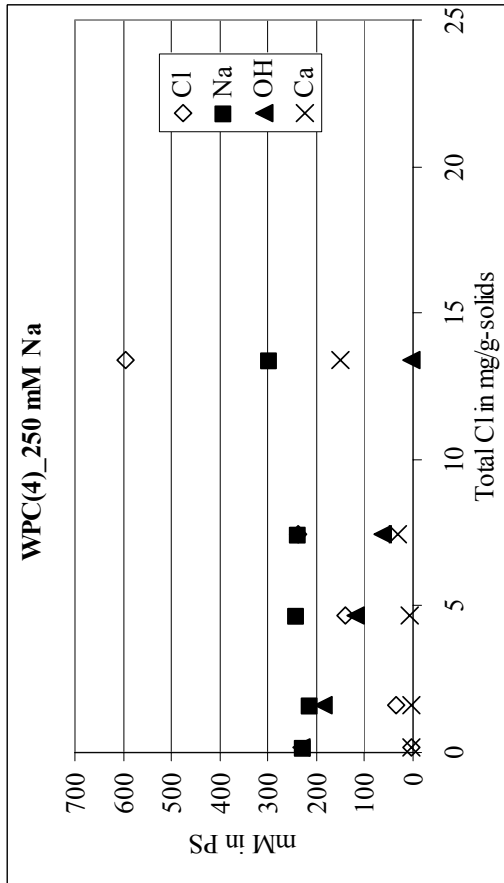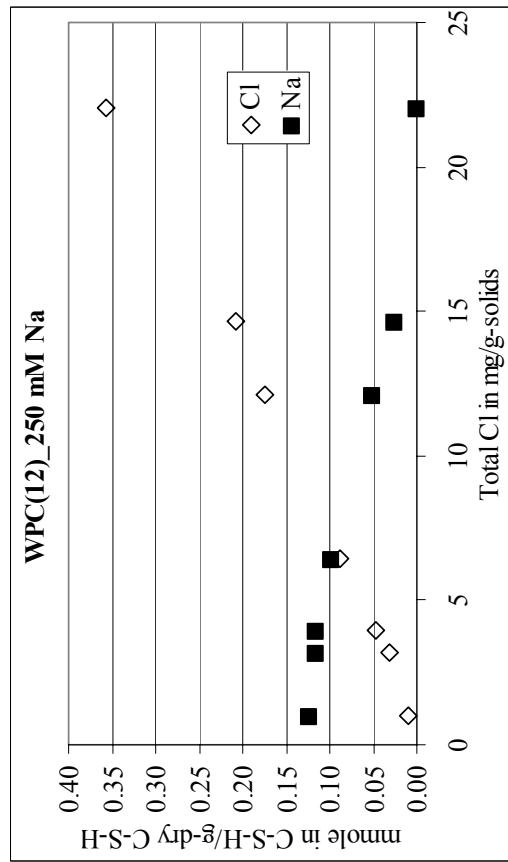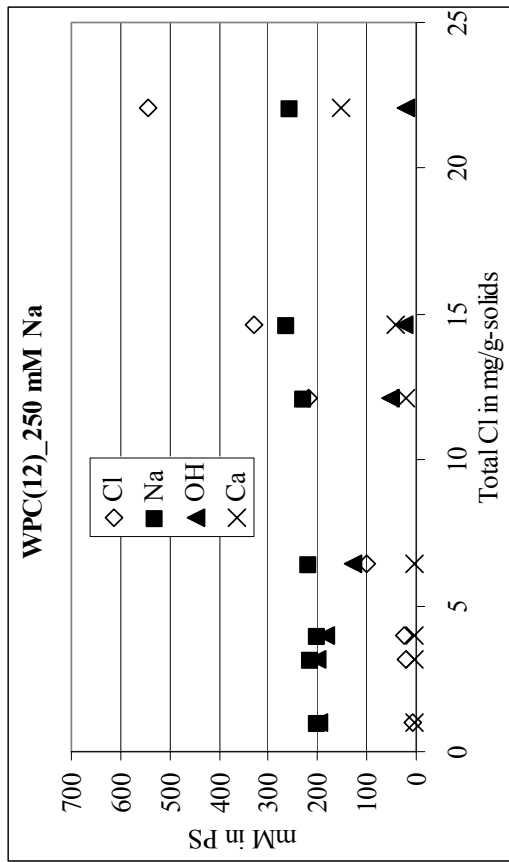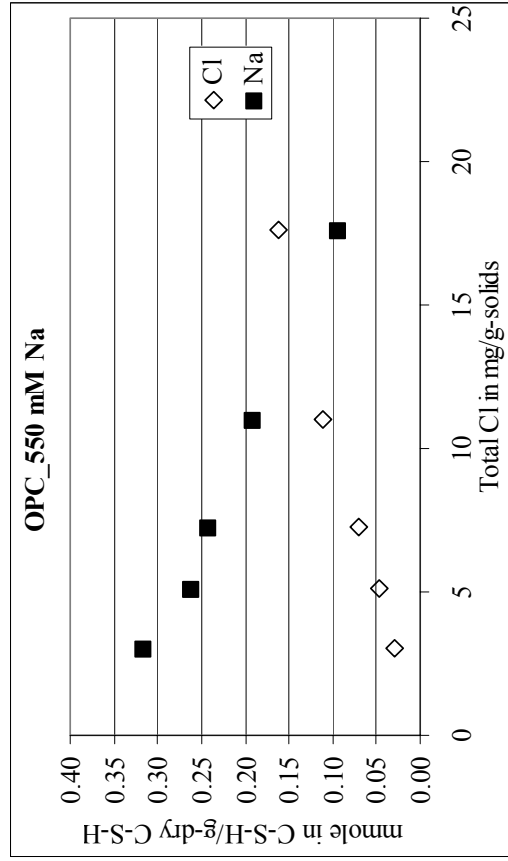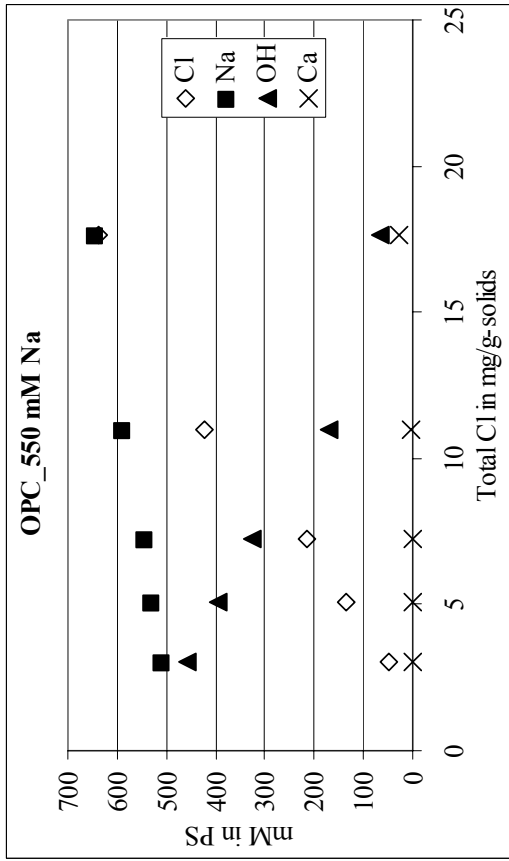
Comparison between measured values for chloride and alkali concentration of the exposure solution, and the predicted by the model described in **sections 2.5** and **2.8**.
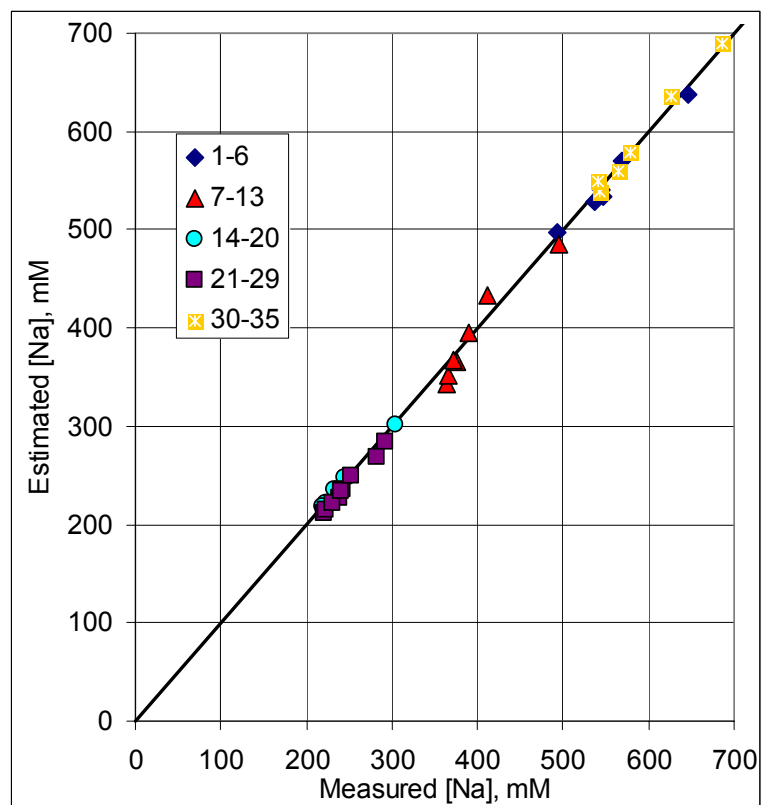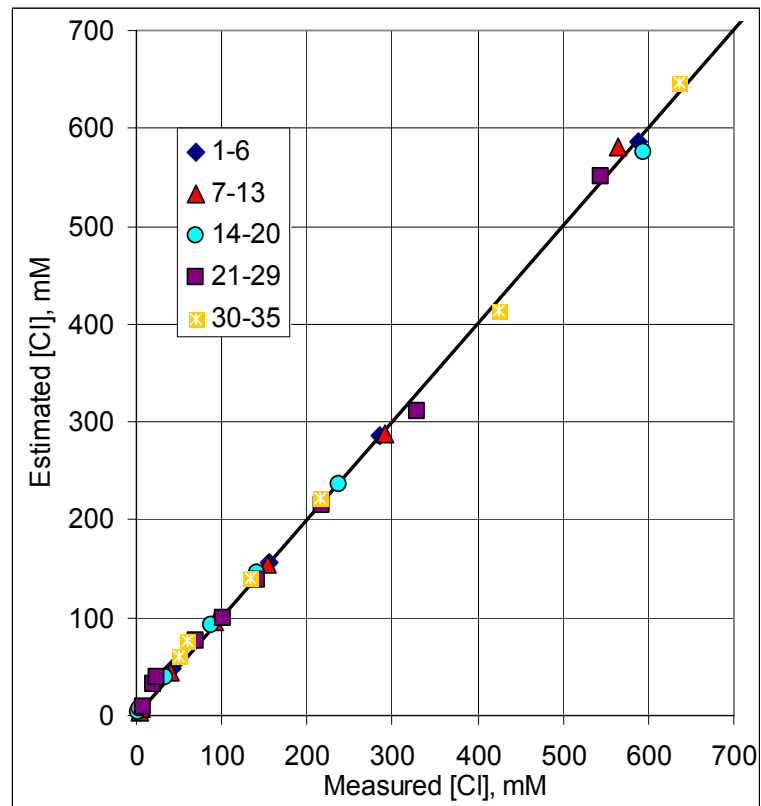
WPC(4) with 10% SF (noted WPC(4)_10%SF).

36-45: WPC(4)_10%SF

| no.	Exposure solution [g]	Pore solution [g]	Dry weight of solids [g]	Dry weight of C-S-H [g]	Composition of pore solution [mmol/l]								Total bound Cl [wt-% to total solids]	Bound Na in C-S-H [wt.% to C-S-H]	Total addition to the system [mmoles]			
					Na+	K+	Cl-	pH	Ca2+	Si4+	Al3+	SO4^2-			Na	Cl	Ca	OH
36	11.02	1.55	5.7	4.95	24.4	6.9	22.4	12.6	17.4	0	0.8	0.0	0.11	0.00	0.100	0.450	0.225	0.100
37	10.24	1.56	5.76	4.95	89.1	7.4	81.7	12.6	16.9	0	0.9	0.0	0.22	0.10	0.988	1.327	0.497	0.657
38	9.58	1.56	5.81	4.94	167.2	7.9	162.6	12.6	18.0	0	0.3	0.3	0.29	0.17	1.959	2.287	0.471	0.615
39	9.54	1.71	6.05	4.96	298.2	8.9	521.2	12.4	137.2	0	1.2	0.0	0.79	0.00	3.019	7.204	0.205	2.194
40	9.51	1.58	5.90	4.95	269.1	8.1	258.9	12.6	24.4	0	0.7	0.2	0.43	0.14	3.015	3.584	0.566	0.564
41	10.06	1.56	5.85	4.95	236.1	7.2	165.6	12.8	8.3	0	0.8	0.6	0.22	0.25	3.005	2.289	0.347	1.411
42	10.24	1.55	5.81	4.95	204.3	6.6	96.4	13.0	3.7	0	0.3	1.4	0.12	0.40	2.994	1.328	0.333	2.334
43	10.24	1.54	5.77	4.95	194.1	6.4	33.0	13.1	2.2	0	0.4	1.8	0.04	0.45	2.986	0.450	0.225	2.987
44	10.50	1.57	5.91	4.95	244.3	7.4	243.5	12.6	19.7	0	0.4	0.0	0.39	0.27	3.257	3.587	0.466	0.604
45	11.08	1.59	6.15	4.96	496.1	7.3	504.3	12.6	25.0	0	0.6	0.0	0.53	0.44	6.954	7.303	0.422	0.498

was added as NaOH and CaCl$_2$, centrifuged, the pH was measured, 12.5 ml were extracted and the concentration of the ions was corrected

due to the common ion effect, which results in the precipitation of Ca(OH)$_2$

WPC(4) with 30% slag (noted WPC(4)_30%slag).

46-61: WPC(4)_30% slag

no.	Exposure solution	Pore solution	Dry weight of solids	Dry weight of C-S-H	Composition of pore solution								Total bound Cl	Bound Na in C-S-H	Total addition to the system			
	[g]	[g]	[g]	[g]	Na$^+$	K$^+$	Cl$^-$	pH	Ca^{2+}	Si^{4+}	Al^{3+}	SO$_4^{2-}$	[wt-% to total solids]	[wt.% to C-S-H]	Na	Cl	Ca	OH
					[mmol/l]										[mmol]			
46	11.103	1.5	6.07	4.32	575.5	10.3	10.0	13.6	1.2	0	0.2	6.0	0.06	0.91	8.659	0.225	0.113	8.662
47	10.92	1.5	6.12	4.32	609.7	11.2	58.8	13.6	1.2	0	0.2	5.6	0.28	0.76	8.698	1.205	0.035	7.565
48	10.746	1.51	6.46	4.32	674.7	11.7	593.6	13.3	11.4	0	0.9	7.3	1.15	0.52	8.940	9.37	0.453	0.479
49	10.043	1.51	6.03	4.32	476.3	11.0	7.8	13.5	1.4	0	0.7	2.5	0.08	0.61	6.347	0.225	0.113	6.337
50	9.916	1.49	6.06	4.32	472.4	11.4	60.6	13.5	1.6	0	0.6	4.2	0.30	0.67	6.354	1.204	0.224	5.600
51	9.788	1.5	6.12	4.33	483.9	11.6	143.1	13.4	2.2	0	1.3	6.1	0.47	0.65	6.388	2.42	0.150	4.271
52	10.19	1.5	6.17	4.32	474.4	11.4	251.0	13.2	3.6	0	1.2	6.2	0.62	0.63	6.43	4.009	0.084	2.590
53	9.301	1.56	6.39	4.32	586.2	13.1	618.2	12.6	41.5	0	1.2	5.2	1.43	0.22	6.488	9.294	1.527	0.250
54	9.172	1.5	6.2	4.31	475.6	12.5	371.3	13.0	10.1	0	0.1	4.3	0.95	0.23	5.204	5.626	0.469	0.518
55	11.028	1.51	5.98	4.33	279.9	10.5	7.3	13.3	1.7	0	0.9	1.5	0.08	0.42	3.998	0.225	0.113	4.000
56	10.814	1.49	6.01	4.32	282.5	10.9	52.5	13.3	2.8	0	0.8	2.5	0.33	0.44	4.013	1.204	0.135	3.080
57	9.878	1.5	6.07	4.33	322.2	11.9	136.1	13.2	4.0	0	0.9	3.0	0.51	0.35	4.032	2.42	0.126	1.865
58	10.14	1.5	6.12	4.32	333.0	12.0	232.2	12.9	8.2	0	0.6	2.8	0.75	0.25	4.053	4.004	0.264	0.579
59	10.78	1.6	6.35	4.33	350.1	12.7	515.9	12.4	98.1	0	0.6	3.0	1.58	0.01	4.059	9.213	2.656	0.160
60	8.182	1.5	6.11	4.32	359.6	13.4	266.1	12.9	9.4	0	0.6	2.8	0.82	0.22	3.591	3.997	0.466	0.527
61	8.921	1.5	5.99	4.33	156.2	12.6	88.0	12.9	9.9	0	0.7	0.9	0.60	0.10	1.518	1.933	0.440	0.466

was added as NaOH and CaCl$_2$, centrifuged, the pH was measured, 12.5 ml were extracted and the concentration of the ions was corrected due to the common ion effect, which results in the precipitation of Ca(OH)$_2$

OPC with 30% slag (noted OPC_30%slag).

| no.	Exposure solution [g]	Pore solution [g]	Dry weight of solids [g]	Dry weight of C-S-H [g]	Composition of pore solution [mmol/l]								Total bound Cl [wt-% to total solids]	Bound Na in C-S-H [wt.% to C-S-H]	Total addition to the system [mmol]			
					Na^+	K^+	Cl^-	pH	Ca^{2+}	Si^{4+}	Al^{3+}	SO_4^{2-}			Na	Cl	Ca	OH
62	8.68	1.47	6.06	3.89	56.1	36.1	20.3	12.8	8.3	0	0.4	0.5	0.42	0.05	0.200	0.925	0.449	0.173
63	10.06	1.48	6.20	3.90	197.4	31.5	112.1	12.9	6.7	0	1.1	0.7	0.96	0.24	2.227	2.970	0.616	0.490
64	11.05	1.48	6.26	3.89	261.8	29.8	166.7	13.0	6.3	0	1.0	1.1	1.15	0.33	3.387	4.121	0.607	0.481
65	10.72	1.48	6.43	3.89	525.2	30.8	323.3	13.2	3.8	0	1.0	3.9	1.35	0.57	6.918	6.396	0.180	0.885
66	10.65	1.48	6.35	3.89	511.0	30.0	233.3	13.3	2.5	0	0.8	5.1	0.92	0.67	6.872	4.473	0.096	2.595
67	9.41	1.48	6.31	3.89	551.0	32.3	178.7	13.4	1.7	0	0.8	6.6	0.71	0.76	6.830	3.208	0.279	4.182
68	11.27	1.47	6.23	3.90	460.0	27.0	34.3	13.5	1.9	0	0.6	3.4	0.28	0.80	6.769	0.926	0.287	6.419
69	11.18	1.47	6.20	3.90	455.3	26.6	9.1	13.5	2.2	0	3.7	2.4	0.06	0.86	6.760	0.225	0.113	6.762
70	10.24	1.49	6.73	3.89	877.7	32.9	702.7	13.1	5.4	0	0.8	6.5	1.41	1.08	11.672	10.914	0.286	0.472
71	10.37	1.49	6.51	3.90	560.8	31.8	411.3	13.0	5.6	0	0.8	4.3	1.63	0.55	7.125	7.872	0.616	0.487
72	9.95	1.49	6.40	3.89	427.6	30.4	335.0	13.0	5.0	0	0.8	2.5	1.00	1.14	6.374	5.645	0.198	0.532
73	11.29	1.47	6.21	3.90	463.5	27.6	23.2	13.5	1.8	0	0.7	3.4	0.22	0.77	6.765	0.676	0.236	6.565
74	9.83	1.48	6.30	3.90	526.9	31.3	156.0	13.4	1.7	0	0.8	6.0	0.68	0.77	6.810	2.972	0.529	4.899
75	9.46	1.48	6.34	3.89	540.0	31.8	227.8	13.3	2.1	0	0.9	6.3	0.92	0.83	6.859	4.135	0.193	3.113
76	9.62	1.49	6.49	3.89	582.5	33.9	433.5	13.1	5.8	0	0.7	4.2	1.15	1.09	7.869	6.930	0.524	0.415
77	7.97	1.48	6.27	3.88	384.5	38.3	238.0	13.0	3.6	0	2.2	0.7	1.25	0.32	3.732	4.455	0.619	0.516
78	8.03	1.48	6.21	3.89	248.9	36.7	162.2	12.9	4.8	0	2.3	1.0	0.95	0.33	2.468	3.200	0.610	0.490

was added as NaOH and CaCl$_2$, centrifuged, the pH was measured, 12.5 ml were extracted and the concentration of the ions was corrected due to the common ion effect, which results in the precipitation of Ca(OH)$_2$

Chloride binding isotherms of all series studied at constant level of alkalis.

Appendix F: Data for equilibria in PC systems at varying MgSO$_4$ content

S1-S6: WPC(4) S7-S12: WPC(12)

No.	Exposure solution [g]	Pore solution [g]	Dry weight of solids [g]	Dry weight of C-S-H [g]	Na$^+$	K$^+$	Cl$^-$	pH	Ca^{2+}	Mg^{2+}	Al^{3+}	SO$_4^{2-}$	Total bound Cl	Bound Cl in C-S-H	Bound Cl in AFm	Bound Na in C-S-H [wt.% to C-S-H]	Na	Cl	MgO	SO3	EDS-file
					Composition of pore solution [mmol/l]								[wt-% to total solids]				Total addition to the system [mmoles]				
S1	12.20	1.71	6.30	3.87	393.1	6.9	336.2	12.8	15.4	0.0	0.8	0.0	0.53	0.53	0.01	0.10	5.625	5.625	0.25	0.25	EDS_S1
S2	12.19	1.70	6.34	3.87	399.7	7.0	344.5	12.8	16.5	0.0	0.7	0.2	0.47	0.47	0.00	0.05	5.625	5.625	0.50	0.50	EDS_S2
S3	12.19	1.68	6.38	3.87	397.4	7.0	343.0	12.8	17.0	0.0	1.2	1.4	0.48	0.48	0.00	0.07	5.625	5.625	0.75	0.75	EDS_S3
S4	12.19	1.66	6.42	3.87	389.5	6.7	344.4	12.8	18.4	0.1	1.1	3.0	0.47	0.47	0.00	0.14	5.625	5.625	1.00	1.00	EDS_S4
S5	12.20	1.65	6.45	3.87	401.3	6.8	353.7	12.8	20.7	1.1	1.2	6.1	0.40	0.40	0.00	0.05	5.625	5.625	1.25	1.25	EDS_S5
S6	10.80	0.97	7.75	3.99	228.0	6.4	88.0	12.6	22.1	0.2	0.5	54.6	0.11	0.11	0.00	0.00	2.675	1.275	12.0	12.0	EDS_S6
S7	12.19	1.54	6.44	3.67	381.8	13.3	300.3	13.0	9.9	0.2	0.5	0.7	0.83	0.29	0.53	0.24	5.625	5.625	0.25	0.25	EDS_S7
S8	12.17	1.57	6.51	3.69	384.0	13.1	302.3	0.0	11.1	0.1	0.4	0.8	0.80	0.31	0.49	0.22	5.625	5.625	0.50	0.50	EDS_S8
S9	12.17	1.53	6.55	3.67	407.4	13.9	328.8	0.0	12.3	0.1	0.7	0.8	0.61	0.25	0.36	0.03	5.625	5.625	0.75	0.75	EDS_S9
S10	12.17	1.49	6.57	3.65	392.9	13.5	316.5	13.0	12.9	0.1	0.8	0.8	0.70	0.29	0.41	0.16	5.625	5.625	1.00	1.00	EDS_S10
S11	12.17	1.45	6.64	3.65	406.8	14.0	333.7	13.0	13.2	0.3	0.8	0.7	0.58	0.26	0.32	0.06	5.625	5.625	1.25	1.25	EDS_S11
S12	11.10	0.50	8.48	3.77	233.5	25.2	271.3	12.5	55.6	0.3	0.9	21.5	0.28	0.28	0.00	0.00	2.675	3.825	12.0	12.0	EDS_S12

Comparison between measured values for chloride and alkali concentration of the exposure solution, and the predicted by the model described in **sections 2.5** and **2.8**.
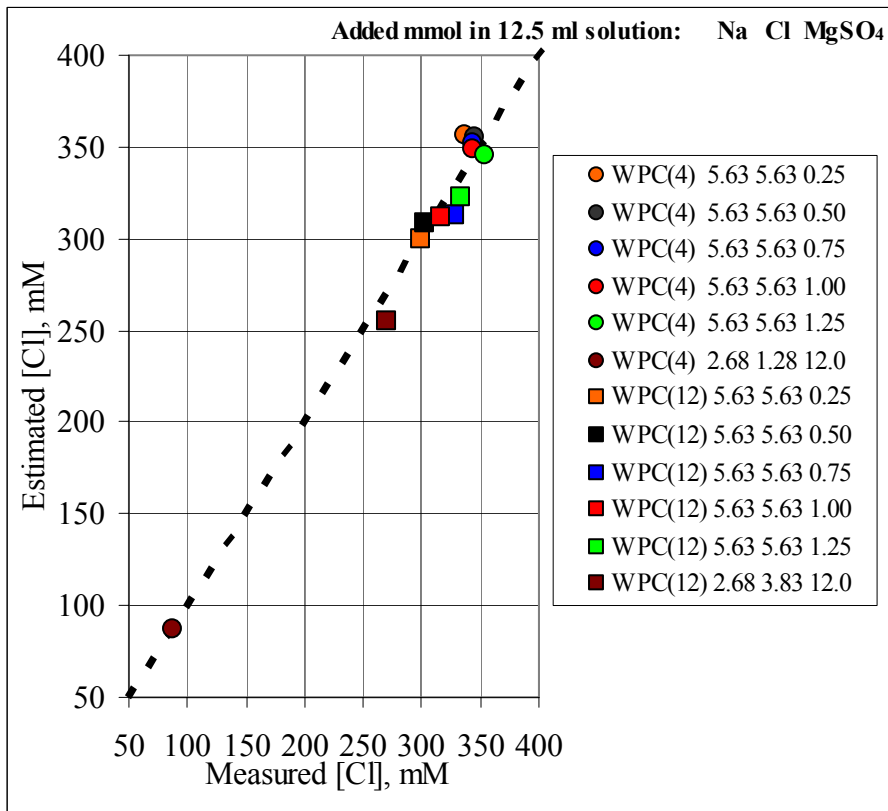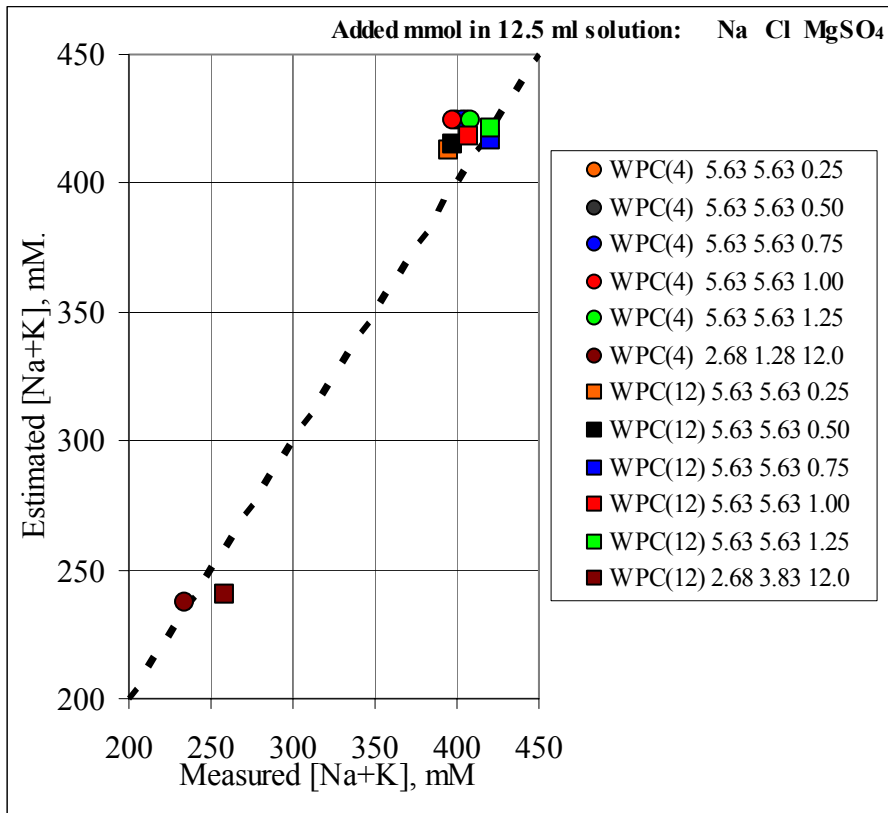
Appendix G: Matlab codes for the FDM for chloride ingress

Main program "main.m"

```
clear all;
%%%%%%%%%%%%%%%%%%%%%%%%%%%%%%%%%%%%%%%%%%%%%%%%%%%%%%%%%%%%%%%%%%%%%%%%%%%%%%
%%%%%%%%%%%%%%%%%%%%%%%%%%%%%%%%%%%%%%%%%%%%%%%%%%%%%%%%%%%%%%%%%%%%%%%%%%%%%%
%%%%%%%%%%              Input                %%%%%%%%%%%%%%%%%%%%%
%%%%%%%%%%%%%%%%%%%%%%%%%%%%%%%%%%%%%%%%%%%%%%%%%%%%%%%%%%%%%%%%%%%%%%%%%%%%%%
%%%%%%%%%%%%%%%%%%%%%%%%%%%%%%%%%%%%%%%%%%%%%%%%%%%%%%%%%%%%%%%%%%%%%%%%%%%%%%
x       = 0.017;        % depth of specimen, in m
delta_x = 0.001;        % depth increment, in m
exp_time = 70*24*60*60; % total exposure time, in seconds
trans_factor = 1;       % factor f1 in eq. 7.9

% Exposure conditions
exp_sol = [0.65 0.65 0.015 0.03 0.0];  % composition of the exposure solution
in mmole/liter, respectively Cl, Na, Ca, OH, K

% Powder properties

% mass percent of each powder, note: the total sum has to be 100
HOCperc  = 99.00;   % wt.% low aluminate white PC, WPC(4)
RCIperc  = 00.00;   % wt.% high aluminate white PC, WPC(12)
OTCperc  = 00.00;   % wt.% ordinary PC, OPC
SACperc  = 00.00;   % wt.% low alkali sulfate resistant grey PC, SRPC
MKperc   = 00.00; % wt.% metakaolin
SFperc   = 00.00; % wt.% silica fume
KSperc   = 01.00; % wt.% CaCO3

% Mix properties

waterpowder= 0.45; % water-to-powder ratio
Vair     = 0.0;   % total volume fraction of air voids
Vagg     = 0.0;   % total volume fraction of aggregate
dagg     = 2.621; % weighed average density of aggregate [g/cm3]
Rd_alkalis = 0.65; % Initial distribution ration for alkalis in the C-S-H, Rd

%%%%%%%%%%%%%%%%%%%%%%%%%%%%%%%%%%%%%%%%%%%%%%%%%%%%%%%%%%%%%%%%%%%%%%%%%%%%%%
%%%%%%%%%%%%%%%%%%%%%%%%%%%%%%%%%%%%%%%%%%%%%%%%%%%%%%%%%%%%%%%%%%%%%%%%%%%%%%
%%%%%%%%%%%%%%%           Calculations                %%%%%%%%%%%%%%%
%%%%%%%%%%%%%%%%%%%%%%%%%%%%%%%%%%%%%%%%%%%%%%%%%%%%%%%%%%%%%%%%%%%%%%%%%%%%%%
%%%%%%%%%%%%%%%%%%%%%%%%%%%%%%%%%%%%%%%%%%%%%%%%%%%%%%%%%%%%%%%%%%%%%%%%%%%%%%
% Determine initial phase assemblage + content and distribution of alkalis

[assem0,molarv,densities,K_concentration,Na_concentration,total_K,total_Na,
total_Cl,FeCa]=initial(HOCperc,RCIperc,OTCperc,SACperc,MKperc,SFperc,
KSperc,waterpowder,Rd_alkalis);
Cl_conc = 0.002;   % minimum conc of Cl
Ca_conc = 0.005;   % minimum conc of Ca
Na_conc = Na_concentration; % initial conc of Na
K_conc = K_concentration; % initial conc of K

Na_tot = zeros(1,abs(x/delta_x)+1);
K_tot = zeros(1,abs(x/delta_x)+1);
Cl_tot = zeros(1,abs(x/delta_x)+1);

Na_tot = Na_tot + total_Na * (1-Vair-Vagg);
K_tot = K_tot + total_K * (1-Vair-Vagg);
Cl_tot = Cl_tot + total_Cl*(1-Vair-Vagg);
```

```
OH_conc = Na_conc + K_conc;  % Approximate concentration of hydroxil ions in
the unexposed sample

PS_init = [Cl_conc Na_conc Ca_conc OH_conc K_conc]; % resp. Cl, Na, Ca, OH, K

% Define matrix for the conc of the different ions in solution, at each depth

conc = zeros(10,abs(x/delta_x)+1);
for (j=1:1:5)
    conc(2*j-1,:)   = conc(2*j-1,:) + PS_init(j);
    conc(2*j,:)     = conc(2*j,:) + PS_init(j);
    conc(2*j-1,1)   = exp_sol(j);
    conc(2*j,1)     = exp_sol(j);
end
assem0 = assem0 * (1-Vair-Vagg);
for (i=1:1:round(x/delta_x)+1)
     for (j=1:1:12)
            assem(j,i)=assem0(j);
       end
end
assem=assem/(1-Vair-Vagg);
assem0=assem0/(1-Vair-Vagg);
Cl_tot= Cl_tot/(1-Vair-Vagg);
Na_tot= Na_tot/(1-Vair-Vagg);
K_tot= K_tot/(1-Vair-Vagg);
[assem_surf,total] =
surf(exp_sol,assem,assem0,molarv,FeCa,Rd_alkalis,molarv);
Cl_tot(1) = total(1);
Na_tot(1) = total(2);
K_tot(1) = total(3);
for(i=1:1:12)
    assem(i,1)= assem_surf(i);
end
delta_t = 0.0;
t=0.0;
leach_CH=zeros(1,(x/delta_x)+1);
while (t<exp_time)
    [conc,Cl_tot,Na_tot,K_tot,delta_t] =
MSing(t,delta_t,conc,exp_sol,x,delta_x,assem,molarv,Vagg,Vair,Cl_tot,Na_tot,
K_tot,trans_factor);

   for (m=2:1:abs(x/delta_x)+1)
      [assem,conc,leach_CH] =
equil(conc,Cl_tot,Na_tot,assem,assem0,molarv,m,K_tot,FeCa,Rd_alkalis,
leach_CH);
   end
   t  = t + delta_t;
end

x1 = zeros(1,(x/delta_x)+1);
for (j=1:1:(x/delta_x)+1)
    x1(1,j)=(j-1)*delta_x;
end
figure
plot(x1,conc(2,:),'r-',x1,conc(4,:),'b-',x1,conc(6,:),'y-',x1,conc(8,:),'c-
',x1,conc(10,:),'m-')
axis([0 max(x1) 0 max(conc(:,1))])
legend('Cl^{-}','Na^{+}','Ca^{2+}','OH^{-}','K^{+}')
xlabel('Depth [m]')
ylabel('Concentration [mM]')

assem = assem*(1-Vair-Vagg);
```

```
assem0= assem0*(1-Vair-Vagg);
Cl_tot= Cl_tot*(1-Vair-Vagg);
Na_tot= Na_tot*(1-Vair-Vagg);
K_tot= K_tot*(1-Vair-Vagg);
mass = zeros(1,(x/delta_x)+1);
for (j=1:1:(x/delta_x)+1)
    for (i=1:1:12)
        assem(i,j)=assem(i,j)*molarv(i)*densities(i);
    end
    mass(j) = (sum(assem(:,j))-assem(5,j)-assem(1,j)*.18+Vagg*dagg);
end
    for (i=1:1:12)
        assem0(i)=assem0(i)*molarv(i)*densities(i);
    end
    Cl_tot = 100*(Cl_tot.*35.45)./mass;
    Na_tot = 100*(Na_tot.*23.0)./mass;
    K_tot = 100*(K_tot*39.1)./mass;
figure
plot(x1,Na_tot,'r-',x1,K_tot,'b-',x1,Cl_tot,'y-')
legend('Na','K','Cl')
xlabel('Depth [m]')
ylabel('Content [mass%]')
figure
for (j=1:1:(x/delta_x)+1)
    CH(j)=100*assem(2,j)./sum(assem(:,j));
    CS(j)=100*assem(9,j)./sum(assem(:,j));
    ETTR(j)=100*assem(8,j)./sum(assem(:,j));
    MS(j)=100*assem(7,j)./sum(assem(:,j));
    C4AH13(j)=100*assem(6,j)./sum(assem(:,j));
    MC(j)=100*assem(10,j)./sum(assem(:,j));
    CC(j)=100*assem(11,j)./sum(assem(:,j));
    FS(j)=100*assem(12,j)./sum(assem(:,j));
end
plot(x1,C4AH13,x1,MS,x1,ETTR,x1,CS,x1,MC,x1,CC,x1,FS)
legend('C4AH13','MS','ETTR','CS','MC','CC','FS')
xlabel('Depth [m]')
ylabel('Content [mass%]')
exp_time = t/(24*3600)
ClOH = zeros(1,(x/delta_x)+1);
for (j=1:1:(x/delta_x)+1)
    ClOH(1,j) = conc(2,j)./conc(8,j);
end
figure
plot(x1,ClOH)
axis([0 max(x1) 0 5 ])
legend('[Cl]/[OH]')
xlabel('Depth [m]')
ylabel('[Cl]/[OH]')
sol=zeros(1,(x/delta_x)+1);
sol(1,:)=conc(2,:); sol(2,:)=conc(4,:); sol(3,:)=conc(6,:);
sol(4,:)=conc(8,:); sol(5,:)=conc(10,:);
save results.xls assem sol Cl_tot K_tot Na_tot mass -ascii
```

Code of function "initial.m"

```
function [assem0,molarv,densities,K_concentration,Na_concentration,total_K,
total_Na,total_Cl,FeCa]=initial(HOCperc,RCIperc,OTCperc,SACperc,MKperc,
SFperc,KSperc,waterpowder,Rd_alkalis)
% Composition of materials
%       SiO2 Al2O3 Fe2O3  CaO  SO3  MgO  H2O CO2  CaCl2 Na2O K2O density
HOC = [24.83 01.87 0.33 68.86 2.20 0.52 0.0 00.14 0.002 0.16 0.11 3.17];
RCI = [23.57 04.49 0.21 65.88 2.38 0.97 0.0 00.72 0.005 0.03 0.20 3.15];
OTC = [20.96 04.90 3.64 65.12 3.00 0.89 0.0 00.08 0.011 0.30 0.41 3.19];
SAC = [24.23 02.92 2.30 66.52 2.06 0.75 0.0 00.11 0.003 0.24 0.15 3.19];
KS  = [03.52 00.42 0.18 52.89 0.07 0.40 0.0 41.71 0.008 0.06 0.07 2.74];
MK  = [52.59 44.31 0.43 00.52 0.20 0.41 0.0 00.07 0.010 0.00 0.02 2.62];
SF  = [95.91 00.15 0.12 00.17 0.20 0.10 0.0 00.00 0.000 0.26 0.07 2.25];
% Properties of phases
%          SiO2  Al2O3 Fe2O3  CaO   SO3   MgO   H2O   CO2   CaCl2 dens Molw
CSH     = [25.24 01.50 00.00 41.23 01.77 00.00 30.27 00.00 00.0  2.1  238.06];
CH      = [00.00 00.00 00.00 75.69 00.00 00.00 24.31 00.00 00.0  2.24 74.09];
MH2     = [00.00 00.00 00.00 00.00 00.00 69.09 30.91 00.00 00.0  2.39 58.32];
FH3     = [00.00 00.00 89.76 00.00 00.00 00.00 10.24 00.00 00.0  4.28 175.01];
CS      = [00.00 00.00 00.00 32.57 46.50 00.00 20.93 00.00 00.0  2.32 72.17];
ETTR    = [00.00 08.12 00.00 26.81 19.14 00.00 45.93 00.00 00.0  1.77 255.10];
MS      = [00.00 16.38 00.00 36.03 12.86 00.00 34.73 00.00 00.0  2.01 622.52];
C4AH13  = [00.00 18.19 00.00 40.02 00.00 00.00 41.79 00.00 00.0  2.05 560.48];
MC      = [00.00 17.94 00.00 39.46 00.00 00.00 34.86 07.74 00.0  2.01 568.46];
CC      = [00.00 00.00 00.00 56.03 00.00 00.00 00.00 43.97 00.0  2.72 100.09];
FS      = [00.00 18.16 00.00 29.97 00.00 00.00 32.09 00.0  19.77 2.08 561.34];
PS      = [00.00 00.00 00.00 00.00 00.00 00.00 100.00 00.00 00.00 1.0  18.02];
% Calculations
for (i=1:1:11)
   powdercomp(i)=(HOC(i)*HOCperc+RCI(i)*RCIperc+OTC(i)*OTCperc+SAC(i)*
SACperc + MK(i)*MKperc + SF(i)*SFperc + KS(i)*KSperc)/100;

end
powderdens = 100/(HOCperc/HOC(12)+RCIperc/RCI(12)+OTCperc/OTC(12)+SACperc
/SAC(12)+SFperc/SF(12)+KSperc/KS(12)+MKperc/MK(12));

pastecomp      = powdercomp;
pastecomp(7)= waterpowder*100;
wetmixdens    = (100+waterpowder*100)/(100/powderdens + waterpowder*100);
vol_system    = (100+waterpowder*100)/wetmixdens;

for (i=1:1:9)
   ConstitutiveM1(i,:) = [CSH(i) CH(i) MH2(i) FH3(i) PS(i) MS(i) C4AH13(i)
MC(i) FS(i)];
   ConstitutiveM2(i,:) = [CSH(i) CH(i) MH2(i) FH3(i) PS(i) MS(i) ETTR(i)
MC(i) FS(i)];
   ConstitutiveM3(i,:) = [CSH(i) CH(i) MH2(i) FH3(i) PS(i) CC(i) ETTR(i)
MC(i) FS(i)];
   ConstitutiveM4(i,:) = [CSH(i) CH(i) MH2(i) FH3(i) PS(i) CC(i) ETTR(i)
CS(i) FS(i)];
end
phasedensities(1,:) = [CSH(10) CH(10) MH2(10) FH3(10) PS(10) MS(10)
C4AH13(10) MC(10) FS(10)];
phasedensities(2,:) = [CSH(10) CH(10) MH2(10) FH3(10) PS(10) MS(10) ETTR(10)
MC(10) FS(10)];
phasedensities(3,:) = [CSH(10) CH(10) MH2(10) FH3(10) PS(10) CC(10) ETTR(10)
MC(10) FS(10)];
phasedensities(4,:) = [CSH(10) CH(10) MH2(10) FH3(10) PS(10) CC(10) ETTR(10)
CS(10) FS(10)];
invM1 = inv(ConstitutiveM1);
```

```
invM2 = inv(ConstitutiveM2);
invM3 = inv(ConstitutiveM3);
invM4 = inv(ConstitutiveM4);
volassemblage = zeros(1,4);
assemblage = zeros(4,9);
p = zeros(1,4);

for (i=1:1:9)
     for (j=1:1:9)
       assemblage(1,i) = assemblage(1,i)+ invM1(i,j)*pastecomp(j)*100;
       assemblage(2,i) = assemblage(2,i)+ invM2(i,j)*pastecomp(j)*100;
       assemblage(3,i) = assemblage(3,i)+ invM3(i,j)*pastecomp(j)*100;
       assemblage(4,i) = assemblage(4,i)+ invM4(i,j)*pastecomp(j)*100;
   end
end
for (i=1:1:4)
   for (j=1:1:9)
      volassemblage(i)=volassemblage(i)+ assemblage(i,j)/phasedensities(i,j);

   end
   assemblage(i,5)=assemblage(i,5)+vol_system-volassemblage(i);
end

for (i=1:1:4)
    for (j=1:1:9)
        if (assemblage(i,j)<0)
            p(i)=1;
        end
    end
end

phase_assem = zeros(1,9);
for (i=1:1:4)
   if (p(i)<1)
      phase_assem = assemblage(i,:);
      vol_assem   = volassemblage(i);
   end
end
density_system= sum(phase_assem)/vol_system;

% Total assemblage used for later calculations
% CSH CH MH2 FH3 PS C4AH13 MS ETTR CS MC CC FS
total_assem = zeros(1,12);
for (i=1:1:5)
    total_assem(i)=phase_assem(i);
end
if (p(1)<1)
    total_assem(7)=phase_assem(6);
    total_assem(6)=phase_assem(7);
    total_assem(10)=phase_assem(8);
    total_assem(12)=phase_assem(9);
end
if (p(2)<1)
    total_assem(7)=phase_assem(6);
    total_assem(8)=phase_assem(7);
    total_assem(10)=phase_assem(8);
    total_assem(12)=phase_assem(9);
end
if (p(3)<1)
    total_assem(11)=phase_assem(6);
    total_assem(8)=phase_assem(7);
    total_assem(10)=phase_assem(8);
    total_assem(12)=phase_assem(9);
```

```
end
if (p(4)<1)
    total_assem(11)=phase_assem(6);
    total_assem(8)=phase_assem(7);
    total_assem(9)=phase_assem(8);
    total_assem(12)=phase_assem(9);
end
% Define molar volumes and transform to moles per cm3
for (i=1:1:12)
   bigM(1,:)=CSH;
   bigM(2,:)=CH;
   bigM(3,:)=MH2;
   bigM(4,:)=FH3;
   bigM(5,:)=PS;
   bigM(6,:)=C4AH13;
   bigM(7,:)=MS;
   bigM(8,:)=ETTR;
   bigM(9,:)=CS;
   bigM(10,:)=MC;
   bigM(11,:)=CC;
   bigM(12,:)=FS;
end
densities = zeros(1,12);
densities = [CSH(10) CH(10) MH2(10) FH3(10) PS(10) C4AH13(10) MS(10) ETTR(10)
CS(10) MC(10) CC(10) FS(10)];
molarv   = zeros (1,12);
for (i=1:1:12)
    molarv(i)=(bigM(i,11)/bigM(i,10));
    % units are in cm3 per mole of each phase
end
factor = sum(total_assem)/density_system;
for (i=1:1:12)
    total_assem(i)= (total_assem(i)/factor)/bigM(i,11);
    % units are in mole per cm3 hydrated paste
end
FeCa = (total_assem(4)*2)/(1.75*total_assem(1));

% Defining elements in pore solution and distribution of alkalis
total_Na    = (powdercomp(10)/factor)*2/(2*23+16); % in 1 cm3
Na_concentration =
(total_Na/(1+(Rd_alkalis/(total_assem(5)*molarv(5)))/(total_assem(1)*235.69*
.81)))*1000/(molarv(5)*total_assem(5));
total_K    = (powdercomp(11)/factor)*2/(2*39.1+16); % in 1 cm3
K_concentration      = (total_K/(1+(Rd_alkalis/(total_assem(5)*molarv(5)))
/(total_assem(1)*235.69*.81)))*1000/(molarv(5)*total_assem(5));

total_Cl = (powdercomp(9)/factor)*2/(2*35.45+40.08); % in 1 cm3
assem0 = total_assem;
```

Code of function "surf.m"

```
function [assem_surf,total] = surf(exp_sol,assem,assem0,molarv,FeCa,
Rd_alkalis,molarv)

assem_surf=zeros(12,1);
if(FeCa>0.02)
   Fex2 = 0.0376; % y = Fex2 * x^2 + Fex * x
   Fex = 0.0046; % y [mol CaCl2/mol CSH], x [mol CaCl2/mol s.s. phase]
else
```

```
    Fex2 = 0.0601;
    Fex = 0.0164;
end
tot_Na = exp_sol(2)*assem_surf(5)*molarv(5)/1000000;
tot_K = exp_sol(5)*assem_surf(5)*molarv(5)/1000000;
conc_Na = 0.0;
conc_K = 0.0;
while((conc_Na+conc_K)<(exp_sol(2)+exp_sol(5)))
for(i=1:1:12)
    assem_surf(i)=assem(i,1);
end
z_Na = tot_Na/(1+assem_surf(5)*molarv(5)/(assem_surf(1)*243.46*.81*
Rd_alkalis))/assem_surf(1);
z_K = tot_K/(1+assem_surf(5)*molarv(5)/(assem_surf(1)*243.46*.81*
Rd_alkalis))/assem_surf(1);

conc_Na = (tot_Na-z_Na*assem_surf(1))/(assem_surf(5)*molarv(5)/1000);
conc_K = (tot_K-z_K*assem_surf(1))/(assem_surf(5)*molarv(5)/1000);
x = 0.0;
y0 = 0.0;  % introduce variables
y1 = 0.0;
z1_Na = z_Na; %help variables
z1_K = z_K;   %help variables
converted = 0; % help variable for converted mol of relevant phases
if (exp_sol(1)>0.0)
    increment_x= 0.01;
    conc_Cl = 0.0; % initial concentration of chlorides, mol/liter
    while(conc_Cl<exp_sol(1))
        if (assem_surf(6)>0.0)        %--------- case C4AH13 > 0
            x = x + increment_x;
            y1 = Fex2 * x^2 + Fex * x;
            converted = (assem_surf(12)+assem_surf(10))^2*increment_x
/(assem_surf(10)-increment_x*(assem_surf(10)+assem_surf(12)));
            assem_surf(6) = assem_surf(6)-converted;
            assem_surf(12)= assem_surf(12)+converted;
            assem_surf(5)= assem_surf(5)+converted*(molarv(6)-molarv(12))
/molarv(5);
            if(z1_Na>0)             %--------- case: alkali-containing C-S-H
                conc_Cl =
conc_Cl+(((z_Na+z_K)*(assem_surf(5)*molarv(5)*25/assem_surf(1))/
(0.81*243*Rd_alkalis))/0.83)*(y1-y0)*2*assem_surf(1)/(assem_surf(5)
*molarv(5)/1000);
                conc_Na = conc_Na+ ((z_Na*(assem_surf(5)*molarv(5)*25/
assem_surf(1))/ (.81*243*Rd_alkalis))/.83)*.34*(y1-y0)*assem_surf(1)
/(assem_surf(5)*molarv(5)/1000);
                conc_K = conc_K + ((z_K*(assem_surf(5)*molarv(5)*25/
assem_surf(1))/(.81*243*Rd_alkalis))/.83)*.34*(y1-y0)*assem_surf(1)
/(assem_surf(5)*molarv(5)/1000);
                z1_Na = z1_Na-((z_Na*(assem_surf(5)*molarv(5)*25/assem_surf(1))
/(0.81*243*Rd_alkalis))/0.83)*0.34*(y1-y0);
                z1_K = z1_K-((z_K*(assem_surf(5)*molarv(5)*25/assem_surf(1))
/(0.81*243*Rd_alkalis))/0.83)*0.34*(y1-y0);
                y0=y1;
            else                 %--------- case: alkali-free C-S-H
                conc_Cl    = conc_Cl+((assem_surf(5)*molarv(5)/assem_surf(1))
/75)*(y1-y0)*2*assem_surf(1)/(assem_surf(5)*molarv(5)/1000);
                conc_Na = tot_Na/(assem_surf(5)*molarv(5)/1000);
                conc_K = tot_K/(assem_surf(5)*molarv(5)/1000);
                y0=y1;
            end
        else
            if(assem_surf(7)>0) %-------- case C4AH13 = 0, C3A.CaSO4.12H2O >0
                x = x + increment_x;
```

```
            y1 = Fex2*x^2+Fex*x;
            converted = (assem_surf(12)+assem_surf(10))^2*increment_x
/(assem_surf(10)-increment_x*(assem_surf(10)+assem_surf(12)));
            assem_surf(6)=0.0;
            assem_surf(7)=assem_surf(7)-3*converted/2;
            assem_surf(8)=assem_surf(8)+0.5*converted;
            assem_surf(12)=assem_surf(12)+converted;
            assem_surf(5)= assem_surf(5)+converted*(3*molarv(7)/2-0.5*
molarv(8)-molarv(12))/molarv(5);
                if(z1_Na>0)      %--------- case: alkali-containing C-S-H
                    conc_Cl = conc_Cl+(((z_Na+z_K)*(assem_surf(5)*molarv(5)*25
/assem_surf(1))/(0.81*243*Rd_alkalis))/0.83)*(y1-y0)*2*assem_surf(1)
/(assem_surf(5)*molarv(5)/1000);
                    conc_Na = conc_Na + ((z_Na*(assem_surf(5)*molarv(5)*25
/assem_surf(1))/(.81*243*Rd_alkalis))/.83)*.34*(y1-y0)*assem_surf(1)
/(assem_surf(5)*molarv(5)/1000);
                    conc_K = conc_K + ((z_K*(assem_surf(5)*molarv(5)*25
/assem_surf(1))/(.81*243*Rd_alkalis))/.83)*.34*(y1-y0)*assem_surf(1)
/(assem_surf(5)*molarv(5)/1000);
                    z1_Na = z1_Na-((z_Na*(assem_surf(5)*molarv(5)*25
/assem_surf(1))/(0.81*243*Rd_alkalis))/0.83)*0.34*(y1-y0);
                    z1_K = z1_K-((z_K*(assem_surf(5)*molarv(5)*25
/assem_surf(1))/(0.81*243*Rd_alkalis))/0.83)*0.34*(y1-y0);
                y0=y1;
            else              %--------- case: alkali-free C-S-H
                conc_Cl    = conc_Cl+((assem_surf(5)*molarv(5)
/assem_surf(1))/75)*(y1-y0)*2*assem_surf(1)/(assem_surf(5)*molarv(5)/1000);
                conc_Na = tot_Na/(assem_surf(5)*molarv(5)/1000);
                conc_K = tot_K/(assem_surf(5)*molarv(5)/1000);
                y0=y1;
            end
        else  %--case C4AH13 = 0, C3A.CaSO4.12H2O = 0, C3A.CaCO3.11H2O > 0
            assem_surf(7)=0.0;
            x=x+increment_x;
            y1=Fex2*x^2+Fex*x;
            converted = (assem_surf(12)+assem_surf(10))*increment_x;
            assem_surf(10)=assem_surf(10)-converted;
            assem_surf(12)=assem_surf(12)+converted;
            assem_surf(11)=assem_surf(11)+converted;
            assem_surf(5)= assem_surf(5)+converted*(molarv(10)-molarv(12)-
molarv(11))/molarv(5);
                if(z1_Na>0)       %--------- case: alkali-containing C-S-H
                    conc_Cl = conc_Cl+(((z_Na+z_K)*(assem_surf(5)*molarv(5)
*25/assem_surf(1))/(0.81*243*Rd_alkalis))/0.83)*(y1-y0)*2*assem_surf(1)
/(assem_surf(5)*molarv(5)/1000);
                    conc_Na = conc_Na + ((z_Na*(assem_surf(5)*molarv(5)*25
/assem_surf(1))/(.81*243*Rd_alkalis))/.83)*.34*(y1-y0)*assem_surf(1)
/(assem_surf(5)*molarv(5)/1000);
                    conc_K = conc_K + ((z_K*(assem_surf(5)*molarv(5)*25
/assem_surf(1))/(.81*243*Rd_alkalis))/.83)*.34*(y1-y0)*assem_surf(1)
/(assem_surf(5)*molarv(5)/1000);
                    z1_Na = z1_Na-((z_Na*(assem_surf(5)*molarv(5)*25
/assem_surf(1))/(0.81*243*Rd_alkalis))/0.83)*0.34*(y1-y0);
                    z1_K = z1_K-((z_K*(assem_surf(5)*molarv(5)*25
/assem_surf(1))/(0.81*243*Rd_alkalis))/0.83)*0.34*(y1-y0);
                    y0=y1;

                else              %--------- case: alkali-free C-S-H
                    conc_Cl    = conc_Cl+((assem_surf(5)*molarv(5)
/assem_surf(1))/75)*(y1-y0)*2*assem_surf(1)/(assem_surf(5)*molarv(5)/1000);
                    conc_Na = tot_Na/(assem_surf(5)*molarv(5)/1000);
                    conc_K = tot_K/(assem_surf(5)*molarv(5)/1000);
                    y0=y1;
```

```
            end
        end
    end
  end
end

if(conc_Na < exp_sol(2))
    tot_Na = tot_Na + 0.00002;
end
if(conc_K < exp_sol(5))
    tot_K = tot_K + 0.00002;
end
end

assem_surf(2) = assem_surf(2)-assem_surf(12)-assem_surf(1)*y1;
assem_surf(5) = assem_surf(5)+(assem_surf(12)+assem_surf(1)*y1)*molarv(2)
/molarv(5);

if(assem_surf(2)<0)
    assem_surf(2)=0;
end

if(exp_sol(3)<0.015)
    assem_surf(2)=0.0;
    assem_surf(5)=assem_surf(5)-assem0(2)*molarv(2)/molarv(5);
end

conc(1,1) = conc_Cl;
conc(2,1) = conc_Cl;
conc(3,1) = conc_Na;
conc(4,1) = conc_Na;
conc(9,1) = conc_K;
conc(10,1) = conc_K;
conc(5,1) = exp_sol(3);
conc(6,1) = exp_sol(3);
conc(7,1) = exp_sol(4);
conc(8,1) = exp_sol(4);

Cl =
(assem_surf(10)+assem_surf(12))*x*2+assem_surf(1)*2*y1+conc_Cl*(assem_surf(5)
* molarv(5)/1000);
Na = z1_Na*assem_surf(1)+conc_Na*(assem_surf(5)*molarv(5)/1000);
K  = z1_K*assem_surf(1)+conc_K*(assem_surf(5)*molarv(5)/1000);

total = [Cl Na K];
```

Code of function "MSing.m"

```
function [conc,Cl_tot,Na_tot,K_tot,delta_t] = MSing(t,delta_t,conc,exp_sol,x,
delta_x,assem,molarv,Vagg,Vair,Cl_tot,Na_tot,K_tot,trans_factor)

Di= [2.032 1.333 0.793 5.303 1.957]*1e-9;
% Intrinsic diffusioncoefficients for each species resp. Cl, Na, Ca, OH, K
Di(2)=Di(2)/100;
Di(5)=Di(5)/100;
z_i = [-1 1 2 -1 1];
D_factor = zeros(1,round(x/delta_x)+1);
% concentration profiles
delta_c_p  = zeros(5,abs(x/delta_x)+1);
delta_c_m  = zeros(5,abs(x/delta_x)+1);
avg_c_p    = zeros(5,abs(x/delta_x)+1);
```

```
avg_c_m      = zeros(5,abs(x/delta_x)+1);
    for (i=1:1:abs(x/delta_x)+1)
        c = assem(5,i).*molarv(5);
        Vgp = 1 - (assem(2,i).*molarv(2)) - (assem(3,i).*molarv(3)) -
(assem(4,i).*molarv(4)) - (assem(5,i).*molarv(5)) - (assem(9,i).*molarv(9)) -
(assem(11,i).*molarv(11));
        n=400;
        Dgm_factor = Vgp/(n*(1.5-0.5*Vgp-1.5*c));
        Dp_factor  = Dgm_factor*(n+2*sqrt(n)*(1+c*(n-1)))/
(n+2*sqrt(n)-c*(n-1));
        D_factor(i)= trans_factor*Dp_factor*(1-Vair-Vagg)/
(1+(Vair+Vagg)/2);
    end
    if (delta_t==0.0)
        delta_t = (0.5*(delta_x)^2)./(D_factor(1)*Di(4))
    end
    for (i=2:1:abs(x/delta_x))
        for (j=1:1:5)
            delta_c_p(j,i)  = (conc(2*j-1,i)-conc(2*j-1,i+1));
            delta_c_m(j,i)  = (conc(2*j-1,i-1)-conc(2*j-1,i));
            avg_c_p(j,i)    = (conc(2*j-1,i)+conc(2*j-1,i+1))./2;
            avg_c_m(j,i)    = (conc(2*j-1,i-1)+conc(2*j-1,i))./2;
        end
    end
    for (i=2:1:abs(x/delta_x))
        sum_delta_c_p   = 0.0;
        sum_delta_c_m   = 0.0;
        sum_avg_c_p     = 0.0;
        sum_avg_c_m     = 0.0;
        for (k=1:1:5)
            sum_delta_c_p   = sum_delta_c_p + z_i(k).*Di(k).*
((D_factor(i)+D_factor(i+1))/2).*delta_c_p(k,i);
            sum_delta_c_m   = sum_delta_c_m + z_i(k).*Di(k).*
((D_factor(i)+D_factor(i-1))/2).*delta_c_m(k,i);
            sum_avg_c_p     = sum_avg_c_p + (z_i(k).^2)*Di(k).*
((D_factor(i)+D_factor(i+1))/2).*avg_c_p(k,i)+1e-100;
            sum_avg_c_m     = sum_avg_c_m + (z_i(k).^2)*Di(k).*
((D_factor(i)+D_factor(i-1))/2).*avg_c_m(k,i)+1e-100;
        end
        share_m = 0.0;
        share_p = 0.0;
        for (j=1:1:5)
            share_m = -(((conc(2*j-1,i-1)-conc(2*j-1,i))./delta_x)
-z_i(j).*((conc(2*j-1,i-1)+conc(2*j-1,i))/(2*delta_x))*sum_delta_c_m
/sum_avg_c_m);
            share_p = -(((conc(2*j-1,i)-conc(2*j-1,i+1))./delta_x)
-z_i(j).*((conc(2*j-1,i)+conc(2*j-1,i+1))/(2*delta_x))*sum_delta_c_p
/sum_avg_c_p);
            conc(2*j,i) = conc(2*j-1,i) - (delta_t*Di(j).*D_factor(i).
/delta_x).*(+share_m-share_p);
        end
    end
    for(j=2:1:abs(x/delta_x)+1)
      Cl_tot(j) = Cl_tot(j)+(conc(2,j)-conc(1,j)).*assem(5,j).*molarv(5)/1e3;
      Na_tot(j) = Na_tot(j)+(conc(4,j)-conc(3,j)).*assem(5,j).*molarv(5)/1e3;
      K_tot(j) = K_tot(j)+(conc(10,j)-conc(9,j)).*assem(5,j).*molarv(5)/1e3;
    end
    for(i=2:1:abs(x/delta_x)+1)
        for(j=1:1:5)
            conc(2*j-1,i)=conc(2*j,i);
        end
    end
```

Code of function "equil.m"

```
function [assem,conc,leach_CH] = equil(conc,Cl_tot,Na_tot,assem,assem0,
molarv,m,K_tot,FeCa,Rd_alkalis,leach_CH)

Ca_conc=zeros(1,2);
Ca_conc(1) = conc(6,m);
Ca_conc(2) = conc(5,m);
OH_conc = conc(8,m);
total_Cl = Cl_tot(m);   %mol
total_Na = Na_tot(m);   %mol
total_K = K_tot(m);     %mol
if(FeCa>0.02)
   Fex2 = 0.0376; % y = Fex2 * x^2 + Fex * x
   Fex = 0.0046; % y [mol CaCl2/mol CSH], x [mol CaCl2/mol s.s. phase]
else
   Fex2 = 0.0601;
   Fex = 0.0164;
end
for(i=1:1:12)
   assem(i,m)=assem0(i); % return to original assemblage
end

z_Na = (total_Na/(1+(assem(5,m)*molarv(5))/(assem(1,m)*243.46*0.81
*Rd_alkalis)))/assem(1,m);
z_K = (total_K/(1+(assem(5,m)*molarv(5))/(assem(1,m)*243.46*0.81
*Rd_alkalis)))/assem(1,m);

conc_Na = (total_Na-z_Na*assem(1,m))/(assem(5,m)*molarv(5)/1000);
conc_K = (total_K-z_K*assem(1,m))/(assem(5,m)*molarv(5)/1000);   %mol/liter

x = 0.0;
y0 = 0.0;  % introduce variables
y1 = 0.0;
z1_Na = z_Na; %help variables
z1_K = z_K;   %help variables
converted = 0; % help variable for converted mol of relevant phases
leach_CH(m)= leach_CH(m)-(Ca_conc(2)-Ca_conc(1))*(assem(5,m)*molarv(5)/1000);
assem(5,m) = assem(5,m)+leach_CH(m)*molarv(2)/molarv(5);
Ca_conc(2) = 0.015;
if (total_Cl>0.0)
   increment_x= 0.01;
   conc_Cl = 0.0; % initial concentration of chlorides, mol/liter
   Cl_used = 0.0; % amount of chlorides accounted for, mol
   while(Cl_used<total_Cl)
      if(assem(6,m)>0.0)        %--------- case C4AH13 > 0
         x = x + increment_x;
         y1 = Fex2 * x^2 + Fex * x;
         converted = (assem(12,m)+assem(10,m))^2*increment_x/(assem(10,m)
-increment_x*(assem(10,m)+assem(12,m)));
         assem(6,m) = assem(6,m)-converted;
         assem(12,m)= assem(12,m)+converted;
         assem(5,m)= assem(5,m)+converted*(molarv(6)-molarv(12))/molarv(5);
         if(z1_Na>0)        %--------- case: alkali-containing C-S-H
            conc_Cl = conc_Cl+(((z_Na+z_K)*(assem(5,m)*molarv(5)*25
/assem(1,m))/(0.81*243*Rd_alkalis))/0.83)*(y1-y0)*2*assem(1,m)
/(assem(5,m)*molarv(5)/1000);
            conc_Na = conc_Na+(((z_Na)*(assem(5,m)*molarv(5)*25
/assem(1,m))/(0.81*243*Rd_alkalis))/0.83)*0.34*(y1-y0)*assem(1,m)
/(assem(5,m)*molarv(5)/1000);
```

```
            conc_K = conc_K+(((z_K)*(assem(5,m)*molarv(5)*25/assem(1,m))
/(0.81*243*Rd_alkalis))/0.83)*0.34*(y1-y0)*assem(1,m)/(assem(5,m)*
molarv(5)/1000);
            z1_Na = z1_Na-((z_Na*(assem(5,m)*molarv(5)*25/assem(1,m))
/(0.81*243*Rd_alkalis))/0.83)*0.34*(y1-y0);
            z1_K = z1_K-((z_K*(assem(5,m)*molarv(5)*25/assem(1,m))
/(0.81*243*Rd_alkalis))/0.83)*0.34*(y1-y0);
            Cl_used = assem(12,m)*2+assem(1,m)*y1*2+conc_Cl*
(assem(5,m)*molarv(5)/1000);
            y0=y1;
        else                    %--------- case: alkali-free C-S-H
            conc_Cl   = conc_Cl+(assem(5,m)*molarv(5)/(assem(1,m)*75))
*(y1-y0)*2*assem(1,m)/(assem(5,m)*molarv(5)/1000);
            conc_Na = total_Na/(assem(5,m)*molarv(5)/1000);
            conc_K = total_K/(assem(5,m)*molarv(5)/1000);
            y0=y1;
            Cl_used = assem(12,m)*2+assem(1,m)*y1*2+conc_Cl*(assem(5,m)*
molarv(5)/1000);
        end
      else
         if(assem(7,m)>0.0)  %------ case C4AH13 = 0, C3A.CaSO4.12H2O >0
            x = x + increment_x;
            y1 = Fex2*x^2+Fex*x;
            converted = (assem(12,m)+assem(10,m))^2*increment_x/
(assem(10,m)-increment_x*(assem(10,m)+assem(12,m)));
            assem(6,m)=0.0;
            assem(7,m)=assem(7,m)-3*converted/2;
            assem(8,m)=assem(8,m)+0.5*converted;
            assem(12,m)=assem(12,m)+converted;
            assem(5,m)= assem(5,m)+converted*(3*molarv(7)/2-
molarv(12)-0.5*molarv(8))/molarv(5);
            if(z1_Na>0)      %--------- case: alkali-containing C-S-H
                conc_Cl =
conc_Cl+(((z_Na+z_K)*(assem(5,m)*molarv(5)*25/assem(1,m))/(0.81*243
*Rd_alkalis))/0.83)*(y1-y0)*2*assem(1,m)/(assem(5,m)*molarv(5)/1000);
                conc_Na =
conc_Na+(((z_Na)*(assem(5,m)*molarv(5)*25/assem(1,m))/(0.81*243
*Rd_alkalis))/0.83)*0.34*(y1-y0)*assem(1,m)/(assem(5,m)*molarv(5)/1000);
                conc_K =
conc_K+(((z_K)*(assem(5,m)*molarv(5)*25/assem(1,m))/(0.81*243
*Rd_alkalis))/0.83)*0.34*(y1-y0)*assem(1,m)/(assem(5,m)*molarv(5)/1000);
                z1_Na = z1_Na-((z_Na*(assem(5,m)*molarv(5)*25/assem(1,m))
/(0.81*243*Rd_alkalis))/0.83)*0.34*(y1-y0);
                z1_K = z1_K-((z_K*(assem(5,m)*molarv(5)*25/assem(1,m))/(0.81
*243*Rd_alkalis))/0.83)*0.34*(y1-y0);
                Cl_used = assem(12,m)*2+assem(1,m)*y1*2+conc_Cl*
(assem(5,m)*molarv(5)/1000);
                y0=y1;
            else                %--------- case: alkali-free C-S-H
                conc_Cl   = conc_Cl+(assem(5,m)*molarv(5)/(assem(1,m)*75))
*(y1-y0)*2*assem(1,m)/(assem(5,m)*molarv(5)/1000);
                conc_Na = total_Na/(assem(5,m)*molarv(5)/1000);
                conc_K = total_K/(assem(5,m)*molarv(5)/1000);
                y0=y1;
                Cl_used = assem(12,m)*2+assem(1,m)*y1*2+conc_Cl*
(assem(5,m)*molarv(5)/1000);
            end
        else  %-- case C4AH13 = 0, C3A.CaSO4.12H2O = 0, C3A.CaCO3.11H2O > 0
            assem(7,m)=0.0;
            x=x+increment_x;
            y1=Fex2*x^2+Fex*x;
            converted = (assem(10,m)+assem(12,m))*increment_x;
            assem(10,m)=assem(10,m)-converted;
```

```
            assem(12,m)=assem(12,m)+converted;
            assem(11,m)=assem(11,m)+converted;
            assem(5,m)= assem(5,m)+converted*(molarv(10)-molarv(12)-
molarv(11))/molarv(5);
                if(z1_Na>0)        %--------- case: alkali-containing C-S-H
                    conc_Cl =
conc_Cl+(((z_Na+z_K)*(assem(5,m)*molarv(5)*25/assem(1,m))/(0.81*243
*Rd_alkalis))/0.83)*(y1-y0)*2*assem(1,m)/(assem(5,m)*molarv(5)/1000);
                    conc_Na =
conc_Na+(((z_Na)*(assem(5,m)*molarv(5)*25/assem(1,m))/(0.81*243
*Rd_alkalis))/0.83)*0.34*(y1-y0)*assem(1,m)/(assem(5,m)*molarv(5)/1000);
                    conc_K =
conc_K+(((z_K)*(assem(5,m)*molarv(5)*25/assem(1,m))/(0.81*243
*Rd_alkalis))/0.83)*0.34*(y1-y0)*assem(1,m)/(assem(5,m)*molarv(5)/1000);
                    z1_Na = z1_Na-((z_Na*(assem(5,m)*molarv(5)*25/assem(1,m))
/(0.81*243*Rd_alkalis))/0.83)*0.34*(y1-y0);
                    z1_K = z1_K-((z_K*(assem(5,m)*molarv(5)*25/assem(1,m))
/(0.81*243*Rd_alkalis))/0.83)*0.34*(y1-y0);
                    Cl_used = assem(12,m)*2+assem(1,m)*y1*2+
conc_Cl*(assem(5,m)*molarv(5)/1000);
                    y0=y1;

                else              %--------- case: alkali-free C-S-H
                    conc_Cl   = conc_Cl+(assem(5,m)*molarv(5)/(assem(1,m)*75))
*(y1-y0)*2*assem(1,m)/(assem(5,m)*molarv(5)/1000);
                    conc_Na = total_Na/(assem(5,m)*molarv(5)/1000);
                    conc_K = total_K/(assem(5,m)*molarv(5)/1000);
                    y0=y1;
                    Cl_used = assem(12,m)*2+assem(1,m)*y1*2+conc_Cl*
(assem(5,m)*molarv(5)/1000);
                end
            end
        end
    end
end

assem(2,m) = assem(2,m)-(Cl_used-conc_Cl*assem(5,m)*molarv(5)/1000)/2;
assem(5,m) = assem(5,m)+((Cl_used-
conc_Cl*assem(5,m)*molarv(5)/1000)/2)*molarv(2)/molarv(5);

if((conc_Na+conc_K-conc_Cl)>0)
   Ca_conc(2)= 0.015;
   OH_conc = conc_Na+conc_K-conc_Cl+2*Ca_conc(2);
else
   OH_conc = 0.030;
   Ca_conc(2) = (conc_Cl+OH_conc-conc_Na-conc_K)/2;
end

if(Ca_conc(2)>0.015)
   assem(2,m) = assem(2,m)-(Ca_conc(2)-0.015)*(assem(5,m)*molarv(5)/1000);
   assem(5,m) = assem(5,m)+( Ca_conc(2)-0.015)*(assem(5,m)*molarv(5)/1000)
*molarv(2)/molarv(5);
end

assem(2,m)= assem(2,m)-leach_CH(m);

if(assem(2,m)<0.0)
   assem(2,m)=0.0;
end

conc(1,m) = conc_Cl;
conc(2,m) = conc_Cl;
conc(3,m) = conc_Na;
```

```
conc(4,m)  = conc_Na;
conc(9,m)  = conc_K;
conc(10,m) = conc_K;
conc(5,m)  = Ca_conc(2);
conc(6,m)  = Ca_conc(2);
conc(7,m)  = OH_conc;
conc(8,m)  = OH_conc;
```

```
conc(4,m)  = conc_Na;
conc(9,m)  = conc_K;
conc(10,m) = conc_K;
conc(5,m)  = Ca_conc(2);
conc(6,m)  = Ca_conc(2);
conc(7,m)  = OH_conc;
conc(8,m)  = OH_conc;
```